

Designing Modular Fibrin Composite Scaffolds for Enhanced Ventricular Myocardium Regeneration

A Dissertation
Submitted to the Faculty of

WORCESTER POLYTECHNIC INSTITUTE

in partial fulfillment of the requirements for the

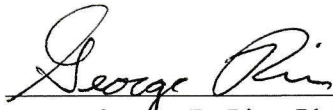
Degree of Doctor of Philosophy in
Biomedical Engineering

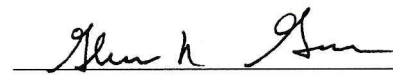
August 29, 2017

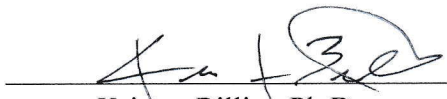
By



Megan O'Brien Chrobak

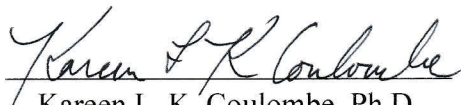
Approved by:


George D. Pins, Ph.D.
Associate Professor, Advisor
Biomedical Engineering
Worcester Polytechnic Institute


Glenn R. Gaudette, Ph.D.
Professor
Biomedical Engineering
Worcester Polytechnic Institute


Kristen Billiar, Ph.D.
Department Head & Professor
Biomedical Engineering
Worcester Polytechnic Institute


Nima Rahbar, Ph.D.
Associate Professor
Civil and Environmental Engineering
Worcester Polytechnic Institute


Karen L. K. Coulombe, Ph.D.
Assistant Professor
Biomedical Engineering
Brown University

Acknowledgements

First and foremost, I would like to thank my husband, Matthew Chrobak, for all of the love and support throughout the years. I can honestly say I likely would not have gone back to school for my Ph.D. without your encouragement and reassurance. I am so grateful to have you in my life. Thank you especially for always knowing how to ease any stress (usually by having chocolate on hand).

To my advisor, George Pins, Ph.D., thank you for helping me develop as a scientist, for encouraging independent thinking and for all of your guidance and support over the years. It was a pleasure working with you and I truly feel that because of you I am more independent and confident in my work. I am incredibly grateful for this!

I would also like to thank our collaborators on this project (Glenn Gaudette, Ph.D., Katrina Hansen and Josh Gershlak) and my dissertation committee (Glenn Gaudette, Ph.D., Kristen Billiar, Ph.D., Nima Rahbar, Ph.D., and Kareen Coulombe, Ph.D.). Thank you for your time, guidance and support. I have learned a great deal from you and your input has helped to develop this project into work that I am very proud of.

Thank you to the rest of the Biomedical Engineering Department faculty and the lab staff at Gateway Park. I have received help from so many of you and am incredibly appreciative of the knowledge and technical expertise you have shared with me.

There were many students who have helped me throughout my time at WPI. To my lab mates in Pins lab (past and present), thank you for the help, encouragement and support. To all of the IGERT students, thank you for the sense of camaraderie. To Marianne Kanellias, Meagan Carnes and David Dolivo, thank you for all of the support (emotional and technical) throughout the years.

Finally, I would also like to thank my family and friends. I am so appreciative of all of the “positive thoughts”, words of encouragement and words of comfort throughout this entire process.

This has been a challenging but rewarding journey, one that I am very grateful to have taken with all of you.

Thank you all!

Table of Contents

	Page
Acknowledgements	i
Table of Contents	ii
Table of Figures	vii
Table of Tables	viii
Abbreviations	ix
Abstract	xii
Chapter 1: Overview	1
1.1 Introduction	1
1.2 Overall Goal and Hypothesis	3
1.3 Specific Aim 1: Develop a fibrin composite layer that enables customizable modulus values while sustaining cardiomyocyte contractility	4
1.4 Specific Aim 2: Develop an aligned composite layer to enhance contractile function	4
1.5 Specific Aim 3: Produce a biomimetic patch with material properties comparable to native myocardium	5
1.6 References	6
Chapter 2: Background	10
2.1 Biomimetics	10
2.1.1 General Tissue Structure	11
2.1.2 Rationale for Biomimetic Tissue Engineered Scaffolds	11
2.2 Composites for Tissue Engineering: Theory and Applications	12
2.2.1 Principle of Combined Action	15
2.2.2 Rule of Mixtures	15
2.2.3 Critical Fiber Length and Integration of Components	16
2.2.4 Alignment of Fibers	17
2.3 Cardiovascular Disease	19
2.4 Heart Anatomy and Ventricular Myocardium	21
2.5 Cardiac Patches: Implantation Strategies	23
2.6 Acellular Cardiac Patches	26
2.7 Cell Populated Cardiac Patches	28
2.7.1 Decellularized Tissues for Cardiac Patch Development	28
2.7.2 Cell Sheets as Cardiac Patches	29
2.7.3 Synthetic Material Cardiac Patch Scaffolds	31

2.7.4	Natural Biopolymer Cardiac Patch Scaffolds	32
2.7.5	Composite Materials for Cardiac Patch Scaffolds	36
2.8	Biopolymer Microthreads for Tissue Regeneration	36
2.9	Fibrin Microthread-Based Composite Scaffolds	38
2.10	References	39
Chapter 3: Design of a Fibrin Microthread-Based Composite Layer for Use in a Cardiac Patch		48
3.1	Introduction	48
3.2	Materials and Methods	49
3.2.1	Fabrication of Fibrin Microthread-Based Composite Scaffolds	49
3.2.1.1	Microthread Extrusion	50
3.2.1.2	Fibrin Microthread Organization	51
3.2.2	Mechanical Characterization of Fibrin Composite Layers	52
3.2.3	Cell Culture	53
3.2.3.1	Rat Neonatal Ventricular Myocyte (rNVM) Isolation	53
3.2.3.2	Composite Layer Fabrication and Tissue Culture	53
3.2.4	Cardiomyocyte Functional Analysis	54
3.2.5	Phenotypic Analyses	55
3.2.5.1	Immunostaining	55
3.2.5.2	Analysis of Nuclear Alignment	55
3.2.6	Statistical Analyses	56
3.3	Results	56
3.3.1	The Fabrication Method Developed for Composite Layers Enables Reproducible Spacing of Aligned Fibrin Microthreads	56
3.3.2	The Modulus of a Composite Layer Can Be Tuned Through Modulation of the Fibrin Microthread Volume Fraction	56
3.3.3	Cardiomyocyte Phenotype is Retained in Fibrin-Microthread Composite Layers	58
3.3.4	Functional Properties of Cardiomyocytes are Maintained in Fibrin Microthread-Based Composites	59
3.3.5	Fibrin Microthreads Increase Alignment in Adjacent Regions	61
3.4	Discussion	62
3.5	Conclusions	66
3.6	Acknowledgements	67
3.7	References	67
Chapter 4: Alignment of Cardiomyocytes Through Static Tension Increases Contractile Strains in Composite Layers		71
4.1	Introduction	71
4.2	Materials and Methods	73
4.2.1	Fabrication of Fibrin Microthread-Based Composite Scaffolds	73
4.2.1.1	Microthread Extrusion	73
4.2.1.2	Fibrin Microthread Organization	73
4.2.2	Rat Neonatal Ventricular Myocyte (rNVM) Isolation	74

4.2.3	Composite Layer Fabrication and Tissue Culture	74
4.2.3.1	Fabrication of Unaligned Controls	74
4.2.3.2	Fabrication of Experimental Composite Samples (A5tC and A20tC)	75
4.2.3.3	Seeding of Gelatin-Coated Glass Coverslip Controls (GCS)	76
4.2.4	Cardiomyocyte Functional Analysis	76
4.2.4.1	High Density Mapping (HDM)	76
4.2.4.2	Contractile Wave Propagation Evaluation	79
4.2.5	Mechanical Characterization of Cultured Composite Layers	80
4.2.5.1	Theoretical Model for Predicting Elastic Modulus of Compacted Composite Layers	80
4.2.5.2	Mechanical Testing of Compacted Composite Layers	82
4.2.6	Phenotypic Analyses	82
4.2.6.1	Immunostaining	82
4.2.6.2	Analysis of Nuclear Alignment	83
4.2.7	Statistical Analyses	84
4.3	Results	84
4.3.1	Static Tension Induced Through Gel Compaction Improves Nuclear Alignment of Incorporated Cells in Composite Layers	84
4.3.2	Immature Connexin-43 Phenotype Observed Across 5tC Layers	85
4.3.3	Composite Layers with Increased Alignment Have Higher Contractile Strains and Larger Contractile Areas Relative to Unaligned Controls	86
4.3.4	The Highest Contractile Strains are Predominantly in Regions Immediately Adjacent to Fibrin Microthreads for Aligned Composite Layers	88
4.3.5	Consistency of Contractile Behavior is Similar for All Composite Layer Groups	88
4.3.6	Composite Layers with Increased Alignment Have Anisotropic Contractile Wave Propagation Speeds	91
4.3.7	A Model Based on Composite Theory Can be Derived to Predict Modulus Values of Fibrin Composite Layers Following Compaction	92
4.3.8	Composite Layers Compact in Culture Resulting in an Increased Modulus for 5tC Layers	93
4.4	Discussion	94
4.5	Conclusions	101
4.6	Acknowledgements	101
4.7	References	101
Chapter 5: Fibrin Composite Layers Can Be Strategically Laminated to Mimic the Mechanical Properties of Ventricular Myocardium		104
5.1	Introduction	104
5.2	Materials and Methods	106
5.2.1	Definition of Material Requirements	106
5.2.2	Composite Theory Model	106
5.2.3	Fibrin Microthread Preparation	108
5.2.4	Composite Layer Fabrication	108
5.2.5	Lamination Method	109

5.2.6 Uniaxial Tensile Test	110
5.2.7 Statistical Analyses	111
5.3 Results	111
5.3.1 Material Property Criteria Can Be Defined for a Cardiac Patch Acting as a Wall Replacement	111
5.3.2 Composite Theory Can Be Utilized to Yield a Model That Informs a Strategic Lamination of Composite Layers to Produce a Biomimetic Patch	112
5.3.3 Fibrin Glue Can Be Used to Laminate Composite Layers Together Without Significantly Impacting Measured Stiffness or Thickness Values	114
5.3.4 When Laminating Composite Layers, Material Properties Similar to Ventricular Myocardium are Achieved	115
5.4 Discussion	118
5.5 Conclusions	121
5.6 Acknowledgements	122
5.7 References	122
Chapter 6: Conclusions and Future Work	124
6.1 Overview	124
6.2 Results and Conclusions	124
6.2.1 Specific Aim 1: Develop a Fibrin Composite Layer that Enables Customizable Modulus Values While Sustaining Cardiomyocyte Contractility	124
6.2.2 Specific Aim 2: Develop an Aligned Composite Layer to Enhance Contractile Function	126
6.2.3 Specific Aim 3: Produce a Biomimetic Patch with Material Properties Comparable to Native Myocardium	129
6.3 Future Work	131
6.3.1 Use of Composite Patches for In-Vitro Drug Testing	131
6.3.2 Modification of Composite Layers for More Uniform Compaction and Cell Function	133
6.3.3 Incorporation of Vasculature in Composite Patch	134
6.3.4 Fibrin Composite Layers as a Platform Technology	136
6.4 Final Conclusions	137
6.5 References	139
Appendices	142
Appendix 1: Summary of Functional Behavior	142
Appendix 2: Comparison of Media Formulations on 2D and 3D Cultures with Rat Neonatal Ventricular Myocytes	143
A.2.1 Introduction	143
A.2.2 Materials and Methods	144
A.2.2.1 Microthread Extrusion	144
A.2.2.2 Fibrin Microthread Organization	144
A.2.2.3 Rat Neonatal Ventricular Myocyte (rNVM) Isolation	144
A.2.2.4 Fabrication of Composite Layers	145
A.2.2.5 Seeding of Gelatin-Coated Glass Coverslip Controls (GCS)	145

A.2.2.6	Media Preparation and Extended Culture	146
A.2.2.7	Cardiomyocyte Functional Analysis Through High Density Mapping (HDM)	147
A.2.2.8	LIVE/DEAD Staining	147
A.2.2.9	Statistical Analysis	148
A.2.3	Results	148
A.2.3.1	M2 Media Promotes Increased Functional Behavior in a 14-Day Culture	148
A.2.3.2	M1 Media May Promote Proliferation of Fibroblasts	152
A.2.4	Discussion	154
A.2.4.1	Study Limitations	154
A.2.5	Conclusions	156
A.2.6	Acknowledgements	156
A.2.7	References	156

Table of Figures

	Page
Figure 2.1. Composite scaffolds can be strategically combined to mimic the structures of target tissues	13
Figure 2.2. Progression of cardiac disease following an MI	20
Figure 2.3. The anatomy of the heart	22
Figure 2.4. Composition of ventricular myocardium	23
Figure 2.5. Biopolymer microthreads for tissue engineering applications	37
Figure 3.1. Fabrication of a biomimetic composite cardiac patch	50
Figure 3.2. Fibrin microthread spacer device	51
Figure 3.3. Evaluation of fibrin microthread spacing in composite layers	52
Figure 3.4. Fibrin microthread volume fraction can be used to mechanically tune a composite layer	57
Figure 3.5. Striated phenotype of rat neonatal ventricular myocytes cultured in composite fibrin scaffolds	59
Figure 3.6. Fibrin composite layers do not hinder the functionality of cardiomyocytes relative to a fibrin hydrogel control	60
Figure 3.7. Nuclear orientation of cells within composite layers	62
Figure 4.1. The materials and procedure for casting the experimental A5tC and A20tC layers	75
Figure 4.2. HDM is a method for evaluating regional mechanical function	77
Figure 4.3. Grid evaluations to determine consistency across a recorded region	79
Figure 4.4. Method for assessing contractile wave propagation	80
Figure 4.5. Nuclear alignment evaluation	85
Figure 4.6. Phenotypic comparison of aligned composite layers, unaligned composite layers and human heart tissue controls	86
Figure 4.7. Contractile behavior evaluation through HDM with a large ROI	87
Figure 4.8. A grid assessment for evaluation of contractile behavior consistency across a recorded region	90
Figure 4.9. Contractile wave propagation speeds of spontaneous contractions at a frequency of ~1.6 Hz through A5tC Max regions	91
Figure 4.10. Comparison of modulus values for predicted and measured cultured composite layers and acellular controls	94
Figure 5.1. Biomimetic patch structure	105
Figure 5.2. Assessment of fibrin glue impact on cardiac patch properties	115
Figure 6.1. Vascular layer fabrication and combination with composite layer	136
Figure A.2.1. Exposure times for fluorescently labeled samples	148
Figure A.2.2. Summary of functional data for 2D and 3D samples in M1 and M2 cultures	151
Figure A.2.3. LIVE/DEAD staining of composite samples	153

Table of Tables

	Page
Table 2.1. Summary of natural biopolymer, fiber-reinforced composites designed for tissue engineering applications	14
Table 3.1. Predicted moduli for fibrin composite layers with varying volume fractions of fibrin microthreads and fibrin hydrogel	57
Table 3.2. Mechanical data from tensile testing evaluation of fibrin-based composite layers	58
Table 4.1. Summary of compaction occurring over 14 days of culture	92
Table 4.2. Stiffness values for acellular and cultured composite layers	92
Table 4.3. Calculated modulus values for microthreads in acellular and cultured composite layers	93
Table 4.4. Predicted moduli values for compacted and non-compacted (acellular) constructs	93
Table 5.1. Value assumptions for acellular and compacted composite layer models	108
Table 5.2. Summary of design criteria for a cardiac patch functioning as a wall replacement	112
Table 5.3. Summary of theoretical moduli values for 70tC, 80tC and 90tC layers with an offset	113
Table 5.4. Summary of theoretical moduli values for acellular and compacted composite layers with an offset	114
Table 5.5. Result comparisons for individual composite layers and glued cardiac patches	117
Table A.1. Summary table of functional behavior	142
Table A.2.1. Media formulations evaluated for experiment	146
Table A.2.2. Outline of sample nomenclatures and study design to compare media formulations in 2D and 3D cultures	147

Abbreviations

2D – 2 Dimensional

3D – 3 Dimensional

5tC – 5 Thread Composite Layer

10tC – 10 Thread Composite Layer

10tC x 20tC – A Composite Patch with 10tC and 20tC Layers

20tC – 20 Thread Composite Layer

70tC – 70 Thread Composite Layer

80tC – 80 Thread Composite Layer

90tC – 90 Thread Composite Layer

σ - Stress

σ^*_f – Tensile Strength of a Fiber

ϵ - Strain

τ_c – Fiber-Matrix Bond Strength

μm – Micrometers

μg - Micrograms

A – Cross-Sectional Area

A5tC – Aligned 5 Thread Composite Layer

A5tC Max – Recorded Region Within an Aligned 5 Thread Composite Layer that had High Global Movement

A5t Min - Recorded Region Within an Aligned 5 Thread Composite Layer that had Low Global Movement

A20tC – Aligned 20 Thread Composite Layer

AC – Aligned Composite Layer

ALS - Amyotrophic Lateral Sclerosis

ANOVA – Analysis of Variance

APS - Poly(ester-amide), 1:2 Poly(1,3-diamino-2-hydroxypropane-*co*-polyol sebacate)

CaCl_2 – Calcium Chloride

cECM – Cardiac Tissue-Derived Extracellular Matrix

CEE – Chick Embryo Extract

CM – Cardiomyocyte

CVD – Cardiovascular Disease

d – Fiber Diameter

DMEM – Dulbecco's Modified Eagle's Medium

E – Modulus of Elasticity

E_{c1} – Modulus of Elasticity of a Composite Layer

ECM – Extracellular Matrix

E_f – Modulus of Elasticity of Fibrous Components

E_m – Modulus of Elasticity of the Matrix

ESC – Embryonic Stem Cells
F50 – A Factor for Evaluating Consistency of Contractile Strains Across an ROI
FBS – Fetal Bovine Serum
FGC – Fibrin Gel Controls
GCS – Gelatin-Coated Coverslips
 G_f = Shear Modulus for the Fibrous Component
 G_m = Shear Modulus for the Matrix Phase
HA – Hyaluronic Acid
HBS – HEPES Buffered Saline
HDM – High Density Mapping
HEPES – N-[2-Hydroxyethyl] piperazine-N'-[2-ethanesulfonic acid]
HGF – Hepatocyte Growth Factor
hMSC – Human Mesenchymal Stem Cells
HS – Horse Serum
Hz - Hertz
i.e. – That Is (To Say)
iPS – Induced Pluripotent Stem Cells
iPS-CMs – Induced Pluripotent Stem Cell-Derived Cardiomyocytes
IQR – Inner Quartile Range
K – Stiffness
kN - Kilonewton
kPa – Kilopascal
L - Length
 l_c – Critical Length
m – Meter
M1 – Media Formulation 1
M2 - Media Formulation 2
MgCl₂: Magnesium Chloride
MI – Myocardial Infarction
min - Minute
mL - Milliliter
mm – Millimeter
mM - Millimolar
mN – Millinewton
MPa – Megapascals
N - Newton
nN – Nanonewton
PBS – Phosphate-buffered Saline
PDMS – Polydimethylsiloxane
PGA – Polyglycolic Acid
PGCL – Poly(glycolide-co-caprolactone)
PGS – Poly(glycerol sebacate)
PIPAAm – Poly-(N-isopropylacrylamide)
PLCL – Poly(lactide-co-epsilon-caprolactone)
PLGA – Poly(lactic-co-glycolic) Acid

POMaC – Poly(octamethylene maleate (anhydride) citrate)
rNVM – Rat Neonatal Ventricular Myocytes
ROI – Region of Interest
SAC – Systolic Area of Contraction
SIS – Small Intestine Submucosa
UA5tC – Unaligned 5 Thread Composite Layer
UAC – Unaligned Composite Layer
UACMAT – Unaligned Composite Layer with Matrigel
UTS – Ultimate Tensile Strength
 ν_f = Poisson's ratio for the fibrous component
 V_f – Volume Fraction of Fibrous Components
 ν_m = Poisson's ratio for the matrix phase
 V_m – Volume Fraction of Matrix

Abstract

Cardiovascular diseases are the leading causes of death globally. One contributing factor that can lead to heart failure is a myocardial infarction. When an infarct occurs, an occlusion in the tissue vasculature prevents blood flow beyond this site. It results in scar tissue formation. The scar is non-contractile and reduces the working efficiency of the heart. To compensate, left ventricular remodeling will ensue resulting in enlarging of the left ventricle. This progression of events ultimately culminates in heart failure. One approach to assist patients who have suffered a heart attack is to implant a cardiac patch. Current patches are acellular and aim to retain the geometry of the left ventricle, limiting any ventricular remodeling from occurring. While these patches provide a passive support, it is hypothesized that incorporation of cells into the patches could result in functional support that could help to restore baseline function. To be effective, a cell-populated cardiac patch would need to integrate with the host tissue functionally and mechanically. In this thesis, we developed a fibrin microthread-based composite scaffold with material properties comparable to left ventricular myocardium that promotes regional cardiomyocyte alignment and physiologically relevant contractile strains. We hypothesized that a composite material could be developed where constituents of the material would complement one another to yield a mechanically reinforced scaffold that promotes cardiomyocyte function. Through manipulation of the volume fraction of the components, we manipulated the modulus of the layer without compromising contractile strain or contractile frequency of incorporated cells. Additionally, through strategic restraint of the scaffolds, we utilized cell-mediated compaction to induce a tension pattern that increased alignment of incorporated cells. This corresponded to an increase in contractile strain magnitudes, and an anisotropic contractile wave propagation through the engineered tissue. Finally, we laminated composite layers into a patch mimicking the architecture of ventricular myocardium and found that material properties of the patch were similar to properties of the target tissue. In summary, we designed a biomimetic composite patch with material properties similar to ventricular myocardium that supports cardiomyocyte alignment and contractility to promote functional and mechanical integration upon implantation.

Chapter 1: Overview

1.1 INTRODUCTION

Every year approximately 500,000 new cases of heart failure are diagnosed in the United States alone,¹ making it the leading cause of death in our society. Heart transplantation remains the only treatment that can restore function for end stage heart failure. However, donors are limited and only ~2,500 cardiac transplantation surgeries occur annually in the United States¹ leaving a majority of affected patients with compromised cardiac function. Other treatments for end stage heart failure include pharmacologic agents and ventricular assist devices, palliative treatments that do not regenerate damaged tissue.² A major cause of heart failure is a myocardial infarction (MI), where blood flow through a coronary artery is blocked, resulting in ischemia of downstream cardiac muscle. Ischemia causes cardiomyocyte (CM) death and a severe inflammatory response that ultimately results in scar tissue formation.³ Because CMs have low proliferation rates,⁴ the heart has a limited capacity to regenerate the myocardium and restore the mechanical function lost after an MI. As such, research over the past decade has focused on delivering cells to the infarct site, and has progressed to clinical trials.⁵ Current cell delivery strategies have demonstrated enhanced cardiac function,⁵⁻⁷ but are associated with poor cell retention.^{2, 4} There is a need for an effective regenerative solution to heart failure.

A cardiac patch is a precisely engineered scaffold that may increase cell retention within the site and promote cell function.^{2, 8-9} Despite significant advances in the design of cardiac patches, there remains a need to develop an implantable scaffold that promotes substantial functional improvements to damaged myocardium. This requires the scaffold to integrate mechanically and functionally with host tissue.^{2, 10} Current cardiac patch strategies to promote regeneration of damaged myocardium use natural materials,¹⁰⁻¹⁶ synthetic materials,¹⁷⁻¹⁹ or

decellularized tissues.²⁰⁻²¹ Decellularized tissues retain the extracellular matrix architecture, but are associated with harsh sterilization methods and difficulty re-populating the scaffolds with cells.²² Synthetic polyesters, such as polyglycolic acid (PGA), enable the engineering of mechanical and degradation profiles.²³ However, synthetic materials lack native cellular niches and require protein coatings for cellular interaction. In contrast, natural biopolymers, such as fibrin, provide physiologic cell attachment sites and degrade into bioactive peptides.¹¹ While various studies have shown that engineered scaffolds are capable of supporting contractile cells^{10, 15, 20, 24} and providing moderate increase in heart function,^{15, 25-26} *there remains a significant need to develop an engineered cardiac patch with physiologically relevant contractility that easily integrates with the surrounding tissue to promote the regeneration of myocardial tissue.*^{2, 10} Integration of a cardiac patch will ultimately require aligned synchronous contractions of the patch that can incorporate with native myocardium in order to generate forces for pumping blood,⁴ and mechanical properties similar to native tissue to avoid mechanical mismatch.⁸

Biopolymer threads are fibrous scaffolding materials comprised of repeating subunits of naturally derived molecules including proteins such as silk,²⁷⁻²⁸ collagen,²⁹⁻³³ and chitosan.³⁴⁻³⁵ These biodegradable materials exhibit a broad range of mechanical and biochemical properties that can be modulated to meet specific applications including cell-mediated regeneration of cartilage, tendon, ligament, and skin.²⁷⁻²⁹ Additionally, thread-based scaffold morphology directs alignment of cells,³⁶ ultimately leading to aligned matrix deposition and tissue regeneration.³⁷⁻³⁸ Our laboratory has developed novel fibrin microthread scaffolds.³⁹⁻⁴⁷ Because fibrin-based matrices are seminal during the early phase of wound healing,⁴⁸ we hypothesize that these fibrin-based microthreads will serve as a facile tool for myocardium regeneration. Additionally, the components of fibrin can be isolated from blood suggesting fibrin scaffolds have the potential to be tailored for personalized healthcare strategies.²⁴ Fibrin has cell adhesive properties, can induce neovascularization and can reduce infarct expansion.¹¹

Fibrin has been used in various conformations such as hydrogels,^{10, 15-16} electrospun scaffolds,⁴⁹ and microthread structures.^{39, 41-43, 50} Hydrogels are compactible and have supported some of the highest contractile forces to date.⁵¹ However, hydrogels are typically mechanically weak⁵²⁻⁵³ and ultimately may fail in the dynamic loading environment of the heart.^{8, 52} Electrospun

scaffolds have been shown to influence cellular orientation through the topography of fibrils,⁴ but they are typically dense. Cells have difficulty penetrating the structure and producing high force cell-mediated contractions.² However, by combining hydrogels with a fibrous scaffold, a more robust material may be realized that supports cell function.

1.2 OVERALL GOAL and HYPOTHESIS

Composites are multiphase materials that exhibit properties of the constituent phases such that a better combination of properties is realized.⁵⁴ We propose to combine fibrin microthreads with a fibrin hydrogel to leverage the benefits of the structural cues and mechanical integrity of threads with the pliable hydrogel environment that is conducive to cell-mediated contractility. With the composite material, we anticipate that functional and mechanical requirements for a cardiac patch to integrate with host tissue will be realized.

We hypothesize that composite myocardial layers of fibrin microthreads within a fibrin gel can be combined to form a cardiac patch with customizable stiffness and enhanced cellular orientation that promotes aligned contractions with physiologically relevant cellular contractile strains.

To systematically test this hypothesis, three specific aims were defined. We evaluated the impact of microthread volume fraction manipulation on cell function and the modulus of the resultant composite layers in Specific Aim 1. In Specific Aim 2, we developed a culturing method for increasing alignment of incorporated cells and evaluated the impact on cell function and phenotype. Additionally, because the method relied on cell-mediated gel compaction to induce alignment, we evaluated how compaction altered the volume fraction of composite constituents and the resultant modulus of the material. Finally, in Specific Aim 3, we determined the lamination angle of composite layers required to yield a patch with material properties comparable to ventricular myocardium. The anticipated outcomes of this thesis were to identify the culturing conditions and configuration of composite layers needed to yield a patch with functional and mechanical properties comparable to ventricular myocardium for integration post-implantation.

1.3 SPECIFIC AIM 1: DEVELOP A FIBRIN COMPOSITE LAYER THAT ENABLES CUSTOMIZABLE MODULUS VALUES WHILE SUSTAINING CARDIOMYOCYTE CONTRACTILITY

The ability to modulate the mechanical properties and cell alignment within a cardiac patch without attenuating cell functionality will have significant impact on developing therapies for treating myocardial infarctions. We developed fibrin-based composite layers comprised of aligned microthreads distributed uniformly throughout a hydrogel. Increasing the microthread volume fraction (~5%, 11% and 22%) significantly increased the moduli of the scaffolds (20.6 ± 8.1 , 46.4 ± 23.0 , 97.5 ± 49.3 kPa, respectively), $p < 0.05$. Analyses of cell-mediated contractile strains and frequencies showed no significant differences among composite layers and fibrin hydrogel controls, suggesting that microthread-based composite layers exhibit similar active functional properties. Nuclear alignment of cells within 100 μm of fibrin microthreads suggests that microthreads influence alignment in adjacent areas. In this study, we developed composite layers with tunable, mechanical patch properties that improve cell alignment and support cell functionality. *Chrobak, M. O.; Hansen, K. J.; Gershlak, J. R.; Vratsanos, M.; Kanellias, M.; Gaudette, G. R.; Pins, G. D., Design of a fibrin microthread-based composite layer for use in a cardiac patch. ACS Biomaterials Science & Engineering 2017; 3 (7): 1394-1403. Copyright 2016 American Chemical Society.*

1.4 SPECIFIC AIM 2: DEVELOP AN ALIGNED COMPOSITE LAYER TO ENHANCE CONTRACTILE FUNCTION

Cell-populated cardiac patches have the potential to provide functional support to damaged myocardium following a myocardial infarction. To do so, a patch must functionally integrate into the adjacent host tissue, requiring alignment, similar contractile behavior, and signal propagation. Fibrin-based composite layers have been shown to support contractile phenotypes of incorporated cardiomyocytes, but alignment was lacking. Here, we describe a culturing method that increased alignment of incorporated cells with trends in nuclear alignment similar to native human heart control tissue. Additionally, samples with increased alignment had significantly greater maximum contractile strains after 10 days in culture relative to unaligned composite layers and gelatin-coated

coverslip controls ($18.4\% \pm 7.9$, $7.1\% \pm 2.1$ and $4.7\% \pm 0.7$, respectively, $p < 0.001$). A similar trend was observed after 14 days in culture, as well as for average contractile strains at days 10 and 14. Contractile areas were significantly higher for aligned composite layers relative to unaligned controls at day 10 ($90.5\% \pm 6.0$ and $81.8\% \pm 4.1$, respectively, $p = 0.037$) with a similar trend observed at day 14. Contractile wave propagation was anisotropic for aligned composites with the fastest average velocity in the direction parallel to the fibrin microthreads (parallel velocity: 11.1 ± 1.5 mm/sec, perpendicular velocity: 4.5 ± 2.0 mm/sec). When evaluating the impact of cell-mediated gel compaction on the modulus for the composite layers, a significant increase was observed for cultured 5-thread composite layers relative to 5-thread layers without cells ($p < 0.05$). This suggests that compaction of the hydrogel increased the volume fraction of the microthreads resulting in an increased modulus. In this study, we improve cellular alignment in composite layers resulting in greater contractile strains, contractile areas and faster signal propagation through the layer.

Chrobak MO, Kanellias M, Hansen KJ, Gershlak JR, Gaudette GR, Pins GD. Alignment of Cardiomyocytes Through Static Tension Increases Contractile Strains in Composite Layers. In preparation 2017.

1.5 SPECIFIC AIM 3: PRODUCE A BIO-INSPIRED PATCH WITH MATERIAL PROPERTIES COMPARABLE TO NATIVE MYOCARDIUM

For a cell-populated cardiac patch to act as a functional therapeutic, it is critical that the patch integrate mechanically with the adjacent host tissue. We recently developed fibrin-based composite layers that support aligned contractions of cardiomyocytes and are mechanically tunable. Because ventricular myocardium is comprised of layers that rotate relative to one another, we hypothesized that lamination of composite layers at strategic offsets would result in a patch that mimics the material properties of ventricular myocardium. We defined material properties for an effective cardiac patch in terms of modulus, anisotropic ratio of modulus values, stiffness, ultimate tensile stress, and strain. We then applied a model based on Hooke's law to determine the anticipated modulus when fibrin microthreads were incorporated at angular offsets from an applied load (30° increments, 30 - 120° .) Using the results of the model, we laminated 10-thread and 20-

thread layers together using fibrin glue at a 90° offset. The glue did not increase patch thickness or patch stiffness ($p > 0.05$). The patch was evaluated through tensile testing with loads applied in the 20-thread direction or 10-thread direction. We compared the measured patch values to our self-defined requirements, meant to serve as first evaluations. Our requirements did not look at important factors such as suturability or response to cyclic loading, but were metrics to conduct an initial evaluation. The resultant material properties of the patch matched the requirements, with the exception of stiffness. It is likely that this is because the geometry of the patch did not match the pre-defined geometry of the defect region. In this study, we develop a cardiac patch with material properties that mimic ventricular myocardium for mechanical integration upon implantation. *Chrobak MO, Kanellias M, Pins GD. Fibrin Composite Layers can be Strategically Laminated to Mimic the Mechanical Properties of Ventricular Myocardium. In preparation 2017.*

1.6 REFERENCES

1. Mozaffarian, D.; Benjamin, E. J.; Go, A. S.; Arnett, D. K.; Blaha, M. J.; Cushman, M.; de Ferranti, S.; Despres, J. P.; Fullerton, H. J.; Howard, V. J.; Huffman, M. D.; Judd, S. E.; Kissela, B. M.; Lackland, D. T.; Lichtman, J. H.; Lisabeth, L. D.; Liu, S.; Mackey, R. H.; Matchar, D. B.; McGuire, D. K.; Mohler, E. R., 3rd; Moy, C. S.; Muntner, P.; Mussolino, M. E.; Nasir, K.; Neumar, R. W.; Nichol, G.; Palaniappan, L.; Pandey, D. K.; Reeves, M. J.; Rodriguez, C. J.; Sorlie, P. D.; Stein, J.; Towfighi, A.; Turan, T. N.; Virani, S. S.; Willey, J. Z.; Woo, D.; Yeh, R. W.; Turner, M. B.; American Heart Association Statistics, C.; Stroke Statistics, S., Heart disease and stroke statistics--2015 update: a report from the American Heart Association. *Circulation* **2015**, *131* (4), e29-322.
2. Radisic, M.; Christman, K. L., Materials science and tissue engineering: repairing the heart. *Mayo Clinic proceedings* **2013**, *88* (8), 884-98.
3. Frangogiannis, N. G.; Smith, C. W.; Entman, M. L., The inflammatory response in myocardial infarction. *Cardiovascular research* **2002**, *53* (1), 31-47.
4. Vunjak-Novakovic, G.; Tandon, N.; Godier, A.; Maidhof, R.; Marsano, A.; Martens, T. P.; Radisic, M., Challenges in cardiac tissue engineering. *Tissue engineering. Part B, Reviews* **2010**, *16* (2), 169-87.
5. Menasche, P., Cardiac cell therapy: lessons from clinical trials. *Journal of molecular and cellular cardiology* **2011**, *50* (2), 258-65.
6. Jakob, P.; Landmesser, U., Current status of cell-based therapy for heart failure. *Current heart failure reports* **2013**, *10* (2), 165-76.
7. Shah, V. K.; Shalia, K. K., Stem Cell Therapy in Acute Myocardial Infarction: A Pot of Gold or Pandora's Box. *Stem cells international* **2011**, *2011*, 536758.
8. Reis, L. A.; Chiu, L. L.; Feric, N.; Fu, L.; Radisic, M., Biomaterials in myocardial tissue engineering. *Journal of tissue engineering and regenerative medicine* **2014**, *10* (1), 11-28.
9. Liau, B.; Zhang, D.; Bursac, N., Functional cardiac tissue engineering. *Regen Med* **2012**, *7* (2), 187-206.
10. Liau, B.; Christoforou, N.; Leong, K. W.; Bursac, N., Pluripotent stem cell-derived cardiac tissue patch with advanced structure and function. *Biomaterials* **2011**, *32* (35), 9180-7.
11. Thomson, K. S.; Korte, F. S.; Giachelli, C. M.; Ratner, B. D.; Regnier, M.; Scatena, M., Prevascularized microtemplated fibrin scaffolds for cardiac tissue engineering applications. *Tissue engineering. Part A* **2013**, *19* (7-8), 967-77.

12. Zhang, D.; Shadrin, I. Y.; Lam, J.; Xian, H. Q.; Snodgrass, H. R.; Bursac, N., Tissue-engineered cardiac patch for advanced functional maturation of human ESC-derived cardiomyocytes. *Biomaterials* **2013**, *34* (23), 5813-20.
13. Miklas, J. W.; Dallabrida, S. M.; Reis, L. A.; Ismail, N.; Rupnick, M.; Radisic, M., QHREDGS enhances tube formation, metabolism and survival of endothelial cells in collagen-chitosan hydrogels. *PloS one* **2013**, *8* (8), e72956.
14. Morin, K. T.; Dries-Devlin, J. L.; Tranquillo, R. T., Engineered microvessels with strong alignment and high lumen density via cell-induced fibrin gel compaction and interstitial flow. *Tissue engineering. Part A* **2014**, *20* (3-4), 553-65.
15. Wendel, J. S.; Ye, L.; Zhang, P.; Tranquillo, R. T.; Zhang, J. J., Functional consequences of a tissue-engineered myocardial patch for cardiac repair in a rat infarct model. *Tissue engineering. Part A* **2014**, *20* (7-8), 1325-35.
16. Xiong, Q.; Hill, K. L.; Li, Q.; Suntharalingam, P.; Mansoor, A.; Wang, X.; Jameel, M. N.; Zhang, P.; Swingen, C.; Kaufman, D. S.; Zhang, J., A fibrin patch-based enhanced delivery of human embryonic stem cell-derived vascular cell transplantation in a porcine model of postinfarction left ventricular remodeling. *Stem cells* **2011**, *29* (2), 367-75.
17. Fleischer, S.; Feiner, R.; Shapira, A.; Ji, J.; Sui, X.; Daniel Wagner, H.; Dvir, T., Spring-like fibers for cardiac tissue engineering. *Biomaterials* **2013**, *34* (34), 8599-606.
18. Jacot, J. G.; McCulloch, A. D.; Omens, J. H., Substrate stiffness affects the functional maturation of neonatal rat ventricular myocytes. *Biophysical journal* **2008**, *95* (7), 3479-87.
19. Ma, Z.; Koo, S.; Finnegan, M. A.; Loskill, P.; Huebsch, N.; Marks, N. C.; Conklin, B. R.; Grigoropoulos, C. P.; Healy, K. E., Three-dimensional filamentous human diseased cardiac tissue model. *Biomaterials* **2014**, *35* (5), 1367-77.
20. Ott, H. C.; Matthiesen, T. S.; Goh, S. K.; Black, L. D.; Kren, S. M.; Netoff, T. I.; Taylor, D. A., Perfusion-decellularized matrix: using nature's platform to engineer a bioartificial heart. *Nature medicine* **2008**, *14* (2), 213-21.
21. Robertson, M. J.; Dries-Devlin, J. L.; Kren, S. M.; Burchfield, J. S.; Taylor, D. A., Optimizing recellularization of whole decellularized heart extracellular matrix. *PloS one* **2014**, *9* (2), e90406.
22. Song, J. J.; Ott, H. C., Organ engineering based on decellularized matrix scaffolds. *Trends in molecular medicine* **2011**, *17* (8), 424-32.
23. Jawad, H.; Lyon, A. R.; Harding, S. E.; Ali, N. N.; Boccaccini, A. R., Myocardial tissue engineering. *British medical bulletin* **2008**, *87*, 31-47.
24. Hogan, M.; Mohamed, M.; Tao, Z. W.; Gutierrez, L.; Birla, R., Establishing the Framework to Support Bioartificial Heart Fabrication Using Fibrin-Based Three-Dimensional Artificial Heart Muscle. *Artificial organs* **2014**, *61* (4), 429-36.
25. Remlinger, N. T.; Gilbert, T. W.; Yoshida, M.; Guest, B. N.; Hashizume, R.; Weaver, M. L.; Wagner, W. R.; Brown, B. N.; Tobita, K.; Wearden, P. D., Urinary bladder matrix promotes site appropriate tissue formation following right ventricle outflow tract repair. *Organogenesis* **2013**, *9* (3), 149-60.
26. Zhang, G.; Hu, Q.; Braunlin, E. A.; Suggs, L. J.; Zhang, J., Enhancing efficacy of stem cell transplantation to the heart with a PEGylated fibrin biomatrix. *Tissue engineering. Part A* **2008**, *14* (6), 1025-36.
27. Altman, G. H.; Diaz, F.; Jakuba, C.; Calabro, T.; Horan, R. L.; Chen, J. S.; Lu, H.; Richmond, J.; Kaplan, D. L., Silk-based biomaterials. *Biomaterials* **2003**, *24* (3), 401-416.
28. Altman, G. H.; Horan, R. L.; Lu, H. H.; Moreau, J.; I, M.; Richmond, J. C.; Kaplan, D. L., Silk matrix for tissue engineered anterior cruciate ligaments. *Biomaterials* **2002**, *23* (20), 4131-4141.
29. Cornwell, K. G.; Lei, P.; Andreadis, S. T.; Pins, G. D., Crosslinking of discrete self-assembled collagen threads: Effects on mechanical strength and cell-matrix interactions. *Journal of Biomedical Materials Research Part A* **2007**, *80A* (2), 362-371.
30. Dunn, M. G.; Avasarala, P. N.; Zawadsky, J. P., Optimization of extruded collagen fibers for ACL reconstruction. *Journal of biomedical materials research* **1993**, *27* (12), 1545-52.
31. Gentleman, E.; Lay, A. N.; Dickerson, D. A.; Nauman, E. A.; Livesay, G. A.; Dee, K. C., Mechanical characterization of collagen fibers and scaffolds for tissue engineering. *Biomaterials* **2003**, *24* (21), 3805-3813.

32. Kato, Y. P.; Dunn, M. G.; Zawadsky, J. P.; Tria, A. J.; Silver, F. H., Regeneration of Achilles tendon with a collagen tendon prosthesis. Results of a one-year implantation study. *J Bone Joint Surg Am* **1991**, *73* (4), 561-74.
33. Pins, G. D.; Silver, F. H., A self-assembled collagen scaffold suitable for use in soft and hard tissue replacement. *Mat Sci Eng C-Biomim* **1995**, *3* (2), 101-107.
34. Funakoshi, T.; Majima, T.; Iwasaki, N.; Suenaga, N.; Sawaguchi, N.; Shimode, K.; Minami, A.; Harada, K.; Nishimura, S., Application of tissue engineering techniques for rotator cuff regeneration using a chitosan-based hyaluronan hybrid fiber scaffold. *Am J Sport Med* **2005**, *33* (8), 1193-1201.
35. Funakoshi, T.; Majima, T.; Iwasaki, N.; Yamane, S.; Masuko, T.; Minami, A.; Harada, K.; Tamura, H.; Tokura, S.; Nishimura, S. I., Novel chitosan-based hyaluronan hybrid polymer fibers as a scaffold in ligament tissue engineering. *Journal of Biomedical Materials Research Part A* **2005**, *74A* (3), 338-346.
36. Rovinsky, Y. A.; Samoilov, V. I., Morphogenetic Response of Cultured Normal and Transformed Fibroblasts, and Epitheliocytes, to a Cylindrical Substratum Surface - Possible Role for the Actin Filament Bundle Pattern. *J Cell Sci* **1994**, *107*, 1255-1263.
37. Canty, E. G.; Starborg, T.; Lu, Y. H.; Humphries, S. M.; Holmes, D. F.; Meadows, R. S.; Huffman, A.; O'Toole, E. T.; Kadler, K. E., Actin filaments are required for fibropositor-mediated collagen fibril alignment in tendon. *Journal of Biological Chemistry* **2006**, *281* (50), 38592-38598.
38. Silver, F. H.; Freeman, J. W.; Seehra, G. P., Collagen self-assembly and the development of tendon mechanical properties. *Journal of biomechanics* **2003**, *36* (10), 1529-1553.
39. Cornwell, K. G.; Pins, G. D., Discrete crosslinked fibrin microthread scaffolds for tissue regeneration. *Journal of biomedical materials research. Part A* **2007**, *82* (1), 104-12.
40. Grasman, J. M.; Do, D. M.; Page, R. L.; Pins, G. D., Rapid release of growth factors regenerates force output in volumetric muscle loss injuries. *Biomaterials* **2015**, *72*, 49-60.
41. Grasman, J. M.; O'Brien, M. P.; Ackerman, K.; Gagnon, K. A.; Wong, G. M.; Pins, G. D., The Effect of Sterilization Methods on the Structural and Chemical Properties of Fibrin Microthread Scaffolds. *Macromolecular bioscience* **2016**, *16* (6), 836-46.
42. Grasman, J. M.; Page, R. L.; Dominko, T.; Pins, G. D., Crosslinking strategies facilitate tunable structural properties of fibrin microthreads. *Acta biomaterialia* **2012**, *8* (11), 4020-30.
43. Grasman, J. M.; Pumphrey, L.; Dunphy, M.; Perez-Rogers, J.; Pins, G. D., Static axial stretching enhances the mechanical properties and cellular responses of fibrin microthreads. *Acta biomaterialia* **2014**, *10* (10), 4367-76.
44. Grasman, J. M.; Zayas, M. J.; Page, R. L.; Pins, G. D., Biomimetic scaffolds for regeneration of volumetric muscle loss in skeletal muscle injuries. *Acta biomaterialia* **2015**, *25*, 2-15.
45. Guyette, J. P.; Fakharzadeh, M.; Burford, E. J.; Tao, Z. W.; Pins, G. D.; Rolle, M. W.; Gaudette, G. R., A novel suture-based method for efficient transplantation of stem cells. *Journal of biomedical materials research. Part A* **2013**, *101* (3), 809-18.
46. Tao, Z. W.; Favreau, J. T.; Guyette, J. P.; Hansen, K. J.; Lessard, J.; Burford, E.; Pins, G. D.; Gaudette, G. R., Delivering stem cells to the healthy heart on biological sutures: effects on regional mechanical function. *Journal of tissue engineering and regenerative medicine* **2014**.
47. Page, R. L.; Malcuit, C.; Vilner, L.; Vojtic, I.; Shaw, S.; Hedblom, E.; Hu, J.; Pins, G. D.; Rolle, M. W.; Dominko, T., Restoration of skeletal muscle defects with adult human cells delivered on fibrin microthreads. *Tissue engineering. Part A* **2011**, *17* (21-22), 2629-40.
48. Thompson, W. D.; Smith, E. B.; Stirk, C. M.; Marshall, F. I.; Stout, A. J.; Kocchar, A., Angiogenic activity of fibrin degradation products is located in fibrin fragment E. *The Journal of pathology* **1992**, *168* (1), 47-53.
49. Perumcherry, S. R.; Chennazhi, K. P.; Nair, S. V.; Menon, D.; Afeesh, R., A novel method for the fabrication of fibrin-based electrospun nanofibrous scaffold for tissue-engineering applications. *Tissue engineering. Part C, Methods* **2011**, *17* (11), 1121-30.
50. O'Brien, M. P.; Carnes, M. E.; Page, R. L.; Gaudette, G. R.; Pins, G. D., Designing biopolymer microthreads for tissue engineering and regenerative medicine. *Current Stem Cell Reports* **2016**, *2*, 147-57.
51. Jackman, C. P.; Carlson, A. L.; Bursac, N., Dynamic culture yields engineered myocardium with near-adult functional output. *Biomaterials* **2016**, *111*, 66-79.

52. Tandon, V.; Zhang, B.; Radisic, M.; Murthy, S. K., Generation of tissue constructs for cardiovascular regenerative medicine: from cell procurement to scaffold design. *Biotechnology advances* **2013**, *31* (5), 722-35.
53. El-Sherbiny, I. M.; Yacoub, M. H., Hydrogel scaffolds for tissue engineering: Progress and challenges. *Global cardiology science & practice* **2013**, *2013* (3), 316-42.
54. Callister, W. D.; Rethwisch, D. G., *Fundamentals of materials science and engineering : an integrated approach*. 4th ed.; Wiley: Hoboken, N.J., 2012; p xxv, 910 p.

Chapter 2: Background

2.1. BIOMIMETICS AND BIO-INSPIRED SOLUTIONS

The field of biomimetics evaluates nature and natural phenomena to understand underlying mechanisms, and to apply those principles to innovate solutions to engineering design problems.¹ The term ‘biomimetics’ was first coined in 1957 by Schmitt² and is still recognized as a promising method to develop the technology of the future. Throughout history, there have been extraordinary achievements through biomimetics and bio-inspired solutions. As an example, the Wright brothers developed an airplane after finding inspiration through eagles’ wings.³⁻⁴ The idea of looking to the sky for inspiration continues today as commercial airplanes are inspired by birds.¹ Velcro® was developed by George de Mastral after observing that burrs often got stuck in his dog’s fur. The hook and loop structure mimicked what had been observed from the burrs interlocking with his pet’s hair, and is today used in a wide variety of applications requiring strong adhesion.¹

Biomimetic approaches are applicable across a wide variety of fields, including tissue engineering. Tissue engineering is traditionally considered the combination of scaffold materials with cells and growth factors to generate tissue-like materials for the regeneration of diseased or damaged tissues.⁵ While progress has been made in this area, currently the most progress has been seen in barrier tissues, like skin. Some of the greatest success stories for tissue engineering are engineered skin scaffolds, with several products reaching the market including Apligraf® and Epicel™.⁶ For more complex connective tissues and hierarchically structured tissues, far less progress has been made. Clinical evaluations are ongoing for bone, cartilage, and muscle. However, complicated multifunctional organ systems like the liver, heart and kidney are significantly challenging. Rather than trying to engineer a spatially controlled organ with multiple tissue types and/or layers with adequate vascularization, work currently focuses on replacing specific functions of these organs.⁶ One of the biggest challenges associated with this approach is the functional assembly of an engineered material into complex tissues or organ systems.⁷

2.1.1. GENERAL TISSUE STRUCTURE

To promote assembly of engineered scaffolds into tissues and organs, it is critical to understand what comprises tissues and how this informs its function. Through strategic biomimicry, there is the potential to understand essential characteristics required in scaffold design and, furthermore, to avoid over-engineering a solution.⁷ Requirements will vary by tissue type, but in general, many tissues within the body are made from similar building blocks. The extracellular matrix (ECM) is comprised of material secreted by the cells within a tissue. The composition, structural organization and corresponding mechanical properties of ECM are tissue dependent. The hierarchical structure and function of the ECM is critical in physiological processes that range from growth and proliferation to cell death.⁸

The ECM is composed of two main components; proteoglycans and insoluble protein fibers.⁸ In native tissue, the fibrillar elements are arranged into hierarchically ordered constructs. These fibrillar elements are composed of protein-based building blocks that form structures 20-200 nanometers in diameter and contain matrix proteins, such as type I collagen and fibrin. The structural arrangement of these fibrils varies from tissue to tissue, in a manner that optimizes their functional mechanical properties. As an example, tendons have cable-like bundles of type I collagen fibers with a crimp pattern that repeats every 45-60 μm . This structure enables uniaxial load transfer from muscle to bone.⁹ The distinct architectures and biochemical compositions of the native tissues also serve a critical function in directing cell-mediated tissue regeneration following injury or trauma.¹⁰ For example, crosslinked fibrin microthreads loaded with hepatocyte growth factor (HGF) were used to promote functional regeneration in a skeletal muscle defect model. The structure of the scaffolds combined with the biochemical signaling of the HGF resulted in a scaffold that promoted ingrowth of myofibers into the wound site and increased differentiation of myoblasts.¹¹

2.1.2. RATIONALE FOR BIOMIMETIC TISSUE ENGINEERED SCAFFOLDS

Tissue engineered scaffolds provide a three-dimensional (3D) structure that can be tailored to support cell types and promote desired tissue formation.¹⁰ For regeneration of tissues that require

mechanical support for the reparative process to occur, scaffold implantation is considered more advantageous than a cell therapy strategy.¹² For a scaffold to be effective at promoting regenerative processes, it is essential for it to integrate with adjacent tissues. To ensure integration of a scaffold and to promote tissue functionality, it is advantageous to recapitulate the structure and composition of distinct tissue regions.⁷ The ECM structure is essential for directing cell functions like survival, differentiation, proliferation, metabolism and integrative function.¹³ These cell behaviors are also influenced by the physiological milieu, levels of nutrients and oxygen, and physical regulatory signals of their environment.¹⁴ Because of this, biomimetic efforts in tissue engineering focus on mimicking these specific areas. This requires an understanding of how structures (from nano to hierarchical) correspond to cellular responses and, ultimately, tissue functions.¹

The strategic design of scaffolds enables the incorporation of biophysical and biochemical cues. The chemical environment of soluble bioactive molecules (i.e. growth factors) and cell-binding peptides (i.e. ECM proteins) is another aspect of the cell environment that can be beneficial to mimic in order to drive specific cell responses.¹⁵ This chemical environment can help drive interactions with surrounding tissues through biomolecular recognition, ultimately aiding with integration. Within their natural environment, cells additionally experience physical cues that influence their behavior. Functional cues like mechanical stretch, electrical stimulation and shear forces are some examples of physical signals that cells encounter in native tissues and organs.¹⁴ By incorporating similar cues into the development of biomimetic scaffolds, the resultant material may more closely mimic the natural tissue to enable facile integration with adjacent tissues.

2.2. COMPOSITES FOR TISSUE ENGINEERING: THEORY AND APPLICATIONS

To achieve a scaffold capable of integrating with host tissue and providing an environment that promotes the proper function, a biomimetic approach is needed. While scaffolds like hydrogels are widely explored for their ability to yield an even distribution of cells and to compact ensuring high cell densities,¹⁶⁻¹⁷ these scaffolds have insufficiencies including reduced mechanical integrity.¹⁸⁻²⁰ Hydrogels typically experience failure under low stress conditions due to the lack of energy dissipation mechanisms within the material.²¹ However, when fibrous networks are

incorporated within a brittle hydrogel, the strength of the resultant composite material is increased through enhanced energy absorption and transfer.²² Composites are materials that combine multiple constituents resulting in a unique combination of, or new properties for the final material.²³ These materials afford an opportunity to generate biomimetic tissues that can better mimic the architecture and mechanical properties of native tissues (**Figure 2.1**).²⁴⁻²⁵

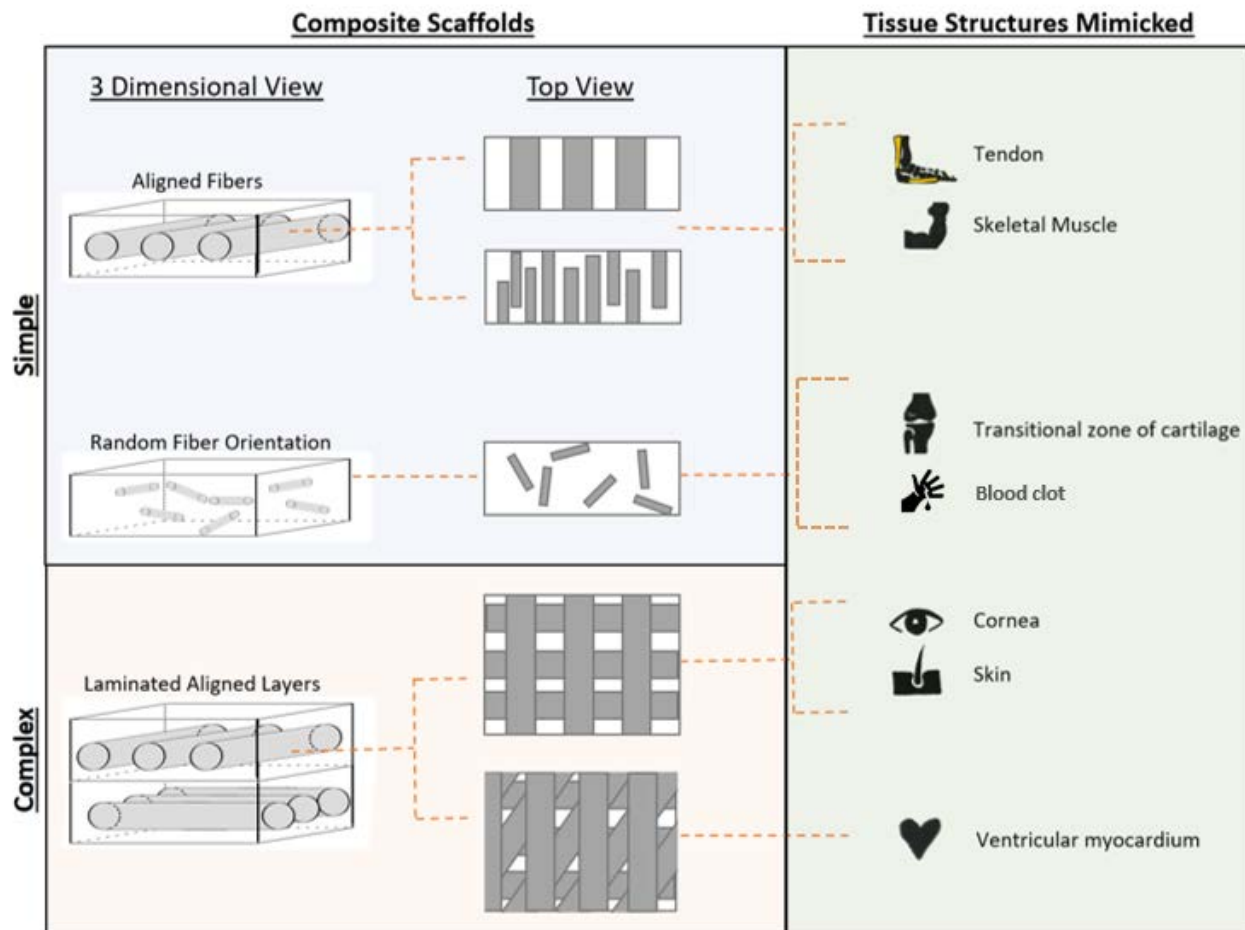


Figure 2.1. Composite scaffolds can be strategically combined to mimic the structures of target tissues.

Additionally, incorporation of biomolecules or therapeutic agents, like growth factors to direct tissue-specific cell functions, can further enhance the biomimetic nature of composite scaffolds.²⁶ An understanding of the theory of composites can inform the strategic design of scaffolding materials. Focus for this work is placed on fiber-reinforced composite samples made of natural biopolymers, summarized in **Table 2.1**.

Table 2.1. Summary of natural biopolymer, fiber-reinforced composites designed for tissue engineering applications.

Classification	Materials	Application	Key Results	Reference
Aligned, non-uniform distribution of fibers	Alginate + collagen fibers	Soft tissues	-Stiffness and strength values tuned through fiber volume fraction modification	27
	Alginate + gelatin nanofibers	Cornea	-Reinforcement with fibers enhanced mechanical properties	28
	Collagen-chondroitin-6-sulfate + collagen fibers	Soft tissues	-Mechanical properties modulated by fiber incorporation and crosslinking.	29
	Pullulan-dextran polysaccharide + chitosan and alginate IPC fibers	Soft tissues	-Demonstrated improvement of cell adhesion, sustained release of drugs, and proliferation with IPC fibers incorporated into hydrogels	26
Aligned, uniform distribution of fibers	Fibrin + fibrin fibers	Cardiac	-Fiber reinforcement enhanced the mechanical properties of the scaffold, increased cellular alignment and did not hinder cell function of incorporated cardiomyocytes.	30
	LysB10 matrix + collagen fibers	Soft tissues	- Fiber concentration, orientation and layout critical for design of composites for mechanical properties	25
	Silk /sodium dodecyl sulfate + silk fibers	Meniscus	-Laminating angles impacted mechanical responses with improved properties observed at 30° and 60° offsets	31
Randomly oriented fibers	Agarose + cellulose nanowhiskers	Biomedical applications	-Significant mechanical reinforcement by nanowhiskers; volume fraction dependent	32
	Collagen + collagen fibers	Tissue engineering	-Fiber addition limited the contraction of the collagen hydrogel with no detrimental effects on cellular response	33-35
	Nano-HA/ Chitosan scaffold + collagen fibers	Bone	- Increased osteoblast differentiation on composites ³⁶ that mimic the hierarchical structure of bone ²⁴	36 24
	Silk + chitin whiskers	Connective tissues	-Improved dimensional stability and compression strength with increased volume fractions of whiskers. Whiskers also promoted cell spreading	37
	Silk + silk fibers	Connective tissues, Bone	-Volume fraction impacted compressive properties ³⁸⁻³⁹ and pore size of composites. ³⁹ Composite use impacted cell adhesion, cell proliferation, and the degradation rate of the matrix ³⁸	38-39
	Silk + silk fibers	Cartilage	- Critical length of fibers needed for sufficient energy transfer for reinforcement identified. Integration of fibers with matrix critical for improved mechanical properties	22
	Silk + silk fibers	Bone	-Fiber length impacted surface roughness, porosity, and compressive strength. Strong integration of fibers and matrix improved compressive properties. Enhanced differentiation of hMSCs was achieved through changes in surface roughness and matrix stiffness	40

2.2.1. PRINCIPLE OF COMBINED ACTION

Fiber-reinforced composites are multiphasic materials comprised of a dispersed, reinforcing phase surrounded by a matrix phase. This composite type is typically designed to achieve high strength or stiffness on a weight basis.²³ By strategically incorporating different materials into a composite, the *principle of combined action* states that new or better properties, or a better combination of properties, can be achieved.²³ These properties will be influenced by the relative amounts of each phase (typically noted as the volume fractions). Additionally, the concentration, size, shape, distribution and orientation of the dispersed phase will impact the resultant composite properties.²³ There have been several recent examples in the literature where composites were designed to incorporate greater cytocompatibility,^{22, 26, 36} to adjust the material degradation rate,³⁸ and to better mimic the structure of native ECM of target tissues.^{24-25, 30} By tactically combining constituents, better scaffold materials for tissue engineering applications were realized in these literature examples.

2.2.2. RULE OF MIXTURES

The *rule of mixtures* enables the estimation of the properties of the composite through weighted averages.⁴¹ This rule uses the volume fractions of each constituent multiplied by a property to estimate what the resultant property of the composite will be.²³ As an example, for an aligned, continuous fiber-reinforced composite, the elastic modulus in the direction of alignment assuming an isostrain state is shown in Equation 2.1²³

$$E_{composite} = E_{matrix}V_{matrix} + E_{Fiber}V_{Fiber} \quad 2.1.$$

where E is representative of the elastic modulus and V is representative of the volume fractions for each component.

Equation 2.1 demonstrates that the resultant modulus of the composite will be intermediate of the moduli values for the matrix and fiber components. By manipulating the volume fraction of each component, engineered tissues can be tailored to have different mechanical properties depending on the desired application. It has been demonstrated that manipulation of the fiber reinforcing component in tissue engineered composites has led to a range of mechanical

properties,^{27, 30, 37, 39} and better maintenance of scaffold shape.^{33-35, 37} Additionally, the utilization of fibers to enhance mechanical properties has been shown to retain the cytocompatibility of the scaffold. In contrast to methods that increase protein concentration and decrease the pore size of the constructs³⁹, fiber incorporation can enhance cell spreading and alignment.^{30, 37} The manipulation of the composition of the composite scaffolds enables the targeting of different tissues,²⁷ suggesting composite scaffolds are a platform technology. However, it should be noted that just increasing volume fraction is not sufficient to manipulate the mechanical properties. It was demonstrated that incorporation of an increasing volume fraction of cellulose nanowhiskers in an agarose hydrogel did not result in mechanical reinforcement. This is likely due to the fact that there were significant disruptions to the matrix with an increased volume fraction.³² This demonstrates that integration of components is a critical factor that must be carefully considered in composite design.

2.2.3. CRITICAL FIBER LENGTH AND INTEGRATION OF COMPONENTS

Mechanical characteristics of composite materials are dependent on the degree to which applied loads are transmitted to reinforcing fibers.²³ The magnitude of the interfacial bond between the fiber and matrix phase is critical. To achieve an isostrain state where deformation of the matrix and dispersed phases are equivalent requires a strong interfacial bond.⁴¹ An isostrain state is an assumption required for the *rule of mixtures* to apply. For incorporated fibers, there is no load transmittance that occurs at the end of each fiber. As such, there is a minimum length that is required for load transmittance to occur along the fiber resulting in effective strengthening and stiffening of the composite material. This “critical length” is dependent on the fiber diameter (d), the tensile strength of the fiber (σ^*_f), and the fiber-matrix bond strength (or shear yield strength of matrix- whichever is smaller)(τ_c). With these values, the critical length required for a composite material can be determined through Equation 2.2.²³

$$l_c = \frac{\sigma^*_f d}{2\tau_c} \quad 2.2.$$

The fiber lengths used for the dispersed phase within a composite will impact the degree of reinforcement. Consider a stress applied to the composite material that is equal to the tensile fiber

strength. When the fibers are equivalent to the critical length, the maximum fiber load is only achieved in the axial center of the fiber. Lengths greater than the critical length result in fiber reinforcement becoming more effective; the maximum fiber load can be achieved over a greater length of the fiber. For any fiber length that is much greater than the critical length (typically 15 times the length of the critical length), the fiber is considered a continuous fiber that provides significant improvement in the strength of the composite. However, with a fiber length smaller than the critical length, the maximum fiber load cannot be achieved. For any fiber length that is much smaller than the critical length, virtually no stress transference will occur, resulting in very little reinforcement (typical of a particulate type of composite).²³

Tissue engineering examples have shown that fiber length is a critical design component for generating fiber reinforced materials.^{22, 40} It was further demonstrated that the integration of the reinforcing fibers with the surrounding matrix influenced the resultant properties.²⁹ When using silk fibers in a silk hydrogel, it was shown that a significant reinforcing effect occurred that was fiber length dependent. However, when using silk fibers in an agarose hydrogel, the reinforcing effect was reduced, and was not fiber length dependent. This was likely due to weaker interfacial bonding between the silk fibers and agarose hydrogel, leading to poor stress transfer to fibers during loading.²²

2.2.4. ALIGNMENT OF FIBERS

Alignment of reinforcing fibers within a composite is another critical design consideration.⁴¹ Fibers may be aligned or have a random orientation throughout the matrix phase. Alignment of fibers results in anisotropic mechanical properties, while random orientation typically results in isotropic properties.²³ Therefore, when evaluating mechanical properties, the direction of the applied load will influence what is measured. For fibrous materials, applying a load in the direction of fiber orientation will yield greater mechanical properties than when evaluating the properties with an applied orthogonal load, as has been shown in the literature.^{27-28, 31} Distribution of the fibers throughout the composite is also key with better composite properties realized when the fibers are uniformly distributed throughout the matrix phase.⁴¹

When designing composite materials, it may be desirable to laminate layers at an offset. As an example, the ventricular myocardium is composed of layers of myocardium that rotate relative to one another from +60 to -60°. ⁴² Using a biomimetic approach to mimic the architecture and material properties of the tissue may require fiber-reinforced composite layers to be laminated at similar offsets. Strategic lamination can be achieved through understanding how the angular offsets will impact the resultant modulus values of the laminated composite material. Hooke's law states that stress and strain are proportional to one another (Equation 2.3) ²³

$$\sigma = E\epsilon \quad 2.3.$$

where σ represents stress, E represents the modulus of elasticity and ϵ represents strain.

A dimensionless analysis based on Hooke's law enables the estimation of the elastic modulus of fibrous composites with various off-axis loadings. ⁴³ The results of this analysis estimate the axial and transverse modulus values (E_x and E_y , respectively) as is shown in Equations 2.4 and 2.5

$$\frac{1}{E_x} = \frac{\cos^4\theta}{E_1} + \frac{\sin^4\theta}{E_2} + \left(\frac{1}{G_{12}} - \frac{2\nu_{12}}{E_1}\right) * \sin^2\theta * \cos^2\theta \quad 2.4.$$

$$\frac{1}{E_y} = \frac{\sin^4\theta}{E_1} + \frac{\cos^4\theta}{E_2} + \left(\frac{1}{G_{12}} - \frac{2\nu_{12}}{E_1}\right) * \sin^2\theta * \cos^2\theta \quad 2.5.$$

where

$$G_{12} = \frac{G_f * G_m}{G_f * V_m + G_m * V_f}$$

$$G_f = \frac{E_f}{2(1 + \nu_f)}$$

$$G_m = \frac{E_m}{2(1 + \nu_m)}$$

$$\nu_{12} = \nu_f * V_f + \nu_m * V_m$$

$$E_1 = E_f * V_f + E_m * V_m$$

$$E_2 = \frac{E_f * E_m}{E_f * V_m + E_m * V_f}$$

E_f = Elastic modulus of the fibrous component

E_m = Elastic modulus of the matrix phase

G_f = Shear modulus for the fibrous component

G_m = Shear modulus for the matrix phase

ν_f = Poisson's ratio for the fibrous component

ν_m = Poisson's ratio for the matrix phase

V_f = Volume fraction of the fibrous component

V_m = Volume fraction of the matrix phase

The analysis is simplified by assuming plane stress conditions where all displacements are occurring within one plane. When using this analysis to evaluate a composite with fibers aligned with the loading direction, these equations simplify to the Rule of Mixtures (Equation 2.1). With this tool, an informed design of composite materials can be achieved for specific applications.

2.3. CARDIOVASCULAR DISEASE

Cardiovascular diseases are currently the leading causes of death in the US. Heart failure is a major contributor with 500,000 new cases diagnosed annually in the United States alone.⁴⁴ The only treatment that can restore function for end stage heart failure is a heart transplant. However, donors are limited. Only ~2,500 cardiac transplantation surgeries occur annually in the United States⁴⁴ leaving the majority of affected patients with compromised cardiac function. Other treatments for end stage heart failure include pharmacologic agents and ventricular assist devices, palliative treatments that do not regenerate damaged tissue.⁴⁵

A major cause of heart failure is a myocardial infarction (MI) where blood flow through a coronary artery is blocked resulting in ischemia of downstream cardiac muscle (**Figure 2.2**). Ischemia causes cardiomyocyte (CM) death and a severe inflammatory response that ultimately results in scar tissue formation.⁴⁶ Because CMs have low proliferation rates,⁴⁷ and due to the scarcity of cardiac stem cells in mature cardiac tissue,⁴⁸ the heart has a limited capacity to

regenerate the myocardium and restore the mechanical function lost after an MI. Instead, highly proliferative cardiac fibroblasts replace the lost cells and become activated, resulting in secretion of type I collagen and formation of a non-functional, mechanically aberrant, fibrous scar that is not conducive to the electrochemical or biomechanical properties of healthy, functional myocardium.⁴⁹⁻⁵¹ Additionally, healthy CMs in the proximity of the infarct site may also die, leading to an increased necrotic tissue region. This process often affects the left ventricle and can lead to left ventricular remodeling, during which the left ventricle wall becomes thinner and structural changes occur⁵⁰ (**Figure 2.2**). To compensate for the reduced functionality, the ventricle becomes larger to try to achieve needed blood flow. This structural change makes the heart more susceptible to dysfunction and eventually leads to heart failure.⁴⁹

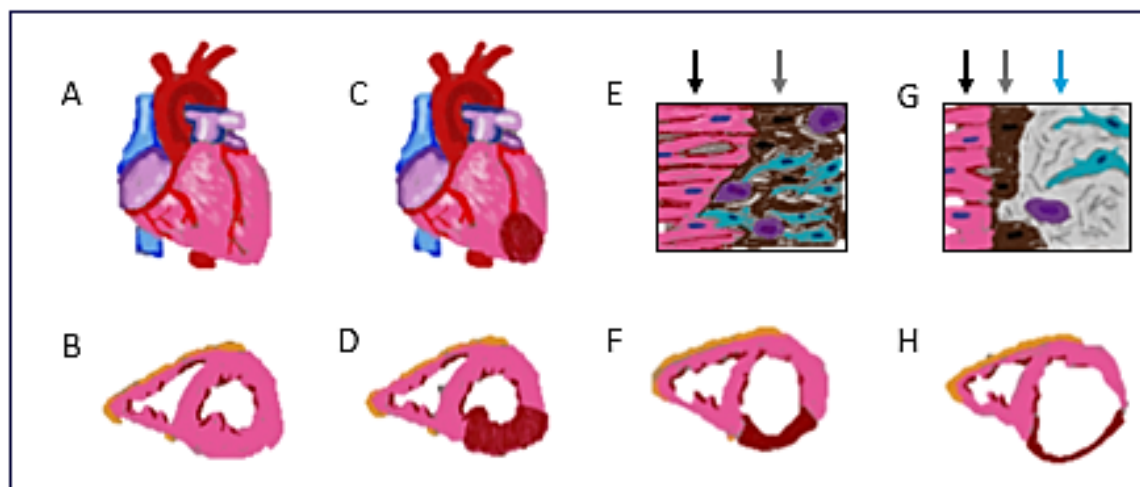


Figure 2.2. Progression of cardiac disease following an MI. Healthy myocardium (A, B) becomes damaged during an MI when an occlusion in the vasculature leads to necrotic tissue beyond the occlusion site (C, D). An acute inflammatory reaction will lead to scar tissue formation (E, F) and ultimately, ventricular remodeling (G, H). Black arrows show healthy myocardium (E,G). Gray arrows show degrading extracellular matrix with macrophages (purple cells) and fibroblasts (blue cells) (E,G). The blue arrow shows the scar tissue region (G). B, D, F and H are displaying cross-sections of the ventricles.

To mitigate this series of events, the CMs lost during a heart attack (on the order of a billion cells)¹³ must be replaced. As such, research over the past decade has focused on delivering cells to the infarct site, and treatments using this method have progressed to clinical trials.⁵² Current cell delivery strategies have demonstrated enhanced cardiac function⁵²⁻⁵⁴ but are associated with poor

cell retention and survival.^{45, 47} The optimal cell source, dose and method for delivery has yet to be defined.⁵⁵ An alternative approach to the regeneration of damaged myocardium is to design a scaffold that can provide mechanical support¹³ and a protective environment against the acute inflammatory environment of an infarct site.⁵⁵ The use of scaffolds provides advantages over cell injection approaches. Namely, the scaffold provides a transitional support, enables control over graft dimensions and mechanical properties, and provides an environment for the survival of incorporated CMs.^{13, 56} While progress has been made in the development of a cardiac patch for myocardial regeneration, there has yet to be a patch able to restore baseline functionality to an infarcted heart. There is a significant need for a regenerative solution for MI patients.⁴⁵

2.4. HEART ANATOMY AND VENTRICULAR MYOCARDIUM

The heart is comprised of 4 chambers: the left atrium, left ventricle, right atrium and right ventricle (**Figure 2.3**). The atrioventricular valves separate the atria from the ventricles. The tricuspid valve separates the right atria from the right ventricle, while the bicuspid valve separates the left atria and left ventricle.⁸ There are two functional phases involved in the heart circulating blood: systole (contraction) and diastole (filling). In late diastole, the ventricles passively fill with blood. During atrial systole, atrial contraction forces a small volume of blood into the ventricles. An isovolumetric ventricular contraction forces the AV valves closed. As pressure builds within the ventricles and eventually exceeds the pressure in the arteries, the semilunar valves (which separate the ventricles from the pathways away from the heart) are forced open and blood is ejected. If leaving from the right ventricle, the blood will pass into the pulmonary arteries, leading to re-oxygenation of the blood via capillary beds in the lungs. If leaving the left ventricle, the blood will pass into the aorta, through which the blood is supplied to the rest of the organs of the body. Action potentials in the heart originate at the SA node in the right atrium. The signal then travels to the atrioventricular node, to the bundle of his and on to Purkinje fibers. This pathway ensures that atria first contract, then the ventricles from the bottom up.

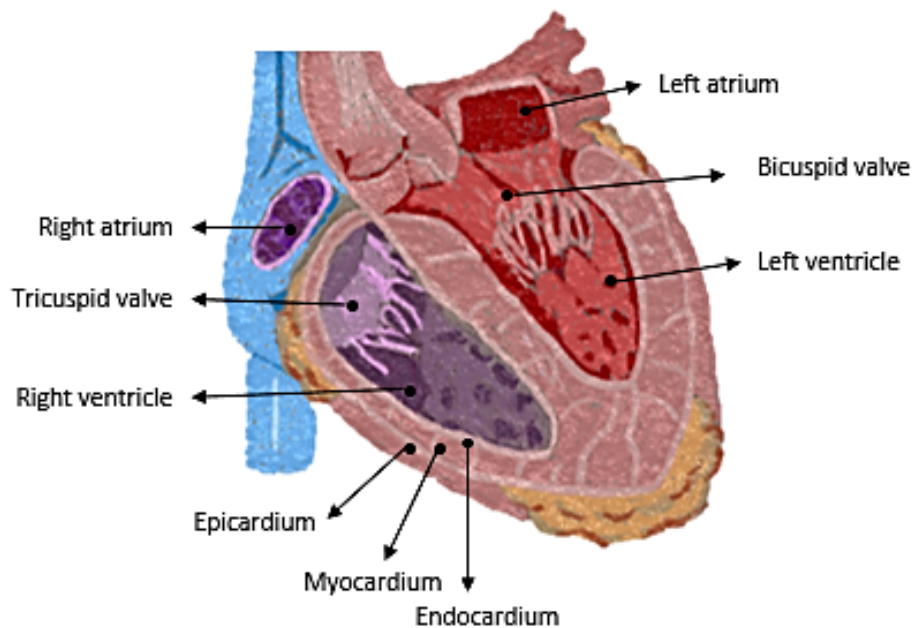


Figure 2.3. The anatomy of the heart.

The anterior myocardium is ~1.5 cm thick and composed of highly aligned CMs and ECM fibrils, predominantly containing collagen.^{42, 57} Ventricular myocardium is arranged in anisotropically aligned sheets of fibrils that are stacked and rotate from +60° (endocardium) to -60° (epicardium) (**Figure 2.4**).⁴² Within each layer, the fibril size can range from 30-120 nm with fibril orientations ranging from +/- 13° relative to one another.⁵⁸⁻⁵⁹ Myocytes closely follow this structure, resulting in highly oriented cells and aligned contraction of cells. This alignment results in high torsional squeezing enabling efficient pumping of blood.⁶⁰ Ventricular myocardium has a modulus ranging from 20 kPa – 500 kPa as it moves from diastole to systole.⁴⁵ To promote functional tissue regeneration, recapitulating the properties of the native tissue may be advantageous.^{45, 61}

Excerpt from: O'Brien, Megan P., et al. "Designing Biopolymer Microthreads for Tissue Engineering and Regenerative Medicine." *Current Stem Cell Reports* 2.2 (2016): 147-157. *Figures original.*

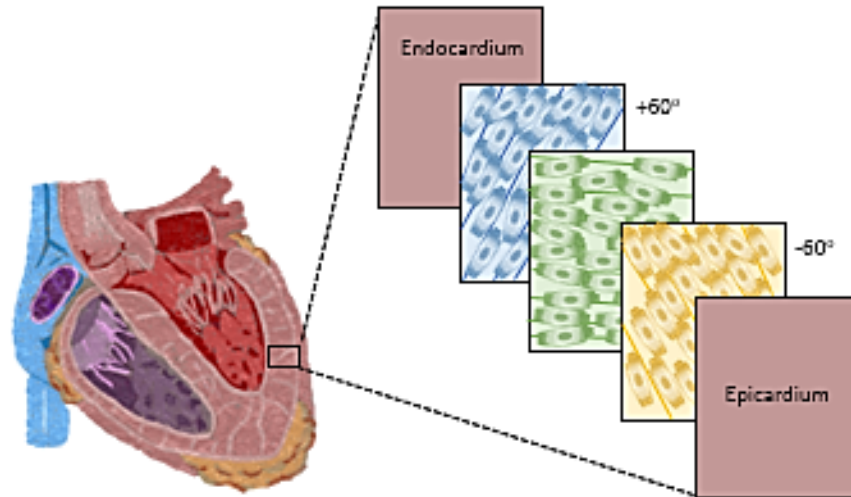


Figure 2.4. Composition of ventricular myocardium. Myocardium is a 3-4 cell layer thick structure. Cells are aligned within each layer, and layers rotate relative to one another from +60 to -60 degrees. Solid colored lines represent ECM fibrils within each layer.

2.5. CARDIAC PATCHES: IMPLANTATION STRATEGIES

A cardiac patch is a precisely engineered scaffold that may help to reverse or prevent further damage to the myocardium following an MI.^{45, 61-62} Following an infarct, a cardiac patch can be used to augment or replace the damaged ventricular myocardium. Augmentation incorporation would involve laying the cardiac patch over the damaged tissue site in an effort to circumvent the scar tissue. Augmentation of the scar region with a cardiac patch may benefit the scarred ventricular wall by increasing tissue thickness and providing structural reinforcement. The Law of Laplace states that the pressure inside a construct is proportional to the thickness and tension of the construct's wall, and inversely proportional to the radius of the construct.⁶³ Equation 2.6 shows the one common representation of the Law of Laplace.⁶⁴

$$\langle \sigma \rangle = \frac{P_i r_i^2}{r_o^2 - r_i^2} \quad 2.6.$$

In 2.6, $\langle \sigma \rangle$ is the average stress, P_i is the internal pressure, r_i is the internal radius and r_o is the outer radius. This simplified analysis as a first approximation assumes a hollow spherical geometry with uniform wall thickness and isotropic, homogenous material properties. These

assumptions are not consistent with left ventricular mechanics, but provide a method for simplifying those relationships as a first estimation of how the parameters are related for this application.⁶⁵ By this common representation of the Law of Laplace, an increase in the ventricular wall thickness through the augmentation of the scar region with a cardiac patch will reduce the average wall stress.⁶⁶ On its own, this effect could help limit ventricular remodeling⁶⁷⁻⁶⁸ improving patient quality of life. Additionally, this approach would be less invasive than replacement therapy. However, a major challenge associated with it is the lack of vascularization in the scar tissue region. This results in the patch having limited contact with the host vasculature.⁴⁵ Maintaining viability of cell populated patches without a well-defined vasculature system may not be feasible. Additionally, this approach does not remove the stiff damaged tissue and does not ultimately heal the myocardium. Replacement of ventricular scar tissue involves excision of the damaged tissue and replacement of that portion of the ventricular wall with a cardiac patch. One technique that can be used for this is a Dor (or modified Dor) procedure. This procedure involves excising the damaged tissue, placing a patch to cover the opening, and then closing the myocardium over the patch. This results in the myocardium that was on either side of the scar being joined and is a typical approach for acellular patches with the goal of preventing remodeling. The operation improves the size and geometry of the left ventricular, reduces wall tension and can enhance the overall systolic function of the heart. Patients typically selected for this type of surgery have large akinetic ventricles, meaning the patients lack either an inward or outward movement of the ventricular region during systole. Patients also typically present with symptoms of angina and /or congestive heart failure.⁶⁹

For cell-populated scaffolds, an incorporation option is to implant the patch in parallel with adjacent tissues so that the patch joins with the tissue that was on either side of the scar region.⁷⁰⁻
⁷¹ This would require vasculature of the patch to anastomose with the host vasculature, and alignment of the patch with the orientation of the cardiomyocytes in the adjacent tissues for effective signal propagation and synchronous contractility. We hypothesize that these techniques will result in the removal of the damaged tissue and promote the regeneration of functional

myocardium. However, this type of approach is challenging; with large, diffuse MI regions it can be difficult to successfully implant a patch and not have lethal excess bleeding.⁷¹

Replacement of an infarct with a vascularized patch may help restore lost cardiac function. However, it should be noted that infarcts do not have specific geometries and do not always transverse the entire width of the ventricular wall.⁷² As such, it is possible that partial removal of the ventricular wall may result in removal of the infarct site while leaving a vascularized region of myocardium. A cardiac patch could then be implanted to fill the defect. While there are many strategies for implanting a cardiac patch, currently there is no consensus on the best approach. For the purposes of this thesis, we have designed a cardiac patch material that can ultimately be implanted in parallel with the myocardium following full-thickness excision of the infarct.

With a patch replacing a portion of the ventricular wall and acting as a functional support, the ideal mechanical properties of the cardiac patch would be comparable to ventricular myocardium. This would result in the patch exhibiting similar behaviors to the native tissue in response to the forces that result from cyclic loading of the ventricles. In ventricular myocardium there are active and passive mechanical aspects that should be considered. When considering passive mechanical properties, it has been shown that cardiomyocytes have the greatest contractile forces on materials with a modulus similar to that of native myocardium.⁷³ Additionally, in order to ensure that a patch was able to withstand and not fail in the demanding mechanical environment of the heart, it is critical that any material considered for a cardiac patch have an ultimate tensile stress that well exceeds the stresses experienced by the ventricular wall.⁷⁴ Another important consideration is suture retention strength. It is vital that the patch be able to be implanted.⁶¹

When considering active mechanical properties, it is important to consider the function of the myocardium. In one heart beat, following depolarization, the ventricles will undergo isovolumeic ventricular contractions (as discussed in section 2.4). During these contractions, the volume of the ventricles does not change, but there is an increase in ventricular pressure, closing the atrioventricular valves. As that pressure rises, the semilunar valves will open and the ventricles will contract, decreasing in volume and ejecting the contained blood.⁸ For a cardiac patch to provide a functional support, the patch itself will need to propagate an electrical signal with a

similar velocity as the adjacent heart tissue.⁴⁷ Should it fail to do so, depolarizations will not occur at the same rate resulting in delayed contractions of the cells incorporated in the cardiac patch. With a delayed contraction, as the pressure builds in the ventricle, the cardiac patch may become a weak point as formed myosin cross-bridges within contracting cardiomyocytes can contribute to the overall stiffness of the material.⁷⁵ With a weak spot, there is the potential for bulging of the ventricle. Perturbated blood may result that can ultimately culminate in the formation of a clot and aneurysm. Therefore, for a cardiac patch to successfully function as a wall replacement, cell function and material properties of the cardiac patch will need to be similar to ventricular myocardium.

Current cardiac patch strategies to promote regeneration of damaged myocardium use natural materials,^{62, 76-81} synthetic materials,⁸²⁻⁸⁴ cell sheets,⁸⁵⁻⁸⁷ or decellularized tissues.⁸⁸⁻⁸⁹ Decellularized tissues retain the extracellular matrix architecture, but are associated with harsh sterilization methods and with difficulty re-populating the scaffolds with cells.⁹⁰ Cell sheets have shown potential as sheets can be stacked and beat synchronously. However, there is no clinically translatable technique for inducing vasculature with these scaffolds, thus limiting their utility⁹¹ and preventing them from reaching a clinically relevant thickness of 1 cm.⁴⁵ Synthetic polyesters, such as polyglycolic acid (PGA), enable the engineering of mechanical and degradation profiles.⁹² However, synthetic materials lack native cellular niches and require protein coatings for cellular interaction. In contrast, natural biopolymers, such as fibrin, provide physiologic cell attachment sites and degrade into bioactive peptides.⁷⁶ However, the weak mechanical nature of natural biopolymers presents a challenge for their use as cardiac patch scaffolding materials.⁹³

2.6. ACELLULAR CARDIAC PATCHES

Acellular patches have been developed from synthetic and natural materials. Dacron and Gore-Tex (W. L. Gore & Associates, Flagstaff, AZ USA) are commercially available synthetic materials that can help prevent remodeling from occurring, but ultimately may result in a foreign body response because of their synthetic nature. This response can lead to increased fibrosis and

may alter the mechanical properties of the tissue in contact with the patch. This can cause functionality to be impaired and may hinder the restorative functionality achieved.⁹⁴

Negative reactions to a synthetic patch were demonstrated in a porcine MI model where a polytetrafluoroethylene patch (same material as Gore-Tex®) was shown to promote inflammation, calcification and cellular necrosis. This tissue response demonstrated a stark contrast to a natural, urinary bladder ECM patch placed in the left ventricle, which supported cell infiltration, production of ECM and pockets of myocyte-like cells.⁹⁵ These results closely mirror what was reported when comparing the synthetic material, Dacron to an ECM-derived cardiac patch.⁹⁴ When using these materials in a canine model for a full thickness right ventricular defect, it was demonstrated that the ECM patch outperformed Dacron through regional systolic and diastolic function evaluations. These findings were likely due to the CMs observed in the ECM implant region, which was not seen with the Dacron® group.

Cormatrix® is a clinically approved, decellularized porcine small intestine submucosa (SIS) matrix that has been used for myocardium repair. In a recent study, patients who had complications resulting from MIs received either a Dor procedure, linear left ventricular aneurysm repair or ventricular septal defect repair with Cormatrix.⁹⁶ Patients had transthoracic echocardiographies prior to discharge and were later evaluated at follow-up appointments. The echocardiographies demonstrated repair integrity and no ventricular thrombus formation. Additionally, no complications such as readmission for any cardiac cause or death occurred. With these results, surgeons felt that the lack of CorMatrix ECM repair failures supported further investigation into the efficacy and regenerative potential of this material.

It is important to note that the benefits of an acellular scaffold may be temporary. As the scaffold degrades the reduced wall stress resulting from an increased wall thickness may be lost. This was demonstrated in a study where a polyethylene glycol hydrogel was injected in to an infarcted rat heart. There was a decrease in end-diastolic volume 4 weeks after MI, but the benefits were gone after 3 months.⁹⁷ Another concern with acellular scaffolds is that patients must rely on cells from adjacent regions repopulating the patch, which may not be restricted to CMs. Reports

have shown patches ultimately supporting a mixture of cell and tissue types including connective tissues, cartilage, and myocardial tissues.^{94, 98}

A cellular approach may have greater regenerative potential than an acellular approach. Studies demonstrate that when small intestine submucosa ECM was combined with mesenchymal stem cells, a greater reparative effect was observed in a chronic MI scar in a rabbit model relative to SIS ECM alone.⁹⁹ It was further demonstrated that these incorporated cells were able to migrate into the infarct site and differentiate into CMs.

2.7. CELL-POPULATED CARDIAC PATCHES

A cell-populated cardiac patch has the potential to restore lost function post-MI. Despite significant advances in the design of cardiac patches, there remains a need to develop an implantable scaffold that promotes substantial functional improvements to damaged myocardium. While various studies have shown that engineered scaffolds are capable of supporting contractile cells^{62, 80, 88, 100} and providing moderate increase in heart function,^{80, 101-102} there remains a significant need to develop an engineered cardiac patch with physiologically relevant contractility that easily integrates with the surrounding tissue to promote the regeneration of myocardial tissue.^{45, 62} Integration of a cardiac patch will require the alignment of incorporated cardiomyocytes to aid in electrical coupling of the patch to native myocardium in order to promote synchronous contractility⁴⁷ and stiffness values similar to native tissue in order to avoid mechanical mismatch.⁶¹

2.7.1. DECELLULARIZED TISSUES FOR CARDIAC PATCH DEVELOPMENT

Decellularized heart tissue has been investigated for use as a cardiac patch. This highly biomimetic approach enables the retention of tissue architecture, vasculature,^{90, 103} and proteins within the structure such as collagen, elastin and fibronectin.¹⁰⁴ Among other scaffold options, this type provides the best cell recognition,¹⁰⁵⁻¹⁰⁶ supports cell growth and tissue organization, and provides cues for adhesion, proliferation, migration, differentiation and function.¹⁰⁷ The removal of cell components and antigens reduces the potential for a foreign body reaction.¹⁰⁸ However, decellularization is difficult to completely accomplish. Residual DNA and other materials can

elicit an immune response and while harsher decellularization methods may result in more complete removal of host cells, they may also compromise tissue architecture.¹⁰⁹

The decellularization process involves physical, chemical, biological or combination treatments of the native tissue.⁸⁸ Once decellularized, the scaffolds can be re-cellularized with selected cell populations. It has been demonstrated that decellularized mouse hearts can be repopulated with human iPS cell-derived multipotent cardiovascular progenitor cells. These scaffolds demonstrated spontaneous contractions and a normal response to drugs.¹¹⁰ Additionally, it has been demonstrated that decellularization of an entire heart can be achieved. Donor hearts not used for transplantation were decellularized and seeded with iPS-derived cardiomyocytes. The authors demonstrated force generation of incorporated myocytes, showed electrical conductivity, pressure development in the left ventricle and metabolic function.¹¹¹

While progress in this area has been made, currently decellularized heart tissues are insufficient to circulate blood by mechanical force and electrical conduction through the scaffold is slower than a healthy heart.⁸⁷ Although there has been progress, the major challenges of decellularization without disruption to the structural and mechanical integrity of the scaffold, recellularization with homogenous distribution of cells, *in vitro* preservation, anticoagulation and endothelialization need to be overcome in order to generate a scaffold capable of *in vivo* functionality.^{104, 111}

2.7.2. CELL SHEETS AS CARDIAC PATCHES

More than a billion cells die following an infarct.¹³ When trying to replace this magnitude of cells, one limitation to scaffold-based patches is that the space occupied by the construct will be ECM, limiting the density of cells that can fill the defect. An alternative method for producing densely cell populated cardiac patches is to use cells alone. While cell suspensions are difficult to deliver and retain in the desired area, confluent cell sheets have been shown to be an alternative strategy. In this approach, confluent cells are harvested as intact sheets by culturing the cells on temperature-responsive polymers, such as poly-(N-isopropylacrylamide) (PIPAAm).¹¹² With this method, cells can adhere and proliferate on the polymer at 37°C, but when the temperature is lowered to below 32°C, the surface becomes hydrophilic and non-adhesive for the cells. This

results in the cells detaching from the polymer, but remaining attached to one another through cell adhesion proteins and deposited ECM.¹¹³ This technique has been used to derive cell sheets from neonatal rat ventricular myocytes and, when two sheets were stacked, synchronous and spontaneous contractions were observed.¹¹⁴⁻¹¹⁵ Additionally, evidence for electrical communication between cells in adjoining layers arising from gap junctions was observed within 1 hour.¹¹⁶ Cell sheets have been transplanted into tissues of rats. When this was done, microvasculature rapidly organized within the sheet, and beating of the transplanted construct continued for up to 1 year.⁸⁶ Despite these successful findings, there are limitations to the use of cell sheets as a cardiac patch. Clinically, stacked, autologous myoblast sheets were implanted in a 56-year-old man with dilated cardiomyopathy.¹¹⁷ This treatment resulted in the patient having an improved prognosis; he had no arrhythmia and was able to discontinue use of a left ventricular assist device. However, these cells do not form gap junctions, preventing them from propagating an electrical signal. In another clinical trial these cells were shown to induce arrhythmias when implanted in cardiac tissue.¹¹⁸

Another challenge is generating a cardiac patch of clinically relevant size. If we consider the perfusion limit of densely populated cell sheets is approximately 50-100 μm , the size of a cardiac patch is then limited to 3 cell layers without a vasculature.⁹¹ However, a clinically relevant cardiac patch needs to be ~1 cm thick,⁴⁵ which is significantly greater than 3 layers of cell sheets. One strategy to overcome this limitation is to create vascularization through the layers, performing a multi-step transplantation. By implanting 3 cell sheets into a rat, and allowing the sheets to become vascularized, the 3 sheets can function as the base for a subsequent transplantation. If this process is repeated 10 times every 24 hours, it will create a vascularized construct that is 3 mm thick. However, this technique will not readily transition to the clinic.⁹¹ Although cell sheets have demonstrated some improvement in cardiac function when implanted in an animal model⁸⁵, the biggest hindrance to use of this technology is developing a vascularization method *in-vitro* that can transition to the clinical setting so that a thick construct can be fabricated.⁸⁷

2.7.3. SYNTHETIC MATERIAL CARDIAC PATCH SCAFFOLDS

Synthetic materials are a promising strategy to create cardiac patches because of their customizable nature, as the mechanical properties and degradation kinetics can be readily tuned and their properties are highly reproducible. Additionally, their use mitigates concern of pathogen transmission risks associated with biological materials.¹¹⁹ Among synthetic materials, some of the most commonly-investigated for application as a cardiac patch are polyesters and polyurethanes, including polyglycolic acid (PGA)¹²⁰⁻¹²¹, poly(lactic-co-glycolic) acid (PLGA)¹²²⁻¹²³, poly(glycolide-co-caprolactone) PGCL¹²⁴, poly(glycerol sebacate) (PGS)¹²⁵⁻¹²⁶, and poly(lactide-co-epsilon-caprolactone) (PLCL)¹²⁷.

PGA has been shown to provide a scaffold environment that can support differentiation of myocytes into organized layers.¹²⁰ Additionally, a PGA patch seeded with embryonic stem cells (ESCs) was implanted onto infarcted mice hearts. At 8 weeks, it was observed that engrafted cells survived, suggesting that the scaffold efficiently served as a cell delivery device.¹²¹

PLGA is the base material of an epicardial patch composed of vicryl® mesh seeded with human fibroblasts that has been investigated as a device to induce angiogenesis in the damaged tissue region following an infarct.¹²² This material was applied as an epicardial patch to an ischemic heart in a Sprague-Dawley rat model.¹²³ The patch provided cytokines, growth factors and proteins to the area contributing to observed arteriogenesis and tissue repair. Functionally, the ejection fraction for the left ventricle increased with application of this patch. Improved left ventricular function was also observed for cellularized patches composed of PLCL that were implanted onto infarcted hearts in an adult rat model, relative to non-cellularized patches.¹²⁷

When implanted onto the epicardial surface, it was demonstrated that a PGCL scaffold populated with bone marrow-derived mononuclear cells attenuated left ventricular remodeling and systolic dysfunction.¹²⁴ Limited remodeling was also observed when PGS films were utilized in an MI in a rat model. Although unable to support systolic function, the patches were able to reduce hypertrophy and may limit remodeling of the tissue.¹²⁶

Research by Lisa Freed's group showed that PGS and PGS-inspired materials created a modular, vascularized cardiac scaffold.¹²⁸ The scaffold is composed of a microfluidic base, a

vascular-parenchymal interface and a heart cell scaffold. By manipulating the degradation rates of the components of this scaffold, the authors designed a scaffold with an interface that enables perfusion-mediated transport *in vitro*, while degrading quickly *in vivo*. The fast degradation of the interface quickly brings the heart cell scaffold in contact with the host-derived blood vessels when implanted. Using a slowly degrading polymer, poly(ester-amide),1:2 poly(1,3-diamino-2-hydroxypropane-*co*-polyol sebacate) (APS), for the heart cell scaffold and microfluidic base provides an anisotropic mechanical support upon implantation. The synthetic materials enabled this clever design as the degradation rates were tunable.

In another strategy, a mosaic patch was created that mimics the structure of Velcro®. This patch was designed to provide a method to incorporate easily stackable units, that could be disassembled on demand while preserving the structure, physical integrity and beating function of the individual layers. This scaffold was made of a honeycomb mesh with hooks comprised of poly(octamethylene maleate (anhydride) citrate) (POMaC). Cells were seeded in Matrigel (an extract from the basal membrane of a sarcoma cell line rich with ECM proteins and bioactive substances). Strong mechanical integration of the layers was observed, as was immediate functional integration of the stacked layers as demonstrated through electrical stimulation.¹²⁹

While considerable progress has been made using synthetic materials, there are still many challenges associated with them. These materials typically have poor interaction with cells because of their hydrophobic nature¹³ and they also have poor interaction with the native biological environment, often inducing an aggressive inflammatory response *in vivo*.¹³⁰ Additionally, synthetic materials tend to crumble rather than slowly degrade, and the degradation products can be acidic, impacting the viability of cells.¹³

2.7.4. NATURAL BIOPOLYMER CARDIAC PATCH SCAFFOLDS

Natural biopolymers are highly compatible materials with native signaling cues for cells to attach, proliferate and differentiate on *in vivo*.¹³ These materials have adhesion-specific sites that promote cellular interaction, unlike synthetic materials.⁹² Additionally, natural biopolymers enable a biomimetic scaffold that closely resembles the ECM of the native tissue. As described earlier, biomimetic approaches may be beneficial in providing instructive cues for tissue regeneration.

Natural hydrogels in particular have proven superior for generating highly functional cardiac tissues, as they support macroscopic contractions and uniform cell density.¹³¹ Some of the most commonly investigated natural biopolymers for use as cardiac patches include collagen, gelatin, fibrin and alginate.⁹³

Collagens types I and III are major components of the ECM of myocardium and are a promising material for a cardiac patch.¹³ When these materials were combined with Matrigel and cultured with rat neonatal ventricular myocytes, an engineered heart tissue was formed that displayed functional and morphological properties similar to differentiated heart muscle. Implantation studies using a Fischer 344 rat model demonstrated that these engineered tissues survive and integrate *in vivo*.¹³² Additionally, the tissues electrically coupled with native tissue upon implantation in a rat MI model, and ultimately improved diastolic and systolic function relative to sham procedure controls.¹³³

In the MAGNUM clinical trial, authors investigated the use of autologous mononuclear bone marrow cells seeded on a collagen matrix. This scaffold was grafted onto infarcted ventricles of patients.¹³⁴ It was observed that the scaffold resulted in improved efficiency of cellular cardiomyoplasty, and that there was an increase in the thickness of the ventricular wall at the infarct site. As mentioned earlier, an increase in ventricular wall thickness can normalize wall stress limiting remodeling and improving diastolic function.¹³⁴

With biomimetic mechanical and electrical stimulations, cells incorporated on collagen scaffolds have a more mature phenotype. In one study, rat neonatal ventricular myocytes in Matrigel were seeded onto Ultrafoam™ collagen sponges. Applications of electrical stimulations that mimicked the native heart resulted in cell alignment, coupling and synchronous contractions.¹³⁵ Additionally, application of mechanical stretch to collagen-based scaffolds has been shown to improve the maturity of incorporated cells. When applying cyclic mechanical stretch to 120% of the initial scaffold length, it was observed that cells incorporated in a collagen/Matrigel matrix underwent hypertrophy and demonstrated functional improvements.¹³⁶

While low-density collagen hydrogels support functionality of incorporated cardiomyocytes, the lack of mechanical integrity is a limiting factor. Interestingly, a recently published study

showed that a high density collagen scaffold could support cardiomyocyte function when co-cultured with matrix-remodeling stromal cells.¹³⁷ This co-culture resulted in a scaffold material that supported a microvasculature and cellular function *in vitro* for two weeks, and appears to be a promising approach for the development of cardiac patches of clinically relevant size.

Silk fibroin is another candidate material for a cardiac patch. Silk fibroin has the highest mechanical performance of all known natural materials. For a 10mm diameter scaffold with a height of 10mm, 84 kPa of compressive strength was reported. This was much greater than collagen or chitosan with reported values of 15 and 45 kPa compressive strength, respectively.¹³ Silk is being explored as a cardiac patch material in combination with cardiac tissue-derived extracellular matrix (cECM)¹³⁸, and will be discussed in the composite patch section (**Section 2.7.5**).

Because fibrin is seminal during the early phase of wound healing,¹³⁹ it is hypothesized that this material will serve as a facile tool for myocardium regeneration. Additionally, the components of fibrin can be isolated from blood suggesting fibrin scaffolds have the potential to be tailored for personalized healthcare strategies.¹⁰⁰ Fibrin has cell adhesive properties, can induce neovascularization¹⁴⁰ and reduce infarct expansion.⁷⁶

Fibrin has been investigated in a hydrogel format and has demonstrated some of the highest contractile forces and action potential propagation speeds to date.^{77, 131, 141} Through patterning of the hydrogel space with ellipsoidal pores, it has been demonstrated that incorporated cells align through gel compaction over time in culture and mature. More recently, bundles of fibrin hydrogel have been cultured on free floating on Nylon frames, and when cultured dynamically with a +/- 30° rotation were shown to achieve conduction velocities and contraction forces approaching values of adult myocardium.¹³¹

Fibrin-based patches with different cell populations have also been considered. In a recent study, the effects of incorporating cardiomyocyte-enriched, or cardiomyocyte-depleted neonatal rat cell hearts in an epicardial patch implanted on the infarct region in a rat model was assessed. This study showed that when CMs were incorporated into the patch, there was a significant improvement in contractile function, and there was elimination of left ventricular wall thinning.

The decreased infarct size and reduced wall thinning were also observed for the patch free of CMs, but there was no subsequent improvement in cardiac function.⁸⁰

Another study utilized cardiac adipose tissue-derived progenitor cells in a fibrin hydrogel patch. Prior to embedding in fibrin, the cells were either electromechanically stimulated and stretched to condition the cells, or were left untreated. The patches were implanted over an infarct region of a murine heart. The findings showed that rodents that received patches with stimulated cells had an increase in cardiac function as evaluated by left ventricular ejection fraction relative to nontreated animals. Trained cells also expressed main cardiac markers such as connexin 43, α -actinin and SERCA2, and migrated into the ischemic tissue of the myocardium.¹⁴² This study demonstrated that conditioning the cells prior to incorporation may increase the functional impact of the patch on the heart.

Other natural materials have also been considered as scaffolds for cardiac patches. A gelatin mesh was combined with rat ventricular fetal or adult cardiomyocytes and used to repair the right ventricular outflow tract in adult rats. In a 12 week study, seeded cells survived in the area even after the scaffold had degraded, demonstrating the cell delivery capability of this material.¹⁴³ Additionally, polysaccharides including alginate¹⁴⁴, cellulose¹⁴⁵, chitosan¹⁴⁶, and hyaluronic acid (HA)¹⁴⁷ have been investigated for use as a cardiac patch.

Natural biopolymers are commonly characterized by poor mechanical properties, limited processing parameters and rapid degradation kinetics.^{92, 148} While crosslinking has been suggested as a method for improving mechanical properties, it can induce modification to the structure impacting the cellular response to the scaffold.¹³ Furthermore, clinical considerations may complicate the use of some natural materials that lack a defined chemical composition. For example, Matrigel™ is a commonly used natural material in the development of cardiac patches, with positive results. However, it is not clear whether Matrigel will be clinically approved for human use.¹¹⁹ Although functionality on natural material scaffolds is some of the highest reported,¹³¹ these challenges still present a barrier for creating implantable, clinically relevant cardiac patches from them.

2.7.5. COMPOSITE MATERIALS FOR CARDIAC PATCH SCAFFOLDS

While progress has been made in the development of cardiac patches using synthetic and natural materials, there are considerable limitations to each. While synthetic materials demonstrate mechanical integrity and tunable degradation, they also can elicit an immune response and do not easily interact with cells or the native tissue environment. Natural materials are highly biocompatible and provide cell attachment sites, but are typically mechanically weak with rapid degradation profiles. As one potential solution, composite materials combining natural and synthetic materials have been investigated for use as cardiac patches. Through the combination of natural and synthetic materials, a more desirable material for cardiac patches may be achieved.

Synthetic materials have been combined with fibrin¹⁴⁹, collagen¹⁵⁰, alginate and gelatin¹⁵¹ for the design of a cardiac patch. The incorporation of natural materials with synthetics enhances the cellular response relative to synthetic materials alone. However, synthetic materials still have drawbacks. One potential strategy to create better cardiac patches may be to generate a natural material that has the mechanical integrity needed for this application.

Silk fibroin has been combined with cardiac tissue-derived extracellular matrix (cECM). This composite material had tunable architectures, degradation rates, and mechanical properties dependent on the concentrations of the components utilized. When implanted subcutaneously in a rat model, the addition of cECM to the acellular silk scaffold lead to high endogenous cellular infiltration. Additionally, the scaffold promoted vascularization after 4 weeks *in vivo*. When evaluating the constructs *in vitro* and seeding cells onto the scaffolds, the incorporation of the cECM promoted greater myosin heavy chain expression, a part of the contractile complex critical to cardiomyocyte function.¹³⁸ This study demonstrates the feasibility of using natural materials to create a mechanically tunable scaffold for a cardiac patch application. Further development of a cell-populated scaffold of clinically relevant size is critical for the development of a successful cardiac patch.

2.8. BIOPOLYMER MICROTHREADS FOR TISSUE REGENERATION

Biopolymer microthreads are discrete, fibrous materials, generated from ECM, polysaccharides and naturally derived proteins such as fibrin,¹⁵²⁻¹⁵⁴ silk,¹⁵⁵⁻¹⁵⁶ collagen,¹⁵⁷⁻¹⁵⁸

chitosan, and alginate.¹⁵⁹⁻¹⁶¹ The morphological and biochemical properties of these microthreads are comparable to native fibrous structures, and they can be precisely engineered into hierarchically ordered, tissue-specific scaffolds with morphological, mechanical and biochemical cues to promote cell-mediated tissue regeneration (**Figure 2.5**). These microthreads can be modified to precisely modulate their material properties including tensile strength and degradation rates. These thread modifications enable the fabrication of scaffolds that closely mimic properties of native tissues.

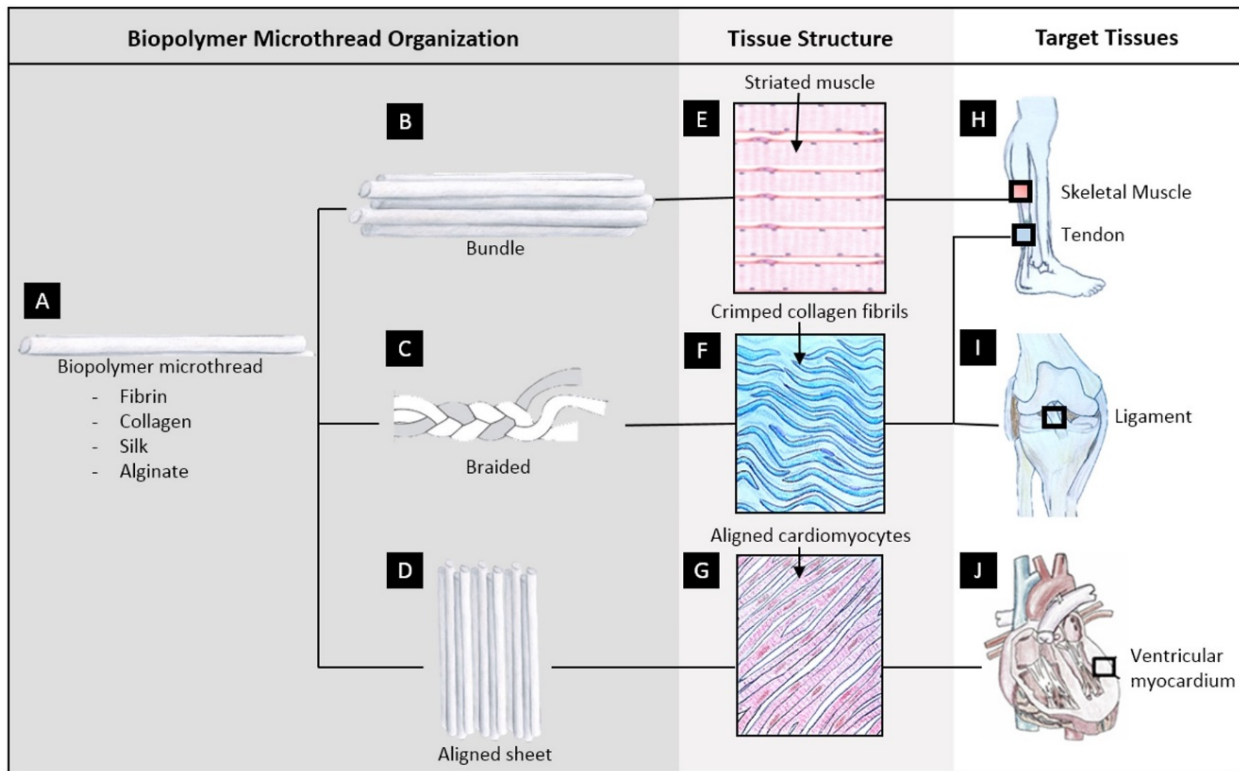


Figure 2.5: Biopolymer microthreads for tissue engineering applications. Biopolymer microthreads composed of different biomaterials (A) can be hierarchically combined to produce scaffolds (B-D). These scaffolds mimic tissue structures (E-G) of targeted diseased or injured tissues (H-J).

To enhance the efficiency of cell delivery to a myocardial infarct, our labs pioneered a cell-seeded fibrin microthread-based suture system to facilitate targeted, localized cell delivery in the heart. Biopolymer threads may mimic the fibril architecture observed in native myocardium and may help cells to incorporate into the infarct tissue.

In one study evaluating the effective delivery of human mesenchymal stem cells (hMSCs), cells were incorporated on a fibrin microthread suture and implanted or delivered via IM injection to the left ventricular wall of non-infarcted normal rat hearts. Delivery efficiency was greatly improved using the fibrin suture relative to the cell injection alone (63.6 +/- 10.6% and 11.8 +/- 6.2%, respectively).¹⁵³ In a more recent study, an acellular suture was compared to an hMSC-seeded suture to assess the impact in normal functioning rat hearts. To compare regional mechanical function, systolic area of contraction (SAC) in the region of biopolymer microthread delivery was evaluated. Compared to native myocardium, SAC was decreased for acellular scaffold implants, while this decrease was less pronounced in the hMSC-seeded suture group. Fibrosis was reduced for the hMSC seeded suture group relative to the acellular suture group,¹⁶² suggesting that hMSCs may release factors limiting the fibrotic response to injury. The incorporation of hMSCs improved regional mechanics when compared to an acellular scaffold, demonstrating the value of delivering healthy cells incorporated onto the biomaterial scaffold. In an *in vitro* analysis, fibrin microthread sutures were able to support viability, proliferative capacity and multipotency in hMSCs, suggesting that the fibrin microthreads may be used as a platform technology¹⁶³ and may be applicable to other applications.

Excerpt from: O'Brien, Megan P., et al. "Designing Biopolymer Microthreads for Tissue Engineering and Regenerative Medicine." *Current Stem Cell Reports* 2.2 (2016): 147-157.

2.9. FIBRIN MICROTHREAD-BASED COMPOSITE SCAFFOLDS

While fibrin microthreads have shown the ability to guide cellular orientation,¹⁵² the microthreads are mechanically stiff relative to myocardium and may limit cell-mediated contractility.¹⁶⁴ In contrast, hydrogels provide compactible environments and have produced some of the highest reported contractile force measurements to date.⁷⁷ However, hydrogels are typically qualitatively characterized as mechanically weak¹⁶⁵⁻¹⁶⁶ and may fail in the dynamic environment of the heart.^{61, 166} A composite material composed of a microthread element and a hydrogel phase may yield a scaffold combining the benefits of structural cues and mechanical integrity of microthreads, with the hydrogel environment that is conducive to cell-mediated contractility. *These materials could be strategically combined to mimic the mechanical environment of native*

myocardium promoting high functionality of incorporated cells. The use of fibrin microthreads within the composite may enable a contractile tissue analog of myocardial tissue.

2.10. REFERENCES

1. Hwang, J.; Jeong, Y.; Park, J. M.; Lee, K. H.; Hong, J. W.; Choi, J., Biomimetics: forecasting the future of science, engineering, and medicine. *International journal of nanomedicine* 2015, 10, 5701-13.
2. Bhushan, B., Biomimetics. *Philos Trans A Math Phys Eng Sci* 2009, 367 (1893), 1443-4.
3. Freedman, R.; Wright, W.; Wright, O., *The Wright brothers : how they invented the airplane*. 1st ed.; Holiday House: New York, 1991; p 129 p.
4. Jakab, P. L., *Visions of a flying machine : the Wright brothers and the process of invention*. Smithsonian Institution Press: Washington, 1990; p xviii, 263 p.
5. Langer, R.; Vacanti, J. P., Tissue engineering. *Science* 1993, 260 (5110), 920-6.
6. Webber, M. J.; Khan, O. F.; Sydlik, S. A.; Tang, B. C.; Langer, R., A perspective on the clinical translation of scaffolds for tissue engineering. *Annals of biomedical engineering* 2015, 43 (3), 641-56.
7. Qu, D.; Mosher, C. Z.; Boushell, M. K.; Lu, H. H., Engineering complex orthopaedic tissues via strategic biomimicry. *Annals of biomedical engineering* 2015, 43 (3), 697-717.
8. Silverthorn, D. U.; Johnson, B. R., *Human physiology : an integrated approach*. 5th ed.; Pearson/Benjamin Cummings: San Francisco, 2010; p xxxiv, 867, 83 p.
9. O'Brien, M. P.; Carnes, M. E.; Page, R. L.; Gaudette, G. R.; Pins, G. D., Designing biopolymer microthreads for tissue engineering and regenerative medicine. *Current Stem Cell Reports* 2016, 2, 147-57.
10. Atala, A.; Kasper, F. K.; Mikos, A. G., Engineering complex tissues. *Science translational medicine* 2012, 4 (160), 160rv12.
11. Grasman, J. M.; Do, D. M.; Page, R. L.; Pins, G. D., Rapid release of growth factors regenerates force output in volumetric muscle loss injuries. *Biomaterials* 2015, 72, 49-60.
12. Leor, J.; Cohen, S., Myocardial tissue engineering: creating a muscle patch for a wounded heart. *Annals of the New York Academy of Sciences* 2004, 1015, 312-9.
13. Silvestri, A.; Boffito, M.; Sartori, S.; Ciardelli, G., Biomimetic materials and scaffolds for myocardial tissue regeneration. *Macromolecular bioscience* 2013, 13 (8), 984-1019.
14. Radisic, M.; Park, H.; Gerecht, S.; Cannizzaro, C.; Langer, R.; Vunjak-Novakovic, G., Biomimetic approach to cardiac tissue engineering. *Philosophical transactions of the Royal Society of London. Series B, Biological sciences* 2007, 362 (1484), 1357-68.
15. Shin, H.; Jo, S.; Mikos, A. G., Biomimetic materials for tissue engineering. *Biomaterials* 2003, 24 (24), 4353-64.
16. Nuernberger, S.; Cyran, N.; Albrecht, C.; Redl, H.; Vecsei, V.; Marlovits, S., The influence of scaffold architecture on chondrocyte distribution and behavior in matrix-associated chondrocyte transplantation grafts. *Biomaterials* 2011, 32 (4), 1032-40.
17. Benya, P. D.; Shaffer, J. D., Dedifferentiated chondrocytes reexpress the differentiated collagen phenotype when cultured in agarose gels. *Cell* 1982, 30 (1), 215-24.
18. Bosworth, L. A.; Turner, L. A.; Cartmell, S. H., State of the art composites comprising electrospun fibres coupled with hydrogels: a review. *Nanomedicine : nanotechnology, biology, and medicine* 2013, 9 (3), 322-35.
19. Anseth, K. S.; Bowman, C. N.; Brannon-Peppas, L., Mechanical properties of hydrogels and their experimental determination. *Biomaterials* 1996, 17 (17), 1647-57.
20. Stammen, J. A.; Williams, S.; Ku, D. N.; Guldberg, R. E., Mechanical properties of a novel PVA hydrogel in shear and unconfined compression. *Biomaterials* 2001, 22 (8), 799-806.
21. Huang, T.; Xu, H.; Jiao, K.; Zhu, L.; Brown, H. R.; Wang, H., A novel hydrogel with high mechanical strength: a macromolecular microsphere composite hydrogel. *Advanced materials* 2007, 19 (1622).

22. Yodmuang, S.; McNamara, S. L.; Nover, A. B.; Mandal, B. B.; Aganwal, M.; Kelly, T. A. N.; Chao, P. H. G.; Hung, C.; Kaplan, D. L.; Vunjak-Novakovic, G., Silk microfiber-reinforced silk hydrogel composites for functional cartilage tissue repair. *Acta biomaterialia* 2015, 11, 27-36.
23. Callister, W. D.; Rethwisch, D. G., *Fundamentals of materials science and engineering : an integrated approach*. 4th ed.; Wiley: Hoboken, N.J., 2012; p xxv, 910 p.
24. Huang, Z.; Feng, Q.; Yu, B.; Li, S., Biomimetic properties of an injectable chitosan/ nano-hydroxyapatite/ collagen composite. *Mat Sci Eng C-Mater* 2011, 31, 683-687.
25. Naik, N.; Caves, J.; Chaikof, E. L.; Allen, M. G., Generation of spatially aligned collagen fiber networks through microtransfer molding. *Adv Healthc Mater* 2014, 3 (3), 367-74.
26. Cutiongco, M. F.; Tan, M. H.; Ng, M. Y.; Le Visage, C.; Yim, E. K., Composite pullulan-dextran polysaccharide scaffold with interfacial polyelectrolyte complexation fibers: a platform with enhanced cell interaction and spatial distribution. *Acta biomaterialia* 2014, 10 (10), 4410-8.
27. Sharabi, M.; Mandelberg, Y.; Benayahu, D.; Benayahu, Y.; Azem, A.; Haj-Ali, R., A new class of bio-composite materials of unique collagen fibers. *Journal of the mechanical behavior of biomedical materials* 2014, 36, 71-81.
28. Tonsomboon, K.; Oyen, M. L., Composite electrospun gelatin fiber-alginate gel scaffolds for mechanically robust tissue engineered cornea. *Journal of the mechanical behavior of biomedical materials* 2013, 21, 185-94.
29. Shepherd, J. H.; Ghose, S.; Kew, S. J.; Moavenian, A.; Best, S. M.; Cameron, R. E., Effect of fiber crosslinking on collagen-fiber reinforced collagen-chondroitin-6-sulfate materials for regenerating load-bearing soft tissues. *Journal of biomedical materials research. Part A* 2013, 101 (1), 176-84.
30. Chrobak, M. O.; Hansen, K. J.; Gershlak, J. R.; Vratsanos, M.; Kanellias, M.; Gaudette, G. R.; Pins, G. D., Design of a fibrin microthread-based composite layer for use in a cardiac patch. *ACS Biomaterials Science & Engineering* 2016.
31. Li, G.; Liu, J.; Zheng, Z.; Wang, X.; Kaplan, D. L., Structural Mimetic Silk Fiber-Reinforced Composite Scaffolds Using Multi-Angle Fibers. *Macromolecular bioscience* 2015, 15 (8), 1125-33.
32. Le Goff, K. J.; Gaillard, C.; Helbert, W.; Garnier, C.; Aubry, T., Rheological study of reinforcement of agarose hydrogels by cellulose nanowhiskers. *Carbohydrate polymers* 2015, 116, 117-23.
33. Gentleman, E.; Nauman, E. A.; Livesay, G. A.; Dee, K. C., Collagen composite biomaterials resist contraction while allowing development of adipocytic soft tissue in vitro. *Tissue engineering* 2006, 12 (6), 1639-49.
34. Gentleman, E.; Dee, K. C.; Livesay, G. A.; Nauman, E. A., Operating curves to characterize the contraction of fibroblast-seeded collagen gel/collagen fiber composite biomaterials: effect of fiber mass. *Plast Reconstr Surg* 2007, 119 (2), 508-16.
35. Gentleman, E.; Nauman, E. A.; Dee, K. C.; Livesay, G. A., Short collagen fibers provide control of contraction and permeability in fibroblast-seeded collagen gels. *Tissue engineering* 2004, 10 (3-4), 421-7.
36. Chen, Y.; Huang, Z.; Li, X.; Li, S.; Zhou, Z.; Zhang, Y.; Feng, Q.; Yu, B., In vitro biocompatibility and osteoblast differentiation of an injectable chitosan/nano-hydroxyapatite/ collagen scaffold. *Journal of Nanomaterials* 2012, 2012.
37. Wongpanit, P.; Sanchavanakit, N.; Pavasant, P.; Bunaprasert, T.; Tabata, Y.; Rujiravanit, R., Preparation and characterization of chitin whisker-reinforced silk fibroin nanocomposite sponges. *Macromolecular Nanotechnology* 2007, 43, 4123-4135.
38. Mobini, S.; Taghizadeh-Jahed, M.; Khanmohammadi, M.; Moshiri, A.; Naderi, M. M.; Heidari-Vala, H.; Ashrafi Helan, J.; Khanjani, S.; Springer, A.; Akhondi, M. M.; Kazemnejad, S., Comparative evaluation of in vivo biocompatibility and biodegradability of regenerated silk scaffolds reinforced with/without natural silk fibers. *Journal of biomaterials applications* 2016, 30 (6), 793-809.
39. Mobini, S.; Hoyer, B.; Solati-Hashjin, M.; Lode, A.; Nosoudi, N.; Samadikuchaksaraei, A.; Gelinsky, M., Fabrication and characterization of regenerated silk scaffolds reinforced with natural silk fibers for bone tissue engineering. *Journal of biomedical materials research. Part A* 2013, 101 (8), 2392-404.

40. Mandal, B. B.; Grinberg, A.; Gil, E. S.; Panilaitis, B.; Kaplan, D. L., High-strength silk protein scaffolds for bone repair. *Proceedings of the National Academy of Sciences of the United States of America* **2012**, *109* (20), 7699-704.
41. Park, J. B.; Lakes, R. S., *Biomaterials: an introduction*. 2nd ed.; Plenum Press: New York, 1992.
42. Sommer, G.; Haspinger, D. C.; Andra, M.; Sacherer, M.; Viertler, C.; Regitnig, P.; Holzapfel, G. A., Quantification of Shear Deformations and Corresponding Stresses in the Biaxially Tested Human Myocardium. *Annals of biomedical engineering* **2015**.
43. Yeh, H. L.; Yeh, H. Y., A dimensionless analysis of young's modulus and stress distribution for orthotropic materials. *Journal of Aeronautics and Aerospace Engineering* **2014**, *3* (1).
44. Mozaffarian, D.; Benjamin, E. J.; Go, A. S.; Arnett, D. K.; Blaha, M. J.; Cushman, M.; de Ferranti, S.; Despres, J. P.; Fullerton, H. J.; Howard, V. J.; Huffman, M. D.; Judd, S. E.; Kissela, B. M.; Lackland, D. T.; Lichtman, J. H.; Lisabeth, L. D.; Liu, S.; Mackey, R. H.; Matchar, D. B.; McGuire, D. K.; Mohler, E. R., 3rd; Moy, C. S.; Muntner, P.; Mussolino, M. E.; Nasir, K.; Neumar, R. W.; Nichol, G.; Palaniappan, L.; Pandey, D. K.; Reeves, M. J.; Rodriguez, C. J.; Sorlie, P. D.; Stein, J.; Towfighi, A.; Turan, T. N.; Virani, S. S.; Willey, J. Z.; Woo, D.; Yeh, R. W.; Turner, M. B.; American Heart Association Statistics, C.; Stroke Statistics, S., Heart disease and stroke statistics--2015 update: a report from the American Heart Association. *Circulation* **2015**, *131* (4), e29-322.
45. Radisic, M.; Christman, K. L., Materials science and tissue engineering: repairing the heart. *Mayo Clinic proceedings* **2013**, *88* (8), 884-98.
46. Frangiannis, N. G.; Smith, C. W.; Entman, M. L., The inflammatory response in myocardial infarction. *Cardiovascular research* **2002**, *53* (1), 31-47.
47. Vunjak-Novakovic, G.; Tandon, N.; Godier, A.; Maidhof, R.; Marsano, A.; Martens, T. P.; Radisic, M., Challenges in cardiac tissue engineering. *Tissue engineering. Part B, Reviews* **2010**, *16* (2), 169-87.
48. Beltrami, A. P.; Barlucchi, L.; Torella, D.; Baker, M.; Limana, F.; Chimenti, S.; Kasahara, H.; Rota, M.; Musso, E.; Urbanek, K.; Leri, A.; Kajstura, J.; Nadal-Ginard, B.; Anversa, P., Adult cardiac stem cells are multipotent and support myocardial regeneration. *Cell* **2003**, *114* (6), 763-76.
49. Cohen, S.; Leor, J., Rebuilding broken hearts. Biologists and engineers working together in the fledgling field of tissue engineering are within reach of one of their greatest goals: constructing a living human heart patch. *Sci Am* **2004**, *291* (5), 44-51.
50. Holmes, J. W.; Borg, T. K.; Covell, J. W., Structure and mechanics of healing myocardial infarcts. *Annual review of biomedical engineering* **2005**, *7*, 223-53.
51. Sun, Y.; Weber, K. T., Infarct scar: a dynamic tissue. *Cardiovascular research* **2000**, *46* (2), 250-6.
52. Menasche, P., Cardiac cell therapy: lessons from clinical trials. *Journal of molecular and cellular cardiology* **2011**, *50* (2), 258-65.
53. Jakob, P.; Landmesser, U., Current status of cell-based therapy for heart failure. *Current heart failure reports* **2013**, *10* (2), 165-76.
54. Shah, V. K.; Shalia, K. K., Stem Cell Therapy in Acute Myocardial Infarction: A Pot of Gold or Pandora's Box. *Stem cells international* **2011**, *2011*, 536758.
55. Li, X.; Tamama, K.; Xie, X.; Guan, J., Improving Cell Engraftment in Cardiac Stem Cell Therapy. *Stem cells international* **2016**, *2016*, 7168797.
56. Vu, D. T.; Martinez, E. C.; Kofidis, T., Myocardial restoration: is it the cell or the architecture or both? *Cardiol Res Pract* **2012**, *2012*, 240497.
57. Black, L. D., 3rd; Meyers, J. D.; Weinbaum, J. S.; Shvelidze, Y. A.; Tranquillo, R. T., Cell-induced alignment augments twitch force in fibrin gel-based engineered myocardium via gap junction modification. *Tissue engineering. Part A* **2009**, *15* (10), 3099-108.
58. Kim, D. H.; Lipke, E. A.; Kim, P.; Cheong, R.; Thompson, S.; Delannoy, M.; Suh, K. Y.; Tung, L.; Levchenko, A., Nanoscale cues regulate the structure and function of macroscopic cardiac tissue constructs. *Proceedings of the National Academy of Sciences of the United States of America* **2010**, *107* (2), 565-70.

59. Lee, W. N.; Pernot, M.; Couade, M.; Messas, E.; Bruneval, P.; Bel, A.; Hagege, A. A.; Fink, M.; Tanter, M., Mapping myocardial fiber orientation using echocardiography-based shear wave imaging. *IEEE transactions on medical imaging* **2012**, *31* (3), 554-62.
60. Coulombe, K. L.; Bajpai, V. K.; Andreadis, S. T.; Murry, C. E., Heart Regeneration with Engineered Myocardial Tissue. *Annual review of biomedical engineering* **2014**.
61. Reis, L. A.; Chiu, L. L.; Feric, N.; Fu, L.; Radisic, M., Biomaterials in myocardial tissue engineering. *Journal of tissue engineering and regenerative medicine* **2014**, *10* (1), 11-28.
62. Liao, B.; Christoforou, N.; Leong, K. W.; Bursac, N., Pluripotent stem cell-derived cardiac tissue patch with advanced structure and function. *Biomaterials* **2011**, *32* (35), 9180-7.
63. Basford, J. R., The Law of Laplace and its relevance to contemporary medicine and rehabilitation. *Arch Phys Med Rehabil* **2002**, *83* (8), 1165-70.
64. Fung, Y. C., *A first course in continuum mechanics*. 2d ed.; Prentice-Hall: Englewood Cliffs, N.J., 1977; p xii, 340 p.
65. Moriarty, T. F., The law of Laplace. Its limitations as a relation for diastolic pressure, volume, or wall stress of the left ventricle. *Circulation research* **1980**, *46* (3), 321-31.
66. Segers, V. F.; Lee, R. T., Biomaterials to enhance stem cell function in the heart. *Circulation research* **2011**, *109* (8), 910-22.
67. Chen, Q. Z.; Harding, S. E.; Ali, N. N.; Lyon, A. R.; Boccaccini, A. R., Biomaterials in cardiac tissue engineering: Ten years of research survey. *Materials Science & Engineering R* **2008**, *59*, 1-37.
68. Ifkovits, J. L.; Tous, E.; Minakawa, M.; Morita, M.; Robb, J. D.; Koomalsingh, K. J.; Gorman, J. H., 3rd; Gorman, R. C.; Burdick, J. A., Injectable hydrogel properties influence infarct expansion and extent of postinfarction left ventricular remodeling in an ovine model. *Proceedings of the National Academy of Sciences of the United States of America* **2010**, *107* (25), 11507-12.
69. Sartipy, U.; Albage, A.; Lindblom, D., The Dor procedure for left ventricular reconstruction. Ten-year clinical experience. *Eur J Cardiothorac Surg* **2005**, *27* (6), 1005-10.
70. Kelly, D. J.; Rosen, A. B.; Schuldt, A. J.; Kochupura, P. V.; Doronin, S. V.; Potapova, I. A.; Azeloglu, E. U.; Badylak, S. F.; Brink, P. R.; Cohen, I. S.; Gaudette, G. R., Increased myocyte content and mechanical function within a tissue-engineered myocardial patch following implantation. *Tissue engineering. Part A* **2009**, *15* (8), 2189-201.
71. Cui, J.; Li, J.; Mathison, M.; Tondato, F.; Mulkey, S. P.; Micko, C.; Chronos, N. A.; Robinson, K. A., A clinically relevant large-animal model for evaluation of tissue-engineered cardiac surgical patch materials. *Cardiovasc Revasc Med* **2005**, *6* (3), 113-20.
72. Ukwatta, E.; Arevalo, H.; Rajchl, M.; White, J.; Pashakhanloo, F.; Prakosa, A.; Herzka, D. A.; McVeigh, E.; Lardo, A. C.; Trayanova, N. A.; Vadakkumpadan, F., Image-based reconstruction of three-dimensional myocardial infarct geometry for patient-specific modeling of cardiac electrophysiology. *Med Phys* **2015**, *42* (8), 4579-90.
73. Tallawi, M.; Rai, R.; Boccaccini, A. R.; Aifantis, K. E., Effect of substrate mechanics on cardiomyocyte maturation and growth. *Tissue engineering. Part B, Reviews* **2015**, *21* (1), 157-65.
74. Pok, S.; Myers, J. D.; Madhally, S. V.; Jacot, J. G., A multilayered scaffold of a chitosan and gelatin hydrogel supported by a PCL core for cardiac tissue engineering. *Acta biomaterialia* **2013**, *9* (3), 5630-42.
75. Campbell, K. S.; Patel, J. R.; Moss, R. L., Cycling cross-bridges increase myocardial stiffness at submaximal levels of Ca²⁺ activation. *Biophysical journal* **2003**, *84* (6), 3807-3815.
76. Thomson, K. S.; Korte, F. S.; Giachelli, C. M.; Ratner, B. D.; Regnier, M.; Scatena, M., Prevascularized microtemplated fibrin scaffolds for cardiac tissue engineering applications. *Tissue engineering. Part A* **2013**, *19* (7-8), 967-77.
77. Zhang, D.; Shadrin, I. Y.; Lam, J.; Xian, H. Q.; Snodgrass, H. R.; Bursac, N., Tissue-engineered cardiac patch for advanced functional maturation of human ESC-derived cardiomyocytes. *Biomaterials* **2013**, *34* (23), 5813-20.

78. Miklas, J. W.; Dallabrida, S. M.; Reis, L. A.; Ismail, N.; Rupnick, M.; Radisic, M., QHREDGS enhances tube formation, metabolism and survival of endothelial cells in collagen-chitosan hydrogels. *PLoS one* 2013, 8 (8), e72956.
79. Morin, K. T.; Dries-Devlin, J. L.; Tranquillo, R. T., Engineered microvessels with strong alignment and high lumen density via cell-induced fibrin gel compaction and interstitial flow. *Tissue engineering. Part A* 2014, 20 (3-4), 553-65.
80. Wendel, J. S.; Ye, L.; Zhang, P.; Tranquillo, R. T.; Zhang, J. J., Functional consequences of a tissue-engineered myocardial patch for cardiac repair in a rat infarct model. *Tissue engineering. Part A* 2014, 20 (7-8), 1325-35.
81. Xiong, Q.; Hill, K. L.; Li, Q.; Suntharalingam, P.; Mansoor, A.; Wang, X.; Jameel, M. N.; Zhang, P.; Swingen, C.; Kaufman, D. S.; Zhang, J., A fibrin patch-based enhanced delivery of human embryonic stem cell-derived vascular cell transplantation in a porcine model of postinfarction left ventricular remodeling. *Stem cells* 2011, 29 (2), 367-75.
82. Fleischer, S.; Feiner, R.; Shapira, A.; Ji, J.; Sui, X.; Daniel Wagner, H.; Dvir, T., Spring-like fibers for cardiac tissue engineering. *Biomaterials* 2013, 34 (34), 8599-606.
83. Jacot, J. G.; McCulloch, A. D.; Omens, J. H., Substrate stiffness affects the functional maturation of neonatal rat ventricular myocytes. *Biophysical journal* 2008, 95 (7), 3479-87.
84. Ma, Z.; Koo, S.; Finnegan, M. A.; Loskill, P.; Huebsch, N.; Marks, N. C.; Conklin, B. R.; Grigoropoulos, C. P.; Healy, K. E., Three-dimensional filamentous human diseased cardiac tissue model. *Biomaterials* 2014, 35 (5), 1367-77.
85. Sekine, H.; Shimizu, T.; Hobo, K.; Sekiya, S.; Yang, J.; Yamato, M.; Kurosawa, H.; Kobayashi, E.; Okano, T., Endothelial cell coculture within tissue-engineered cardiomyocyte sheets enhances neovascularization and improves cardiac function of ischemic hearts. *Circulation* 2008, 118 (14 Suppl), S145-52.
86. Shimizu, T.; Sekine, H.; Isoi, Y.; Yamato, M.; Kikuchi, A.; Okano, T., Long-term survival and growth of pulsatile myocardial tissue grafts engineered by the layering of cardiomyocyte sheets. *Tissue engineering* 2006, 12 (3), 499-507.
87. Masuda, S.; Shimizu, T., Three-dimensional cardiac tissue fabrication based on cell sheet technology. *Adv Drug Deliv Rev* 2016, 96, 103-9.
88. Ott, H. C.; Matthiesen, T. S.; Goh, S. K.; Black, L. D.; Kren, S. M.; Netoff, T. I.; Taylor, D. A., Perfusion-decellularized matrix: using nature's platform to engineer a bioartificial heart. *Nature medicine* 2008, 14 (2), 213-21.
89. Robertson, M. J.; Dries-Devlin, J. L.; Kren, S. M.; Burchfield, J. S.; Taylor, D. A., Optimizing recellularization of whole decellularized heart extracellular matrix. *PLoS one* 2014, 9 (2), e90406.
90. Song, J. J.; Ott, H. C., Organ engineering based on decellularized matrix scaffolds. *Trends in molecular medicine* 2011, 17 (8), 424-32.
91. Shimizu, T.; Sekine, H.; Yang, J.; Isoi, Y.; Yamato, M.; Kikuchi, A.; Kobayashi, E.; Okano, T., Polysurgery of cell sheet grafts overcomes diffusion limits to produce thick, vascularized myocardial tissues. *FASEB J* 2006, 20 (6), 708-10.
92. Jawad, H.; Lyon, A. R.; Harding, S. E.; Ali, N. N.; Boccaccini, A. R., Myocardial tissue engineering. *British medical bulletin* 2008, 87, 31-47.
93. Kaiser, N. J.; Coulombe, K. L., Physiologically inspired cardiac scaffolds for tailored in vivo function and heart regeneration. *Biomedical materials* 2015, 10 (3), 034003.
94. Kochupura, P. V.; Azeloglu, E. U.; Kelly, D. J.; Doronin, S. V.; Badylak, S. F.; Krukenkamp, I. B.; Cohen, I. S.; Gaudette, G. R., Tissue-engineered myocardial patch derived from extracellular matrix provides regional mechanical function. *Circulation* 2005, 112 (9 Suppl), I144-9.
95. Robinson, K. A.; Li, J.; Mathison, M.; Redkar, A.; Cui, J.; Chronos, N. A.; Matheny, R. G.; Badylak, S. F., Extracellular matrix scaffold for cardiac repair. *Circulation* 2005, 112 (9 Suppl), I135-43.
96. Yanagawa, B.; Rao, V.; Yau, T. M.; Cusimano, R. J., Initial experience with intraventricular repair using CorMatrix extracellular matrix. *Innovations (Phila)* 2013, 8 (5), 348-52.

97. Dobner, S.; Bezuidenhout, D.; Govender, P.; Zilla, P.; Davies, N., A synthetic non-degradable polyethylene glycol hydrogel retards adverse post-infarct left ventricular remodeling. *J Card Fail* 2009, 15 (7), 629-36.
98. Badylak, S.; Obermiller, J.; Geddes, L.; Matheny, R., Extracellular matrix for myocardial repair. *Heart Surg Forum* 2003, 6 (2), E20-6.
99. Okada, M.; Payne, T. R.; Oshima, H.; Momoi, N.; Tobita, K.; Huard, J., Differential efficacy of gels derived from small intestinal submucosa as an injectable biomaterial for myocardial infarct repair. *Biomaterials* 2010, 31 (30), 7678-83.
100. Hogan, M.; Mohamed, M.; Tao, Z. W.; Gutierrez, L.; Birla, R., Establishing the Framework to Support Bioartificial Heart Fabrication Using Fibrin-Based Three-Dimensional Artificial Heart Muscle. *Artificial organs* 2014, 61 (4), 429-36.
101. Remlinger, N. T.; Gilbert, T. W.; Yoshida, M.; Guest, B. N.; Hashizume, R.; Weaver, M. L.; Wagner, W. R.; Brown, B. N.; Tobita, K.; Wearden, P. D., Urinary bladder matrix promotes site appropriate tissue formation following right ventricle outflow tract repair. *Organogenesis* 2013, 9 (3), 149-60.
102. Zhang, G.; Hu, Q.; Braunlin, E. A.; Suggs, L. J.; Zhang, J., Enhancing efficacy of stem cell transplantation to the heart with a PEGylated fibrin biomatrix. *Tissue engineering. Part A* 2008, 14 (6), 1025-36.
103. Moroni, F.; Mirabella, T., Decellularized matrices for cardiovascular tissue engineering. *Am J Stem Cells* 2014, 3 (1), 1-20.
104. Rana, D.; Zreiqat, H.; Benkirane-Jessel, N.; Ramakrishna, S.; Ramalingam, M., Development of decellularized scaffolds for stem cell-driven tissue engineering. *Journal of tissue engineering and regenerative medicine* 2015.
105. Lopes, S. A.; Costa, F. D.; Paula, J. B.; Dhomen, P.; Phol, F.; Vilani, R.; Roderjan, J. G.; Vieira, E. D., Decellularized heterografts versus cryopreserved homografts: experimental study in sheep model. *Rev Bras Cir Cardiovasc* 2009, 24 (1), 15-22.
106. Gui, L.; Muto, A.; Chan, S. A.; Breuer, C. K.; Niklason, L. E., Development of decellularized human umbilical arteries as small-diameter vascular grafts. *Tissue engineering. Part A* 2009, 15 (9), 2665-76.
107. Leor, J.; Amsalem, Y.; Cohen, S., Cells, scaffolds, and molecules for myocardial tissue engineering. *Pharmacol Ther* 2005, 105 (2), 151-63.
108. Badylak, S. F.; Tullius, R.; Kokini, K.; Shelbourne, K. D.; Klootwyk, T.; Voytik, S. L.; Kraine, M. R.; Simmons, C., The use of xenogeneic small intestinal submucosa as a biomaterial for Achilles tendon repair in a dog model. *Journal of biomedical materials research* 1995, 29 (8), 977-85.
109. Crapo, P. M.; Gilbert, T. W.; Badylak, S. F., An overview of tissue and whole organ decellularization processes. *Biomaterials* 2011, 32 (12), 3233-43.
110. Lu, T. Y.; Lin, B.; Kim, J.; Sullivan, M.; Tobita, K.; Salama, G.; Yang, L., Repopulation of decellularized mouse heart with human induced pluripotent stem cell-derived cardiovascular progenitor cells. *Nature communications* 2013, 4, 2307.
111. Guyette, J. P.; Charest, J. M.; Mills, R. W.; Jank, B. J.; Moser, P. T.; Gilpin, S. E.; Gershlak, J. R.; Okamoto, T.; Gonzalez, G.; Milan, D. J.; Gaudette, G. R.; Ott, H. C., Bioengineering Human Myocardium on Native Extracellular Matrix. *Circulation research* 2016, 118 (1), 56-72.
112. Okano, T.; Yamada, N.; Sakai, H.; Sakurai, Y., A novel recovery system for cultured cells using plasma-treated polystyrene dishes grafted with poly(N-isopropylacrylamide). *Journal of biomedical materials research* 1993, 27 (10), 1243-51.
113. Kushida, A.; Yamato, M.; Konno, C.; Kikuchi, A.; Sakurai, Y.; Okano, T., Decrease in culture temperature releases monolayer endothelial cell sheets together with deposited fibronectin matrix from temperature-responsive culture surfaces. *Journal of biomedical materials research* 1999, 45 (4), 355-62.
114. Shimizu, T.; Yamato, M.; Akutsu, T.; Shibata, T.; Isoi, Y.; Kikuchi, A.; Umezu, M.; Okano, T., Electrically communicating three-dimensional cardiac tissue mimic fabricated by layered cultured cardiomyocyte sheets. *Journal of biomedical materials research* 2002, 60 (1), 110-7.

115. Shimizu, T.; Yamato, M.; Isoi, Y.; Akutsu, T.; Setomaru, T.; Abe, K.; Kikuchi, A.; Umezu, M.; Okano, T., Fabrication of pulsatile cardiac tissue grafts using a novel 3-dimensional cell sheet manipulation technique and temperature-responsive cell culture surfaces. *Circulation research* **2002**, *90* (3), e40.
116. Haraguchi, Y.; Shimizu, T.; Yamato, M.; Kikuchi, A.; Okano, T., Electrical coupling of cardiomyocyte sheets occurs rapidly via functional gap junction formation. *Biomaterials* **2006**, *27* (27), 4765-74.
117. Sawa, Y.; Miyagawa, S.; Sakaguchi, T.; Fujita, T.; Matsuyama, A.; Saito, A.; Shimizu, T.; Okano, T., Tissue engineered myoblast sheets improved cardiac function sufficiently to discontinue LVAS in a patient with DCM: report of a case. *Surgery today* **2012**, *42* (2), 181-4.
118. Menasche, P.; Hagege, A. A.; Vilquin, J. T.; Desnos, M.; Abergel, E.; Pouzet, B.; Bel, A.; Sarateanu, S.; Scorsin, M.; Schwartz, K.; Bruneval, P.; Benbunan, M.; Marolleau, J. P.; Duboc, D., Autologous skeletal myoblast transplantation for severe postinfarction left ventricular dysfunction. *Journal of the American College of Cardiology* **2003**, *41* (7), 1078-83.
119. Akhyari, P.; Kamiya, H.; Haverich, A.; Karck, M.; Lichtenberg, A., Myocardial tissue engineering: the extracellular matrix. *Eur J Cardiothorac Surg* **2008**, *34* (2), 229-41.
120. Bursac, N.; Papadaki, M.; Cohen, R. J.; Schoen, F. J.; Eisenberg, S. R.; Carrier, R.; Vunjak-Novakovic, G.; Freed, L. E., Cardiac muscle tissue engineering: toward an in vitro model for electrophysiological studies. *The American journal of physiology* **1999**, *277* (2 Pt 2), H433-44.
121. Ke, Q.; Yang, Y.; Rana, J. S.; Chen, Y.; Morgan, J. P.; Xiao, Y. F., Embryonic stem cells cultured in biodegradable scaffold repair infarcted myocardium in mice. *Sheng Li Xue Bao* **2005**, *57* (6), 673-81.
122. Kellar, R. S.; Landeen, L. K.; Shepherd, B. R.; Naughton, G. K.; Ratcliffe, A.; Williams, S. K., Scaffold-based three-dimensional human fibroblast culture provides a structural matrix that supports angiogenesis in infarcted heart tissue. *Circulation* **2001**, *104* (17), 2063-8.
123. Thai, H. M.; Juneman, E.; Lancaster, J.; Hagerty, T.; Do, R.; Castellano, L.; Kellar, R.; Williams, S.; Sethi, G.; Schmelz, M.; Gaballa, M.; Goldman, S., Implantation of a three-dimensional fibroblast matrix improves left ventricular function and blood flow after acute myocardial infarction. *Cell transplantation* **2009**, *18* (3), 283-95.
124. Piao, H.; Kwon, J. S.; Piao, S.; Sohn, J. H.; Lee, Y. S.; Bae, J. W.; Hwang, K. K.; Kim, D. W.; Jeon, O.; Kim, B. S.; Park, Y. B.; Cho, M. C., Effects of cardiac patches engineered with bone marrow-derived mononuclear cells and PGCL scaffolds in a rat myocardial infarction model. *Biomaterials* **2007**, *28* (4), 641-9.
125. Chen, Q. Z.; Bismarck, A.; Hansen, U.; Junaid, S.; Tran, M. Q.; Harding, S. E.; Ali, N. N.; Boccaccini, A. R., Characterisation of a soft elastomer poly(glycerol sebacate) designed to match the mechanical properties of myocardial tissue. *Biomaterials* **2008**, *29* (1), 47-57.
126. Stuckey, D. J.; Ishii, H.; Chen, Q. Z.; Boccaccini, A. R.; Hansen, U.; Carr, C. A.; Roether, J. A.; Jawad, H.; Tyler, D. J.; Ali, N. N.; Clarke, K.; Harding, S. E., Magnetic resonance imaging evaluation of remodeling by cardiac elastomeric tissue scaffold biomaterials in a rat model of myocardial infarction. *Tissue engineering. Part A* **2010**, *16* (11), 3395-402.
127. Jin, J.; Jeong, S. I.; Shin, Y. M.; Lim, K. S.; Shin, H.; Lee, Y. M.; Koh, H. C.; Kim, K. S., Transplantation of mesenchymal stem cells within a poly(lactide-co-epsilon-caprolactone) scaffold improves cardiac function in a rat myocardial infarction model. *Eur J Heart Fail* **2009**, *11* (2), 147-53.
128. Ye, X.; Lu, L.; Kolewe, M. E.; Hearon, K.; Fischer, K. M.; Coppeta, J.; Freed, L. E., Scalable units for building cardiac tissue. *Advanced materials* **2014**, *26* (42), 7202-8.
129. Zhang, B.; Montgomery, M.; Davenport-Huyer, L.; Korolj, A.; Radisic, M., Platform technology for scalable assembly of instantaneously functional mosaic tissues. *Sci Adv* **2015**, *1* (7), e1500423.
130. Causa, F.; Netti, P. A.; Ambrosio, L., A multi-functional scaffold for tissue regeneration: the need to engineer a tissue analogue. *Biomaterials* **2007**, *28* (34), 5093-9.
131. Jackman, C. P.; Carlson, A. L.; Bursac, N., Dynamic culture yields engineered myocardium with near-adult functional output. *Biomaterials* **2016**, *111*, 66-79.

132. Zimmermann, W. H.; Melnychenko, I.; Eschenhagen, T., Engineered heart tissue for regeneration of diseased hearts. *Biomaterials* 2004, 25 (9), 1639-47.
133. Zimmermann, W. H.; Melnychenko, I.; Wasmeier, G.; Didie, M.; Naito, H.; Nixdorff, U.; Hess, A.; Budinsky, L.; Brune, K.; Michaelis, B.; Dhein, S.; Schwoerer, A.; Ehmke, H.; Eschenhagen, T., Engineered heart tissue grafts improve systolic and diastolic function in infarcted rat hearts. *Nature medicine* 2006, 12 (4), 452-8.
134. Chachques, J. C.; Trainini, J. C.; Lago, N.; Cortes-Morichetti, M.; Schussler, O.; Carpentier, A., Myocardial Assistance by Grafting a New Bioartificial Upgraded Myocardium (MAGNUM trial): clinical feasibility study. *Ann Thorac Surg* 2008, 85 (3), 901-8.
135. Radisic, M.; Park, H.; Shing, H.; Consi, T.; Schoen, F. J.; Langer, R.; Freed, L. E.; Vunjak-Novakovic, G., Functional assembly of engineered myocardium by electrical stimulation of cardiac myocytes cultured on scaffolds. *Proceedings of the National Academy of Sciences of the United States of America* 2004, 101 (52), 18129-34.
136. Fink, C.; Ergun, S.; Kralisch, D.; Remmers, U.; Weil, J.; Eschenhagen, T., Chronic stretch of engineered heart tissue induces hypertrophy and functional improvement. *FASEB J* 2000, 14 (5), 669-79.
137. Roberts, M. A.; Tran, D.; Coulombe, K. L.; Razumova, M.; Regnier, M.; Murry, C. E.; Zheng, Y., Stromal Cells in Dense Collagen Promote Cardiomyocyte and Microvascular Patterning in Engineered Human Heart Tissue. *Tissue engineering. Part A* 2016, 22 (7-8), 633-44.
138. Stoppel, W. L.; Hu, D.; Domian, I. J.; Kaplan, D. L.; Black, L. D., 3rd, Anisotropic silk biomaterials containing cardiac extracellular matrix for cardiac tissue engineering. *Biomedical materials* 2015, 10 (3), 034105.
139. Thompson, W. D.; Smith, E. B.; Stirk, C. M.; Marshall, F. I.; Stout, A. J.; Kocchar, A., Angiogenic activity of fibrin degradation products is located in fibrin fragment E. *The Journal of pathology* 1992, 168 (1), 47-53.
140. Ryu, J. H.; Kim, I. K.; Cho, S. W.; Cho, M. C.; Hwang, K. K.; Piao, H.; Piao, S.; Lim, S. H.; Hong, Y. S.; Choi, C. Y.; Yoo, K. J.; Kim, B. S., Implantation of bone marrow mononuclear cells using injectable fibrin matrix enhances neovascularization in infarcted myocardium. *Biomaterials* 2005, 26 (3), 319-26.
141. Bian, W.; Badie, N.; Himel, H. D. t.; Bursac, N., Robust T-tubulation and maturation of cardiomyocytes using tissue-engineered epicardial mimetics. *Biomaterials* 2014, 35 (12), 3819-28.
142. Lluica-Valldeperas, A.; Soler-Botija, C.; Galvez-Monton, C.; Roura, S.; Prat-Vidal, C.; Perea-Gil, I.; Sanchez, B.; Bragos, R.; Vunjak-Novakovic, G.; Bayes-Genis, A., Electromechanical Conditioning of Adult Progenitor Cells Improves Recovery of Cardiac Function After Myocardial Infarction. *Stem cells translational medicine* 2016.
143. Sakai, T.; Li, R. K.; Weisel, R. D.; Mickle, D. A.; Kim, E. T.; Jia, Z. Q.; Yau, T. M., The fate of a tissue-engineered cardiac graft in the right ventricular outflow tract of the rat. *The Journal of thoracic and cardiovascular surgery* 2001, 121 (5), 932-42.
144. Leor, J.; Abouafia-Etzion, S.; Dar, A.; Shapiro, L.; Barbash, I. M.; Battler, A.; Granot, Y.; Cohen, S., Bioengineered cardiac grafts: A new approach to repair the infarcted myocardium? *Circulation* 2000, 102 (19 Suppl 3), III56-61.
145. Entcheva, E.; Bien, H.; Yin, L.; Chung, C. Y.; Farrell, M.; Kostov, Y., Functional cardiac cell constructs on cellulose-based scaffolding. *Biomaterials* 2004, 25 (26), 5753-62.
146. Blan, N. R.; Birla, R. K., Design and fabrication of heart muscle using scaffold-based tissue engineering. *Journal of biomedical materials research. Part A* 2008, 86 (1), 195-208.
147. Khademhosseini, A.; Eng, G.; Yeh, J.; Kucharczyk, P. A.; Langer, R.; Vunjak-Novakovic, G.; Radisic, M., Microfluidic patterning for fabrication of contractile cardiac organoids. *Biomedical microdevices* 2007, 9 (2), 149-57.
148. Jawad, H.; Ali, N. N.; Lyon, A. R.; Chen, Q. Z.; Harding, S. E.; Boccaccini, A. R., Myocardial tissue engineering: a review. *Journal of tissue engineering and regenerative medicine* 2007, 1 (5), 327-42.
149. Lisi, A.; Briganti, E.; Ledda, M.; Losi, P.; Grimaldi, S.; Marchese, R.; Soldani, G., A combined synthetic-fibrin scaffold supports growth and cardiomyogenic commitment of human placental derived stem cells. *PLoS one* 2012, 7 (4), e34284.

150. Mukherjee, S.; Venugopal, J. R.; Ravichandran, R.; Ramakrishna, S.; Raghunath, M., Evaluation of the Biocompatibility of PLACL/Collagen Nanostructured Matrices with Cardiomyocytes as a Model for the Regeneration of Infarcted Myocardium. *Advanced Functional Materials* 2011, 21 (12), 2291-2300.
151. Boccaccini, A. R.; Harding, S. E., *Myocardial tissue engineering*. Springer: Heidelberg, 2011; p x, 268 p.
152. Grasman, J. M.; Pumphrey, L. M.; Dunphy, M.; Perez-Rogers, J.; Pins, G. D., Static axial stretching enhances the mechanical properties and cellular responses of fibrin microthreads. *Acta biomaterialia* 2014, 10 (10), 4367-76.
153. Guyette, J. P.; Fakhazadeh, M.; Burford, E. J.; Tao, Z. W.; Pins, G. D.; Rolle, M. W.; Gaudette, G. R., A novel suture-based method for efficient transplantation of stem cells. *Journal of biomedical materials research. Part A* 2013, 101 (3), 809-18.
154. Page, R. L.; Malcuit, C.; Vilner, L.; Vojtic, I.; Shaw, S.; Hedblom, E.; Hu, J.; Pins, G. D.; Rolle, M. W.; Dominko, T., Restoration of skeletal muscle defects with adult human cells delivered on fibrin microthreads. *Tissue engineering. Part A* 2011, 17 (21-22), 2629-40.
155. Altman, G. H.; Diaz, F.; Jakuba, C.; Calabro, T.; Horan, R. L.; Chen, J. S.; Lu, H.; Richmond, J.; Kaplan, D. L., Silk-based biomaterials. *Biomaterials* 2003, 24 (3), 401-416.
156. Altman, G. H.; Horan, R. L.; Lu, H. H.; Moreau, J.; I, M.; Richmond, J. C.; Kaplan, D. L., Silk matrix for tissue engineered anterior cruciate ligaments. *Biomaterials* 2002, 23 (20), 4131-4141.
157. Cornwell, K. G.; Lei, P.; Andreadis, S. T.; Pins, G. D., Crosslinking of discrete self-assembled collagen threads: Effects on mechanical strength and cell-matrix interactions. *Journal of Biomedical Materials Research Part A* 2007, 80A (2), 362-371.
158. Gentleman, E.; Lay, A. N.; Dickerson, D. A.; Nauman, E. A.; Livesay, G. A.; Dee, K. C., Mechanical characterization of collagen fibers and scaffolds for tissue engineering. *Biomaterials* 2003, 24 (21), 3805-3813.
159. Funakoshi, T.; Majima, T.; Iwasaki, N.; Suenaga, N.; Sawaguchi, N.; Shimode, K.; Minami, A.; Harada, K.; Nishimura, S., Application of tissue engineering techniques for rotator cuff regeneration using a chitosan-based hyaluronan hybrid fiber scaffold. *Am J Sport Med* 2005, 33 (8), 1193-1201.
160. Funakoshi, T.; Majima, T.; Iwasaki, N.; Yamane, S.; Masuko, T.; Minami, A.; Harada, K.; Tamura, H.; Tokura, S.; Nishimura, S. I., Novel chitosan-based hyaluronan hybrid polymer fibers as a scaffold in ligament tissue engineering. *Journal of Biomedical Materials Research Part A* 2005, 74A (3), 338-346.
161. Irie, T.; Majima, T.; Sawaguchi, N.; Funakoshi, T.; Nishimura, S.; Minami, A., Biomechanical and histologic evaluation of tissue engineered ligaments using chitosan and hyaluronan hybrid polymer fibers: A rabbit medial collateral ligament reconstruction model. *Journal of Biomedical Materials Research Part A* 2011, 97A (2), 111-117.
162. Tao, Z. W.; Favreau, J. T.; Guyette, J. P.; Hansen, K. J.; Lessard, J.; Burford, E.; Pins, G. D.; Gaudette, G. R., Delivering stem cells to the healthy heart on biological sutures: effects on regional mechanical function. *Journal of tissue engineering and regenerative medicine* 2014.
163. Proulx, M. K.; Carey, S. P.; Ditroia, L. M.; Jones, C. M.; Fakhazadeh, M.; Guyette, J. P.; Clement, A. L.; Orr, R. G.; Rolle, M. W.; Pins, G. D.; Gaudette, G. R., Fibrin microthreads support mesenchymal stem cell growth while maintaining differentiation potential. *Journal of biomedical materials research. Part A* 2011, 96 (2), 301-12.
164. Bhana, B.; Iyer, R. K.; Chen, W. L.; Zhao, R.; Sider, K. L.; Likhitpanichkul, M.; Simmons, C. A.; Radisic, M., Influence of substrate stiffness on the phenotype of heart cells. *Biotechnology and bioengineering* 2010, 105 (6), 1148-60.
165. El-Sherbiny, I. M.; Yacoub, M. H., Hydrogel scaffolds for tissue engineering: Progress and challenges. *Global cardiology science & practice* 2013, 2013 (3), 316-42.
166. Tandon, V.; Zhang, B.; Radisic, M.; Murthy, S. K., Generation of tissue constructs for cardiovascular regenerative medicine: from cell procurement to scaffold design. *Biotechnology advances* 2013, 31 (5), 722-35.

Chapter 3: Design of a Fibrin Microthread-Based Composite Layer for Use in a Cardiac Patch¹

Reproduced with permission from Chrobak, M. O.; Hansen, K. J.; Gershlak, J. R.; Vratsanos, M.; Kanellias, M.; Gaudette, G. R.; Pins, G. D., Design of a fibrin microthread-based composite layer for use in a cardiac patch. *ACS Biomaterials Science & Engineering* 2017. 3 (7): 1394-1403. Copyright 2016 American Chemical Society.

3.1 INTRODUCTION

Cardiovascular diseases are the leading causes of death globally with 500,000 new cases of heart failure diagnosed in the United States alone.² The major condition leading to heart failure is myocardial infarction (MI), damage of cardiac tissue resulting from oxygen deprivation ultimately reducing functionality. The heart has limited capacity to regenerate damaged myocardium and restore mechanical function lost following an MI.³ As such, a therapy that promotes functional myocardial regeneration is greatly needed.

Cardiac patches can be used to replace scar tissue in the heart and are especially useful in repairing ventricular aneurysms. However, currently available scaffolds are acellular and only provide passive structural support.⁴⁻⁵ Actively contracting cardiac scaffolds may provide better options for patients, as they may contribute to the active mechanical function lost after an MI. Current strategies to promote active regeneration of damaged myocardium use scaffolds composed of natural materials,⁶⁻¹² synthetic materials,¹³⁻¹⁵ extracellular matrix,¹⁶⁻¹⁷ or decellularized tissues.¹⁸⁻¹⁹ Sheets of cardiac “progenitor cells,” or engineered tissues that integrate the promising functions of biomaterials and stem cell therapies, are being investigated as well. Modular scaffolds that integrate myocardial components of the tissue into scalable units²⁰⁻²¹ to guide myocardial regeneration are also being considered. While various studies have shown that engineered scaffolds are capable of contraction,^{6-7, 11, 18, 22} and of providing moderate increases in mechanical function of the injured heart,^{11, 16, 23} there is still a need to develop a functional, engineered cardiac patch that readily integrates with the surrounding tissue to promote the regeneration of myocardial tissue with physiologically relevant contractility.^{7, 24}

Fibrin-based hydrogels have been extensively researched in the field of cardiac engineering. Cell-seeded hydrogels have demonstrated functionality such as high twitch forces comparable to

neonatal rat myocardium (8.9 ± 1.1 and 7.8 - 8.7 mN/mm², respectively).²⁵ However, hydrogels are typically mechanically weak²⁶⁻²⁷ and ultimately may fail in the dynamic loading environment of the heart.^{26, 28} Thus, it is critical for myocardial regeneration strategies that a cardiac patch be able to mechanically²⁹ and functionally integrate with native myocardium.^{7, 24} To achieve this, a cardiac patch should mimic the properties of native myocardium, a highly aligned tissue with modulus values ranging from 20 to 500 kPa.²⁴

In this chapter, we report the development of discrete layers of a microthread-based composite scaffold that can be fabricated into engineered myocardial tissue with precisely designed structural mechanical properties. Microthreads derived from natural biopolymers, such as fibrin, have been investigated for a wide range of tissue engineering applications.³⁰ These microthreads exhibit tunable mechanical properties³¹ and drive cellular orientation.³² Here, we hypothesize that fibrin microthreads can be strategically combined with fibrin-based hydrogels to create a composite layer that will enable the design of a scaffold that provides mechanical properties similar to that of native myocardium, supports cell contractility, and promotes cellular orientation. To test this hypothesis, we systematically varied the fibrin microthread volume fractions in composite layers and evaluated the moduli of the composite scaffolds. We incorporated rat neonatal ventricular myocytes into the composite layers and analyzed the cell-mediated contractile behavior of the scaffolds by measuring contractile strains and contractile frequencies. Finally, we evaluated the effect of the microthreads on cell alignment by measuring the nuclear orientation of incorporated cells in the composite scaffolds. Ultimately, we envision that these fibrin composite layers will enable the development of an implantable, multilayered cardiac patch to facilitate the regeneration of damaged ventricular myocardium.

3.2 MATERIALS and METHODS

3.2.1 Fabrication of Fibrin Microthread-Based Composite Scaffolds

To generate biomimetic composite layers, varied densities of fibrin microthreads were precisely aligned and integrated into fibrin hydrogels (**Figure 3.1**).

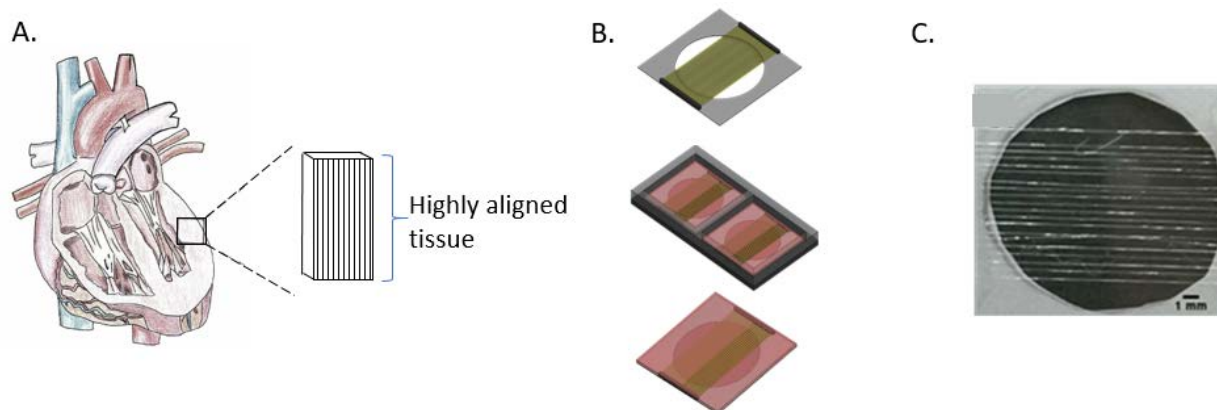


Figure 3.1. Fabrication of a biomimetic composite cardiac patch. Ventricular myocardium is arranged in highly aligned layers (A). To fabricate an aligned composite layer, fibrin microthreads are organized (B, C) and embedded in a fibrin hydrogel (B). Ultimately, we anticipate that these individual layers will be stacked to form a multilayered scaffold that mimics native myocardium.

3.2.1.1 Microthread Extrusion

Fibrin microthreads were generated through the co-extrusion of fibrinogen and thrombin solutions using techniques described previously.³¹⁻³⁴ Briefly, fibrinogen isolated from bovine plasma (Sigma, St. Louis, MO) was dissolved in HEPES (N-[2-Hydroxyethyl] piperazine-N'-[2-ethanesulfonic acid]) buffered saline (HBS, 20 mM HEPES, 0.9% NaCl; pH 7.4) at a concentration of 70 mg/mL. The solution was stored at -20°C until use. Thrombin from bovine plasma (Sigma) was dissolved in HBS at 40 U/mL and stored at -20°C until use.

To generate microthreads, fibrinogen and thrombin solutions were thawed to room temperature. A 40 mM solution of CaCl₂ was mixed with the thrombin solution resulting in a working solution of 6 U/mL. Equal volumes of fibrinogen and thrombin/CaCl₂ solutions were loaded into separate 1 mL syringes. A blending applicator tip (Micromedics Inc., St. Paul, MN) was connected to the loaded 1 mL syringes. The solutions were mixed in the applicator tip and extruded through polyethylene tubing (BD, Sparks, MD) with an inner diameter of 0.86 mm into a buffer bath of 10 mM HEPES (pH 7.4). Microthreads were extruded into a Teflon-coated pan at a flow rate of 0.225 mL/min using a dual syringe pump. Following a 10-15 minute polymerization time, the scaffolds were carefully removed and stretched to ~150% of their original length to create a high strength microthread, and hung to dry under the tension of their own weight.³²

3.2.1.2 Fibrin Microthread Organization

A custom fibrin microthread spacer was used to align fibrin microthreads at set distances to ensure a uniform layer (**Figure 3.2A**). The device has evenly spaced ridges with ports and is coupled to a house vacuum enabling the placement and maintenance of threads in configurations with defined spacing. Layers were organized with either 5, 10, or 20 threads across a 1 cm length to vary the volume fraction in the composite (**Figure 3.2B**). Once organized, threads were mounted along the edge, the vacuum was turned off, and aligned microthreads were transferred and secured to vellum frames with precut windows using medical grade silicone adhesive.

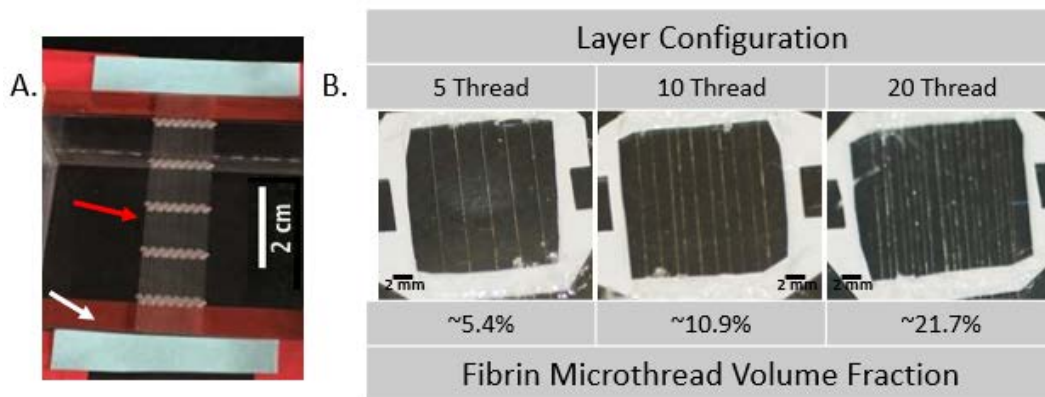


Figure 3.2. Fibrin microthread spacer device. Fibrin microthreads are organized using a custom microthread spacer (A) by placing microthreads into grooves (red arrow). Microthreads are secured with frames following alignment (white arrow). By incorporating different thread counts into the layer, the volume fraction of fibrin microthreads is adjusted (B). Volume fractions were calculated with the assumptions that microthreads have a cylindrical shape, and the shape of the scaffolds are rectangular.

To evaluate the consistency of spacing for organized threads, 20 microthreads secured to vellum frames were divided into 9 segments (**Figure 3.3 A-C**), and imaged under 2X magnification. For each image, 3 regions (represented as lines in **Figure 3.3C**) were evaluated. For each region, distances between all threads were measured using ImageJ. To ensure results were not user-dependent, 4 different users generated samples using the spacing device. A total of 16 samples were analyzed. A one-way ANOVA was run to determine if statistical differences existed in thread spacings between users. Significance level was set to a p value of $p < 0.05$.

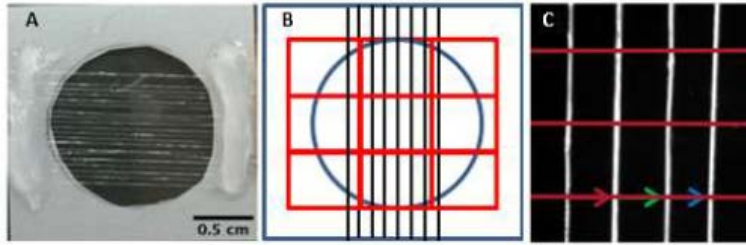


Figure 3.3. Evaluation of fibrin microthread spacing in composite layers. Twenty-thread fibrin based composite layers (A) were evaluated to determine thread spacing consistency. Samples were divided into 9 regions (B) and imaged under 2X magnification. For all 9 images, 3 regions were identified (red lines in C). For these regions, spacing between all threads was determined.

3.2.2 Mechanical Characterization of Fibrin Composite Layers

To predict the moduli of fibrin microthread-based composite layers with varying volume fractions of components, classical composite theory for aligned, fiber-reinforced composites was utilized. This theory enables the estimation of modulus of elasticity (E_{cl}) of a composite layer in the direction of alignment as shown in Equation 3.1,

$$E_{cl} = E_m V_m + E_f V_f \quad 3.1.$$

where E_m and E_f are the elastic moduli of the matrix and fibrous components, respectively and V_m and V_f are the volume fractions of the matrix and fibrous components, respectively.³⁵

Mechanical characterization of acellular fibrin composite layers was completed using a submerged, uniaxial tensile test. Fibrin composite layers were prepared using modified vellum frames that enabled the mechanical characterization of the scaffolds, independent of the frame. A hydrogel solution containing 1.6 U/mL thrombin and 3.1 mg/mL fibrinogen was combined and mixed on ice, cast over the vellum frames and spread using a pipette tip to provide an even layer. For a 144 mm² area, 150 uL of hydrogel solution was utilized. Following a 30 minute polymerization period, a laser displacement technique was used to measure the thickness of the composite layer in 3 places per sample.³⁶ These thicknesses were averaged together to obtain a representative measurement, and were used with the width of the sample to calculate the cross-sectional area, assuming a rectangular geometry. Samples were then secured in grips of a uniaxial testing machine (ElectroPuls E1000; Instron, Norwood, MA) and a 1 N load cell, with an initial gauge length of 13 mm. The sample and grips were submerged in a PBS bath, then uniaxially loaded until failure at a strain rate of 10 mm/min.³⁷ Force and displacement values were recorded continuously throughout the test at a frequency of 10 Hz. Prior to determining the modulus and

phase I and II maximum stress and strain values, all initial load and deformation values were zeroed to a baseline value at the onset of each test. Engineering stress was calculated as the amount of force recorded divided by the initial cross-sectional area. Strain was calculated as the increased extension from the initial length of the composite layer.

A MATLAB (MathWorks, Natick, MA) script was written to analyze the modulus of the layers. With aligned fiber-reinforced composites, there are generally two phases observable on stress strain curves.³⁵ For our analysis, we analyzed the slope of the stress strain curves in phase I (elastic deformation). This region is typically between 0-30% strain, a physiologically relevant strain regime as the average peak shortening in the midwall of the left ventricle is ~23 – 30%.³⁸⁻³⁹ Outliers were identified as any modulus value that was 1.5 times greater than the inner quartile range (IQR) for each sample set (average modulus $\pm 1.5 \times \text{IQR}$) and were subsequently removed from further analysis.³²

3.2.3 Cell Culture

3.2.3.1 Rat Neonatal Ventricular Myocyte (rNVM) Isolation

All animal experiments were performed under the guidance of and approved by the Institutional Animal Care and Use Committee at Worcester Polytechnic Institute. As previously described, cardiomyocytes were isolated from 2 and 3 day old neonatal Sprague Dawley rats (Charles River, Wilmington, MA).⁴⁰ In short, hearts were removed from the neonatal rat, ventricles were separated from atria, and then ventricles were minced into $\sim 1\text{mm}^2$ sized pieces. Ventricle pieces were digested at 37°C in type II collagenase (Thermo Fisher Scientific, Waltham, MA) serially in 7x7 minute digestions. To enrich the fraction of cardiac myocytes, one 45-minute pre-plating step was performed.⁴¹ Isolated cardiomyocytes were used immediately for experimental samples as described below.

3.2.3.2 Composite Layer Fabrication and Tissue Culture

To ensure that samples remained in the same orientation throughout culture for functional evaluations, a purpose-built culture dish and framing system was developed to maintain sample orientation throughout the culture period. For hydrogel casting, PDMS sheets were autoclaved and coated with sterile 1% Pluronic-F127 in DI water (Sigma, St. Louis, MO) solution for 1 hour.

Vellum frames with 5, 10 or 20 aligned threads, or without threads (hydrogel controls), were rehydrated in PBS for one hour, then placed on top of the coated PDMS immediately prior to gel casting. A hydrogel solution containing 4×10^6 cells/mL, 1.6 U/mL thrombin, and 3.1 mg/mL fibrinogen was combined and mixed on ice, cast over the vellum frames and spread using a pipette tip to provide an even layer. For a 144 mm^2 area, 150 μL of hydrogel solution was utilized. Samples polymerized in an incubator at 37°C for 30 minutes, then were moved into wells containing DMEM (Iscove's, VWR, Radnor, PA) supplemented with 10% fetal bovine serum (VWR) 2% heat inactivated horse serum (Fisher Scientific, Waltham, MA) 1% penicillin streptomycin (Thermo Fisher Scientific, Waltham, MA) 1% amphotericin B (Thermo Fisher Scientific), 0.5% gentamicin (Thermo Fisher Scientific), 1% glutamax (Thermo Fisher Scientific), 0.0007% B-mercaptoethanol (Thermo Fisher Scientific), 50 $\mu\text{g/mL}$ aprotinin, and 1.2 mM CaCl_2 and 0.8 mM MgCl_2 .

For cell culture controls, glass coverslips (10 x 10mm) (VWR) were coated with 0.7% gelatin in DI water (Sigma Aldrich) for 4 hours and secured to the bottom of wells in a 12 well plate using autoclaved vacuum grease. Cells were seeded on coverslips with 100 μL of cell suspension (2×10^6 cells/mL), incubated for 18 hours, rinsed and covered with medium for extended culture. All cell culture experiments were maintained for 14 days with medium changes every other day. For this work, individual composite layers were evaluated and were identified using the following nomenclature scheme:

5 Thread Composite Layers (5tC), 10 Thread Composite Layers (10tC), 20 Thread Composite Layers (20tC), Fibrin Gel Controls (FGC), or Gelatin-coated Coverslips (GCS).

3.2.4 *Cardiomyocyte Functional Analysis*

To evaluate cardiomyocyte functionality, spontaneous contractions were recorded at 60 frames per second with a high speed camera (HiSpec 4, Fastec Imaging Corp, San Diego, CA) attached to an inverted microscope (DMIL, Leica Microsystems, Buffalo Grove, IL) at 7, 10, and 14 days of culture. High density mapping (HDM), an optical technique used to evaluate regional mechanical function with high spatial resolution, was applied by selecting a region of interest (size dependent on contractile region) and dividing it into 16×16 pixel subwindows to track displacements of sequential frames over several images, with an 8 pixel shift and noise threshold of 1% strain.⁴²⁻⁴⁴ The displacement fields are used to determine maximum contractile strain,

average contractile strain, and frequency of contraction. To ensure representative data for each sample was obtained, samples were divided into quadrants and one region of interest was identified per quadrant per sample, per time point. Each sample represents the average value from multiple regions of interest at each time point.

3.2.5 Phenotypic Analyses

3.2.5.1 Immunostaining

To confirm the cardiomyocyte phenotype and evaluate alignment, cell-seeded constructs were immunostained to assess the sarcomeric structure of cardiomyocytes and the nuclear orientation of all cells incorporated into the layer. At day 14, samples were fixed with 4% paraformaldehyde, permeabilized with 0.1% Triton and blocked with 5% BSA in PBS. After blocking, tissues were incubated overnight at 4°C with mouse monoclonal to sarcomeric α -actinin primary antibody (Abcam, Cambridge, MA) in a blocking solution. Samples were rinsed in PBS and a secondary antibody (Goat anti-mouse Alexa Fluor 546, Life Technologies, Waltham, MA) was incubated at room temperature for 30 minutes. A Hoechst counterstain (Thermo Fisher Scientific) was incubated with the samples at room temperature for 10 minutes. Tissue samples were imaged using a confocal microscope (TCS SP5 Point Scanning Confocal, Leica, Germany). For each sample, 3 representative images of the width of the construct were obtained at 200X.

3.2.5.2 Analysis of Nuclear Alignment

To determine the alignment of cells within the composite layer relative to fibrin microthreads, fluorescent images were analyzed using ImageJ (NIH). For each condition, a total of 3 samples (9 representative images) were evaluated after 14 days in culture. A binary image from the blue channel (representing nuclear staining by Hoechst) was generated, and analyzed using the particle analysis function within the ImageJ software to obtain the orientation of the long axis of the nucleus with respect to the microthread. Nuclei that were on the edge of the image or in contact with other nuclei were excluded from analysis. All values were binned in 15° increments and plotted as a histogram to present the distribution of nuclear orientations observed for each group.

3.2.6 Statistical Analyses

All statistical analyses were performed using SigmaPlot 12.5 software, with $p < 0.05$ indicating a significant difference between groups. For contractile strains and frequencies, statistical analyses were performed using a two-way analysis of variance (ANOVA). For the uniaxial testing data, statistical analyses were performed using a one-way ANOVA. Holm-Sidak pairwise multiple comparison tests were performed for all post-hoc analyses with $p < 0.05$ indicating significant differences between samples. For functional data including maximum contractile strain, average contractile strain, and frequency of contraction data are reported as means \pm standard error. For the reported elastic modulus values, data are presented as means \pm standard deviation.

3.3 RESULTS

3.3.1 The Fabrication Method Developed for Composite Layers Enables Reproducible Spacing of Aligned Fibrin Microthreads.

Four users generated 20tC samples using the fibrin microthread spacer. Fibrin microthread spacing distances averaged 140 μm for each user, with a standard deviation of 21.74 μm , ~15.5% of the average spacing distance. The average thread separation distances for each user were compared with, a one-way ANOVA. This analysis demonstrated that no significant differences were observed, suggesting that the automated thread spacing system creates aligned microthread-based scaffolds with reproducible morphological properties.

3.3.2 The Modulus of a Composite Layer Can Be Tuned Through Modulation of the Fibrin Microthread Volume Fraction

The computational model using classic composite theory demonstrated that with an increasing volume fraction of fibrin microthreads there should be an increase in modulus of the composite layer. Predicted values ranged from 48 – 190 kPa with microthread volume fractions increasing from 2.2% to 8.6%. Assumptions included that the fibrin microthreads had a diameter of 130 μm and a stiffness value near 2.2 MPa,³² and that the hydrogel had a stiffness near 0.25 kPa.⁴⁵ As the number of fibrin microthreads doubled, the predicted moduli values approximately doubled as well. This trend is summarized in Table 3.1.

Table 3.1. Predicted moduli for fibrin composite layers with varying volume fractions of fibrin microthreads and fibrin hydrogel.

<i>Number of Threads</i>	<i>Volume Fraction of Threads</i>	<i>Volume Fraction of Gel</i>	<i>Predicted Modulus (kPa)</i>
5	2.2%	97.8%	48
10	4.3%	95.7%	95
20	8.6%	91.4%	190

Composite layers were evaluated using uniaxial tensile testing to determine the effect of fibrin microthread volume fractions on the moduli of the scaffolds. Aligned fibrous composite materials typically have two phases (**Figure 3.4A**).³⁵ Characteristic stress-strain curves for the composite layers showed the anticipated two phases followed by multiple points of failure as components of the composite failed (**Figure 3.4B**). Our analyses characterized the elastic deformation of the scaffolds (phase I) for calculating the modulus values of the composites (**Figure 3.4A**). Qualitative observations of uniaxial tensile tests suggest that the composite layers remain as one cohesive, integrated material upon full failure. As the number of fibrin microthreads was doubled, the moduli increased to slightly greater than double values. Significant differences in the elastic modulus values were observed between all groups (**Figure 3.4 C**) (5tC vs 10tC $p = 0.048$; 5tC vs 20tC $p < 0.001$; 10tC vs 20tC $p < 0.001$).

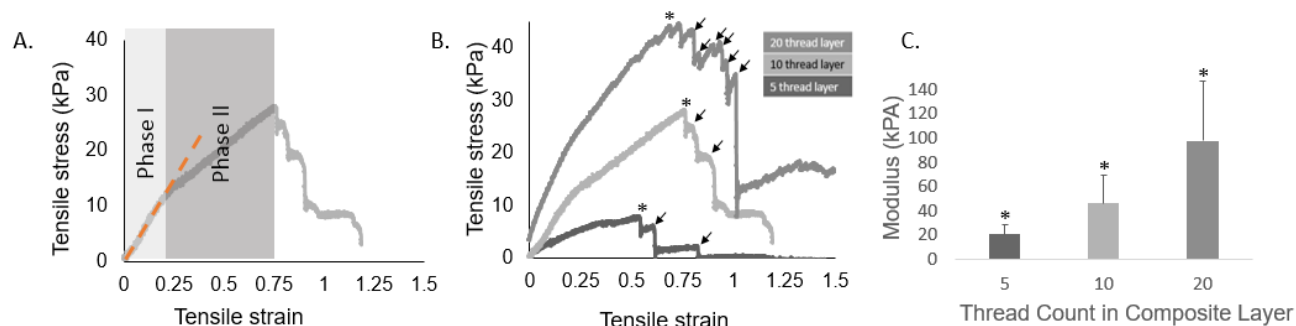


Figure 3.4. Fibrin microthread volume fraction can be used to mechanically tune a composite layer. Stress strain curves for composites generally have two phases (A). All modulus values were taken from phase I of the curves (dotted line in A). Characteristic stress strain curves of 5, 10, and 20 thread composite layers are shown in B. * marks first point of failure for each sample and arrows show subsequent microthread failure points. Modulus values were significantly different between each sample group (denoted with a *) as determined by a one-way ANOVA with Holm-Sidak post-hoc analysis, $p < 0.05$ (C).

The mechanical data from the tensile testing is further summarized in **Table 3.2**.

Table 3.2. Mechanical data from tensile testing evaluation of fibrin-based composite layers.

Composite Group	n	Tensile Stress (Phase I) (kPa)	Tensile Strain (Phase I) (mm/mm)	Elastic Modulus (kPa)		Tensile Stress (Phase II) (kPa)	Tensile Strain (Phase II) (mm/mm)
				Predicted	Measured		
5tC	15	12.9 ± 5.3 [‡] (p=0.002)	0.31 ± 0.08	48	20.6 ± 8.1* (10tC: p=0.048) (20tC: p<0.001)	23.2 ± 9.6 [‡] (p<0.001)	1.03 ± 0.25
10tC	12	13.6 ± 6.0 [‡] (p=0.005)	0.21 ± 0.06	95	46.4 ± 23.0* (5tC: p=0.048) (20tC: p<0.001)	42.1 ± 25.2 [‡] (p=0.007)	0.99 ± 0.34
20tC	12	27.7 ± 15.4	0.24 ± 0.09	190	97.5 ± 49.3* (5tC: p<0.001) (10tC: p<0.001)	83.0 ± 45.8	1.07 ± 0.22

[‡]: Significant difference from the 20tC group

*: Significant difference from all other groups

3.3.3 Cardiomyocyte Phenotype is Retained in Fibrin-Microthread Composite Layers

Rat neonatal cardiomyocytes were isolated and incorporated into fibrin-microthread composite layers with varied thread densities, fibrin hydrogels, or seeded onto gelatin coated coverslips. To ensure that the cells in the scaffolds maintained functional cardiomyocyte properties, sarcomeric α -actinin protein expression was evaluated with putative sarcomeric arrangement being considered a hallmark of functional cardiomyocytes.⁴⁶ For all groups, cells exhibited characteristic sarcomeric striations for the duration of the 14 day culture period, confirming that the cells in the composite scaffolds maintained phenotypic properties of cardiomyocytes (**Figure 3.5**).

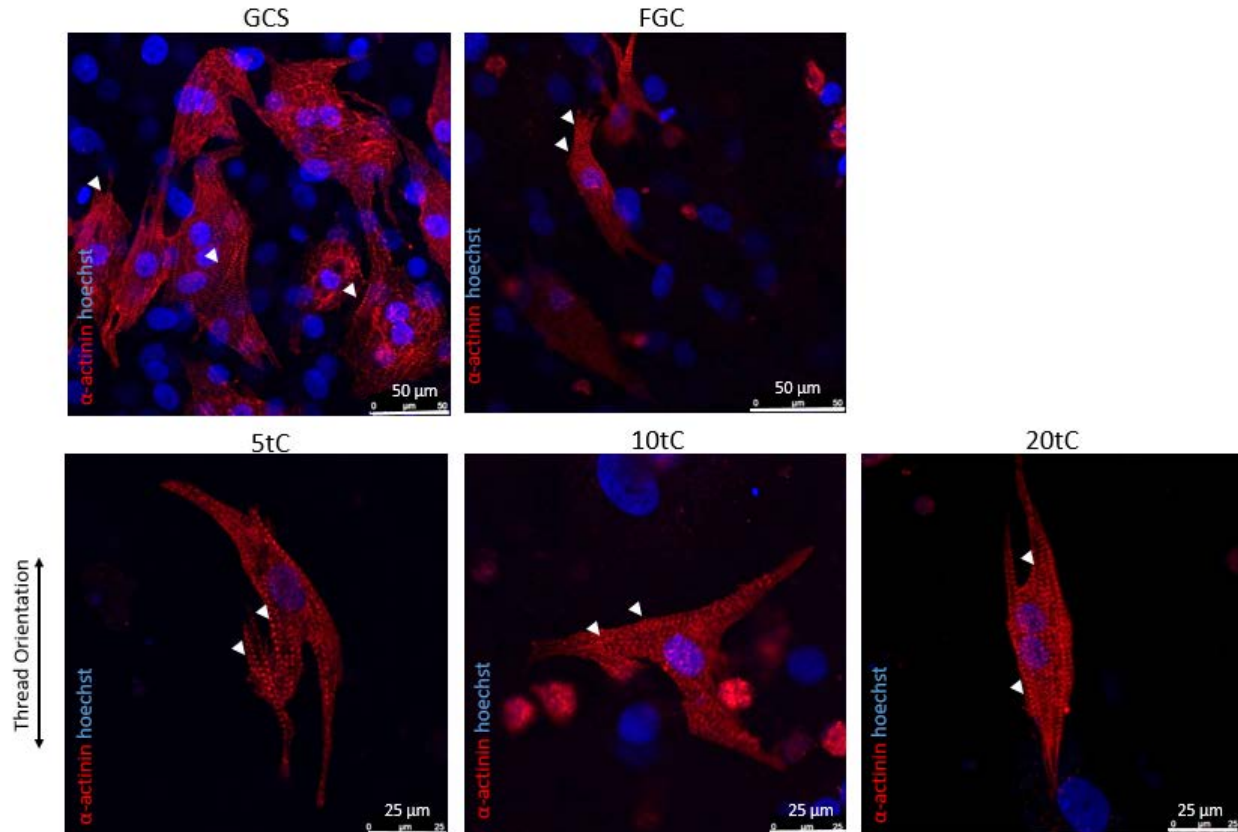


Figure 3.5. Striated phenotype of rat neonatal ventricular myocytes cultured in composite fibrin scaffolds. Cells were stained with sarcomeric α -actinin (red) and Hoechst (blue). All controls and test groups exhibited a striated pattern characteristic of functional cardiomyocytes. White arrows indicate α -actinin striations.

3.3.4 Functional Properties of Cardiomyocytes are Maintained in Fibrin Microthread-Based Composites

The active functional properties of cardiomyocytes were evaluated by measuring the maximum contractile strain, average contractile strain, and contraction frequency using HDM applied to high speed videos of contractile regions taken at 7, 10, and 14 days in culture (**Figure 3.6**). The maximum and average contractile strain measurements followed similar trends for all groups (**Figures 3.6A and B**). Only the 5tC group had a significant decrease in strain measurements between days 10 and 14 ($p=0.007$ for maximum contractile strain and $p=0.048$ for average contractile strain) (**Figure 3.6 A, B**). When comparing groups at each time point, all groups were significantly greater than the gelatin coated coverslips (GCS) at day 10 for both maximum and average contractile strains (for maximum contractile strains $p<0.001$ for 5tC, $p<0.001$ for 10tC, $p=0.044$ for 20tC, $p=0.010$ for FGC. For average contractile strains, $p=0.001$ for 5tC, $p=0.006$ for 10tC, $p=0.002$ for 20tC, $p=0.023$ for FGC) (**Figure 3.6 D, E**). Significant

differences were observed at day 7 for the average contractile strain, with FGC, 5tC, and 10tC exhibiting significantly greater ($p=0.006$ for 5tC, $p=0.006$ for 10tC, $p=0.023$ for FGC) average strains than GCS (**Figure 3.6 E**).

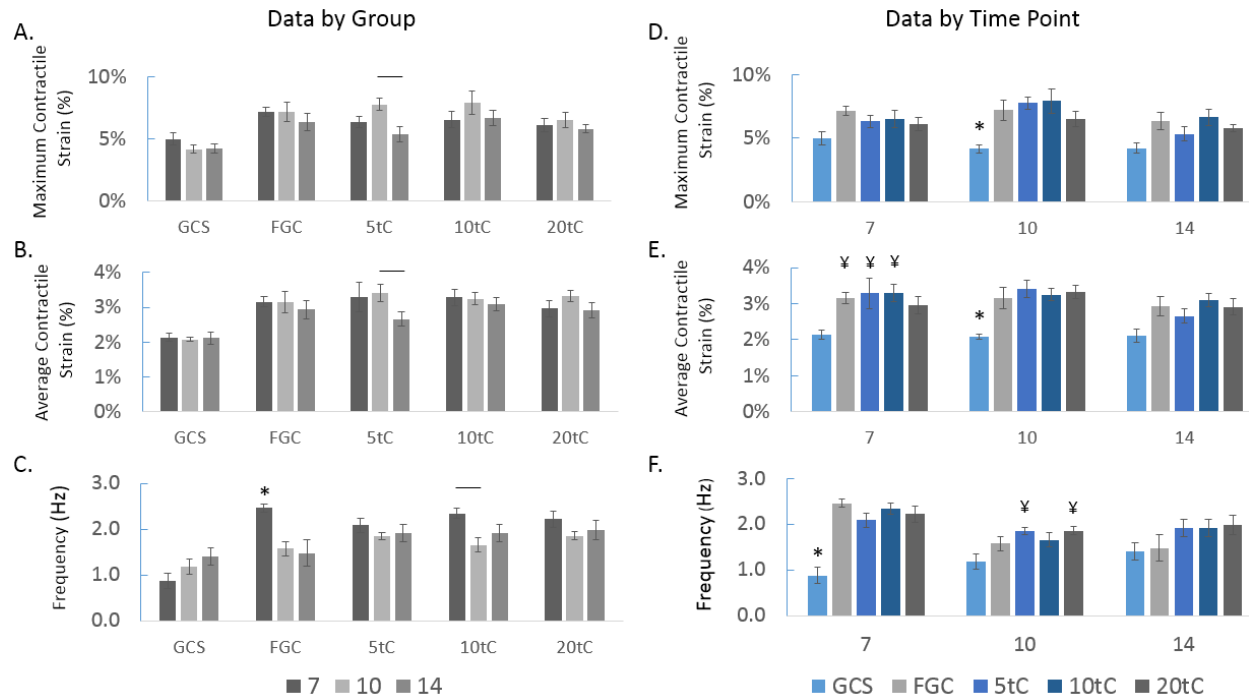


Figure 3.6. Fibrin composite layers do not hinder the functionality of cardiomyocytes relative to a fibrin hydrogel control. Cardiomyocyte functionality is summarized by group (A-C) and by time point (D-F). Maximum contractile strain (A,D) values showed that composite layers behaved similarly to fibrin hydrogel controls. Differences were evaluated through a Two-Way ANOVA with Holm-Sidak post hoc analysis with $p < 0.05$. A bar denotes a significant difference, * denotes significant differences relative to all other groups within cluster, ¥ denotes significant difference relative to coverslip controls.

When evaluating contraction frequency, a significant decrease was observed for FGC at days 10 and 14 relative to day 7 samples ($p < 0.001$ for day 10, $p < 0.001$ for day 14). The 10tC group also exhibited a significant decrease at day 10 relative to day 7 ($p = 0.006$) (**Figure 3.6 C**). All groups had significantly higher frequencies at day 7 relative to GCS ($p < 0.001$ for all groups). At day 10, 5tC and 20tC maintained a significantly higher frequency relative to GCS ($p = 0.035$ for 5tC, $p = 0.037$ for 20tC) (**Figure 3.6 F**). By day 14, no significant differences were observed for any of the functional data among groups. A critical observation is that at no time point were there any significant differences between the FGC and composite groups (5tC, 10tC, 20tC) when

comparing any of the functional data (**Figure 3.6 D, E, F**). **Table A.1** in Appendix 1 summarizes the functional evaluations with data presented as mean \pm standard error.

3.3.5 Fibrin Microthreads Increase Alignment in Adjacent Regions

To assess the effect of microthread-based composites on the alignment of cells, confocal images of Hoechst-stained samples were analyzed using ImageJ to quantify nuclear orientation. When evaluating all cells within the images, nuclear orientation appeared random for FGC and for the bulk phase of the composite layers (**Figure 3.7 A, B**). When analyzing nuclei within 100 μm of fibrin microthreads in composite layers, nuclei demonstrated increased orientation with respect to the long axes of the microthreads (**Figure 3.7 C**). The highest percentage of cells for all composite groups clustered in the 0-15° orientation bin, with respect to the long axes of the threads: 26%, 24%, and 23% for 5tC, 10tC and 20tC, respectively. These observations suggest that the highest number of cells aligned along the direction of the microthreads when they were cultured adjacent to the fibers.

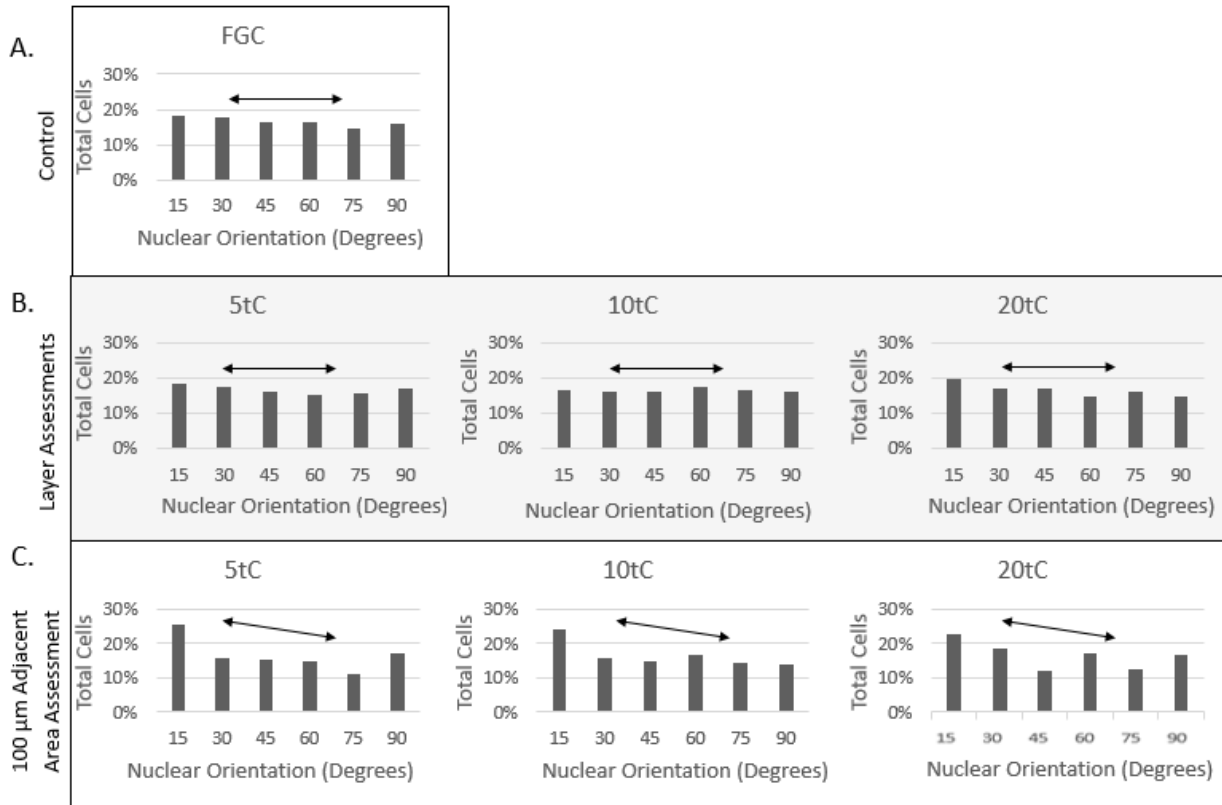


Figure 3.7. Nuclear orientation of cells within composite layers. When assessing nuclear alignment in fibrin hydrogel controls and composite layers, no trend was observed. However, when assessing regions adjacent to fibrin microthreads (within 100 μm), there was a trend suggesting an increase in nuclear orientation as shown by the non-uniform distribution. All nuclear orientations were taken with respect to the long axes of the fibrin microthreads within the composite layer. For fibrin gel controls, the nuclear orientation was taken with respect to the x axis.

3.4 DISCUSSION

The goal of this study was to develop an aligned fibrin microthread-based composite scaffold that enables modulation of the structural properties of the composite material while supporting the cell-mediated contractility comparable to that of conventional fibrin hydrogels. To achieve this, changes in a composite layer were controlled through the addition of fibrin microthreads in varying volume fractions. We demonstrated that through this manipulation, (1) an increase in fibrin microthread volume fraction resulted in an increase in modulus for the layer, and (2) increasing the fibrin microthread volume fraction supported cell-mediated contractile strains and frequency of contractions comparable to hydrogel controls. All composite layers and fibrin hydrogel controls significantly increased these parameters relative to a gelatin coated coverslip control group (GCS). We also found that (3) fibrin microthreads within the composite layer

influence the nuclear orientation of cells immediately adjacent to the fibers (up to a distance of 100 μm).

Upon implantation, it is critical that a cardiac patch have similar mechanical properties to the host myocardium to avoid mechanical mismatch.^{24, 29} It has also been found that scaffold modulus is an important influence on cardiomyocyte contractile force, phenotype and gene expression.^{14, 24, 46-47} Using composite theory, we predicted that the trend for doubling fibrin microthread counts from 5 to 10 and from 10 to 20 microthreads should result in a two-fold increase in scaffold moduli (48 kPa to 95 kPa, and 95 kPa to 190 kPa, respectively). We found that a comparable trend was observed when scaffolds were subjected to submerged uniaxial tensile testing, with moduli increasing two-fold when fibrin microthread counts in the composites were increased from 5 to 10 (20.6 kPa to 46.4 kPa), and from 10 to 20 (46.4 kPa to 97.5 kPa). While the trends for predicted and measured moduli values were comparable, the magnitudes of moduli values were greater for the computational model than for the experimental measurements. The stress-strain curves for the composite layers had two phases which is common for composite materials.³⁵ The first phase is characteristic of elastic deformation, both of the matrix and fibrous components. The second phase is characteristic of elastic deformation of the fiber phase and plastic deformation of the matrix phase. We evaluated the first phase which is more likely to have stronger interfacial bonding between components than the second phase. However, composite theory for aligned, fiber-reinforced composites assumes an isostrain state.³⁵ It is possible that bonding of microthreads and hydrogel within the composite layer was not sufficient to ensure equal deformation of components in the first phase, resulting in the observed reduced moduli values. Future studies in our laboratory will focus on characterizing the shear strength of the fibrin microthread/hydrogel interface to refine the robustness of our predictive model regarding our experimental data. Additionally, manipulation of the interfacial bond strength through techniques like crosslinking offer a potential method for tuning the resultant modulus of the composite layers.

The modulus of the patches we developed can be altered through fibrin microthread volume fraction. The range of modulus values observed was from $20.6 \pm 8.1 - 97.5 \pm 49.3$ kPa. Rat myocardium stiffness can range from 0.1 – 140 kPa²⁴ with neonatal myocardium ranging from 10-20 kPa.¹⁴ To match rat neonatal myocardium, the most appropriate configuration was 5tC (20.6 ± 8.1 kPa). This may not be the case for other species. If working with a more clinically relevant cell

type such as a matured human induced pluripotent stem cell-derived cardiomyocyte, 20tC (97.5 ± 49.3 kPa) may be more appropriate as human myocardium ranges in stiffness from 20 kPa – 500 kPa.²⁴

Composites with a higher fibrin microthread volume fraction are feasible. A distinct advantage of our microthread-based composite scaffold is that we anticipate that we could fabricate layers with 40 microthreads across a 1 cm width. Based on the relationship between our composite theory model and our experimental findings, we hypothesize that this scaffold would exhibit a modulus of 195 kPa. This would result in spacing between threads of approximately 100 μm , a distance shorter than the diameter of a fibrin microthread ($\sim 150 \mu\text{m}$)³² and a modulus closer to the mid-range of stiffness values observed for human myocardium. While a higher thread count may increase the modulus to the mid-range, it will reduce the hydrogel volume and therefore the volume available to the incorporated cells. There is likely a trade-off in the design for mechanical reinforcement and cell function. We hypothesize that crosslinking the fibrin microthreads could further enhance the mechanical properties of the layer, allowing for additional control of the modulus to ensure the fabrication of composite scaffolds with material properties that match native tissue.³¹ However, it is critical that resultant patch stiffness remains within the physiological range; too stiff of a patch could induce a tethering effect, inhibiting contractility of adjacent tissue.²⁹

Samples were evaluated over a 14 day culture period as neonatal rat cardiomyocytes functionally mature in the first postnatal week¹⁴, and it has been reported that fibrin-based hydrogels typically reach a steady-state for compaction between days 8-13.⁴¹ It has also been reported that functional assessments of 3-dimensional (3D) scaffolds with rat neonatal cardiomyocytes can be assessed for 14 days in culture without significant cell death or scaffold breakdown.⁴⁸ As such, we did not conduct a quantitative analysis of the changes in cell viability for this study. However, we plan to conduct future cell viability studies to confirm these observations. A critical observation from these evaluations was that at no time point did the contractile strain or frequency of any composite sample (5tC, 10tC, 20tC) differ significantly from FGC. This observation demonstrates that composite layers and fibrin hydrogels exhibit comparable active, cell-mediated mechanical properties.

Fibrin hydrogels have been extensively investigated for use as cardiac patches,^{6, 25, 49-50} and our results show that relative to fibrin hydrogels, our composite improves the modulus and cell

alignment without compromising contractile strain or contractile frequency. For the GCS group, a beating frequency of ~ 1 Hz was observed, similar to reported literature (61 ± 9 events / min⁵¹ and 40-90 beats/min).⁵² All hydrogel and composite groups had significantly higher contractile frequencies at day 7 with values ~ 2.5 Hz, comparable to reported frequencies for neonatal cardiomyocytes in a 3D environment (180 beats/min⁵³ and 2.5-3Hz⁴⁸). The contractile frequency decreased significantly for FGC and 10tC after day 7. This is a similar trend to reported literature where a decrease in neonatal cardiomyocyte contraction frequency was observed as early as day 6.⁴⁸

When evaluating the maximum and average contractile strains, similar trends were observed where all groups remained stable over 14 days with the exception of the 5tC group where a significant decrease from day 10 to day 14 was observed. While this decrease was unexpected, it is important to note that at both the day 10 and day 14 time points, 5tC was not significantly different from any other composite group (10tC, 20tC) or FGC. It is possible that with this cell type, a peak in cell function was achieved at day 10. This is further supported by the observation that all samples cultured in a 3D environment had significantly higher contractile strains at the day 10 time point relative to GCS, and that no significant difference was present for contractile strains by day 14. Together these findings suggest that cardiomyocytes cultured in our fibrin-microthread composite scaffolds exhibit contractile properties comparable to those observed when cells were cultured in fibrin hydrogels.

Cardiomyocyte alignment may contribute to enhanced functional maturation and integration upon implantation with native myocardium.^{25, 50, 54-55} In healthy myocardium, cardiomyocytes in a layer of tissue are aligned within $\pm 13^\circ$ of each other.⁵⁶ When initially evaluating nuclear alignment of cells within the composite layers, no alignment was observed, similar to FGC. When we focused the evaluation on nuclear alignment of cells within a 100 μ m distance from a fibrin microthread, we observed trends in all composite groups towards alignment with respect to the long axes of the fibrin microthreads. The greatest percentage of cells were oriented between 0-15 $^\circ$ of the direction of the microthreads, orientations comparable to native tissue. This suggests that fibrin microthreads influence cellular orientation for a limited distance in the fibrin hydrogel. This is similar to reports of cellular sensing of rigid bodies not in direct cellular contact for a limited distance.⁵⁷ Cell sensing can influence a range of cell behaviors

including cell spreading and migration. When cultured on polyacrylamide gels mimicking soft tissues (~1 kPa), it was demonstrated through cell spreading that mesenchymal stem cells were able to sense a rigid underlying surface 10-20 μm away, with an average sensing distance of <5 μm .⁵⁸ When considering a fibrous biopolymer (specifically, fibrin and collagen hydrogels), fibroblasts demonstrated changes in spreading at distances as great as 150 μm from a rigid boundary with an average sensing distance of greater than 65 μm .⁵⁷ It is possible that the rat neonatal ventricular myocytes incorporated into our composite layers did not sense fibrin microthreads beyond 150 μm and may exhibit random orientation at distances greater than this. The gel phase of the composite material will require additional stimuli to ensure alignment of cells throughout the layer is comparable to healthy myocardium. Static tension has been shown to influence alignment of muscle cells,⁵⁹ and could potentially further induce alignment in composite layers. Other potential options are to increase the number of microthreads, pattern the hydrogel phase⁴⁹ or electrically stimulate the cells.⁶⁰

Ultimately, using a layer-by-layer approach, we anticipate that our composite fibrin layers can be strategically combined to create and assess an implantable active composite cardiac patch. In the future, we plan to laminate composite layers together with rotating orientation to mimic the structure of native myocardium (**Figure 3.1**). We also aim to couple our composite layers with a fibrin-based vascular network to enable the generation of a perfusable, thick, implantable construct with cell-mediated contractile properties and signal propagation rates that will ultimately facilitate mechanical and electrical coupling to the host tissue and promote the regeneration of functional myocardial tissue within an infarcted environment.

3.5 CONCLUSIONS

In this study, we have shown that increasing the volume fraction of fibrin microthreads in a composite layer increases the modulus, enabling the strategic design of the layer composition to mimic native tissue. Fibrin microthreads within the layer also increased alignment of cells within 100 μm of microthreads. Most importantly, these changes occurred without inhibiting contractile function. All composite groups demonstrated similar contractile strain behavior relative to a hydrogel control, while all composite groups and the hydrogel control showed significantly improved contractile function relative to gelatin-coated coverslips. We anticipate that

reinforcement of hydrogel materials by microthreads will enable the design of cardiac patches that are more suited for implantation. In the future, we plan to assess the effects of static tension on aligning cells within the gel space that do not lie in close proximity to a microthread. This will be critical to achieve an aligned, highly functional layer.

3.6 ACKNOWLEDGEMENTS

The authors wish to thank Kara McCluskey, Laura Pumphrey, Gabriela Romero and Aubrie Vannasse for their work in providing the microthread spacing analysis for this study. This work was funded by NIH R01-HL115282 (G.R.G.), NSF IGERT DGE 1144804, and NSF REU EEC-1156821.

3.7 REFERENCES

1. Chrobak, M. O.; Hansen, K. J.; Gershlak, J. R.; Vratanos, M.; Kanellias, M.; Gaudette, G. R.; Pins, G. D., Design of a fibrin microthread-based composite layer for use in a cardiac patch. *ACS Biomaterials Science & Engineering* **2016**.
2. Mozaffarian, D.; Benjamin, E. J.; Go, A. S.; Arnett, D. K.; Blaha, M. J.; Cushman, M.; de Ferranti, S.; Despres, J. P.; Fullerton, H. J.; Howard, V. J.; Huffman, M. D.; Judd, S. E.; Kissela, B. M.; Lackland, D. T.; Lichtman, J. H.; Lisabeth, L. D.; Liu, S.; Mackey, R. H.; Matchar, D. B.; McGuire, D. K.; Mohler, E. R., 3rd; Moy, C. S.; Muntner, P.; Mussolino, M. E.; Nasir, K.; Neumar, R. W.; Nichol, G.; Palaniappan, L.; Pandey, D. K.; Reeves, M. J.; Rodriguez, C. J.; Sorlie, P. D.; Stein, J.; Towfighi, A.; Turan, T. N.; Virani, S. S.; Willey, J. Z.; Woo, D.; Yeh, R. W.; Turner, M. B.; American Heart Association Statistics, C.; Stroke Statistics, S., Heart disease and stroke statistics--2015 update: a report from the American Heart Association. *Circulation* **2015**, *131* (4), e29-322.
3. Sutton, M. G.; Sharpe, N., Left ventricular remodeling after myocardial infarction: pathophysiology and therapy. *Circulation* **2000**, *101* (25), 2981-8.
4. Badylak, S.; Obermiller, J.; Geddes, L.; Matheny, R., Extracellular matrix for myocardial repair. *Heart Surg Forum* **2003**, *6* (2), E20-6.
5. Ozawa, T.; Mickle, D. A.; Weisel, R. D.; Koyama, N.; Ozawa, S.; Li, R. K., Optimal biomaterial for creation of autologous cardiac grafts. *Circulation* **2002**, *106* (12 Suppl 1), I176-82.
6. Zhang, D.; Shadrin, I. Y.; Lam, J.; Xian, H. Q.; Snodgrass, H. R.; Bursac, N., Tissue-engineered cardiac patch for advanced functional maturation of human ESC-derived cardiomyocytes. *Biomaterials* **2013**, *34* (23), 5813-20.
7. Liao, B.; Christoforou, N.; Leong, K. W.; Bursac, N., Pluripotent stem cell-derived cardiac tissue patch with advanced structure and function. *Biomaterials* **2011**, *32* (35), 9180-7.
8. Miklas, J. W.; Dallabrida, S. M.; Reis, L. A.; Ismail, N.; Rupnick, M.; Radisic, M., QHREDGS enhances tube formation, metabolism and survival of endothelial cells in collagen-chitosan hydrogels. *PLoS one* **2013**, *8* (8), e72956.
9. Morin, K. T.; Dries-Devlin, J. L.; Tranquillo, R. T., Engineered microvessels with strong alignment and high lumen density via cell-induced fibrin gel compaction and interstitial flow. *Tissue engineering. Part A* **2014**, *20* (3-4), 553-65.
10. Thomson, K. S.; Korte, F. S.; Giachelli, C. M.; Ratner, B. D.; Regnier, M.; Scatena, M., Prevascularized microtemplated fibrin scaffolds for cardiac tissue engineering applications. *Tissue engineering. Part A* **2013**, *19* (7-8), 967-77.

11. Wendel, J. S.; Ye, L.; Zhang, P.; Tranquillo, R. T.; Zhang, J. J., Functional consequences of a tissue-engineered myocardial patch for cardiac repair in a rat infarct model. *Tissue engineering. Part A* **2014**, *20* (7-8), 1325-35.
12. Xiong, Q.; Hill, K. L.; Li, Q.; Suntharalingam, P.; Mansoor, A.; Wang, X.; Jameel, M. N.; Zhang, P.; Swingen, C.; Kaufman, D. S.; Zhang, J., A fibrin patch-based enhanced delivery of human embryonic stem cell-derived vascular cell transplantation in a porcine model of postinfarction left ventricular remodeling. *Stem cells* **2011**, *29* (2), 367-75.
13. Fleischer, S.; Feiner, R.; Shapira, A.; Ji, J.; Sui, X.; Daniel Wagner, H.; Dvir, T., Spring-like fibers for cardiac tissue engineering. *Biomaterials* **2013**, *34* (34), 8599-606.
14. Jacot, J. G.; McCulloch, A. D.; Omens, J. H., Substrate stiffness affects the functional maturation of neonatal rat ventricular myocytes. *Biophysical journal* **2008**, *95* (7), 3479-87.
15. Ma, Z.; Koo, S.; Finnegan, M. A.; Loskill, P.; Huebsch, N.; Marks, N. C.; Conklin, B. R.; Grigoropoulos, C. P.; Healy, K. E., Three-dimensional filamentous human diseased cardiac tissue model. *Biomaterials* **2014**, *35* (5), 1367-77.
16. Remlinger, N. T.; Gilbert, T. W.; Yoshida, M.; Guest, B. N.; Hashizume, R.; Weaver, M. L.; Wagner, W. R.; Brown, B. N.; Tobita, K.; Wearden, P. D., Urinary bladder matrix promotes site appropriate tissue formation following right ventricle outflow tract repair. *Organogenesis* **2013**, *9* (3), 149-60.
17. Vukadinovic-Nikolic, Z.; Andree, B.; Dorfman, S. E.; Pflaum, M.; Horvath, T.; Lux, M.; Venturini, L.; Bar, A.; Kensah, G.; Lara, A. R.; Tudorache, I.; Cebotari, S.; Hilfiker-Kleiner, D.; Haverich, A.; Hilfiker, A., Generation of bioartificial heart tissue by combining a three-dimensional gel-based cardiac construct with decellularized small intestinal submucosa. *Tissue engineering. Part A* **2014**, *20* (3-4), 799-809.
18. Ott, H. C.; Matthiesen, T. S.; Goh, S. K.; Black, L. D.; Kren, S. M.; Netoff, T. I.; Taylor, D. A., Perfusion-decellularized matrix: using nature's platform to engineer a bioartificial heart. *Nature medicine* **2008**, *14* (2), 213-21.
19. Robertson, M. J.; Dries-Devlin, J. L.; Kren, S. M.; Burchfield, J. S.; Taylor, D. A., Optimizing recellularization of whole decellularized heart extracellular matrix. *PloS one* **2014**, *9* (2), e90406.
20. Thavandiran, N.; Dubois, N.; Mikryukov, A.; Masse, S.; Beca, B.; Simmons, C. A.; Deshpande, V. S.; McGarry, J. P.; Chen, C. S.; Nanthakumar, K.; Keller, G. M.; Radisic, M.; Zandstra, P. W., Design and formulation of functional pluripotent stem cell-derived cardiac microtissues. *Proceedings of the National Academy of Sciences of the United States of America* **2013**, *110* (49), E4698-707.
21. Ye, X.; Lu, L.; Kolewe, M. E.; Hearon, K.; Fischer, K. M.; Coppeta, J.; Freed, L. E., Scalable units for building cardiac tissue. *Advanced materials* **2014**, *26* (42), 7202-8.
22. Hogan, M.; Mohamed, M.; Tao, Z. W.; Gutierrez, L.; Birla, R., Establishing the Framework to Support Bioartificial Heart Fabrication Using Fibrin-Based Three-Dimensional Artificial Heart Muscle. *Artificial organs* **2014**, *61* (4), 429-36.
23. Zhang, G.; Hu, Q.; Braunlin, E. A.; Suggs, L. J.; Zhang, J., Enhancing efficacy of stem cell transplantation to the heart with a PEGylated fibrin biomatrix. *Tissue engineering. Part A* **2008**, *14* (6), 1025-36.
24. Radisic, M.; Christman, K. L., Materials science and tissue engineering: repairing the heart. *Mayo Clinic proceedings* **2013**, *88* (8), 884-98.
25. Bian, W.; Jackman, C. P.; Bursac, N., Controlling the structural and functional anisotropy of engineered cardiac tissues. *Biofabrication* **2014**, *6* (2), 024109.
26. Tandon, V.; Zhang, B.; Radisic, M.; Murthy, S. K., Generation of tissue constructs for cardiovascular regenerative medicine: from cell procurement to scaffold design. *Biotechnology advances* **2013**, *31* (5), 722-35.
27. El-Sherbiny, I. M.; Yacoub, M. H., Hydrogel scaffolds for tissue engineering: Progress and challenges. *Global cardiology science & practice* **2013**, *2013* (3), 316-42.
28. Reis, L. A.; Chiu, L. L.; Feric, N.; Fu, L.; Radisic, M., Biomaterials in myocardial tissue engineering. *Journal of tissue engineering and regenerative medicine* **2014**, *10* (1), 11-28.
29. Kochupura, P. V.; Azeloglu, E. U.; Kelly, D. J.; Doronin, S. V.; Badylak, S. F.; Krukenkamp, I. B.; Cohen, I. S.; Gaudette, G. R., Tissue-engineered myocardial patch derived from extracellular matrix provides regional mechanical function. *Circulation* **2005**, *112* (9 Suppl), I144-9.
30. O'Brien, M. P.; Carnes, M. E.; Page, R. L.; Gaudette, G. R.; Pins, G. D., Designing biopolymer microthreads for tissue engineering and regenerative medicine. *Current Stem Cell Reports* **2016**, *2*, 147-57.

31. Grasman, J. M.; Page, R. L.; Dominko, T.; Pins, G. D., Crosslinking strategies facilitate tunable structural properties of fibrin microthreads. *Acta biomaterialia* **2012**, *8* (11), 4020-30.
32. Grasman, J. M.; Pumphrey, L. M.; Dunphy, M.; Perez-Rogers, J.; Pins, G. D., Static axial stretching enhances the mechanical properties and cellular responses of fibrin microthreads. *Acta biomaterialia* **2014**, *10* (10), 4367-76.
33. Cornwell, K. G.; Pins, G. D., Discrete crosslinked fibrin microthread scaffolds for tissue regeneration. *Journal of biomedical materials research. Part A* **2007**, *82* (1), 104-12.
34. Grasman, J. M.; O'Brien, M. P.; Ackerman, K.; Gagnon, K. A.; Wong, G. M.; Pins, G. D., The Effect of Sterilization Methods on the Structural and Chemical Properties of Fibrin Microthread Scaffolds. *Macromolecular bioscience* **2016**, *16* (6), 836-46.
35. Callister, W. D.; Rethwisch, D. G., *Fundamentals of materials science and engineering : an integrated approach*. 4th ed.; Wiley: Hoboken, N.J., 2012; p xxv, 910 p.
36. Billiar, K. L.; Throm, A. M.; Frey, M. T., Biaxial failure properties of planar living tissue equivalents. *Journal of biomedical materials research. Part A* **2005**, *73* (2), 182-91.
37. Grasman, J. M.; Pumphrey, L.; Dunphy, M.; Perez-Rogers, J.; Pins, G. D., Static axial stretching enhances the mechanical properties and cellular responses of fibrin microthreads. *Acta biomaterialia* **2014**, *10* (10), 4367-76.
38. Moore, C. C.; Lugo-Olivieri, C. H.; McVeigh, E. R.; Zerhouni, E. A., Three-dimensional systolic strain patterns in the normal human left ventricle: characterization with tagged MR imaging. *Radiology* **2000**, *214* (2), 453-66.
39. Clark, N. R.; Reichek, N.; Bergey, P.; Hoffman, E. A.; Brownson, D.; Palmon, L.; Axel, L., Circumferential myocardial shortening in the normal human left ventricle. Assessment by magnetic resonance imaging using spatial modulation of magnetization. *Circulation* **1991**, *84* (1), 67-74.
40. Morgan, K. Y.; Black, L. D., 3rd, Mimicking isovolumic contraction with combined electromechanical stimulation improves the development of engineered cardiac constructs. *Tissue engineering. Part A* **2014**, *20* (11-12), 1654-67.
41. Bian, W.; Liao, B.; Badie, N.; Bursac, N., Mesoscopic hydrogel molding to control the 3D geometry of bioartificial muscle tissues. *Nature protocols* **2009**, *4* (10), 1522-34.
42. Kelly, D. J.; Rosen, A. B.; Schuldt, A. J.; Kochupura, P. V.; Doronin, S. V.; Potapova, I. A.; Azeloglu, E. U.; Badylak, S. F.; Brink, P. R.; Cohen, I. S.; Gaudette, G. R., Increased myocyte content and mechanical function within a tissue-engineered myocardial patch following implantation. *Tissue engineering. Part A* **2009**, *15* (8), 2189-201.
43. Tao, Z. W.; Favreau, J. T.; Guyette, J. P.; Hansen, K. J.; Lessard, J.; Burford, E.; Pins, G. D.; Gaudette, G. R., Delivering stem cells to the healthy heart on biological sutures: effects on regional mechanical function. *Journal of tissue engineering and regenerative medicine* **2014**.
44. Hansen, K. J.; Favreau, J. T.; Gershlak, J. R.; Laflamme, M. A.; Albrecht, D. R.; Gaudette, G. R., Optical Method to Quantify Mechanical Contraction and Calcium Transients of Human Pluripotent Stem Cell-Derived Cardiomyocytes. *Tissue engineering. Part C, Methods* **2017**.
45. Duong, H.; Wu, B.; Tawil, B., Modulation of 3D fibrin matrix stiffness by intrinsic fibrinogen-thrombin compositions and by extrinsic cellular activity. *Tissue engineering. Part A* **2009**, *15* (7), 1865-76.
46. Forte, G.; Pagliari, S.; Ebara, M.; Uto, K.; Tam, J. K.; Romanazzo, S.; Escobedo-Lucea, C.; Romano, E.; Di Nardo, P.; Traversa, E.; Aoyagi, T., Substrate stiffness modulates gene expression and phenotype in neonatal cardiomyocytes in vitro. *Tissue engineering. Part A* **2012**, *18* (17-18), 1837-48.
47. Marsano, A.; Maidhof, R.; Wan, L. Q.; Wang, Y.; Gao, J.; Tandon, N.; Vunjak-Novakovic, G., Scaffold stiffness affects the contractile function of three-dimensional engineered cardiac constructs. *Biotechnol Prog* **2010**, *26* (5), 1382-90.
48. Bursac, N.; Loo, Y.; Leong, K.; Tung, L., Novel anisotropic engineered cardiac tissues: studies of electrical propagation. *Biochemical and biophysical research communications* **2007**, *361* (4), 847-53.
49. Bian, W.; Badie, N.; Himel, H. D. t.; Bursac, N., Robust T-tubulation and maturation of cardiomyocytes using tissue-engineered epicardial mimetics. *Biomaterials* **2014**, *35* (12), 3819-28.
50. Black, L. D., 3rd; Meyers, J. D.; Weinbaum, J. S.; Shvelidze, Y. A.; Tranquillo, R. T., Cell-induced alignment augments twitch force in fibrin gel-based engineered myocardium via gap junction modification. *Tissue engineering. Part A* **2009**, *15* (10), 3099-108.

51. Lalevee, N.; Rebsamen, M. C.; Barrere-Lemaire, S.; Perrier, E.; Nargeot, J.; Benitah, J. P.; Rossier, M. F., Aldosterone increases T-type calcium channel expression and in vitro beating frequency in neonatal rat cardiomyocytes. *Cardiovascular research* **2005**, *67* (2), 216-24.
52. Fleischman, A.; Vecchio, C.; Sunny, Y.; Bawiec, C. R.; Lewin, P. A.; Kresh, J. Y.; Kohut, A. R., Ultrasound-induced modulation of cardiac rhythm in neonatal rat ventricular cardiomyocytes. *J Appl Physiol (1985)* **2015**, *118* (11), 1423-8.
53. Zimmermann, W. H.; Fink, C.; Kralisch, D.; Remmers, U.; Weil, J.; Eschenhagen, T., Three-dimensional engineered heart tissue from neonatal rat cardiac myocytes. *Biotechnology and bioengineering* **2000**, *68* (1), 106-14.
54. Chung, C. Y.; Bien, H.; Entcheva, E., The role of cardiac tissue alignment in modulating electrical function. *J Cardiovasc Electrophysiol* **2007**, *18* (12), 1323-9.
55. Pong, T.; Adams, W. J.; Bray, M. A.; Feinberg, A. W.; Sheehy, S. P.; Werdich, A. A.; Parker, K. K., Hierarchical architecture influences calcium dynamics in engineered cardiac muscle. *Exp Biol Med (Maywood)* **2011**, *236* (3), 366-73.
56. Lee, W. N.; Pernot, M.; Couade, M.; Messas, E.; Bruneval, P.; Bel, A.; Hagege, A. A.; Fink, M.; Tanter, M., Mapping myocardial fiber orientation using echocardiography-based shear wave imaging. *IEEE transactions on medical imaging* **2012**, *31* (3), 554-62.
57. Rudnicki, M. S.; Cirka, H. A.; Aghvami, M.; Sander, E. A.; Wen, Q.; Billiar, K. L., Nonlinear strain stiffening is not sufficient to explain how far cells can feel on fibrous protein gels. *Biophysical journal* **2013**, *105* (1), 11-20.
58. Buxboim, A.; Rajagopal, K.; Brown, A. E. X.; Discher, D. E., How deeply cells feel: methods for thin gels. *J Phys-Condens Mat* **2010**, *22* (19), 194116.
59. Heher, P.; Maleiner, B.; Pruller, J.; Teuschl, A. H.; Kollmitzer, J.; Monforte, X.; Wolbank, S.; Redl, H.; Runzler, D.; Fuchs, C., A novel bioreactor for the generation of highly aligned 3D skeletal muscle-like constructs through orientation of fibrin via application of static strain. *Acta biomaterialia* **2015**, *24*, 251-265.
60. Tandon, N.; Marsano, A.; Maidhof, R.; Wan, L.; Park, H.; Vunjak-Novakovic, G., Optimization of electrical stimulation parameters for cardiac tissue engineering. *Journal of tissue engineering and regenerative medicine* **2011**, *5* (6), E115-E125.

Chapter 4: Alignment of Cardiomyocytes Through Static Tension Increases Contractile Strains in Composite Layers

4.1 INTRODUCTION

Approximately 1 in 3 deaths in the United States is due to cardiovascular disease (CVD).¹ A major contributing factor to CVD is a heart attack. When a heart attack occurs, oxygen deficiency results in necrotic tissue and ultimately a harsh inflammatory reaction that leaves a scar in place of functional ventricular myocardium.² The scar tissue is non-contractile and reduces the working efficiency of the heart. To compensate, ventricular remodeling occurs which can ultimately lead to heart failure.³ While treatment options exist, the only treatment that can restore baseline function for end stage heart failure is a heart transplant. However, donors are limited restricting use of this treatment option.⁴ There is a need for a regenerative solution for heart attack patients.

A cardiac patch is a material that is used to augment or replace scar tissue resulting from a heart attack.⁵⁻⁶ Clinically available cardiac patches are acellular⁷ and aim to limit ventricular remodeling. While this approach can attenuate the progression towards heart failure, these patches do not restore baseline function to the patients. It has been hypothesized that a cell-populated cardiac patch could overcome this limitation by providing a functional rather than just passive support. Research on the development of cell-populated patches has demonstrated promising contractility with contractile forces and action potential propagation speeds approaching adult myocardium values,⁸ however the materials that yield the highest cell function are typically hydrogels that lack robust mechanical properties.⁹⁻¹² In the dynamic environment of the heart, it is important that the material exhibit similar mechanical properties to native tissue. Weak materials may bulge, resulting in an aneurysm, or rupture during the cyclic loading. Materials that are too stiff may result in a tethering effect, limiting the function of the adjacent heart tissue.¹³

We recently developed a fibrin-based composite material for use as a cardiac patch.¹⁴ This material is comprised of a fibrin hydrogel reinforced with fibrin microthreads. We demonstrated

that the stiffness of this material can be modulated by manipulating the volume fraction of the components. When the volume fraction of the fibrin microthreads increased, we observed a corresponding increase in the stiffness values of the material. Additionally, we observed that the contractile strains and frequencies of the cardiomyocytes in the scaffold did not vary significantly with the increased volume fractions. However, the alignment of incorporated cells was random throughout the layer. Only slight improvements in alignment were observed in areas immediately adjacent to fibrin microthreads (within 100 μm).

Native ventricular myocardium is a highly aligned tissue, comprised of anisotropically organized layers. Each layer of the myocardium contains fibrils that run $\pm 13^\circ$ relative to the mean fiber direction.¹⁵⁻¹⁶ The orientation of the cardiomyocytes within the tissue closely follows this organization. For a cardiac patch to restore baseline function, it is critical that the patch exhibits functional properties that are comparable to healthy ventricular myocardium. A critical factor that impacts these functional properties is cell alignment, which drives the magnitude and direction of the contractility of the patch.

Previous studies showed that fibrin hydrogels can be compacted by incorporated cells.¹⁷ If the hydrogel is strategically constrained, the compaction can induce a static tension. Static tension has been used in conjunction with hydrogel patterning to induce alignment of incorporated cells.¹⁸⁻²⁰ To orient the cells in our composite layers, we hypothesize that we can use cell-mediated compaction to induce static tension ultimately aligning incorporated cells. To test this hypothesis, we created a method for inducing static tension consistently and predominantly in one direction within composite layers. In our previous work, we observed no significant alignment for the bulk layers.¹⁴ Using these layers as an unaligned control, we evaluated a novel experimental culturing method that influenced nuclear orientation and cell function of incorporated primary neonatal rat ventricular myocytes. To analyze the functional properties of the cells, we evaluated contractile principal strains, principal angles, total contractile area, and contractile frequencies. In addition to these assessments for the entire recorded region, we also completed a grid assessment breaking the recorded region into smaller sub-regions to evaluate regional consistency. Further we evaluated whether cell-mediated compaction altered the volume fractions of the composite constituents and impacted the stiffness of the scaffolds. To assess the impact on the mechanical properties, we modeled the effect volume fraction changes of composite constituents resulting from compaction

would have on layer stiffness using composite theory and performed uniaxial tensile testing on compacted layers. The results of these analyses will inform the material properties and functionality of individual composite layers. Ultimately, we anticipate that composite fibrin layers can be strategically laminated to mimic the architecture, function and mechanical properties of ventricular myocardium.

4.2 MATERIALS and METHODS

4.2.1 Fabrication of Fibrin Microthread-Based Composite Scaffolds

4.2.1.1 Microthread Extrusion

Fibrin microthreads were generated by co-extruding fibrinogen and thrombin solutions.²¹⁻²⁴ Briefly, a 70 mg/mL solution of fibrinogen (from bovine plasma, Sigma, St. Louis, MO) in HEPES (N-[2-Hydroxyethyl] piperazine-N'-[2-ethanesulfonic acid]) buffered saline (HBS, 20 mM HEPES, 0.9% NaCl; pH 7.4) was made and stored at -20°C until use. A 40 U/mL solution of thrombin isolated from bovine plasma (Sigma) in HBS was also made and stored at -20°C. Solutions were thawed to room temperature prior to use. The thrombin solution was mixed with a 40 mM solution of CaCl₂ yielding a working solution of 6 U/mL. Equal volumes of fibrinogen and thrombin/CaCl₂ solutions were loaded into separate 1 mL syringes and connected to a blending applicator tip (Micromedics Inc., St. Paul, MN) to mix the solutions. The mixed solution was then extruded using a dual syringe pump through polyethylene tubing (BD, Sparks, MD) with an inner diameter of 0.86 mm into a 10 mM HEPES buffer bath (pH 7.4) in a Teflon coated pan at a flow rate of 0.225 mL/min. After a 10-15-minute polymerization time, the scaffolds were stretched to ~150% of their original length and hung to dry.²⁴

4.2.1.2 Fibrin Microthread Organization

Dried fibrin microthreads were organized as previously reported.¹⁴ Briefly, a purpose-built fibrin microthread spacer was used to align fibrin microthreads at set distances to ensure a uniform layer. The device has aligned grooves with pores. This system couples with a house vacuum enabling the placement of fibrin microthreads threads at defined spacing. For this work, evaluations were completed utilizing composite layers with 5 fibrin microthreads (5tC) or 20 fibrin microthreads (20tC) evenly spaced across a 12 mm width. Once organized, threads were secured

and were transferred to precut vellum frames. Threads were glued to the vellum frames using medical grade silicone adhesive (Factor II, Inc, Lakeside, AZ).

4.2.2 Rat Neonatal Ventricular Myocyte (rNVM) Isolation

All work involving animals was submitted to and approved by the Institutional Animal Care and Use Committee at Worcester Polytechnic Institute. Rat neonatal ventricular myocytes were isolated following a previously described protocol.²⁵ Briefly, hearts were excised from 2 and 3-day old neonatal Sprague Dawley rats (Charles River, Wilmington, MA). The ventricles were then separated from the atria and were subsequently minced into ~1mm² sized pieces. Digestion of the ventricle pieces was completed at 37°C using type II collagenase (Thermo Fisher Scientific, Waltham, MA) serially in 7x7 minute digestions. One 45-minute pre-plating step was performed to enrich the volume of cardiomyocytes in the isolation.¹⁹ Cells were used immediately for experimentation.

4.2.3 Composite Layer Fabrication and Tissue Culture

All samples used in cell culture were maintained in medium comprised of DMEM (VWR, Radnor, PA) supplemented with 10% defined donor equine serum (Fisher Scientific, Waltham, MA), 2% chick embryo extract (United States Biological Corp, Salem, MA), 1% penicillin streptomycin (Thermo Fisher Scientific, Waltham, MA), 1% amphotericin B (Thermo Fisher Scientific) and 50 ug/mL aprotinin (Sigma Aldrich, St. Louis, MO). All cell culture experiments were maintained for 14 days with medium changes every other day.

The following nomenclature scheme was used for all experimental conditions: unaligned controls of 5 thread composite layers (UA5tC), aligned 5 thread composite layers (A5tC), aligned 20 thread composite layers (A20tC) and gelatin-coated coverslips (GCS). Each experimental condition was tested in triplicate.

4.2.3.1 Fabrication of Unaligned Controls (UA5tC)

Autoclaved polydimethylsiloxane (PDMS) sheets were coated with sterile 1% Pluronic-F127 (Sigma, St. Louis, MO) in DI water for 1 hour. Organized fibrin microthreads secured to vellum frames were rehydrated in phosphate buffered saline (PBS) (VWR, Radnor, PA) for 1 hour.

Immediately prior to gel casting, rehydrated samples were placed on the coated PDMS sheets. A hydrogel solution of 4×10^6 cells/mL, 4% (v/v) 40 U/mL thrombin, and 28% (v/v) 11 mg/mL fibrinogen was mixed on ice, cast over the vellum frames and spread using a pipette tip to provide an even layer. For the 144 mm^2 area of the sample, 150 μL of hydrogel solution was used. Samples were placed in an incubator at 37°C for 30 minutes to polymerize and were then transferred into wells.

4.2.3.2 Fabrication of Experimental Composite Samples (A5tC and A20tC)

Custom hydrogel-casting and culturing devices were generated by casting PDMS into a purpose-built aluminum mold (**Figure 4.1**). Casting devices are $19 \times 25 \text{ mm}$ with 2 mm diameter posts 1 mm in height, and 1 mm thick walls to restrict the geometry of the cast hydrogel. Culturing devices are $19 \times 25 \text{ mm}$ with 2 mm diameter posts 5 mm in height, and couple with 4 X 1 mm wide, 2 mm inner-diameter high-temperature silicone o-rings with a durometer of 70A.

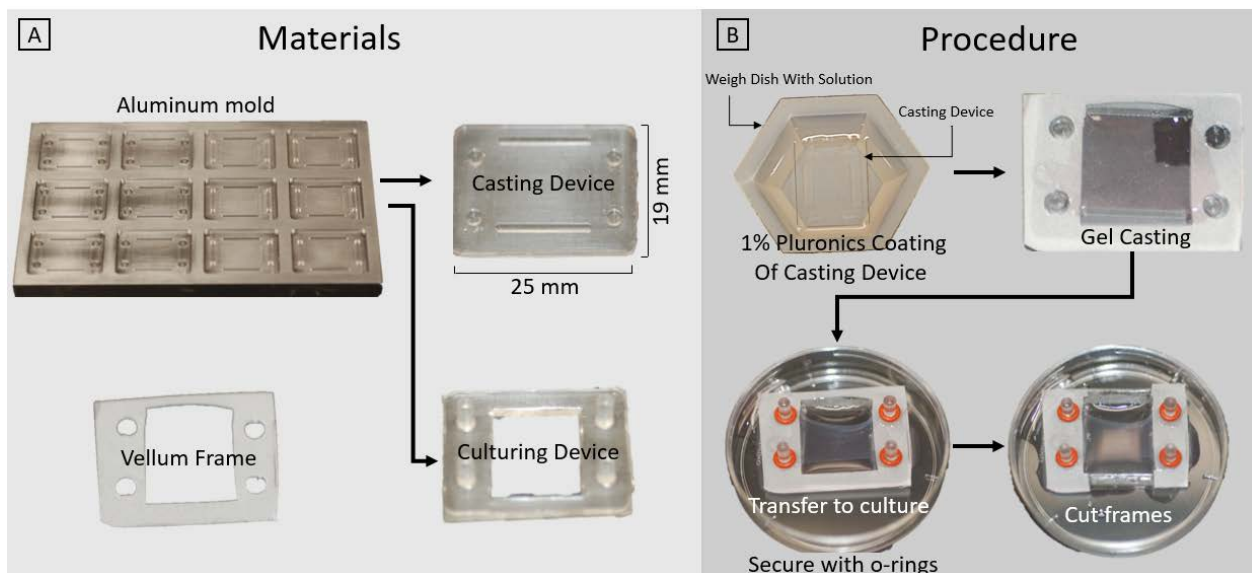


Figure 4.1. The materials and procedure for casting the experimental A5tC and A20tC layers. PDMS is used with an aluminum mold to create casting and culturing devices that couple with vellum frames (A). The casting device is coated with 1% Pluronic which enables hydrogel incorporation into only 2 of the vellum frame sides. The samples are transferred to the culturing device, secured with o-rings and frame side-arms cut for culture (B).

Hydrogel-casting devices were autoclaved and coated with sterile 1% Pluronic-F127 in DI water (Sigma, St. Louis, MO) solution for 1 hour. Vellum frames with secured fibrin microthreads (5 or 20 threads) were rehydrated in PBS for 1 hour. Immediately prior to hydrogel casting, samples

were placed on the casting devices. A hydrogel solution of 4×10^6 cells/mL, 4% (v/v) 40 U/mL thrombin, and 28% (v/v) 11 mg/mL fibrinogen was mixed on ice, cast over the samples and spread using a pipette tip to provide an even layer. The casting device prohibited any hydrogel from binding to the side arms of the vellum frames. For the sample area of 144 mm^2 , 150 μL of hydrogel solution was utilized. Polymerization occurred in an incubator at 37°C for 30 minutes. Following this, samples were moved to culturing devices in wells, and secured to the PDMS posts of the device with silicone o-rings (McMaster-Carr, Princeton, NJ). The side arms of the vellum frames were then cut, and samples were covered with medium.

4.2.3.3 Seeding of Gelatin-Coated Glass Coverslip Controls (GCS)

Gelatin coated coverslips (GCS) were used as a control to assess batch-to-batch variation. Glass coverslips (VWR) were cut to $10 \times 10\text{mm}$ dimensions, autoclaved, and coated with sterile 0.7% gelatin (Sigma Aldrich) in DI water for 4 hours. Following coating, coverslips were secured to the bottom of wells in a 12 well plate using autoclaved vacuum grease. The plate was stored in an incubator at 37°C until use. Following casting of all other samples, 100 μL of cell suspension (2×10^6 cells/mL) was seeded on each coverslip and incubated at 37°C for 18 hours. Samples were then rinsed and covered with medium for extended culture.

4.2.4 Cardiomyocyte Functional Analysis

4.2.4.1 High Density Mapping (HDM)

For functional analyses, UA5tC, A5tC and GCS controls were evaluated. Spontaneous contractions were recorded at 100X magnification and 60 frames per second with a high-speed camera (HiSpec 4, Fastec Imaging Corp, San Diego, CA) attached to an inverted microscope (DMIL, Leica Microsystems, Buffalo Grove, IL). Recordings of ~ 1300 frames were completed at 7, 10 and 14 days of culture. Because of visible differences in the regional function of A5tC layers, two videos per sample per timepoint were collected, one at a region of larger global movements (“max”, as identified by thread movement) and one at a region of low global movements (“min”, as identified by little if any thread movement). An optical technique, high density mapping (HDM), was used to evaluate regional mechanical function with high spatial resolution.²⁶ Two methods were utilized to assess the contractile behaviors of incorporated cardiomyocytes; a large region

assessment and a grid assessment (**Figure 4.2**). Regions of interest (ROIs) for each sample were selected (large region size: 1200 x 986 pixels, grid size: 20 squares, each 300 x 197 pixels). Each ROI was divided into 16 x 16 pixel subwindows, with an 8 pixel shift and 5 averaging windows to track displacements of sequential frames over several images, ultimately yielding displacement fields.²⁷⁻²⁸

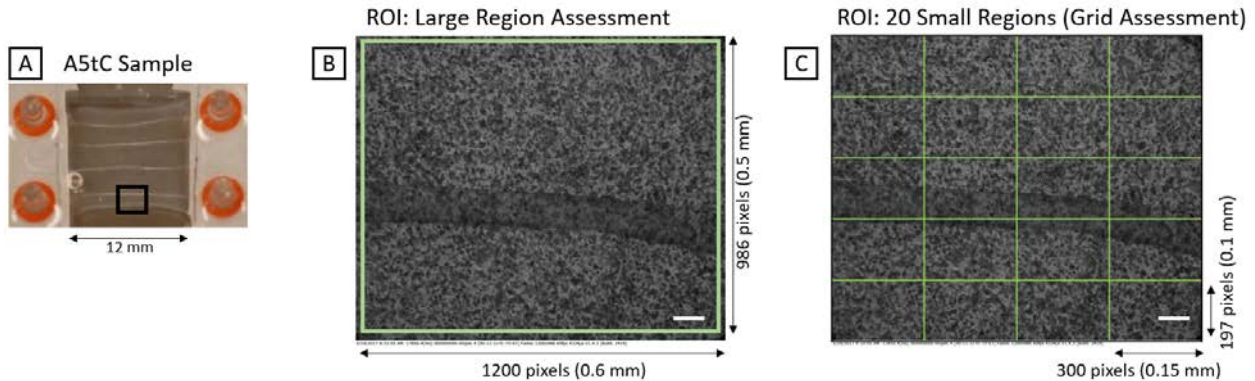


Figure 4.2. HDM is a method for evaluating regional mechanical function.²⁶ Recordings were taken of regions of samples (A). From the recorded images, ROIs were selected. For the large region assessment (B) an ROI of ~1200 x 986 pixels was selected. For the grid assessment, 20 regions 197 x 300 pixels in size were selected (C). The scale bar is 0.05 mm.

For the large region assessment, the displacement fields were used to determine the maximum principal contractile strain for the ROI, the average principal contractile strain across the ROI, the frequency of contractions and the percent contractile area. Outliers were identified as any strain or frequency value that was 1.5 times greater than the inner quartile range (IQR) for each sample set (min: quartile 1 - 1.5*IQR, max: quartile 3 + 1.5*IQR) and were subsequently removed from further analysis.²⁴

Additionally, with the large region assessment the principal angles of 5 contractile strains per sample were evaluated. For each sample, a range of principal angles was calculated as a measure of how synchronous the sample was contracting. A small range would imply that the layer was beating synchronously as the angles were not changing for different contraction cycles. A large range however, could result from multiple contractions occurring asynchronously.

The grid assessment yielded information about the uniformity of the incorporated cells' contractile behavior across the recorded region. For this assessment, the recorded region was subdivided into 20 ROIs forming a grid. Each ROI was evaluated individually for maximum

principal contractile strain and the associated principal angle value. Additionally, each ROI was evaluated for the average principal contractile strain. With this data, 3 evaluations were completed (**Figure 4.3**). To determine the principal angle consistency across the entire recorded region, the range of principal angles for the maximum contractile strains of each sample's 20 ROIs was calculated (**Figure 4.3 B**). This is different from the analysis completed for the large ROI assessment. Consistency between contractions for an ROI was not determined; rather, consistency across all ROIs in a recorded region was calculated. To evaluate the consistency of the maximum and average contractile strain values, a factor we have termed F50 was calculated (**Figure 4.3 C**). This factor is equivalent to the percentage of ROIs within a sample that are equal to or greater than 50% of the highest maximum contractile strain value calculated for the recorded area. As an example, if the highest maximum contractile strain was found to be 10% across the recorded area and 5 of the 20 grid blocks had maximum contractile strains $\geq 5\%$, the F50 value would be 25%. This calculation was also completed for the highest average contractile strain for each sample.

Additionally, to evaluate the distribution of the maximum contractile strains relative to incorporated fibrin microthreads, distances of the highest maximum contractile strains for recorded regions from microthreads were determined (**Figure 4.3 D**). To do so, grid blocks were identified where the highest maximum contractile strains were observed. The distance from the center of this block to the center of the closest block containing a thread was calculated. If any of the highest maximum contractile strains were observed in blocks containing a microthread, the distance was evaluated as 0 mm. The same evaluation was completed for the blocks containing the highest average contractile strains for the recorded samples.

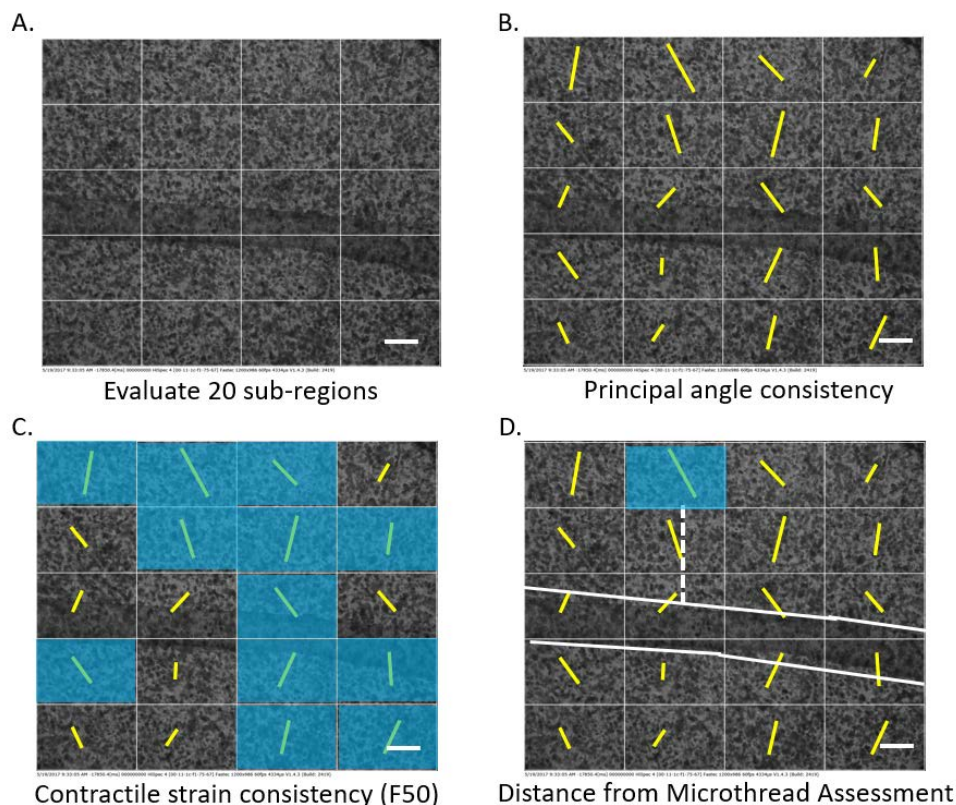


Figure 4.3. Grid evaluations to determine consistency across a recorded region. The recorded region was subdivided into a grid of 20 sub-regions (A) and evaluated for contractile strains and principal angles. In B-D, the yellow bars indicate the principal angle calculated for the region, and are scaled depending on the calculated maximum contractile strain value. Longer bars correspond to greater contractile strains. With this data, the consistency of the principal angles (B) and the contractile strains (C) can be evaluated. In C, blue highlighted regions show values greater than 50% of the maximum contractile strain. For this example, the F50 factor would be 60%. The distance of the highest contractile strains relative to fibrin microthreads was also evaluated (D). Scale bars are 0.05mm.

4.2.4.2 Contractile Wave Propagation Evaluation

To evaluate contractile wave propagation through the composite layers, cell shortening patterns were compared. ROIs (~50 x 150 μm) within the recorded areas were selected that ran parallel and perpendicular to the incorporated fibrin microthreads for videos collected at day 14 of culture, when areas appeared to be spontaneously, synchronously contracting at a frequency of approximately 1.6 Hz (**Figure 4.4**). For each ROI, contractile strains were plotted against frame numbers yielding a strain trace. Traces for regions running parallel to the thread were overlaid. Frame differences in contractile peaks were taken and averaged for 5 contractions per sample. This value was then multiplied by the framerate used to record the images, 60 fps, to yield a time difference. The distance between the two ROIs was measured using ImageJ. The distance was then

divided by the time difference to obtain an approximate velocity. This evaluation was repeated for regions that ran perpendicular to the incorporated fibrin microthread. To calculate the noise of the assessment method, the time that would be required for the signal to travel at the fastest velocity found was calculated. This time value was then compared to the rate at which frames were captured to determine if the framerate used was sufficient for capturing the propagation. Outliers were identified as any velocity value that was 1.5 times greater than the inner quartile range (IQR) for each sample set (min: quartile 1 - 1.5*IQR, max: quartile 3 + 1.5*IQR) and were subsequently removed from further analysis.²⁴

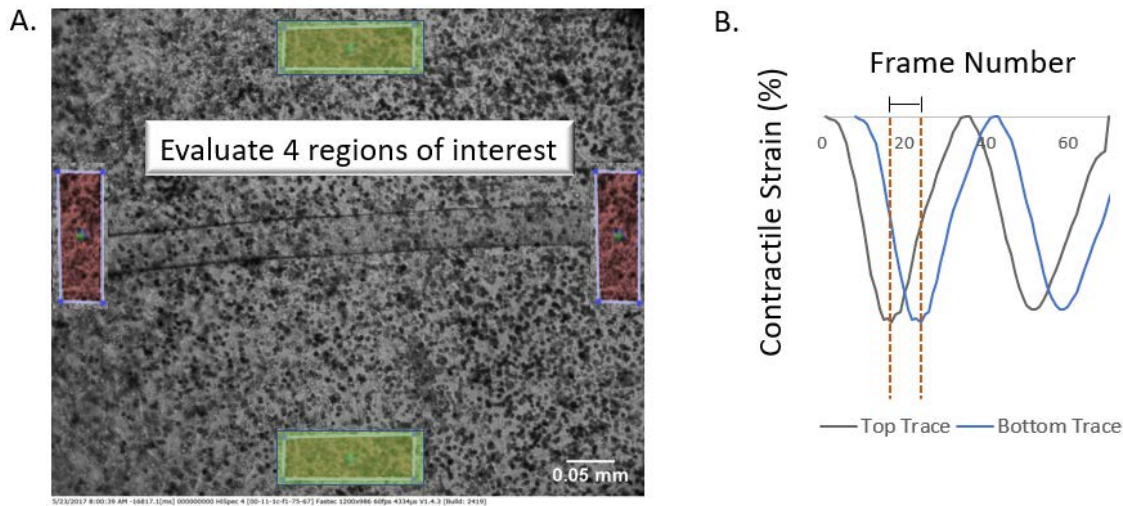


Figure 4.4. Method for assessing contractile wave propagation. To determine how a signal may be traveling through the layer, 4 ROIs that ran parallel (red regions) and perpendicular (green regions) to the incorporated fibrin microthreads were analyzed using HDM (A). Traces were then compared to evaluate the time delay between peaks (B). Using the time delay and distance between ROIs, propagation velocities were estimated.

4.2.5 Mechanical Characterization of Cultured Composite Layers

4.2.5.1. Theoretical Model for Predicting Elastic Modulus of Compacted Composite Layers.

To generate a model for predicting moduli of fibrin microthread-based composite layers following compaction in a 14-day culture, classical composite theory for aligned, fiber-reinforced composites was utilized. With this theory, the elastic modulus (E_{cl}) of a composite layer in the direction of microthread alignment can be estimated as shown in Equation 4.1²⁹

$$E_{cl} = E_m V_m + E_f V_f \quad 4.1.$$

where E_m and E_f are the elastic moduli of the matrix and fibrous components, respectively and V_m and V_f are the volume fractions of the matrix and fibrous components, respectively.²⁹

For this assessment, UA5tC, A5tC and A20tC were analyzed. To evaluate the amount of compaction that occurred, the volumes of the compacted layers following 14 days of culture were calculated. To do so, a laser displacement technique was used to measure the thickness of the composite layer in 3 places per sample.³⁰ A disk with diameter 13 mm, thickness of 1.3mm and weight of 1.3 g was placed on the top of the sample prior to measuring. The disk did not deform the layers, but enabled a reflective surface for accurate thickness measurements. The widths of the constructs were also measured using calipers. For both metrics, 3 measurements were taken and averaged. To calculate the volume, a rectangular geometry was assumed. Calculations were also completed for acellular (non-compacted) composite layers.

Unsterilized fibrin microthreads (in acellular layers) were assumed to have a diameter of ~110 μm while ethanol-sterilized fibrin microthreads (in cultured layers) were assumed to have a diameter of ~99 μm .²² Reported modulus values for uncrosslinked fibrin microthreads range from 2.2 to 22.3 ± 15.1 MPa.^{22-23, 31} Additionally, fibrin microthreads with human MSCs seeded on the surface and cultured with aprotinin supplementation for 3 days have reported modulus values of ~0.07 MPa.³² To incorporate the most appropriate parameters into our model, the stiffness values of compacted layers following 14 days in culture were compared to stiffness values of acellular composite layers with the same microthread configuration (i.e. cultured 5tC layers were compared to acellular 5tC layers). The stiffness was determined to be the slope of the load versus extension curve. We assumed that the stiffness of the composite layer was predominantly from the microthreads. If changes in the mechanical properties of the microthreads occurred over the culture period, differences in the stiffness values would be evident. With an understanding of the impact of culture on the mechanical nature of the microthreads, we then back-calculated what modulus values corresponded to the observed stiffnesses using Equation 4.2,

$$E = \frac{K \times L}{A} \quad 4.2.$$

where E is the modulus, K is the stiffness, L is the length of the fibrin microthreads, and A is the cross-sectional area of the fibrin microthreads. With the calculated modulus values and volume fractions of each component, Equation 4.1 was used to estimate the elastic modulus of the compacted layers.

4.2.5.2. Mechanical Testing of Compacted Composite Layers.

A submerged uniaxial tensile test was used to characterize cell-populated fibrin composite layers. To ensure that contractions of incorporated cells did not impact the evaluation of the material, scaffolds were cooled to room temperature in PBS and monitored for cessation of contractions. Frames of composite layers were glued using medical grade silicone adhesive (Factor II, Inc, Lakeside, AZ) to modified vellum frames for securing into the test apparatus. Mechanical characterization of the scaffolds was independent of the frame. To assess the cross sectional area of the samples, a laser displacement technique was used to measure the thickness of the composite layer in 3 places per sample.³⁰ For these measurements, a reflective disk diameter 13 mm, thickness of 1.3mm and weight of 1.3 g was used to ensure a highly reflective surface and accurate thickness measurements. The width of the samples were measured in 3 places and averaged, and used with the thicknesses to calculate the cross-sectional area, assuming a rectangular geometry.

Samples were secured in an ElectroPuls E1000 Instron (Norwood, MA) with a 1 N load cell and an initial gauge length of 12 mm. The sample and grips were submerged in a PBS bath. Uniaxial loading until failure was completed at a strain rate of 10 mm/min. Displacement and force values were recorded throughout the test at a frequency of 10 Hz. Engineering stress was calculated by dividing the amount of force recorded by the initial cross-sectional area. Strain was calculated as the increased extension from the initial length of the samples. The modulus of the layers was evaluated with a MATLAB (MathWorks, Natick, MA) script. Composite materials characteristically have two phases in the plotted stress strain curves.²⁹ Because in native tissue the myocardium is loaded cyclically experiencing strains often exceeding 20% strain,³³ we analyzed the modulus in the first phase (0-30% strain range). Outliers were identified as any modulus value that was 1.5 times greater than the inner quartile range (IQR) for each sample set (min: quartile 1 - 1.5*IQR, max: quartile 3 + 1.5*IQR) and were subsequently removed from further analysis.²⁴

4.2.6 Phenotypic Analyses

4.2.6.1 Immunostaining

To evaluate alignment and the cardiomyocyte phenotype sarcomeric α -actinin, connexin-43 and Hoechst were used to visualize the sarcomeric structure of cardiomyocytes, distribution of gap junction protein and the orientation of nuclei, respectively. Human myocardium was used for the

positive and negative control tissues. The heart tissue was cut into 1-inch cubes prior to fixation. Cubes were fixed in 4% paraformaldehyde overnight, then incubated in a 30% sucrose solution for 24 hours. The heart tissue was embedded using OCT and cryosectioned at 10 μm thick using a Leica CM 3050 cryostat (Leica Microsystems). Composite samples were fixed with 4% paraformaldehyde after 14 days in culture. Samples and control tissues were permeabilized with 0.1% Triton, then blocked using 5% goat serum in PBS (Invitrogen, Carlsbad, CA). Samples and positive controls were incubated for 60 minutes with mouse monoclonal to sarcomeric α -actinin primary antibody (Abcam, Cambridge, MA), and rabbit polyclonal to connexin 43 (Abcam) in a blocking solution. The negative control was incubated for 60 minutes in PBS and blocking solution with no primary antibodies. All samples then were incubated with secondary antibodies (Goat anti-mouse Alexa Fluor 546, Life Technologies, Waltham, MA and Goat anti-rabbit Alexa Fluor 488, Life Technologies) at room temperature for 30 minutes. Hoechst counterstain (Thermo Fisher Scientific) was incubated with the samples at room temperature for 10 minutes. Samples and control tissues were imaged using a confocal microscope (TCS SP5 Point Scanning Confocal, Leica, Germany). For the nuclear orientation evaluation, 3 representative images of the width of each construct were obtained at 200X. To visualize connexin-43 distribution and sarcomeric α -actinin, an image at 400X was obtained.

4.2.6.2 Analysis of Nuclear Alignment

Nuclear alignment was evaluated for the positive control, UA5tC and A5tC constructs. The fluorescent images were analyzed using ImageJ (NIH). For each condition, a total of 6 samples (18 representative images) were evaluated after 14 days in culture. A binary image was generated after isolating the blue channel (representing nuclear staining by Hoechst). The particle analysis function within the ImageJ software was used to analyze the particles. The orientation of the long axis of the nucleus was taken relative to the incorporated fibrin microthreads. For positive controls, the nuclei were analyzed with respect to the predominant direction of alignment within each image. Any nuclei on the edge of the image, or in contact with any other nuclei were excluded from analysis. Values were plotted as histograms in 15° increments as representative of the distribution of the nuclear orientations within each group.

4.2.7 *Statistical Analyses*

Statistical analyses were run using SigmaPlot 13 (SYSTAT software, Chicago, IL) software. For all comparisons, a significance level of $p < 0.05$ was utilized. For contractile strains and frequencies, comparisons were made using a Two-way ANOVA on ranked data with a Holm-Sidak post-hoc analysis. For signal propagation speed comparisons, a t-test was used to compare speeds parallel and perpendicular to the fibrin microthreads. For the uniaxial tensile data, a one-way ANOVA on ranks with Dunn's post-hoc comparison was used to compare 5tC and 10tC cultured and acellular layers. A Students t-test was used to compare the 20tC acellular and cultured layers. For all data presented, data are reported as means \pm standard deviation.

4.3 RESULTS

4.3.1 *Static Tension Induced Through Gel Compaction Improves Nuclear Alignment of Incorporated Cells in Composite Layers.*

Evaluations were completed of the nuclear orientation of cells relative to the fibrin microthread for composite layers and relative to the predominant direction of alignment for positive control samples of human myocardium. With this analysis method, the positive control has the highest alignment of incorporated cells as is shown in **Figure 4.5**. The majority (46%) of the nuclei were within the $0-15^\circ$ bin with the lowest percentage of cells (~5%) in the $60^\circ < x < 75^\circ$ and $75^\circ < x < 90^\circ$ bins. The A5tC layers had a skewed distribution qualitatively similar to the positive controls with the majority of the nuclei (28%) falling with the $0-15^\circ$ bin. The lowest number of nuclei (12%) for the A5tC group fell within the $75^\circ < x < 90^\circ$ bin. The UA5tC group had a uniform distribution across all bins with 15-20% of nuclei falling within each bin range as would be expected from random alignment.

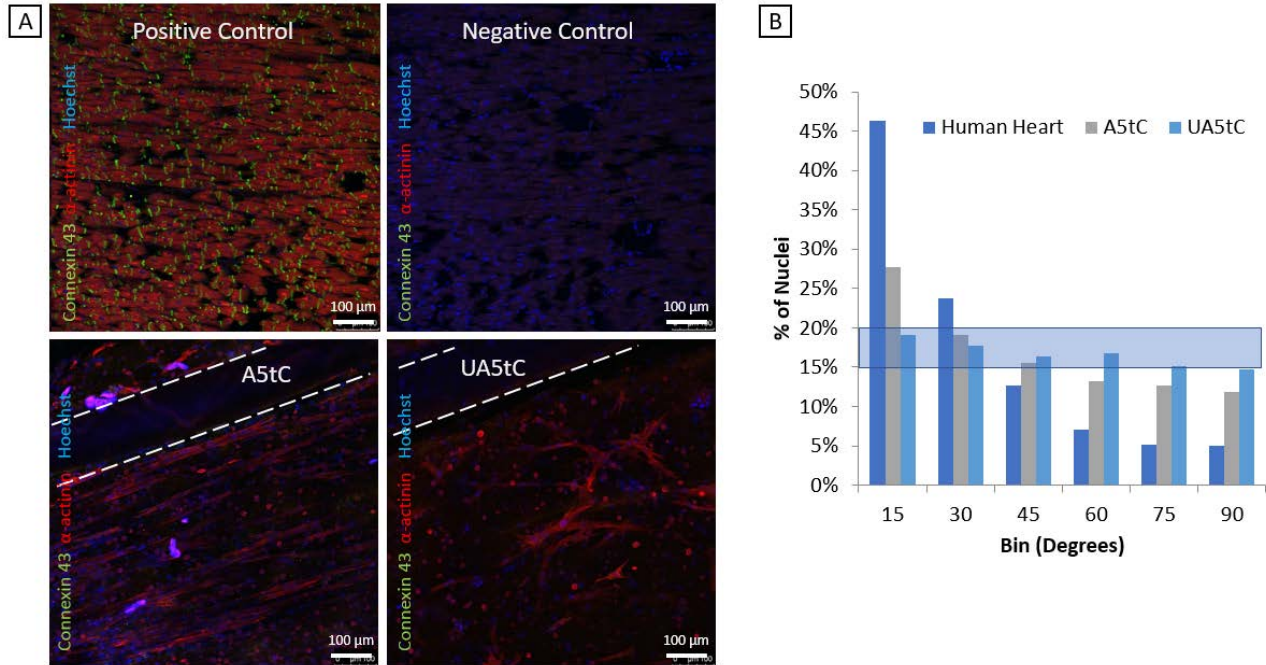


Figure 4.5. Nuclear alignment evaluation. Representative images of positive controls (human heart tissue), A5tC and UA5tC composite layer groups stained with sarcomeric α -actinin, connexin 43 and Hoechst are shown in A. When isolating the Hoechst channel, nucleus orientation was evaluated relative to fibrin microthreads (white dotted lines) or the predominant direction of alignment for positive controls. Distribution of nuclei orientations is shown in B, with human heart demonstrating the greatest alignment. When comparing to the positive control group, A5tC layers more closely mimic the control distribution than UA5tC layers.

4.3.2 Immature Connexin-43 Phenotype Observed Across 5tC Layers.

Positive control samples (human heart sections), A5tC layers and UA5tC layers were stained with sarcomeric α -actinin, connexin 43 and Hoechst. When evaluating the phenotype of incorporated cells, it was observed that all cells demonstrated a striated appearance (α -actinin) characteristic of a contractile cardiomyocyte phenotype (**Figure 4.6**). Connexin 43 distribution in the positive controls was polarized with clear banding visible at the ends of the cells, a phenotype characteristic of mature cardiomyocytes. Connexin 43 distribution in the A5tC and UA5tC groups was more circumferential with positive staining visible between cells, but not polarized. This staining pattern is characteristic of an immature cardiomyocyte phenotype.³⁴

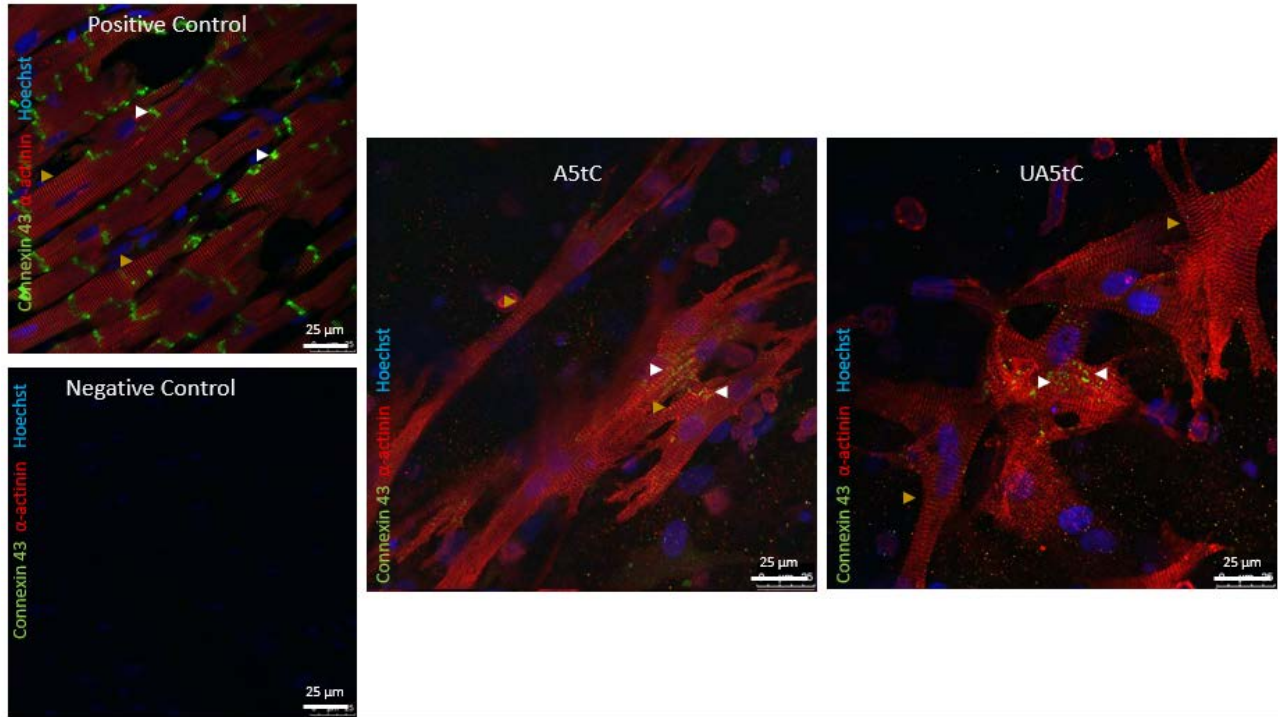


Figure 4.6. Phenotypic comparison of aligned composite layers, unaligned composite layers and human heart tissue controls. Positive and negative control tissue was cryosectioned human heart tissue. All samples were stained with connexin 43, sarcomeric α -actinin, and Hoechst. Yellow arrows show striations from α -actinin and white arrows show positive connexin 43 staining.

4.3.3 Composite Layers with Increased Alignment Have Higher Contractile Strains and Larger Contractile Areas Relative to Unaligned Controls.

Macroscopic differences among UA5tC and A5tC groups were visible at day 14. While the UA5tC group had contractions occurring all over the layer, they appeared to not have a uniform direction. This was in contrast to the A5tC layers which appear to contract in the same direction across the layer. For the large ROI assessment, HDM was utilized to assess the functional behavior of incorporated rNVMs in composite layers and on gelatin-coated coverslip controls (GCS) (**Figure 4.7 A**). For each sample, the principal angle was determined for 5 contractions. The range of the determined angles was then calculated. Ranges were averaged for each group at each timepoint and are summarized in (**Figure 4.7 B**). At day 7, maximum principal contractile strains were greatest in the UA5tC group (**Figure 4.7 C**) ($10.4\% \pm 3.1$). By day 10, A5tC min and A5tC max regions were greater than UA5tC and GCS ($10.3\% \pm 3.5$, $18.4\% \pm 7.9$, $7.1\% \pm 2.1$ and $4.7\% \pm 0.7$, respectively). A similar trend was observed at day 14. Average principal contractile strains followed a similar pattern to the maximum principal strains (**Figure 4.7 D**). Significant increases

in strain relative to the GCS controls were evident at day 14 for UA5tC, A5tC min and A5tC max groups ($1.4\% \pm 0.2$, $2.5\% \pm 0.7$, $3.2\% \pm 1.9$ and $4.6\% \pm 2.4$, respectively). Contractile areas were similar between all groups at day 7 with a significant increase observed for A5tC regions (min and max) by day 10. At day 10, A5tC max areas had significantly greater contractile areas relative to the UA5tC group ($90.5\% \pm 6.0$ and $81.8\% \pm 4.1$, respectively). By day 14, all groups had similar contractile areas again ranging from $84.1\% \pm 5.3$ (GCS) to $91.5\% \pm 3.9$ (A5tC Max) (**Figure 4.7 E**). All groups had similar contractile frequencies across the 14-day culture period with no significant differences observed (values ranging from 1.6 to 2.1 Hz) (**Figure 4.7 E**).

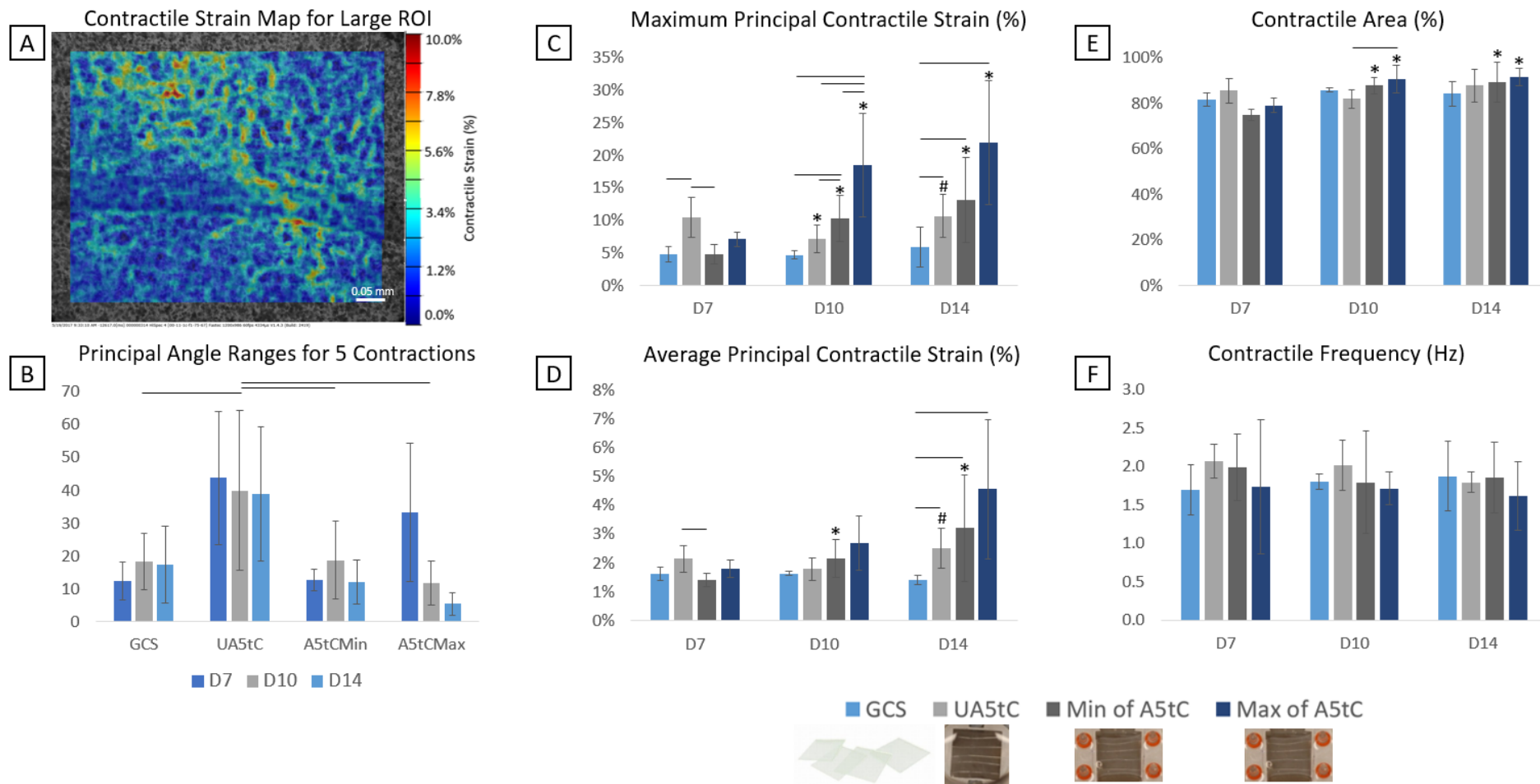


Figure 4.7. Contractile behavior evaluation through HDM with a large ROI. The ROI and distribution of contractile strains across the region are shown in A. The uniformity of contractions was evaluated with a principal angle assessment (B). Maximum principal contractile strains (C), average principal contractile strains (D), contractile areas (E), and contractile frequencies (F) were calculated for GCS, UA5tC, A5tC- Min and A5tC- Max regions. Statistical differences were evaluated through a two-way ANOVA on ranked data with a Holm-Sidak pos-hoc analysis, $p < 0.05$. Differences are shown within timepoints by a bar. Statistical differences within groups across timepoints are shown with *= significantly different from day 7 timepoint and # = significantly different from day 10 timepoint. Data are presented as averages \pm standard deviations.

4.3.4. The Highest Contractile Strains are Predominantly in Regions Immediately Adjacent to Fibrin Microthreads for Aligned Composite Layers.

To assess variations across a recorded region, a grid assessment was completed with HDM in which 20 smaller sub-regions were analyzed to quantify the maximum contractile strain and its associated principal angle (**Figure 4.8 A**). Additionally, the average contractile strain was evaluated for each sub-region. With this data, the distance of the region with the highest maximum contractile strain, and highest average contractile strain from the nearest incorporated fibrin microthread was calculated (**Figure 4.8 C-D**). For the highest maximum contractile strains, an overall trend showed that these regions were typically regions that contained fibrin microthreads (a distance of 0 mm). An increasing distance from microthreads corresponded to decreasing occurrences of the highest maximum contractile strains. When evaluating this data on a group-by-group basis, the same distribution was observed for the A5tC layers (max and min regions). The UA5tC layers did not have the same trend; the highest maximum contractile strains were observed ~200 μm from the nearest fibrin microthread. When evaluating the highest average contractile strains, a similar overall trend was observed to the highest maximum contractile strains, although not as prominent. Again, the A5tC layers had the same trend as with the highest maximum contractile strains. The UA5tC layers had the same trend, where the highest average strains were observed ~200 μm from the nearest fibrin microthread.

4.3.5. Consistency of Contractile Behavior is Similar for All Composite Layer Groups.

The grid assessment was used to evaluate the consistency of contractile behavior across the entire recorded region. Principal angles for all 20 ROIs within a grid were compared and a range of angles calculated for each sample group at timepoints 7, 10 and 14 days in culture (**Figure 4.8 B**). When comparing the principal angle ranges through a Two-way ANOVA, no significant differences based on group were observed. Significant differences based on timepoint were found with day 14 having significantly lower ranges than day 7 and day 10 (day 14 and day 7: $p=0.038$, day 14 and day 10: $p=0.025$). This suggests that all groups experienced a decrease in principal angle range over time as contraction angles across the recorded region became more consistent. An F50 factor was also calculated to quantify the consistency of the contractile strains observed across the recorded region. All groups had similar distributions with most samples having an F50

of ~80% for the maximum contractile strains. For the average contractile strains, an overall trend was that the majority of samples had an F50 value of 100% suggesting consistent contractile behavior across recorded regions. For A5tC max regions, the majority of samples had an F50 value of 80%, unlike the A5tC min and UA5tC groups whose majorities were F50 values of 100%. However, the majority of samples for all groups had F50 values $\geq 80\%$ suggesting similar consistencies in contractile behaviors across all groups.

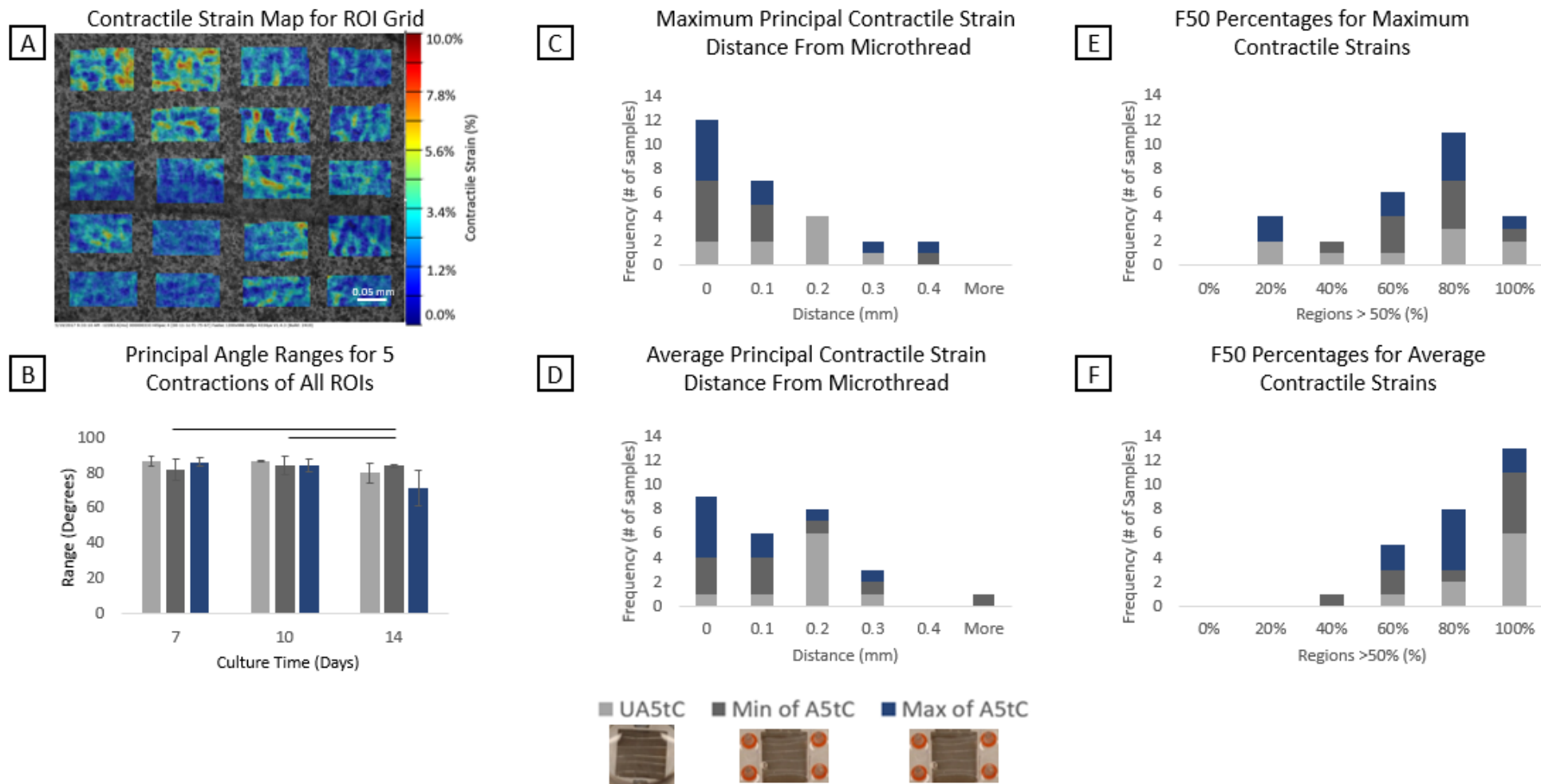


Figure 4.8 A grid assessment for evaluation of contractile behavior consistency across a recorded region. Recorded regions were broken up into 20 sub-regions to evaluate contractile strains (A) and associated principal angles (B). No significant differences in principal angle ranges were observed suggesting similar behavior across all groups. Evaluation of the distance for the highest maximum and highest average contractile strains from the incorporated fibrin microthreads were evaluated (C-D). Similar trends were observed for A5tC layer regions, with highest strains being in regions immediately adjacent to microthreads. Additionally, consistency of contractile strain values across ROIs was compared using a F50 factor (E-F) with similar behavior across all groups.

4.3.6 Composite Layers with Increased Alignment Have Anisotropic Contractile Wave Propagation Speeds

With the large ROI assessment, the smallest range in principal angles was observed for the A5tC Max group suggesting that this group had the most synchronous contractions. As such, contractile wave propagation assessments focused on this sample group specifically. Contractile wave propagation speeds through the A5tC max regions were evaluated at day 14 for directions parallel and perpendicular to the incorporated fibrin microthreads. These assessments were completed of spontaneously occurring contractions that occurred at a frequency of ~1.6 Hz. The fastest velocity evaluated across all samples was 19.1 mm/s. At that velocity, the distance traveled was ~0.5mm. The time required to travel this distance at that speed was 0.03 s. With a recording framerate of 60fps, 1 frame is recorded every 0.017 s. This implies that at that speed, 2 frames would be taken. The recording framerate was sufficient for capturing the fastest velocity observed in this work.

Samples from 3 separate trials (2 samples per trial) were evaluated. Velocities were anisotropic for the A5tC- Max group; 11.1 ± 1.5 mm/sec and 4.5 ± 2.0 mm/sec in directions parallel to and perpendicular to the fibrin microthreads, respectively (**Figure 4.9**). There was a significant difference between these speeds, as evaluated through a t-test, $p < 0.05$.

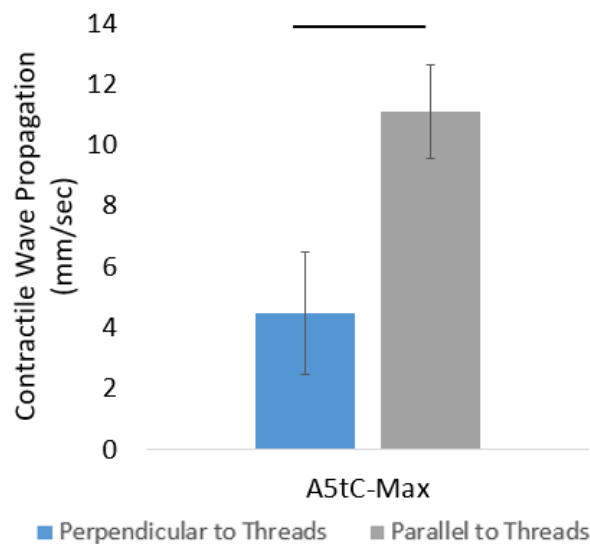


Figure 4.9. Contractile wave propagation speeds of spontaneous contractions at a frequency of ~1.6 Hz through A5tC Max regions. Velocities parallel to the threads were compared to speeds perpendicular to threads through a t-test. A bar represents significant difference, $p < 0.05$, $n = 3$.

4.3.7 A Model Based on Composite Theory Can be Derived to Predict Modulus Values of Fibrin Composite Layers Following Compaction

Following a 14-day culture, A5tC, UA5tC, and A20tC samples were measured to determine the new volume of each construct and the amount of compaction that occurred (**Table 4.1**). The greatest amount of compaction was observed in A5tC samples (65%). The UA5tC and A20tC samples had similar compaction with values near 50%.

Table 4.1. Summary of compaction occurring over 14 days of culture.

<i>Group</i>	<i>Average Volume Compaction Relative to Acellular Scaffolds</i>
<i>UA5tC</i>	54%
<i>A5tC</i>	65%
<i>A20tC</i>	48%

Stiffness values were determined by taking the slope of load versus extension curves for acellular and cultured A5tC and 20tC layers (**Table 4.2**). The stiffness values were compared to determine whether any changes in the mechanical integrity of the microthreads occurred over the 14-day culture period. For 5tC layers, no difference was observed across any groups. For the 20tC layers, a significant difference between the acellular and cultured layer stiffness values was observed, as evaluated through a t-test with $p < 0.05$.

Table 4.2. Stiffness values for acellular and cultured composite layers. * indicates significant difference as evaluated through a t-test, $p < 0.05$.

<i>Group</i>	<i>Stiffness (N/m)</i>
<i>A5tC- Acellular</i>	7 ± 3
<i>UA5tC- Cultured</i>	7 ± 2
<i>A5tC- Cultured</i>	7 ± 6
<i>A20tC - Acellular</i>	$26 \pm 7^*$
<i>A20tC- Cultured</i>	$20 \pm 8^*$

The stiffness values for the 20tC layers were evaluated to determine the respective modulus values for microthreads incorporated in acellular and cultured layers (**Table 4.3**) The modulus was

reduced ~7% for the microthreads in the cultured layers relative to the acellular layers, again with the assumption that the any stiffness contributed by the matrix component of the composite layer was negligible relative to the stiffness of the microthreads.

Table 4.3. Calculated modulus values for microthreads in acellular and cultured composite layers.

<i>Group</i>	<i>K (N/m)</i>	<i>L (m)</i>	<i>A (m²)</i>	<i>E (kPa)</i>
<i>A20tC - Acellular</i>	26 ± 7	0.012	1.9 x 10 ⁻⁷	1642
<i>A20tC- Cultured</i>	20 ± 8	0.012	1.6 x 10 ⁻⁷	1528

Volume fractions of each component were calculated factoring in the compaction observed. These values in combination with the calculated fibrin microthread modulus values were used to estimate the modulus of acellular and compacted composite layers. When comparing measured acellular modulus values for 5tC and 20tC layers¹⁴ to model predictions, values were very similar. When comparing the measured acellular values to predicted values for cultured layers, all moduli values increased (**Table 4.4**).

Table 4.4. Predicted moduli values for compacted and non-compacted (acellular) constructs.

<i>Group</i>	<i>Predicted Acellular Modulus (kPa)</i>	<i>Measured Acellular Modulus Value (kPa)¹⁴</i>	<i>Predicted Compacted Modulus (kPa)</i>
<i>UA5tC</i>	24	20.6 ± 8.1	38
<i>A5tC</i>	24	20.6 ± 8.1	51
<i>A20tC</i>	94	97.5 ± 49.3	142

4.3.8 Composite Layers Compact in Culture Resulting in an Increased Modulus for 5tC Layers.

Submerged, uniaxial tensile testing was completed to evaluate layers following a 14-day culture. Elastic modulus values were calculated as the slope of the engineering stress vs engineering strain curves in the first phase of the curves (~0-30% strain). The UA5tC, A5tC and A20tC groups had an elastic modulus of 47 ± 21, 40 ± 26 and 97 ± 29 kPa, respectively (**Figure 4.10**).

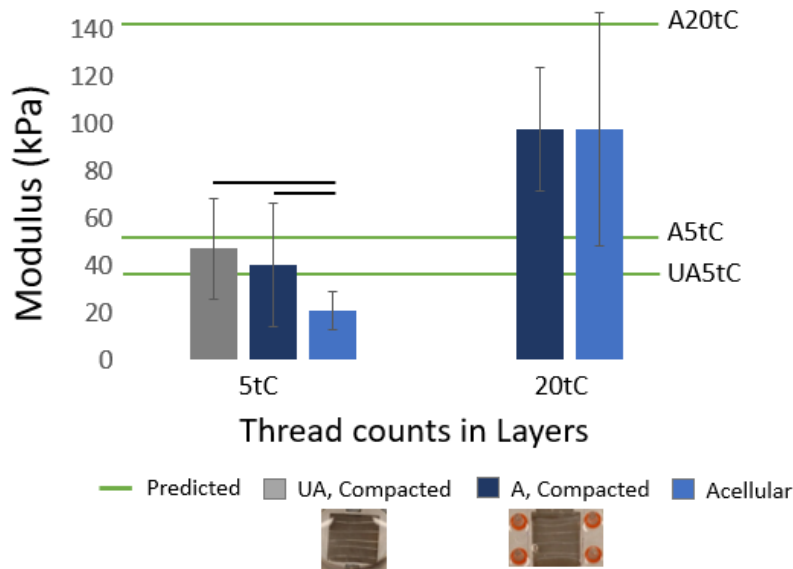


Figure 4.10. Comparison of modulus values for predicted and measured cultured composite layers and acellular controls. UA5tC, A5tC and A20tC layers were cultured for 14 days and then uniaxially tensile tested to determine the modulus for each group. Green lines represent the predicted modulus values from the developed model. Black bars represent significant difference as evaluated through an ANOVA on ranks with Dunn’s post-hoc comparison, $p < 0.05$.

The predicted values for 5tC layers were similar to the measured values, and were within 1 standard deviation of the measured values. When comparing the modulus values for cultured 5tC layers to previously reported acellular 5tC layers,¹⁴ UA5tC and A5tC groups had significantly increased modulus values as evaluated through an ANOVA on ranks with Dunn’s post-hoc comparison, $p < 0.05$. In fact, the UA5tC and A5tC groups were closer to the measured acellular 10tC layers with no significant differences observed in modulus values (47 ± 21 kPa, 40 ± 26 kPa, 46 ± 23 kPa, respectively). The A20tC predicted value was greater than the measured value, and was slightly more than ~ 1.5 standard deviations greater than the measured value. The cultured 20tC layer did not increase relative to the acellular 20tC layers (97 ± 29 kPa and 98 ± 49 kPa, respectively).

4.4 DISCUSSION

The goal of this study was to evaluate how alignment induced by cell-mediated compaction of composite layers would impact cell function. We compared GCS and UA5tC controls to A5tC layers for functional assessments of principal contractile strains and the associated principal angle, contractile areas, and contractile frequencies via HDM analysis. Large region ROIs and grid ROIs

were utilized to assess contractile behaviors for a recorded region and to assess variations across the recorded region, respectively. All efforts for functional evaluations were completed with rat neonatal ventricular myocytes in 5tC layers as the acellular modulus (20.6 ± 8.1 kPa)¹⁴ most closely mimics the modulus of rat neonatal myocardium ($10 - 20$ kPa)³⁵. Further, we compared the phenotype of incorporated rNVMs in A5tC and UA5tC layers to human heart tissue controls. Finally, we evaluated how compaction impacted the mechanical properties of the composite layers. For this assessment, we not only evaluated UA5tC and A5tC groups, but also A20tC groups to determine whether the impact in compaction was evident across samples with a larger volume fraction of microthreads.

We demonstrated that the culturing method presented increases nuclear alignment relative to UA5tC controls. When evaluating human heart tissue as a control, only ~46% of the nuclei had an offset of 0-15°. It has been reported that myocardium is a highly aligned tissue where fibers within each layer of the tissue are within 0-13° of the mean fiber direction. The orientation of the cells within each layer closely follow the fiber orientation.¹⁶ The method used to evaluate nuclear alignment involved taking a confocal image and isolating the blue (Hoechst) channel. It is possible that the confocal image had nuclei that were not entirely within the plane imaged. If a nucleus were out of plane but partially imaged, it may appear to have a different orientation than it truly does. While this may have reduced the alignment measured, it was done consistently for each sample, enabling comparisons.

When evaluating the orientation of nuclei within the A5tC layers, it was impossible to separate out the max and min regions that were analyzed for function. This is because without seeing the contractions occurring within each region, we were not able to ensure that we were evaluating alignment in those specific areas. Instead, we evaluated the entire A5tC layer and reported alignment for the overall group. However, there were visible differences in alignment for the A5tC layers regionally, as was observed in the functional analysis. It is possible that compaction did not occur uniformly throughout the layer. Inducing alignment through cell-mediated gel compaction is similar to other published methods where ends of the scaffolding material are restricted. In a pioneering work completed by Zimmermann et al, edges of a fibrin hydrogel-based scaffold were restricted by pieces of Velcro. The authors observed variations in alignment with the greatest concentration of longitudinally oriented cells at the free edges of the

construct.¹⁷ While we observed spatial variations as well, the variations were not consistently at the edges across all samples. In some cases, the greatest functionality and alignment was within the center areas of the constructs. The fibrin microthreads may have acted as a barrier for compaction, or influenced the areas that most greatly compacted resulting in regional variability.

A potential alternative in the future is to utilize a smaller fibrin microthread length. While these layers used continuous fibers that extended through the entire length of the construct, mechanical reinforcement can be achieved as long as the fiber length is greater than the critical length needed for the material.²⁹ The critical length is dependent on fiber diameter, the tensile strength of the fiber and the fiber-matrix bond strength. In reports of utilizing a silk fiber to reinforce silk hydrogels, critical lengths reported were on the order of 500 μm .³⁶ It is likely that the critical length for fibrin microthreads in a fibrin hydrogel is reduced from the current length used (12 mm). If we used shorter, discrete, aligned fibers it is possible that more uniform compaction could be achieved. With more uniform compaction, it is possible that greater alignment and more uniform functionality throughout the layer could result.

HDM evaluations were completed for large ROI regions. In those comparisons, A5tC layers had greater contractile strains and larger contractile areas relative to GCS and UA5tC controls. This is likely due to the increased alignment of incorporated rNVMs as cardiomyocyte alignment may contribute to enhanced functional maturation.^{18, 37-39} All functional parameters increased over the culture period, with the exception of contractile frequency which was maintained at a consistent level from 7- 14 days. It has been reported that, for a fibrin hydrogel, constructs finished compaction at days 8-13 in culture.¹⁹ It is possible that the increase over the culture period in contractile strains and areas was due to compaction occurring throughout the 14 days, resulting in increased alignment throughout the culture period.

Contractile strains measured in normal myocardium have been reported to be ~19%.⁴⁰ Maximum contractile strains observed for the A5tC max areas were near ~18% on day 10 and ~22% on day 14. While these values are very near the reported value for healthy myocardium, it should be noted that different methods were used to assess the contractile strains. With HDM, the use of different parameters (averaging windows, subimage size and subimage shift) can greatly impact the measured values.²⁶ While we optimized these parameters to improve the signal to noise

ratio and believe the results to be near the actual values, the best comparison would be to evaluate healthy myocardium using the same method.

We observed lower contractile frequencies for all groups (1-5- 2.0 Hz) than reported frequencies for neonatal cardiomyocytes in a 3D environment (2.5-3Hz^{17, 41}). Data collection for the functional experiments was completed on days 7, 10 and 14. However, it has been reported that contractile frequencies for rNVMs have decreased in culture as early as day 6.⁴¹ It is possible that the contractile frequencies reduced prior to the data collection timepoints.

For the large ROI evaluations, one assessment focused on the consistency of principal angles for different contraction cycles. If all cells are contracting in sync, one principal angle should be observed for the entire ROI. However, if multiple contractions are occurring out of sync, then when evaluating different contraction cycles different principal angles may be observed. With this evaluation, the 2D GCS controls had reduced ranges relative to UA5tC 3D controls. This is likely because in a 2D environment, all cells are within one plane and may more easily make cell-cell connections than in a 3D environment. The A5tC Max group was the only group to show a decreasing trend in the principal angle ranges observed. By day 14, the A5tC Max group had the smallest ranges observed of all groups suggesting that this group had the most synchronous contractile behavior. Because the A5tC max regions had the lowest ranges shown for the large region ROI principal angle assessment, the contractile wave propagation speed was evaluated for this sample group at day 14.

The A5tC layers have anisotropic contractile wave propagation occurring, a sign of highly aligned tissue.¹⁵ This assessment does not conclusively show that conduction is occurring as we did not inhibit spontaneous contractions from occurring. While we did overlay and match strain curves, it is possible that spontaneous contractions were occurring at different locations in the layer. However, this method enables visualizations of cell shortening and does estimate contractile wave propagation speeds. Healthy myocardium has anisotropic propagation speeds with conduction velocities in the longitudinal direction and transverse direction being 73 ± 4 cm/s and 11 ± 3 cm/s, respectively³³ (anisotropic ratio = $\frac{\text{longitudinal}-\text{transverse}}{\text{longitudinal}+\text{transverse}} = 0.7$). The A5tC max regions had contractile wave velocities of 11.1 ± 1.5 mm/sec and 4.5 ± 2.0 mm/sec in directions parallel to and perpendicular to the fibrin microthreads, respectively (anisotropic ratio = 0.4). The magnitude of the velocities and the ratio of them was reduced relative to conduction speeds that

occur in healthy myocardium. It is likely due to immature gap junction formation as was confirmed with connexin 43 staining and imaging. Polarized gap junctions are characteristic of highly mature, functional myocardium.³⁴ We observed circumferential staining of connexin 43, characteristic of immature cardiomyocytes. This study utilized rat neonatal ventricular myocytes from 2- and 3-day old rats. Connexin-43 has been shown to exhibit dispersed distributions within the first 20 days of postnatal life with polarizations of gap junction proteins being more evident between 20-90 days of postnatal life.⁴² With an improvement in gap junction formation, it is likely that the signal propagation speed would increase. Additionally, the alignment of cells within the A5tC layers was reduced relative to human myocardium. Further increased alignment could also contribute to faster propagation speeds.

A grid assessment was completed for evaluation of regional variations within a recorded region. Consistency across samples was similar for all sample groups. The principal angle ranges for all groups significantly decreased over time. However, no significant differences in ranges were observed among groups. This was unexpected as it was hypothesized that, with increased alignment, a reduction in the range of principal angles across the grid ROIs would be observed. The high variation was expected for UA5tC samples as contractions were not aligned. For A5tC samples, contractions were visibly highly aligned and resulted in a wave-like motion. It is possible that this wave motion is what caused such high variability in the observed principal angles. This is because if one region contracting caused it to not only contract inward, but pull upward (like a wave), it would also pull adjacent regions. In those regions, when contractions would begin, pixels may have already been at a different angular offset from one another than when no cells in the recorded region were contracting. Another factor with this assessment was that in each trial, primary isolations of cells were utilized. Primary isolations can result in variations in the ratios of cells isolated. We have used a pre-plating step following isolation to try to enrich the number of cardiomyocytes and minimize this issue.¹⁹

The F50 factor was a method for quantifying the uniformity of contractile strains across the entire grid. Overall trends showed that the majority of samples had F50 values of 80% and 100% for maximum contractile strains and average contractile strains, respectively. The increased F50 value for the average strains relative to the maximum strains is not surprising; the maximum values were the highest values across the entire sample while the average was closer to the overall

mid-line contractile behavior observed. The similar distributions suggest that across all sample groups, contractile behavior is similarly consistent. The distributions would change with the factor level being set to a different threshold (i.e. 75% instead of 50%). For our purposes, the 50% benchmark resulted in non-flat distribution plots to assess patterns in behavior.

The grid assessment was also utilized to evaluate the distance of the highest maximum and highest average contractile strains from incorporated fibrin microthreads. What was observed is that overall, the highest values for both categories were in regions immediately adjacent to fibrin microthreads. It is possible that the microthreads may increase alignment in the immediately adjacent areas,¹⁴ resulting in greater contractile function. This pattern was observed for the A5tC max and min regions, but was not observed for the UA5tC samples whose highest contractile strains were $\sim 200\mu\text{m}$ from the nearest fibrin microthread. It is possible that this trend may be observed because, with the A5tC layers compaction brings more of the total gel phase in closer proximity to the incorporated fibrin microthreads. With the UA5tC samples, distances of the gel phase from the microthreads are consistently maintained. It is also possible that there are regional variations in the mechanical environment that are present for the UA5tC samples that are not observed with the A5tC layers. Cells have been shown to have the ability to sense rigid bodies not in direct cellular contact.⁴³ In fibrous polymers like fibrin, cell sensing distances of $\sim 150\mu\text{m}$ have been reported.⁴⁴ One hypothesis for the observed outcome is that the observed distance was a result of the cells no longer sensing the incorporated fibrin microthreads.

Compaction reduces the volume fraction of the gel phase of the composite layer. We developed a model for predicting modulus values of cultured, compacted layers. First, we evaluated the stiffness of acellular and cultured layers for 5tC and 20tC layers. Stiffness is a metric that can be utilized to compare the mechanical nature of the incorporated fibrin microthreads; cross-sectional area is not factored into stiffness. Stiffness was calculated by taking the slope of the load versus extension curve. We assumed that the contribution of the gel phase to the stiffness of the material was negligible. We found that the 5tC layers all had similar stiffnesses, suggesting that the culture did not impact the mechanical integrity of the incorporated fibrin microthreads. We did observe a significant difference between the acellular 20tC layer and the cultured 20tC layer. When calculating the modulus from the stiffness values for the 20tC samples, the difference resulted in a change of $\sim 7\%$. It is likely that this difference was not observed with the 5tC layers

as the standard deviations for each layer when evaluating stiffness was much greater than 7%. With fewer threads, the change may have been masked by variations observed in the data. As such, for the predictive model we incorporated the reduced modulus value for all cultured groups. The change in mechanical properties of 7% was reduced from previous reports of seeded microthread bundles cultured with aprotinin supplementation having modulus values reduced by an order of magnitude after 3 days in culture.³² This is likely because, in that particular study, the cells were seeded directly onto the microthreads while in our system cells were dispersed throughout the gel phase.

Through composite theory, we anticipated that we should see an increase in the measured modulus values for each group. While the anticipated trend was evident for the 5tC layers, when testing a 20tC layer, no increase was observed. Potentially because the 5tC layers initially began with a higher volume fraction of hydrogel relative to the 20tC layers, the effect of compaction on the modulus may have been more apparent with the 5tC groups. Another possibility is that the volume fractions were not estimated accurately with the method reported. As an example, if the diameter of the microthreads was overestimated, this would result in an overestimation of the volume fraction of the microthreads and ultimately an overestimation of the modulus of the layer. This may explain why the measured A20tC modulus was lower than anticipated. Additionally, the assumption of a rectangular geometry of the cross-section of the composite layers may not have been an accurate assumption. Compaction may have resulted in narrower hydrogel regions relative to regions with fibrin microthreads. This also could impact the calculated volume fractions. A potentially better way to estimate the volume fractions would be to measure images of the cross-sections of the composite layers using imaging software such as ImageJ.

In the future, we plan to investigate the critical lengths of fibrin microthreads needed for mechanical reinforcement. We hypothesize that shorter fibers will enable a more uniform compaction, increasing alignment and ultimately cell function. We further plan to laminate composite layers to mimic the hierarchical architecture and mechanical properties of ventricular myocardium. With lamination, an increase in patch thickness will be observed. To circumvent diffusion limitations and ensure cell viability, we plan to incorporate a fibrin gel-based vasculature into the cardiac patch. Ultimately, we anticipate that fibrin composite layers can be used to

generate a patch that is able to mechanically and functionally integrate into the host myocardium, promoting regeneration of functional myocardial tissue in an infarct environment.

4.5 CONCLUSIONS

In this work, we demonstrated that cell-mediated compaction of composite layers can increase the alignment of incorporated cells. With increased alignment, increases in contractile strain and contractile area were also observed. A grid assessment showed that consistency of contractile behavior of incorporated cardiomyocytes was similar across all sample groups. Additionally, for aligned samples, the highest contractile strains are predominantly found in regions immediately adjacent to fibrin microthreads. Contractile wave propagation occurring throughout the layer was anisotropic and fastest in the direction parallel to the threads for the aligned samples. However, signal propagation was slow relative to healthy myocardium and was likely due to the immature phenotype of the cells (circumferential distribution of the gap junction protein connexin 43). Compaction resulted in significantly increased modulus values for 5tC layers, but not for 20tC layers. Regional variations that were observed for alignment and function may have been due to non-uniform compaction occurring across the layers. In the future, we plan to investigate the critical length of microthread required for mechanical reinforcement to see if with a shorter length, more uniform compaction result increasing alignment and cell function.

4.6 ACKNOWLEDGEMENTS

This work was funded by NIH R01-HL115282 (G.R.G.), NSF IGERT DGE 1144804 and NIH 1R15HL137145-01 (G.D.P.).

4.7 REFERENCES

1. Kochanek, K. D.; Murphy, S. L.; Xu, J.; Tejada-Vera, B., Deaths: Final Data for 2014. *Natl Vital Stat Rep* **2016**, *65* (4), 1-122.
2. Frangogiannis, N. G.; Smith, C. W.; Entman, M. L., The inflammatory response in myocardial infarction. *Cardiovascular research* **2002**, *53* (1), 31-47.
3. Cohen, S.; Leor, J., Rebuilding broken hearts. Biologists and engineers working together in the fledgling field of tissue engineering are within reach of one of their greatest goals: constructing a living human heart patch. *Sci Am* **2004**, *291* (5), 44-51.
4. Mozaffarian, D.; Benjamin, E. J.; Go, A. S.; Arnett, D. K.; Blaha, M. J.; Cushman, M.; de Ferranti, S.; Despres, J. P.; Fullerton, H. J.; Howard, V. J.; Huffman, M. D.; Judd, S. E.; Kissela, B. M.; Lackland, D. T.; Lichtman, J. H.; Lisabeth, L. D.; Liu, S.; Mackey, R. H.; Matchar, D. B.; McGuire, D. K.; Mohler, E. R., 3rd; Moy, C. S.; Muntner, P.; Mussolino, M. E.; Nasir, K.; Neumar, R. W.; Nichol, G.; Palaniappan, L.; Pandey,

- D. K.; Reeves, M. J.; Rodriguez, C. J.; Sorlie, P. D.; Stein, J.; Towfighi, A.; Turan, T. N.; Virani, S. S.; Willey, J. Z.; Woo, D.; Yeh, R. W.; Turner, M. B.; American Heart Association Statistics, C.; Stroke Statistics, S., Heart disease and stroke statistics--2015 update: a report from the American Heart Association. *Circulation* **2015**, *131* (4), e29-322.
5. Radisic, M.; Christman, K. L., Materials science and tissue engineering: repairing the heart. *Mayo Clinic proceedings* **2013**, *88* (8), 884-98.
 6. Reis, L. A.; Chiu, L. L.; Feric, N.; Fu, L.; Radisic, M., Biomaterials in myocardial tissue engineering. *Journal of tissue engineering and regenerative medicine* **2014**, *10* (1), 11-28.
 7. Yanagawa, B.; Rao, V.; Yau, T. M.; Cusimano, R. J., Initial experience with intraventricular repair using CorMatrix extracellular matrix. *Innovations (Phila)* **2013**, *8* (5), 348-52.
 8. Jackman, C. P.; Carlson, A. L.; Bursac, N., Dynamic culture yields engineered myocardium with near-adult functional output. *Biomaterials* **2016**, *111*, 66-79.
 9. Jawad, H.; Lyon, A. R.; Harding, S. E.; Ali, N. N.; Boccaccini, A. R., Myocardial tissue engineering. *British medical bulletin* **2008**, *87*, 31-47.
 10. Kaiser, N. J.; Coulombe, K. L., Physiologically inspired cardiac scaffolds for tailored in vivo function and heart regeneration. *Biomedical materials* **2015**, *10* (3), 034003.
 11. El-Sherbiny, I. M.; Yacoub, M. H., Hydrogel scaffolds for tissue engineering: Progress and challenges. *Global cardiology science & practice* **2013**, *2013* (3), 316-42.
 12. Tandon, V.; Zhang, B.; Radisic, M.; Murthy, S. K., Generation of tissue constructs for cardiovascular regenerative medicine: from cell procurement to scaffold design. *Biotechnology advances* **2013**, *31* (5), 722-35.
 13. Kochupura, P. V.; Azeloglu, E. U.; Kelly, D. J.; Doronin, S. V.; Badylak, S. F.; Krukenkamp, I. B.; Cohen, I. S.; Gaudette, G. R., Tissue-engineered myocardial patch derived from extracellular matrix provides regional mechanical function. *Circulation* **2005**, *112* (9 Suppl), I144-9.
 14. Chrobak, M. O.; Hansen, K. J.; Gershlak, J. R.; Vratsanos, M.; Kanellias, M.; Gaudette, G. R.; Pins, G. D., Design of a fibrin microthread-based composite layer for use in a cardiac patch. *ACS Biomaterials Science & Engineering* **2016**.
 15. Kim, D. H.; Lipke, E. A.; Kim, P.; Cheong, R.; Thompson, S.; Delannoy, M.; Suh, K. Y.; Tung, L.; Levchenko, A., Nanoscale cues regulate the structure and function of macroscopic cardiac tissue constructs. *Proceedings of the National Academy of Sciences of the United States of America* **2010**, *107* (2), 565-70.
 16. Lee, W. N.; Pernot, M.; Couade, M.; Messas, E.; Bruneval, P.; Bel, A.; Hagege, A. A.; Fink, M.; Tanter, M., Mapping myocardial fiber orientation using echocardiography-based shear wave imaging. *IEEE transactions on medical imaging* **2012**, *31* (3), 554-62.
 17. Zimmermann, W. H.; Fink, C.; Kralisch, D.; Remmers, U.; Weil, J.; Eschenhagen, T., Three-dimensional engineered heart tissue from neonatal rat cardiac myocytes. *Biotechnology and bioengineering* **2000**, *68* (1), 106-14.
 18. Bian, W.; Jackman, C. P.; Bursac, N., Controlling the structural and functional anisotropy of engineered cardiac tissues. *Biofabrication* **2014**, *6* (2), 024109.
 19. Bian, W.; Liao, B.; Badie, N.; Bursac, N., Mesoscopic hydrogel molding to control the 3D geometry of bioartificial muscle tissues. *Nature protocols* **2009**, *4* (10), 1522-34.
 20. Liao, B.; Christoforou, N.; Leong, K. W.; Bursac, N., Pluripotent stem cell-derived cardiac tissue patch with advanced structure and function. *Biomaterials* **2011**, *32* (35), 9180-7.
 21. Cornwell, K. G.; Pins, G. D., Discrete crosslinked fibrin microthread scaffolds for tissue regeneration. *Journal of biomedical materials research. Part A* **2007**, *82* (1), 104-12.
 22. Grasman, J. M.; O'Brien, M. P.; Ackerman, K.; Gagnon, K. A.; Wong, G. M.; Pins, G. D., The Effect of Sterilization Methods on the Structural and Chemical Properties of Fibrin Microthread Scaffolds. *Macromolecular bioscience* **2016**, *16* (6), 836-46.
 23. Grasman, J. M.; Page, R. L.; Dominko, T.; Pins, G. D., Crosslinking strategies facilitate tunable structural properties of fibrin microthreads. *Acta biomaterialia* **2012**, *8* (11), 4020-30.
 24. Grasman, J. M.; Pumphrey, L. M.; Dunphy, M.; Perez-Rogers, J.; Pins, G. D., Static axial stretching enhances the mechanical properties and cellular responses of fibrin microthreads. *Acta biomaterialia* **2014**, *10* (10), 4367-76.

25. Morgan, K. Y.; Black, L. D., 3rd, Mimicking isovolumic contraction with combined electromechanical stimulation improves the development of engineered cardiac constructs. *Tissue engineering. Part A* **2014**, *20* (11-12), 1654-67.
26. Hansen, K. J.; Favreau, J. T.; Gershlak, J. R.; Laflamme, M. A.; Albrecht, D. R.; Gaudette, G. R., Optical Method to Quantify Mechanical Contraction and Calcium Transients of Human Pluripotent Stem Cell-Derived Cardiomyocytes. *Tissue engineering. Part C, Methods* **2017**.
27. Kelly, D. J.; Rosen, A. B.; Schuldt, A. J.; Kochupura, P. V.; Doronin, S. V.; Potapova, I. A.; Azeloglu, E. U.; Badylak, S. F.; Brink, P. R.; Cohen, I. S.; Gaudette, G. R., Increased myocyte content and mechanical function within a tissue-engineered myocardial patch following implantation. *Tissue engineering. Part A* **2009**, *15* (8), 2189-201.
28. Tao, Z. W.; Favreau, J. T.; Guyette, J. P.; Hansen, K. J.; Lessard, J.; Burford, E.; Pins, G. D.; Gaudette, G. R., Delivering stem cells to the healthy heart on biological sutures: effects on regional mechanical function. *Journal of tissue engineering and regenerative medicine* **2014**.
29. Callister, W. D.; Rethwisch, D. G., *Fundamentals of materials science and engineering : an integrated approach*. 4th ed.; Wiley: Hoboken, N.J., 2012; p xxv, 910 p.
30. Billiar, K. L.; Throm, A. M.; Frey, M. T., Biaxial failure properties of planar living tissue equivalents. *Journal of biomedical materials research. Part A* **2005**, *73* (2), 182-91.
31. Grasman, J. M.; Pumphrey, L.; Dunphy, M.; Perez-Rogers, J.; Pins, G. D., Static axial stretching enhances the mechanical properties and cellular responses of fibrin microthreads. *Acta biomaterialia* **2014**, *10* (10), 4367-76.
32. Coffin, S. T.; Gaudette, G. R., Aprotinin extends mechanical integrity time of cell-seeded fibrin sutures. *Journal of biomedical materials research. Part A* **2016**, *104* (9), 2271-9.
33. Capulli, A. K.; MacQueen, L. A.; Sheehy, S. P.; Parker, K. K., Fibrous scaffolds for building hearts and heart parts. *Adv Drug Deliv Rev* **2016**, *96*, 83-102.
34. Yang, X.; Pabon, L.; Murry, C. E., Engineering adolescence: maturation of human pluripotent stem cell-derived cardiomyocytes. *Circulation research* **2014**, *114* (3), 511-23.
35. Jacot, J. G.; McCulloch, A. D.; Omens, J. H., Substrate stiffness affects the functional maturation of neonatal rat ventricular myocytes. *Biophysical journal* **2008**, *95* (7), 3479-87.
36. Yodmuang, S.; McNamara, S. L.; Nover, A. B.; Mandal, B. B.; Aganwal, M.; Kelly, T. A. N.; Chao, P. H. G.; Hung, C.; Kaplan, D. L.; Vunjak-Novakovic, G., Silk microfiber-reinforced silk hydrogel composites for functional cartilage tissue repair. *Acta biomaterialia* **2015**, *11*, 27-36.
37. Black, L. D., 3rd; Meyers, J. D.; Weinbaum, J. S.; Shvelidze, Y. A.; Tranquillo, R. T., Cell-induced alignment augments twitch force in fibrin gel-based engineered myocardium via gap junction modification. *Tissue engineering. Part A* **2009**, *15* (10), 3099-108.
38. Chung, C. Y.; Bien, H.; Entcheva, E., The role of cardiac tissue alignment in modulating electrical function. *J Cardiovasc Electrophysiol* **2007**, *18* (12), 1323-9.
39. Pong, T.; Adams, W. J.; Bray, M. A.; Feinberg, A. W.; Sheehy, S. P.; Werdich, A. A.; Parker, K. K., Hierarchical architecture influences calcium dynamics in engineered cardiac muscle. *Exp Biol Med (Maywood)* **2011**, *236* (3), 366-73.
40. Taylor, R. J.; Moody, W. E.; Umar, F.; Edwards, N. C.; Taylor, T. J.; Stegemann, B.; Townend, J. N.; Hor, K. N.; Steeds, R. P.; Mazur, W.; Leyva, F., Myocardial strain measurement with feature-tracking cardiovascular magnetic resonance: normal values. *European heart journal cardiovascular Imaging* **2015**.
41. Bursac, N.; Loo, Y.; Leong, K.; Tung, L., Novel anisotropic engineered cardiac tissues: studies of electrical propagation. *Biochemical and biophysical research communications* **2007**, *361* (4), 847-53.
42. Angst, B. D.; Khan, L. U.; Severs, N. J.; Whitely, K.; Rothery, S.; Thompson, R. P.; Magee, A. I.; Gourdie, R. G., Dissociated spatial patterning of gap junctions and cell adhesion junctions during postnatal differentiation of ventricular myocardium. *Circulation research* **1997**, *80* (1), 88-94.
43. Buxboim, A.; Rajagopal, K.; Brown, A. E. X.; Discher, D. E., How deeply cells feel: methods for thin gels. *J Phys-Condens Mat* **2010**, *22* (19), 194116.
44. Rudnicki, M. S.; Cirka, H. A.; Aghvami, M.; Sander, E. A.; Wen, Q.; Billiar, K. L., Nonlinear strain stiffening is not sufficient to explain how far cells can feel on fibrous protein gels. *Biophysical journal* **2013**, *105* (1), 11-20.

Chapter 5: Fibrin Composite Layers Can Be Strategically Laminated to Mimic the Mechanical Anisotropy of Ventricular Myocardium

5.1 INTRODUCTION

Approximately 614,000 people died in 2014 from heart disease in the United States alone.¹ A key event that begins the progression towards heart failure is a heart attack. A heart attack initiates a series of events that ultimately culminate in scar tissue formation.² Scar tissue hinders the heart from performing as it should. While treatment options exist, they are palliative in nature and no current treatment acts to regenerate the damaged heart tissue. As such, there is a clinical need for a regenerative therapy for those with damaged myocardium.

A cardiac patch is one treatment option available to patients that aims to stop progression towards heart failure by limiting ventricular remodeling from occurring. Current patches are acellular and do not contribute to the active function of the heart.³ These approaches do not restore baseline function, but a cell-populated cardiac patch may be able to do so. For a patch to be able to provide functional assistance, it will need to integrate functionally and mechanically into the host myocardium. Matching mechanical properties of the laminated composite tissue with the surrounding myocardium is critical for efficiently coupling load transfer between the scaffold and the native tissue.⁴ For a material stiffer than myocardium, a tethering effect may be observed that hinders the mechanical functioning of the surrounding tissue. For materials less stiff than myocardium, the material may fail in the dynamic environment of the heart.⁵⁻⁶

We recently created fibrin composite layers for use in a cardiac patch.⁷ To date, we have demonstrated that fibrin hydrogels can be mechanically reinforced with fibrin microthreads with no impact to incorporated cardiomyocyte contractile strain or frequency. We showed that manipulation of the fibrin microthread volume fraction could tune the elastic modulus of the composite layers. Further, we observed that orientation of incorporated cells could be improved through cell-mediated compaction of the construct, inducing a static tension through the layer.

Compaction of the gel phase resulted in a significant increase in the composite modulus for 5-thread composite (5tC) layers, but did not result in a change for 20-thread composite (20tC) layers.

The material is an aligned, fiber reinforced anisotropic material. Ventricular myocardium is an anisotropic tissue that is comprised of multiple layers that rotate relative to one another from the endocardium to the epicardium (**Figure 5.1**). As such, we hypothesize that through the strategic lamination of composite layers, we can mimic the hierarchical and mechanical properties of ventricular myocardium.

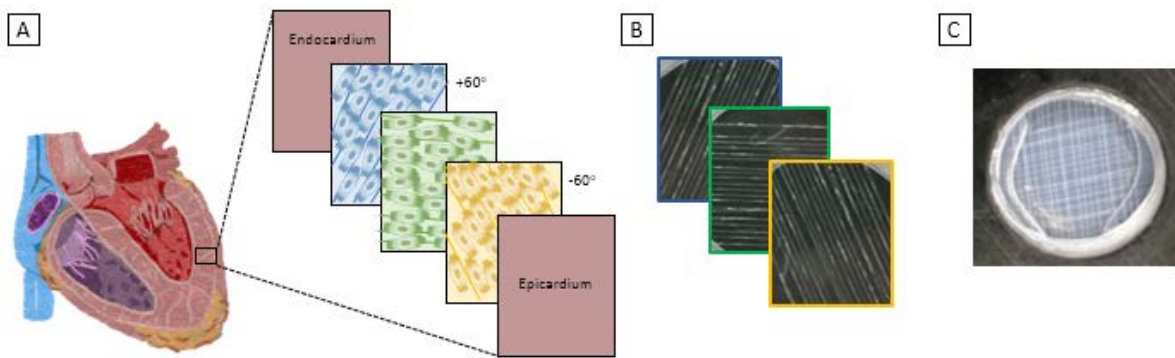


Figure 5.1. Biomimetic patch structure. Ventricular myocardium is comprised of layers that rotate relative to one another (A). We plan to mimic this structure with fibrin-based composite layers (B), ultimately producing a cardiac patch (C) with mechanical and hierarchical properties similar to ventricular myocardium.

To test our hypothesis, we first defined required material properties of a cardiac patch functioning as a wall replacement. We then generated a model using laminar composite theory to determine what angular offset of laminated layers would best mimic the anisotropic nature of the elastic modulus of ventricular myocardium. A lamination method was generated that utilized a fibrin glue to adhere layers together. In order to evaluate the effects of the fibrin glue on the mechanical properties, a control of two layers cast in one hydrogel and two layers glued together were uniaxially tensile tested. Uniaxial tensile testing was further completed to evaluate the mechanical properties of a cardiac patch with layers laminated to mimic the mechanical nature of ventricular myocardium. We then compared material properties of individual composite layers, laminated cardiac patches and target values of healthy myocardium. Ultimately, we envision this patch as a wall replacement that, when coupled with a vasculature system, could functionally and mechanically integrate with adjacent healthy myocardial tissue.

5.2 MATERIALS and METHODS

5.2.1 Definition of Material Requirements

Design criteria for the mechanical properties of a cardiac patch can be created from understanding the material properties of the ventricular myocardium. A defect area for an infarct is on average approximately 10-50 cm².⁸ By assuming a square defect area of 16 cm², we can define the length and width as 4 cm. The thickness of ventricular myocardium is approximately 1.5 cm.⁹ and the modulus of the myocardium ranges from 20-500 kPa.¹⁰ With this information, we can determine a membrane stiffness of ventricular myocardium using Equation 5.1.

$$E \times t = k \quad 5.1.$$

In Equation 5.1, E is the elastic modulus, t is the thickness and k is the membrane stiffness. For an axial elastic modulus, the slope of the stress strain curve would be evaluated where stress is calculated as the force applied divided by the initial cross-sectional area. For the membrane stiffness, the value would equate to the slope of a stress strain curve where the stress was calculated as the force applied divided by the initial width. Because loads in native myocardium are applied across the width of the sample rather than in a tensile fashion, this parameter is a more relevant comparison term. A literature search was conducted to evaluate the wall stress that the ventricular myocardium experiences. Information for a patient population with abnormally high ventricular pressure was used as this value is towards the upper range of what the patch would experience in vivo. To ensure the patch could withstand this stress, the ultimate tensile stress (UTS) of the patch will need to exceed this value. For our design criteria, the stress was multiplied by the thickness of the ventricular myocardium to determine force per width that would be required for a cardiac patch. Additionally, the corresponding strain at that stress value should correspond to what the heart typically experiences cyclically. With these values, design criteria for the cardiac patch were defined.

5.2.2 Composite Theory Model

Myocardium is composed of highly aligned layers that rotate relative to one another +/- 60°.⁹ To produce a cardiac patch with structural and mechanical properties similar to native tissue, we anticipate that lamination of composite sheets will need to occur at an angular offset. To understand which layer orientations may best mimic native myocardium, a model developed from the

generalized Hooke's law was used to estimate the contribution of a composite layer to the y and x direction moduli at various offset angles with assumed plane stress conditions.¹¹ Offset values ranged in 30 degree increments from 0- 120 degrees (the rotation observed of layers through the width of the ventricular wall of myocardium)¹². To calculate the modulus value of one individual layer in the x and y directions at an offset, the following equations were used:¹¹

$$\frac{1}{E_x} = \frac{\cos^4\theta}{E_1} + \frac{\sin^4\theta}{E_2} + \left(\frac{1}{G_{12}} - \frac{2\nu_{12}}{E_1}\right) * \sin^2\theta * \cos^2\theta \quad 5.4.$$

$$\frac{1}{E_y} = \frac{\sin^4\theta}{E_1} + \frac{\cos^4\theta}{E_2} + \left(\frac{1}{G_{12}} - \frac{2\nu_{12}}{E_1}\right) * \sin^2\theta * \cos^2\theta \quad 5.5.$$

Where

$$G_{12} = \frac{G_f * G_m}{G_f * V_m + G_m * V_f}$$

$$G_f = \frac{E_f}{2(1 + \nu_f)}$$

$$G_m = \frac{E_m}{2(1 + \nu_m)}$$

$$\nu_{12} = \nu_f * V_f + \nu_m * V_m$$

$$E_1 = E_f * V_f + E_m * V_m$$

$$E_2 = \frac{E_f * E_m}{E_f * V_m + E_m * V_f}$$

E_f = Elastic modulus of the fibrous component

E_m = Elastic modulus of the matrix phase

G_f = Shear modulus for the fibrous component

G_m = Shear modulus for the matrix phase

ν_f = Poisson's ratio for the fibrous component

ν_m = Poisson's ratio for the matrix phase

V_f = Volume fraction of the fibrous component

V_m = Volume fraction of the matrix phase

Because a significant difference was observed for 5tC layers following compaction in a 14-day culture period, two models were generated; an acellular model and a compacted model. Assumptions for each model are summarized in **Table 5.1**.

Table 5.1. Value assumptions for acellular and compacted composite layer models.

<i>Parameter</i>	<i>Acellular Model Value</i>	<i>Compacted Model Value</i>
Ef	1642 kPa*	1528 kPa*
Em	0.25 kPa ¹³	0.25 kPa ¹³
Layer Volume	40 mm ³	14 mm ³ for 5tC layers 20 mm ³ for all others
vf	0.3 ¹⁴	0.3 ¹⁴
vm	0.25 (Assumes perfectly isotropic material) ¹³	0.25 (Assumes perfectly isotropic material) ¹³

*Values calculated in Chapter 4: Alignment of Cardiomyocytes Through Static Tension Increases Contractile Strains in Composite Layers

5.2.3 Fibrin Microthread Preparation

Fibrin microthreads were prepared through the co-extrusion of fibrinogen and thrombin solutions as has been previously reported.¹⁴⁻¹⁷ Briefly, a 70 mg/mL solution of fibrinogen from bovine plasma (Sigma, St. Louis, MO) dissolved in HEPES (N-[2-Hydroxyethyl] piperazine-N'-[2-ethanesulfonic acid]) buffered saline (HBS, 20 mM HEPES, 0.9% NaCl; pH 7.4) was prepared. A 40 U/mL solution of thrombin from bovine plasma (Sigma) dissolved in HBS was also made and both solutions were stored at -20°C until use. A working solution of 6 U/mL of thrombin was made by diluting the stock thrombin solution with 40 mM solution of CaCl₂. Equal volumes of fibrinogen and thrombin/CaCl₂ solutions were loaded into separate 1 mL syringes and extruded through a blending applicator tip (Micromedics Inc., St. Paul, MN). Solutions were extruded at a flow rate of 0.225 mL/min through polyethylene tubing (BD, Sparks, MD) into a buffer bath of 10 mM HEPES (pH 7.4) in a Teflon coated pan. Following a 10-15 minute polymerization time, the scaffolds were carefully stretched to ~150% of their original length and hung to dry under the tension of their own weight.¹⁴

5.2.4 Composite Layer Fabrication

Composite layer fabrication was completed as was previously reported.⁷ Briefly, a custom built fibrin microthread spacer with ridges was used to align fibrin microthreads. The device couples to a house vacuum enabling placement of threads with defined spacing. Layers were organized with

either 5 (5tC), 10 (10tC) or 20 (20tC) fibrin microthreads across a 1 cm length. Once organized, threads were transferred to vellum frames and secured with medical grade silicone adhesive. Polydimethylsiloxane (PDMS) sheets were coated with 1% Pluronic-F127 in DI water (Sigma, St. Louis, MO) solution for 1 hour. A hydrogel solution containing 1.6 U/mL thrombin, and 3.1 mg/mL fibrinogen was mixed in media on ice, cast over the vellum frames and spread using a pipette tip to provide an even layer. Media was used as the source of calcium in the polymerization reaction. This was done to closely mimic what is done in tissue culture. The media is composed of DMEM (+L-glutamine, VWR, Radnor, PA), 10% defined donor equine serum (Fisher Scientific, Waltham, MA), 2% chick embryo extract (US Biological Life Sciences, Salem, MA), 1% penicillin streptomycin (Thermo Fisher Scientific, Waltham, MA), 1% amphotericin B (Thermo Fisher Scientific) and 1% 5 mg/mL aprotinin, (Sigma Aldrich, St. Louis, MO). For the sample size of 12 x 12 mm (144 mm² area), 150 μ L of hydrogel solution was utilized. Samples polymerized at room temperature for 30 minutes, then were moved into wells with 1X PBS, and stored at -4C until use.

5.2.5 Lamination Method

When fabricating cardiac patches, two composite layers were glued together using a fibrin-based glue. The glue is comprised of HBS, 17.5 mg/mL fibrinogen, 5 U/mL thrombin, and media. The media is the same composition as described in 4.2.4. *Composite Layer Fabrication*. 150 μ L of glue was placed on the top of one of the composite layers. The second layer was then pressed down onto the first layer at the desired angular offset. When pressing, excess glue was secreted from the sides and removed. This method ensured even coverage of glue across the layer.

As a control, patches were also generated that did not utilize glue. These patches were fabricated by casting 1 gel over 2 layers of organized fibrin microthreads. The same gel volume that would have been utilized for 2 separate layers was cast to create 1 larger hydrogel. To evaluate the impact of the glue on the thickness of the patch, thicknesses for glued layers and control patches were compared. Additionally, to evaluate whether the glue had an impact on the measured mechanical properties, glued layers and control patches were uniaxially tensile tested and the stiffness values were compared. For this comparison, we evaluated the maximum slope of the force versus displacement curve.

5.2.6 Uniaxial Tensile Test

Submerged uniaxial tensile testing was completed on individual composite layers (5tC, 10tC and 20tC), glued composite layer patches and control patches (without glue). Each patch consisted of a 10tC and 20tC layer orthogonally aligned to one another. For patches, mechanical characterization was completed by applying load in the direction of the threads for 2 different samples; i.e. when testing a patch with layers perpendicular to one another, applied loads were parallel to threads of the 10tC in one sample, and parallel to threads of the 20tC in a second sample. This was done to evaluate the anisotropic nature of the patch.

Prior to testing, the thickness of each sample was determined using a laser displacement technique.¹⁸ A disk with dimensions of diameter 13 mm, thickness of 1.3mm and weight of 1.3 g was used to create a reflective surface for accurate measurements. The disk did not deform the layers; no indentations upon removal were evident. Thicknesses in three different areas were measured and averaged together to obtain a representative measurement. These were used in combination with the width of the sample to calculate the cross-sectional area, assuming a rectangular geometry. Samples were gripped into an ElectroPuls E1000 testing system (Instron, Norwood, MA) with a 1 N load cell. The initial gauge length of all samples was 15 mm. Samples were submerged in a PBS bath before being uniaxially loaded to failure at a strain rate of 10 mm/min. Throughout the test, force and displacement values were recorded at a frequency of 10 Hz. Prior to evaluating the parameters of interest, all initial load and deformation values were zeroed, baselining the onset value for each test. Engineering stress was determined by dividing the recorded force by the initial cross-sectional area. Strain was calculated as the extension in length from the initial length of the material. To analyze the modulus, a MATLAB (MathWorks, Natick, MA) script was written. Fiber-reinforced composite materials generally have two observable phases on stress strain curves.¹⁹ Because the heart experiences strain values cyclically up to ~30%,²⁰ our analysis took the slope of the first phase of the curves (0-30%). To analyze membrane stiffness, a curve was generated that plotted the recorded force divided by the initial width, against the extension. The slope of the first phase of this curve was used to calculate the membrane stiffness. Outliers were identified as any modulus value that was 1.5 times greater than the inner

quartile range (IQR) for each sample set (min: quartile 1 - 1.5*IQR, max: quartile 3 + 1.5*IQR) and were subsequently removed from further analysis.¹⁴

5.2.7 Statistical Analyses

All statistical analyses were run using SigmaPlot 12.5 software, with all comparisons using a significance level of $p < 0.05$. For patch mechanical properties, loads applied in each of the two directions were compared through a t-test (applied load parallel to 10tC layer direction compared to applied load in the 20tC layer direction). Comparisons of mechanical properties for individual layers were compared through a one-way ANOVA with Holm-Sidak post-hoc pairwise multiple comparison tests for all post-hoc analyses.

5.3 RESULTS

5.3.1 Material Property Criteria Can Be Defined for a Cardiac Patch Acting as a Wall Replacement

The modulus, an inherent material property not dependent on geometry, ranges for the myocardium from 20- 500 kPa depending on whether the heart is in systole or diastole.¹⁰ Ventricular myocardium is an anisotropic tissue. Measured values from biaxial mechanical testing showed that in the direction along the base/apex axis, cadaveric heart tissue is $\sim 376.3 \pm 191.7$ kPa while in the direction along the septum/free-wall axis the tissue is 581.4 kPa, yielding an anisotropic ratio of 0.314 ± 0.196 . ($Anisotropic\ ratio = \frac{Axis\ 1 - Axis\ 2}{Axis\ 1 + Axis\ 2}$).²¹ Membrane stiffness is another important consideration. The range of required membrane stiffness for a patch acting as a wall replacement was calculated to be 300-7500 N/m, as explained in **5.2.1**.

Ideally, the patch should react to load in a similar manner to adjacent healthy myocardium. A patient population with high blood pressure experienced wall stress of 16.1 kPa on average.²² For our design criteria, this value was multiplied by the thickness of ventricular myocardium to yield a required ultimate stress per width of 242 N/m. Furthermore, when experiencing a stress of 16.1 kPa, the strain would need to be comparable to the strain that the heart experiences cyclically. The average peak shortening in the left ventricle at the midwall has been reported to be $\sim 23\% \pm 4$,²³ and $30\% \pm 6$.²⁴ All design criteria are summarized in **Table 5.2**.

Table 5.2. Summary of design criteria for a cardiac patch functioning as a wall replacement.

<i>Parameter</i>	<i>Value</i>
Modulus	20 – 500 kPa * ¹⁰
Anisotropic Ratio of Modulus Values	0.314 ²¹
Membrane Stiffness	300 – 7500 N/m
Ultimate Tensile Stress	242 N/m
Strain at 16.1 kPa of Stress	~23- 30% ²³⁻²⁴

*For a wall replacement, a value closer to the upper limit of the modulus would be beneficial.¹⁰

5.3.2 Composite Theory Can Be Utilized to Yield a Model That Informs a Strategic Lamination of Composite Layers to Produce a Biomimetic Patch

For individual layers, Chapter 4: Alignment of Cardiomyocytes Through Static Tension Increases Contractile Strains in Composite Layers demonstrated that the 5tC, 10tC and 20tC layers were predicted to have modulus values of 24 kPa, 47 kPa and 94 kPa, respectively. Actual measured modulus values of these composite layers were 20 ± 8 kPa, 46 ± 23 kPa and 98 ± 49 kPa.⁷ Additionally, for compacted layers modulus values were predicted to be 51 kPa and 142 kPa for aligned 5tC and aligned 20tC layers. Measured values were similar for the 5tC layers (40 ± 26 kPa), but were reduced for the 20tC layers (97 ± 29 kPa). The compacted 20tC layer had very similar mechanical properties to the acellular 20tC layer with average modulus values of 97 and 98 kPa, respectively. For a wall replacement, modulus values closer to the upper value of the range (500 kPa) would be beneficial.¹⁰

One potential method to increase the modulus values of composite layers is to increase the volume fraction of fibrin microthreads. Using equations 5.4 and 5.5, 70-thread (70tC), 80-thread (80tC) and 90-thread (90tC) composite layers were analyzed with modulus values for offsets ranging from 0-120° summarized in **Table 5.3**.

Table 5.3. Summary of theoretical moduli values for 70tC, 80tC and 90tC layers with an offset. Offsets are taken from the x-axis. Ey and Ex show the modulus values with loads applied in the direction of the y and x axes, respectively

<i>Thread Count</i>	<i>Offset (degrees)</i>	<i>Ey (kPa)</i>	<i>Ex (kPa)</i>
70	0	0.3	<u>327.7</u>
	30	0.3	0.6
	60	0.6	0.3
	90	<u>327.7</u>	0.3
	120	0.6	0.3
80	0	0.3	<u>374.5</u>
	30	0.3	0.6
	60	0.6	0.3
	90	<u>374.5</u>	0.3
	120	0.6	0.3
90	0	0.3	<u>421.3</u>
	30	0.3	0.6
	60	0.6	0.3
	90	<u>421.3</u>	0.3
	120	0.6	0.3

For layers constructed with 70, 80 or 90 fibrin microthreads, the resultant theoretical modulus values are much closer to the upper range of the modulus for ventricular myocardium of 500 kPa. The average diameter for a fibrin microthread is $\sim 110 \mu\text{m}$.¹⁶ For this average diameter, the spacing required for a 70tC layer is $57.5 \mu\text{m}$; a distance approximately half of the diameter of one thread. For 80tC and 90tC layers this value decreases to $24 \mu\text{m}$ and $2 \mu\text{m}$, respectively. Such precise spacing will likely require a 3D printing method for exact placements of microthreads. Additionally, an important consideration is that there is likely a trade-off in cell volume and loss of contractile function if stiffness were to be increased in this manner. Because of the potential for a reduction in function with these increased volume fractions, focus for patch development remained on the 10tC and 20tC layers. Application of laminate composite theory for offsets ranging from 0- 120 degrees in 30-degree increments yielded the results summarized in **Table 5.4**.

Table 5.4. Summary of theoretical moduli values for acellular and compacted composite layers with an offset. Offsets are taken from the x-axis. Ey and Ex show the modulus values with loads applied in the direction of the y and x axes, respectively.

<i>Thread Count</i>	<i>Offset (degrees)</i>	<i>Acellular Ey (kPa)</i>	<i>Acellular Ex (kPa)</i>	<i>Compacted Ey (kPa)</i>	<i>Compacted Ex (kPa)</i>
5	0	0.3	23.6	0.3	50.6
	30	0.2	0.5	0.3	0.5
	60	0.5	0.2	0.5	0.3
	90	23.6	0.3	50.6	0.3
	120	0.5	0.2	0.5	0.3
10	<u>0</u>	<u>0.3</u>	<u>47.0</u>	<u>0.3</u>	<u>70.8</u>
	30	0.2	0.5	0.3	0.5
	60	0.5	0.2	0.5	0.3
	90	47.0	0.3	70.8	0.3
	120	0.5	0.2	0.5	0.3
20	0	0.3	93.8	0.3	141.3
	30	0.3	0.5	0.3	0.5
	60	0.5	0.3	0.5	0.3
	<u>90</u>	<u>93.8</u>	<u>0.3</u>	<u>141.3</u>	<u>0.3</u>
	120	0.5	0.3	0.5	0.3

The computational model demonstrated that it is likely that a 90 degree offset of layers with different microthread volume fractions will be necessary to mimic the anisotropic moduli observed of myocardium. When layers are offset, there is negligible contribution to the x and y moduli unless the x and y axes align with the fibrin microthread axes. Otherwise, moduli were predicted to be below 1 kPa in these directions. Reinforcement of a 20-thread composite layer with a 10-thread composite layer at a 90-degree offset may yield a patch with an anisotropic ratio similar to myocardium.

5.3.3 Fibrin Glue Can Be Used to Laminate Composite Layers Together Without Significantly Impacting Measured Stiffness or Thickness Values.

Fibrin glue was used to laminate layers yielding a composite patch. As a control, two layers of organized fibrin microthreads were cast in 1 hydrogel eliminating the glue component entirely. This control was used to evaluate how the glue impacted patch thickness and patch stiffness (Figure 5.2).

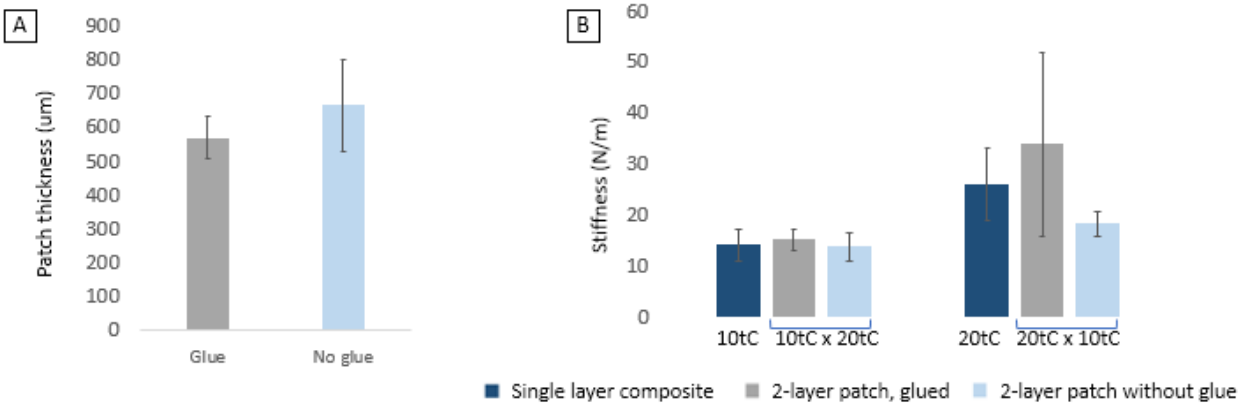


Figure 5.2. Assessment of fibrin glue impact on cardiac patch properties. The thicknesses of glued patches and control patches (no glue) were not significantly different when compared with a t-test, $p < 0.05$ ($n = 7$ for each group) (A). The stiffness values for the patches when loads were applied in the 10tC direction did not significantly vary from a single 10tC layer when compared with a one-way ANOVA, $p > 0.05$ (B). The same was true of stiffness values for patches when loads were applied in the 20tC direction; these values did not significantly vary from a single 20tC layer (B). For stiffness evaluations, $n = 3$ for both glued and control patches, $n = 12$ for single layer assessments. For patches, loads were applied in the direction of the first listed composite layer (i.e., 10tC x 20tC implies load was applied in the direction of the 10tC layer).

The use of fibrin glue did not significantly increase patch thickness, as evaluated through a t-test, $p < 0.05$. The average thickness for patches laminated together with glue were $569.8 \pm 62.6 \mu\text{m}$. Patches generated without glue were on average $665.1 \pm 134.5 \mu\text{m}$ thick.

For comparison of stiffness values, patches were also compared to individual composite layers with the load applied in the direction of the threads. Similar to the thickness assessment, no significant difference was observed between glued samples and controls without glue. Additionally, no differences were observed between the patches and individual layers. The stiffness values for the 10tC single layer, glued patch with load in the 10tC direction, and control patch without glue and load applied in the 10tC direction were $14.1 \pm 3.1 \text{ N/m}$, $15.2 \pm 2.0 \text{ N/m}$ and $13.8 \pm 2.7 \text{ N/m}$, respectively. The 20tC single layer, glued patch with load applied in the 20tC direction, and control patch without glue and load applied in the 20tC direction were $26.0 \pm 7.2 \text{ N/m}$, $33.9 \pm 17.9 \text{ N/m}$ and $18.3 \pm 2.5 \text{ N/m}$, respectively.

5.3.4 When Laminating Composite Layers, Material Properties Similar to Ventricular Myocardium are Achieved

For material property evaluations, all patches included in the assessment were laminated with fibrin glue. When evaluating individual layers through submerged tensile testing, it was

observed that all modulus values were within the range for myocardium (20-500 kPa), but were on the low end of the range (20 ± 8 , 46 ± 23 , and 98 ± 49 kPa for 5tC, 10tC and 20tC layers, respectively). Similarly, a cardiac patch comprised of a 10tC and 20tC layers had modulus values of 45 ± 9 and 96 ± 42 kPa for loads aligned with the 10tC layer and 20tC layer, respectively (**Table 5.5**).

The anisotropic ratio, calculated as $Anisotropic\ ratio = \frac{Axis\ 1 - Axis\ 2}{Axis\ 1 + Axis\ 2}$, of the 10tC x 20tC patch was found to be 0.36, very near the target value of ventricular myocardium. Anisotropic ratios were not calculated for individual layers as the layers were not tested in the direction perpendicular to the alignment of the fibrin microthreads. This was not completed because, without threads aligned with the direction of applied force, the only phase contributing to the measured mechanical properties would be the gel phase. It was anticipated that these measured modulus values would be much lower (<1 kPa) than the modulus values measured when load was applied in the direction of the threads, yielding an anisotropic ratio much greater than the desired 0.314.

The membrane stiffness values for all individual layers and for the 10tC x 20tC patch were below the target stiffness range of 300 – 7500 N/m. This is expected as the modulus values were within range, but the geometry of the patches do not match the geometry of the assumed defect region. Similarly, the ultimate tensile stress (UTS) values were all lower than the target value of 241.5 N/m. When comparing to the ventricular myocardium strain of 16.1 kPa experienced by a patient population with high ventricular pressure, 10 of 16 samples failed prior to reaching 16.1 kPa for the 5tC group. For the 10tC layers, 2 of 12 samples failed before reaching this stress level. The 20tC layers and the 10tC x 20tC did not have any samples fail prior to reaching 16.1 kPa. Strain at 16.1 kPa of stress for all groups except the 5tC layers were near the target value range of 23-30%. The 5tC layer group had strain that was much higher than this target range ($70\% \pm 36$).

Table 5.5. Result comparisons for individual composite layers and glued cardiac patches. Values shown are averages \pm standard deviations. Significant differences are noted. All single layers were compared with a one-way ANOVA and holm-sidak post-hoc analysis, $p < 0.05$. All patch parameters were compared using a two-tailed t-test, $p < 0.05$. All values that are near the target values are bolded.

<i>Parameter</i>	<i>Target Value</i>	<i>5tC</i> (<i>n=16</i>)	<i>10tC</i> (<i>n=12</i>)	<i>20tC</i> (<i>n=12</i>)	<i>10tC x 20tC</i> (<i>n=9 for each, 18 total</i>) #
Modulus (kPa)	20 – 500 ¹⁰	20 \pm 8 (10tC: $p=0.048$) (20tC: $p<0.001$)	46 \pm 23 (5tC: $p=0.048$) (20tC: $p<0.001$)	98 \pm 49 (5tC: $p<0.001$) (10tC: $p<0.001$)	45 \pm 9 x 96 \pm 42 $p=0.007$
Anisotropic Ratio of Modulus Values	0.314 ²¹	NA	NA	NA	0.36
Membrane Stiffness (N/m)	300-7500	6 \pm 2 (10tC: $p=0.022$) (20tC: $p<0.001$)	13 \pm 7 (5tC: $p=0.022$) (20tC: $p=0.002$)	26 \pm 13 (5tC: $p<0.001$) (10tC: $p=0.002$)	25 \pm 5 x 54 \pm 24 $p=0.007$
UTS (N/m)	241.5 ²²	3 \pm 2 * (10tC: $p=0.001$) (20tC: $p<0.001$)	13 \pm 8 ** (5tC: $p=0.001$)	17 \pm 8 (5tC: $p<0.001$)	19 \pm 5 x 42 \pm 10 $p<0.001$
Strain at 16.1 kPa of Stress	~23- 30% ²³⁻²⁴	70% \pm 36 (10tC and 20tC $p<0.001$)	26% \pm 14 (5tC: $p<0.001$)	14% \pm 7 (5tC: $p<0.001$)	28% \pm 16 x 14% \pm 5 $p=0.036$

*10/16 samples failed before reaching minimum value of 16.1 kPa.

** 2/12 samples failed before reaching minimum value of 16.1 kPa.

Values are presented as load in the direction of 10 threads x load in the direction of 20 threads.

5.4 DISCUSSION

The goal of this study was to evaluate whether strategic lamination of fibrin-based composite layers could mimic the mechanical properties of ventricular myocardium. We defined important mechanical properties of modulus, anisotropic ratio of modulus, membrane stiffness, UTS and strain at a specific ventricular wall stress characteristic of patients with high blood pressure. The use of a high ventricular stress to calculate the required force per width (UTS) and ensuring strain at this value did not exceed normal deformations anticipated of myocardial tissue was a method for ensuring that, for the target patient population, the patch would not fail in vivo.

Through laminar composite theory, a model was used to determine that, theoretically, a patch with a 20tC layer arranged orthogonally to a 10tC layer would yield an anisotropic patch that would mimic the modulus values of ventricular myocardium. In theory, measured modulus values with loads applied in the 10tC layer and 20tC layer directions were 47 kPa and 94 kPa, respectively. When measuring the actual values through tensile testing, the modulus values were very similar to what the model predicted for the 10tC and 20tC layers (45 ± 9 kPa and 96 ± 42 kPa, respectively). Because the patch will ultimately use cultured, compacted composite layers, a secondary model was generated that incorporated properties for compacted layers. In previous work, we found that this model accurately predicted a modulus increase for 5tC layers. However, we found that this model also anticipated a modulus increase for 20tC layers. When mechanically tested, the compacted 20tC layers had remarkably similar mechanical properties to acellular 20tC layers. The compaction model was based on volumes measured for the layer and assumed a rectangular geometry for the cross-sectional area of the layers. It is possible that the volumes were not estimated accurately enough to better predict the layer modulus for 20tC layers. Because the 20tC layers behaved similarly when cultured or acellular, it is possible that the better predictive model for compacted layers with more than 5 threads is the acellular model.

One critical factor that influences a composite material's properties is integration between components. To achieve an isostrain state where deformation of all phases of the composite material are equivalent requires a strong interfacial bond.²⁵ While we anticipate a strong interfacial bond as the microthread and hydrogel components of the composite layer are comprised of the same polymer, the strength of the bond has not been assessed. In future work, we plan to perform

pull-out tests to better understand the strength of the bond, and how the strength may be increased through techniques like crosslinking.²⁶

When looking at potential angular offsets for the layers, 0-120° offsets were considered as ventricular myocardium rotates $\pm 60^\circ$ from the endocardium to the epicardium. However, when fibers in a layer are at an angle from the applied load, very low modulus values were anticipated (<1 kPa). The hydrogel phase would be the primary phase contributing to the modulus values at these particular angular offsets. The hydrogel component has a low modulus (assumed to be ~0.25kPa).¹³ To ensure that the anisotropic behavior of the patches mimicked ventricular myocardium, it was critical to have microthreads aligned with the x and y axes (in line with applied loads). It is critical to remember that myocardium is not solely loaded in the x and y directions but rather in all directions. As such, future work for the development of this patch will need to include mechanical testing with a more physiologically relevant loading such as a burst test.²⁷

To generate a patch, layers were laminated using a fibrin glue. A control patch with layers cast within one gel was also evaluated. While there are benefits to casting one hydrogel and having a more uniform cardiac patch material, it is necessary that the layers be glued together to form a patch for this system. Each layer is approximately 300 μm thick when initially cast. In the patch thickness assessment, patches were $569.8 \pm 62.6 \mu\text{m}$ thick when laminated with fibrin glue. Patches without glue were similar in thickness; $665.1 \pm 134.5 \mu\text{m}$. The oxygen diffusion limit is 100 -200 μm .^{8, 28-29} As such, it is important that the lamination technique not significantly increase the thickness of the patch as diffusion will be problematic, likely resulting in the necrosis of the central portion of the patch. Fortunately, the composite layers compact when in culture. Observed thicknesses at day 14 of culture for individual layers were $131 \pm 48 \mu\text{m}$ and $193 \pm 42 \mu\text{m}$ for 5tC and 20tC layers, respectively. While the compacted layers laminated will have a reduced thickness, in the future it will still be necessary to incorporate a vasculature system into this patch to maintain cell viability.

Additionally, it was important to evaluate whether the fibrin glue would alter the material properties of the scaffold. No significant difference was observed between control patches and glued patches demonstrating that the glue did not change anticipated behaviors of the cardiac patch. The reported stiffness values had a tighter distribution for loads applied in the 10tC layer direction relative to loads applied in the 20tC layer direction. Fibrin microthread diameter can vary

with average diameter reported as $110 \pm 18 \mu\text{m}$.³⁰ A variation of $18 \mu\text{m}$ in diameter will impact the volume fraction of the microthreads, ultimately impacting the mechanical properties of the composite material. Because the 20tC layers have more fibrin microthreads relative to the 10tC layers, there is the potential for more variation of fibrin microthread diameter.

The cardiac patches (laminated with glue) and individual composite layers (5tC, 10tC and 20tC) were further evaluated to see how the material properties compared to ventricular myocardium. All modulus values were found to be on the lower end of the range of ventricular myocardium. The anisotropic ratio of the modulus values was also evaluated. A value close to zero would indicate little or no anisotropy. A value close to 1 would indicate a high degree of anisotropy.²¹ The anisotropic ratio of the patch was very near the anisotropic ratio of the native tissue (0.314).²¹ Evaluating the strain at a stress level of 1601 kPa demonstrated that 5tC composite layers are not sufficient. The strain observed was on average $70\% \pm 36$. This deformation is much greater than the deformation that would be anticipated of the myocardium. In contrast, the 10tC layer, 20tC layer and the patch were near the anticipated strain values of myocardium.

The patch matched all required values except for UTS and stiffness. This is not surprising; the modulus values were within the desired range. If the modulus values match, the stiffness will only match if the same geometry is used. The patches tested were $\sim 600 \mu\text{m}$ thick, but the defect area had an assumed thickness of 1.5 cm. This implies that we would need 3 patches laminated to have approximately the same thickness, and ultimately the same stiffness. Using equation 1 and the measured modulus values for the patch, we can estimate the stiffness with an increase in volume of the patch to match the size of the myocardium defect:

$$k = E \times t = 45 \text{ kPa} \times 1.5 \text{ cm} = 675 \frac{\text{N}}{\text{m}}$$

$$k = E \times t = 96 \text{ kPa} \times 1.5 \text{ cm} = 1440 \frac{\text{N}}{\text{m}}$$

Theoretically, with a patch that has a volume matching the defect size, the stiffness values of the patch are within the range desired to mimic ventricular myocardium (300-7500 N/m). Similarly, we can estimate what the UTS would be for a patch with a specific thickness. Looking at the engineering stress versus strain curves, and taking the greatest engineering stress value for each composite type (5tC, 10tC and 20tC), we can multiply that value by the specified thickness to see what the UTS (in terms of force over width) would be.

$$\textit{With load applied in the 10tC direction: } 33 \text{ kPa} \times 1.5 \text{ cm} = 495 \frac{\text{N}}{\text{m}}$$

$$\textit{With load applied in the 20tC direction: } 74 \text{ kPa} \times 1.5 \text{ cm} = 1110 \frac{\text{N}}{\text{m}}$$

The design criteria was for the patch to have a UTS of at least 241 N/m. When scaling up to the same thickness as ventricular myocardium, in theory all composite compositions satisfy this requirement. This suggests that it may be possible to generate thinner patches that satisfy this mechanical requirement. For example, for a patch to have a UTS of 241 N/m with load applied in the direction of the 20tC layers, a thickness of 0.3 cm would be needed.

The design parameters were based on a literature search for this work but, in the future, could be based on patient data. Because each patient is unique, defect sizes may vary as may ventricular wall stresses and associated cyclic strains. This study provides a framework for modeling a patch that can function as a wall replacement with a specific defect geometry and patient requirements. If access to these parameters were available on a patient-by-patient basis, a patch could be designed for each case using this modeling method.

While the patch is promising with the data presented here, it is important to note that an important parameter that was not investigated is fatigue strength. Upon implantation the scaffold will be subjected to cyclic loading. It is critical that the integrity of the patch not vary pre- and post- loading. In the future, we plan to cyclically load the patches in a manner that will mimic physiologic loading. Patches will be subjected to cyclic loading at 1 Hz at a peak strain of 10% for 1 week.³¹ Additionally, degradation of the patch will need to be characterized to determine if replacement of the matrix with extracellular matrix occurs at the same rate. This important metric will also be evaluated in future work. Finally, we also plan to perform suture pullout tests to ensure that the patch can be implanted with a suturing technique. Ultimately, we plan to couple our patch with a fibrin-based vasculature to enable the generation of a thick, implantable construct that can serve as a functional wall replacement for damaged ventricular myocardium.

5.5 CONCLUSIONS

In this study, we have shown that strategic lamination of composite layers can yield a cardiac patch with material properties comparable to ventricular myocardium. While the stiffness and UTS of the patch was not in the desired range, the modulus values were within range. Both parameters

will likely be in range when the thickness of the patch is equivalent to that of ventricular myocardium (1.5 cm). A necessary component for the thick patch is a vasculature to ensure cell viability throughout the construct thickness. Future work will focus on integrating a vasculature and performing long-term mechanical evaluations to ensure that the patch can withstand cyclic loading without a significant change to the failure strength.

5.6 ACKNOWLEDGEMENTS

This work was funded by NIH R01-HL115282 (G.R.G.), NSF IGERT DGE 1144804 and NIH 1R15HL137145-01 (G.D.P.)

5.7 REFERENCES

1. Kochanek, K. D.; Murphy, S. L.; Xu, J.; Tejada-Vera, B., Deaths: Final Data for 2014. *Natl Vital Stat Rep* **2016**, *65* (4), 1-122.
2. Frangogiannis, N. G.; Smith, C. W.; Entman, M. L., The inflammatory response in myocardial infarction. *Cardiovascular research* **2002**, *53* (1), 31-47.
3. Yanagawa, B.; Rao, V.; Yau, T. M.; Cusimano, R. J., Initial experience with intraventricular repair using CorMatrix extracellular matrix. *Innovations (Phila)* **2013**, *8* (5), 348-52.
4. Kochupura, P. V.; Azeloglu, E. U.; Kelly, D. J.; Doronin, S. V.; Badylak, S. F.; Krukenkamp, I. B.; Cohen, I. S.; Gaudette, G. R., Tissue-engineered myocardial patch derived from extracellular matrix provides regional mechanical function. *Circulation* **2005**, *112* (9 Suppl), I144-9.
5. Reis, L. A.; Chiu, L. L.; Feric, N.; Fu, L.; Radisic, M., Biomaterials in myocardial tissue engineering. *Journal of tissue engineering and regenerative medicine* **2014**, *10* (1), 11-28.
6. Tandon, V.; Zhang, B.; Radisic, M.; Murthy, S. K., Generation of tissue constructs for cardiovascular regenerative medicine: from cell procurement to scaffold design. *Biotechnology advances* **2013**, *31* (5), 722-35.
7. Chrobak, M. O.; Hansen, K. J.; Gershlak, J. R.; Vratsanos, M.; Kanellias, M.; Gaudette, G. R.; Pins, G. D., Design of a fibrin microthread-based composite layer for use in a cardiac patch. *ACS Biomaterials Science & Engineering* **2016**.
8. Vunjak-Novakovic, G.; Tandon, N.; Godier, A.; Maidhof, R.; Marsano, A.; Martens, T. P.; Radisic, M., Challenges in cardiac tissue engineering. *Tissue engineering. Part B, Reviews* **2010**, *16* (2), 169-87.
9. Sommer, G.; Haspinger, D. C.; Andra, M.; Sacherer, M.; Viertler, C.; Regitnig, P.; Holzapfel, G. A., Quantification of Shear Deformations and Corresponding Stresses in the Biaxially Tested Human Myocardium. *Annals of biomedical engineering* **2015**.
10. Radisic, M.; Christman, K. L., Materials science and tissue engineering: repairing the heart. *Mayo Clinic proceedings* **2013**, *88* (8), 884-98.
11. Yeh, H. L.; Yeh, H. Y., A dimensionless analysis of young's modulus and stress distribution for orthotropic materials. *Journal of Aeronautics and Aerospace Engineering* **2014**, *3* (1).
12. Sommer, G.; Schriebl, A. J.; Andra, M.; Sacherer, M.; Viertler, C.; Wolinski, H.; Holzapfel, G. A., Biomechanical properties and microstructure of human ventricular myocardium. *Acta biomaterialia* **2015**, *24*, 172-92.
13. Duong, H.; Wu, B.; Tawil, B., Modulation of 3D fibrin matrix stiffness by intrinsic fibrinogen-thrombin compositions and by extrinsic cellular activity. *Tissue engineering. Part A* **2009**, *15* (7), 1865-76.
14. Grasman, J. M.; Pumphrey, L. M.; Dunphy, M.; Perez-Rogers, J.; Pins, G. D., Static axial stretching enhances the mechanical properties and cellular responses of fibrin microthreads. *Acta biomaterialia* **2014**, *10* (10), 4367-76.

15. Cornwell, K. G.; Pins, G. D., Discrete crosslinked fibrin microthread scaffolds for tissue regeneration. *Journal of biomedical materials research. Part A* **2007**, *82* (1), 104-12.
16. Grasman, J. M.; O'Brien, M. P.; Ackerman, K.; Gagnon, K. A.; Wong, G. M.; Pins, G. D., The Effect of Sterilization Methods on the Structural and Chemical Properties of Fibrin Microthread Scaffolds. *Macromolecular bioscience* **2016**, *16* (6), 836-46.
17. Grasman, J. M.; Page, R. L.; Dominko, T.; Pins, G. D., Crosslinking strategies facilitate tunable structural properties of fibrin microthreads. *Acta biomaterialia* **2012**, *8* (11), 4020-30.
18. Billiar, K. L.; Throm, A. M.; Frey, M. T., Biaxial failure properties of planar living tissue equivalents. *Journal of biomedical materials research. Part A* **2005**, *73* (2), 182-91.
19. Callister, W. D.; Rethwisch, D. G., *Fundamentals of materials science and engineering : an integrated approach*. 4th ed.; Wiley: Hoboken, N.J., 2012; p xxv, 910 p.
20. Capulli, A. K.; MacQueen, L. A.; Sheehy, S. P.; Parker, K. K., Fibrous scaffolds for building hearts and heart parts. *Adv Drug Deliv Rev* **2016**, *96*, 83-102.
21. Guyette, J. P.; Charest, J. M.; Mills, R. W.; Jank, B. J.; Moser, P. T.; Gilpin, S. E.; Gershlak, J. R.; Okamoto, T.; Gonzalez, G.; Milan, D. J.; Gaudette, G. R.; Ott, H. C., Bioengineering Human Myocardium on Native Extracellular Matrix. *Circulation research* **2016**, *118* (1), 56-72.
22. Grossman, W.; Jones, D.; McLaurin, L. P., Wall stress and patterns of hypertrophy in the human left ventricle. *The Journal of clinical investigation* **1975**, *56* (1), 56-64.
23. Moore, C. C.; Lugo-Olivieri, C. H.; McVeigh, E. R.; Zerhouni, E. A., Three-dimensional systolic strain patterns in the normal human left ventricle: characterization with tagged MR imaging. *Radiology* **2000**, *214* (2), 453-66.
24. Clark, N. R.; Reichek, N.; Bergey, P.; Hoffman, E. A.; Brownson, D.; Palmon, L.; Axel, L., Circumferential myocardial shortening in the normal human left ventricle. Assessment by magnetic resonance imaging using spatial modulation of magnetization. *Circulation* **1991**, *84* (1), 67-74.
25. Park, J. B.; Lakes, R. S., *Biomaterials: an introduction*. 2nd ed.; Plenum Press: New York, 1992.
26. Shepherd, J. H.; Ghose, S.; Kew, S. J.; Moavenian, A.; Best, S. M.; Cameron, R. E., Effect of fiber crosslinking on collagen-fiber reinforced collagen-chondroitin-6-sulfate materials for regenerating load-bearing soft tissues. *Journal of biomedical materials research. Part A* **2013**, *101* (1), 176-84.
27. Coburn, J. C.; Brody, S.; Billiar, K. L.; Pandit, A., Biaxial mechanical evaluation of cholecyst-derived extracellular matrix: a weakly anisotropic potential tissue engineered biomaterial. *Journal of biomedical materials research. Part A* **2007**, *81* (1), 250-6.
28. Carmeliet, P.; Jain, R. K., Angiogenesis in cancer and other diseases. *Nature* **2000**, *407* (6801), 249-57.
29. Novosel, E. C.; Kleinhans, C.; Kluger, P. J., Vascularization is the key challenge in tissue engineering. *Adv Drug Deliv Rev* **2011**, *63* (4-5), 300-11.
30. Grasman, J. M.; Pumphrey, L.; Dunphy, M.; Perez-Rogers, J.; Pins, G. D., Static axial stretching enhances the mechanical properties and cellular responses of fibrin microthreads. *Acta biomaterialia* **2014**, *10* (10), 4367-76.
31. Engelmayer, G. C., Jr.; Cheng, M.; Bettinger, C. J.; Borenstein, J. T.; Langer, R.; Freed, L. E., Accordion-like honeycombs for tissue engineering of cardiac anisotropy. *Nat Mater* **2008**, *7* (12), 1003-10.

Chapter 6: Conclusions and Future Work

6.1 OVERVIEW

The work in this thesis describes the development of a biomimetic composite scaffold that recapitulates the architectural and material properties of ventricular myocardium to enable functional and mechanical integration with adjacent host tissue upon implantation. Modulation of the volume fractions of the composite phases enabled control over the mechanical properties of the material without attenuating cell function. Further, we developed a culturing method for increasing alignment of incorporated cells. Increased alignment correlated with increased cell function. Finally, we demonstrated that the composite layers can be strategically laminated to further mimic the structural and mechanical properties of ventricular myocardium.

6.2 RESULTS AND CONCLUSIONS

6.2.1 *Specific Aim 1: Develop a Fibrin Composite Layer that Enables Customizable Modulus Values While Sustaining Cardiomyocyte Contractility*

Based on composite theory,¹ we hypothesized that fibrin microthreads could be combined with fibrin-based hydrogels forming a composite layer scaffold with tunable mechanical properties that supports cell contractility. Further, based on earlier work we hypothesized that the incorporated fibrin microthreads would promote cellular orientation.² We developed a methodology for generating evenly-spaced fibrin-based composite layers. To do so, a custom-built fibrin microthread spacer was developed that yields average thread spacing of 140 ± 21.7 μm . When comparing the spacing between 4 individual users, a one-way ANOVA demonstrated that no significant difference in spacing existed. This analysis showed that the method we developed is reproducible.

We then evaluated 3 different volume fractions of fibrin microthreads in a fibrin hydrogel through submerged uniaxial tensile testing. We observed that the modulus for the layer was tunable through modulation of the volume fraction of fibrin microthreads. Further, the trend observed was predicted by using composite theory to estimate what modulus values were

expected for the different layer conformations. It is critical that a scaffold have comparable mechanical properties to avoid mechanical mismatch upon implantation,³ and to promote proper contractile force, phenotype, and gene expression.⁴⁻⁷ Moduli for all configurations (thread counts of 5, 10 and 20 per layer) were within the desired range for human ventricular myocardium of 20 – 500 kPa.⁵

To ensure that increasing the volume fraction of fibrin microthreads did not hinder cell function, samples were evaluated using high density mapping (HDM) at days 7, 10 and 14 in culture. We observed that at no time point did the contractile strain or frequency differ for any composite layer relative to a fibrin hydrogel control. Using Hooke's Law to predict the contractile forces, we found that the contractile forces increased with an increasing layer modulus maintaining similar contractile strain values for all groups. This demonstrates that with an increasing modulus, we can improve the mechanical properties without compromising contractile function. The contractile frequencies for all groups were ~2.5 Hz; comparable to reported frequencies for neonatal cardiomyocytes in a 3D environment.⁸ Additionally, when evaluating the phenotype of incorporated cells, sarcomeric α -actinin showed striated appearances of cells in all composite layer and control groups. This phenotype is considered a hallmark of functional cardiomyocytes,⁶ further supporting that increasing volume fractions of fibrin microthreads without attenuating cell function.

We anticipated that incorporating fibrin microthreads in a gel would provide an instructive cue that would promote cellular alignment, similar to results shown previously.² Alignment has been correlated with enhanced functional maturation and it is needed for integration upon implantation.⁹⁻¹² When evaluating the nuclear orientation of cells within the layer, we first evaluated all regions. We found that no alignment of cells was observed. Following this assessment, we evaluated nuclear orientation of cells within 100 μm of the fibrin microthreads. We found a slight improvement with alignment; the greatest percentage of cells were oriented between 0-15° of the direction of the fibrin microthreads. In ventricular myocardium, alignment of the cells closely follows alignment of the fibrils of the tissue. Within each layer, fibrils rotate relative to one another $\pm 13^\circ$.¹³ The majority of nuclei within a 100 μm distance of fibrin microthreads had similar alignment. The fibrin microthreads may be providing an instructive cue for a limited distance in the fibrin hydrogel. This is similar to cells sensing

rigid bodies not in direct contact. It has been reported that cells in a fibrous biopolymer, like fibrin, can sense rigid bodies at distances as great as 150 μm .¹⁴

In conclusion of Specific Aim 1: Develop a Fibrin Composite Layer that Enables Customizable Modulus Values While Sustaining Cardiomyocyte Contractility of this thesis, we determined that fibrin microthreads can be incorporated in a fibrin hydrogel generating a composite layer. Through manipulation of volume fractions of the components of the composite, tuning of the mechanical properties is possible. An increase in volume fraction of fibrin microthreads correlates to an increase in layer modulus. Changes in fibrin microthread volume fraction did not impact the functionality of incorporated cells; all contractile strain and contractile frequency values were not significantly different for 5, 10 or 20 thread composite layers relative to a hydrogel control. When evaluating nuclear orientation, there was no alignment observed when evaluating all cells. When limiting the evaluation to 100 μm distances from the incorporated microthreads, an increase in alignment was observed, suggesting that the impact of microthreads on alignment is limited in distance. The composite material overcomes limitations of hydrogel materials with weak mechanical properties, but does not promote the necessary alignment for functional integration upon implantation.

6.2.2 Specific Aim 2: Develop an Aligned Composite Layer to Enhance Contractile Function

In this section of this thesis, we incorporated the findings from Specific Aim 1: Develop a Fibrin Composite Layer that Enables Customizable Modulus Values While Sustaining Cardiomyocyte Contractility, and aimed to increase the observed alignment of incorporated cells in the composite layers. To do so, we developed a new culturing method that directed tension patterns created by cell-mediated gel compaction. We restricted the scaffold as compaction occurred over a 14 day culture period, similar to other reported methods.^{9, 15} The method utilized a PDMS post system coupled with customized vellum frames. When analyzing the orientation of incorporated cells, it was found that samples cultured using this method had nuclear alignment more similar to human heart controls than unaligned controls prepared using the method developed in Aim 1.

Functional evaluations were completed on large regions of interest (ROIs) and grid ROIs which divided the recorded region into 20 smaller sub-regions. The large ROI evaluation showed

that composite layers with improved alignment had greater contractile strains and larger contractile areas relative to gelatin-coated coverslip and unaligned controls. This is anticipated as alignment of cardiomyocytes may contribute to enhanced functional maturation.⁹⁻¹² For all groups, an increase in functional parameters was observed over the culture period, likely because compaction was occurring throughout. Compaction has been shown to equilibrate 8-13 days in culture for fibrin hydrogels.¹⁶ For healthy myocardium, contractile strains have been reported to be ~19%.¹⁷ For the samples with increased alignment, the highest functioning regions had similar contractile strains with average values of ~18% and 22% after 10 and 14 days in culture, respectively.

A grid assessment was used to evaluate consistency of contractile behavior across the entire recorded region. Three assessments were completed that evaluated the consistency of contractile strains, the consistency of principal angles of the greatest contractile strains in each region, and the distance of the greatest contractile strain from the incorporated fibrin microthreads. The contractile strain and principal angle assessments demonstrated that all groups had similar consistency levels. Interestingly the distance assessment showed that aligned samples had the highest contractile strains typically occurring in areas immediately adjacent to the fibrin microthreads while in unaligned layers, the highest contractile strains were ~200 μm from the nearest microthread. It is possible that compaction of the aligned composite layers results in a greater percentage of the gel phase being in close proximity to the incorporated fibrin microthreads. Additionally, it is possible that the unaligned composite layers have regional variations in the mechanical environment that are not present for the aligned composite layers.

Contractile wave propagation through the composite layers was also evaluated for samples on day 14. It was observed that aligned 5-thread composite layers demonstrated anisotropic propagation; comparable to that observed in highly aligned tissue.¹⁸ The aligned, 5-thread layer had contractile wave propagation speeds of 11.1 ± 1.5 mm/sec and 4.5 ± 2.0 mm/sec in directions parallel to and perpendicular to the fibrin microthreads, respectively. These speeds are an order of magnitude slower than signal propagation speeds of healthy myocardium (73 ± 4 cm/s and 11 ± 3 cm/s for the longitudinal and transverse directions, respectively).¹⁹ Phenotypic evaluations of incorporated cells demonstrated that relative to human heart controls, the experimental (aligned) and unaligned control groups had immature expression of connexin 43.

The distribution was circumferential, which is comparable to neonatal rat ventricular myocytes within the first 20 days of postnatal life.²⁰ This is in contrast to mature, highly functional myocardium which exhibits polarized distribution.²¹ It is likely that the immature gap junction formation is a contributing factor to the reduced signal propagation occurring in the composite layers.

For functional evaluations (large ROI assessment of contractile strains) and nuclear alignment measurements, it was observed that in the experimental group that there were regional differences. This may be because compaction did not occur uniformly across the composite layer. When evaluating compaction and its impact on mechanical properties, no significant difference was observed between the acellular and compacted 20-thread composite layers. However, a significant modulus increase was observed for 5-thread compacted layers relative to acellular 5-thread composite layers. It is possible that because the 5-thread layers began with a larger hydrogel volume fraction the effect was more pronounced.

In conclusion of Specific Aim 2: Develop an Aligned Composite Layer to Enhance Contractile Function, we demonstrated that tension resulting from cell-mediated compaction can be used to increase alignment of incorporated cells. The samples with increased alignment also demonstrated increased contractile strain and contractile areas. Additionally, contractile wave propagation in the layer was anisotropic, characteristic of highly aligned native tissue. Relative to healthy myocardium, contractile wave propagation speeds were reduced, while contractile strains were near native values. This may be because of immature gap junction formations throughout the layer. Compaction did not appear to be uniform throughout the composite. When evaluating the impact of compaction on the modulus of the layer, a significant increase was observed for 5-thread layers, which was anticipated with the predictive model. No significant increase was observed for the 20-thread layers. The 20-thread layers had similar values to the acellular samples and acellular predictive model. It is possible that the volume fractions of the components may not be accurately calculated for the compacted layer predictive model.

6.2.3 Specific Aim 3: Produce a Biomimetic Patch with Material Properties Comparable to Native Myocardium

In the final section of this thesis, we incorporated the findings from Specific Aims 1: Develop a Fibrin Composite Layer that Enables Customizable Modulus Values While Sustaining Cardiomyocyte Contractility and 2: Develop an Aligned Composite Layer to Enhance Contractile Function to determine if strategic lamination of composite layers would yield a patch with comparable material properties to ventricular myocardium. First, material requirements for a cardiac patch acting as a wall replacement were defined; including a range of modulus values (20-500 kPa)⁵, anisotropic modulus ratio (~0.3)²², membrane stiffness (300-7500 N/m)^{5, 23-24}, ultimate tensile strength (UTS) (242 N/m)²⁵, and strain at 16.1 kPa (23-30%).²⁶⁻²⁷ These metrics provided criteria for evaluating whether a patch configuration would warrant further investigation as a wall replacement.

We modeled the theoretical modulus values for a composite layer when the load was applied at an angular offset from the direction of the incorporated microthreads. We utilized a model developed from the generalized Hooke's law with assumed planar stress conditions.²⁸ We considered angular offsets ranging from 0- 120° in 30° increments as ventricular myocardium layers rotate relative to one another from +60° to -60° through the ventricular wall. Using this assessment, we found that lamination of a 20-thread composite layer at a 90° offset from a 10-thread composite layer would yield a patch with an anisotropic modulus ratio, and modulus values comparable to ventricular myocardium.

Because the layers are initially ~300µm thick, it is necessary to culture the layers enabling compaction and reduction in thickness prior to laminating them with a fibrin glue. Otherwise, necrosis of the central region of the patch may be observed as oxygen diffusion through a confluent cell layer is ~ 100 -200µm.^{23, 29-30} To evaluate how the fibrin glue may impact the thickness of the patch and the resulting stiffness values, glued layers were compared to a patch generated by casting 1 gel over 2 layers of organized microthreads (no glue control). Uniaxial tensile testing was performed in two directions; with loads applied in the direction of the 10-thread layer, and with loads applied in the direction of the 20-thread layer. Because it is a destructive test, two separate samples were needed for these evaluations. Importantly, we found that the fibrin glue did not increase the thickness of the patch and further, that the glue did not

significantly change the stiffness. The stiffness values were comparable to the stiffness values of individual layers of 10-thread and 20-thread composite layers as well, demonstrating that the patch configuration did not alter this mechanical property significantly.

For a patch laminated with fibrin glue, the material properties were similar to ventricular myocardium. For all data listed, the data are shown as loads applied in the 10-thread direction x loads applied in the 20-thread directions, respectively. The modulus values (45 ± 9 x 96 ± 42 kPa) were comparable to the range of ventricular myocardium values. The anisotropic ratio of modulus values was similar to the desired ratio value (0.36 and 0.314, respectively). The strains at 16.1 kPa of stress were near the desired values as well ($28\% \pm 16$ x $14\% \pm 5$). The only parameters not within range of native tissue were the stiffness and UTS. This is not surprising because the thickness of myocardium was not the same as the thickness of the cardiac patch. When calculating the stiffness values for a cardiac patch with thickness matching that of the assumed defect (1.5 cm), the stiffness values were 675 N/m and 1440 N/m for loads in the 10-thread layer direction and 20-thread layer direction, respectively. For the UTS when considering a patch of 1.5 cm thickness, the values were calculated to be 495 and 1110 N/m for a patch with loads applied in the 10tC and 20tC directions, respectively. These values are within the desired range for stiffness (300-7500 N/m) and above the desired value for UTS (241 N/m).

In conclusion of Specific Aim 3: Produce a Biomimetic Patch with Material Properties Comparable to Native Myocardium, we established material requirements for a cardiac patch functioning as a wall replacement. Additionally, we evaluated theoretical angular offsets that would enable the development of a patch to mimic the material properties of ventricular myocardium. A lamination method was established utilizing fibrin glue that does not increase patch thickness, or alter the stiffness of the resultant patch. Further, we evaluated a patch composed of a 10-thread layer laminated at a 90° offset to a 20-thread layer. This patch was within range for all desired material parameters, except for stiffness and UTS. This is likely because the thickness of the patch does not match the thickness of the assumed defect size. Calculations show that with an increase in thickness of the patch to match the defect size, the stiffness and UTS values should meet the design criteria outlined for a cardiac patch. This work demonstrated that patches could be strategically designed to meet specified criteria. We hypothesize that similar work could be done to produce patient-specific patches.

6.3 FUTURE WORK

The ultimate goal of this dissertation was to develop a biomimetic cardiac patch that will ultimately serve as a functional wall replacement following a myocardial infarction. In accomplishing this goal, we created a composite patch with tunable mechanical properties, layers that promote aligned contractions, and a cardiac patch with structural and functional properties comparable to native ventricular myocardium. To further develop the patch technology, work can be done to extend application of the patch for *in vitro* drug testing. Additionally, modification of the patch configuration can be completed to enable more uniform compaction and ultimately cell function. Further, to ensure that the patch can maintain cell viability, incorporation of a vasculature in the composite patch is needed. Ultimately, we envision this composite material as a platform technology that could be investigated for use in a wide range of tissue engineering applications.

6.3.1 Use of Composite Patches for In-Vitro Drug Testing

While we ultimately envision the cardiac patch as providing a functional therapeutic for heart attack patients, there is the potential to apply the composite patch in a different application while still benefiting many patients. The cost of bringing a new drug to market is approximately \$1 billion.³¹ Unfortunately, with current development techniques and conventional testing methods, complications that may result from drug use are not always identified. Approximately 1/3 of these complications are cardiovascular effects. Without adequate in-vitro testing methods, the cost of drug development can be inflated to \$11 billion in order to detect adverse effects.³²

Recently, in the Pins lab in collaboration with the Gaudette lab, a universal microscope incubator for drug screening of 3D models of engineered myocardium was created.³³ In this work, a cost-effective device houses a 6-well plate and enables perfusion to individual wells while maintaining carbon dioxide, humidity and temperature levels. The system couples with a microscope allowing visualization of samples while maintaining the desired culturing environment. Through a biomimetic screening platform, assays could potentially have significantly improved predictive power in informing which compounds should progress to clinical trials.³⁴ As such, a highly biomimetic scaffold is needed.

With this thesis work, we found that while contractile strains for aligned composite layers were comparable to healthy myocardium, action potential propagation speeds were greatly reduced likely due to the immature phenotype of the incorporated cardiomyocytes. This thesis utilized rat neonatal ventricular myocytes; a cell type not likely to transfer to the clinic. Isolation of primary human cardiomyocytes is difficult, and isolated cells have a short lifespan in culture before dedifferentiating.³⁵ Another option is to utilize induced pluripotent stem cell derived cardiomyocytes (iPS-CMs).

In 2006, Yamanaka et al demonstrated the ability to generate embryonic like stem cells from dermal fibroblasts via transfection with 4 factors; Oct3/4, Sox2, c-Myc, and Klf4. These induced pluripotent stem cells (iPSCs) were able to differentiate into the three different germ lineages as demonstrated by tumor formation in a mouse model,³⁶ and exhibited morphology and growth properties similar to ESCs. While micro-array research has demonstrated that hundreds of genes and DNA methylation patterns are expressed differently for ESCs and iPSCs,³⁷⁻³⁸ it is not conclusive that cardiomyocytes derived from either cell type differ in any meaningful way.³⁵ Similar to ESC derived CMs, iPSC derived CMs (iPS-CMs) can provide a large cell source and have been shown to enhance the ejection fraction in an *in vivo* model.³⁹ Unlike ESCs, iPS-CMs have the potential to be autologous without associated ethical concerns.³⁵ With the potential to isolate cells from patients, patient specific disease models such as spinal muscular atrophy,⁴⁰ amyotrophic lateral sclerosis (ALS)⁴¹ and Huntington's disease⁴² are possible. This cell type has a great deal of potential for disease modeling, drug screening, and potentially therapeutics in the future.³⁵

Currently, iPS-CMs have slower conduction velocities and shorter action potential durations relative to human myocardium. This is likely due to the lack of cell maturity.³⁵ Efforts are on-going for increasing the maturity levels of iPS-CMs through methods like long-term culture, electrical stimulation and mechanical loading.²¹ There is the potential for the composite patch developed in this thesis to become a better biomimetic scaffold through incorporation of iPS-CMs and the maturation of incorporated cells through stimulations mimicking those anticipated *in vivo*. A more biomimetic patch will not only be applicable for drug testing, but will also likely have better integration upon implantation if utilized as a patch. It is likely that an *in*

in vitro testing system is a more realistic near-term goal, while the cardiac patch application is something that will require a lengthier development time.

6.3.2 *Modification of Composite Layers for More Uniform Compaction and Cell Function*

In this thesis, continuous aligned fibrin microthreads were used as a reinforcing agent for fibrin hydrogels. For composite materials, the lengths of the fibers are critical for determining the amount of reinforcement achieved. As a material, fibers are able to withstand a maximum fiber load. For the fibers to be able to withstand the same load when in a composite material, a critical length of fiber must be utilized. At the critical length, the fiber will be able to withstand the maximum fiber load at the center of the fiber. For any fiber lengths lower than the critical length, virtually no stress transfer occurs from the matrix to the fibers resulting in little reinforcement. For lengths greater than the critical length, the reinforcement becomes more effective; the maximum fiber load can be achieved over a greater length. When using a fiber that is much greater (~15 times greater) than the critical length, the fiber is considered continuous and provides a significant improvement in the strength of the overall material.¹

The critical length needed is dependent on the fiber diameter, tensile strength of the fiber and the fiber-matrix bond strength. To design a scaffold material for cartilage regeneration, Yodmuong et al developed silk microfiber reinforced silk hydrogel composites.⁴³ The goal of this work was to improve the mechanical properties of a silk hydrogel scaffold.⁴⁴ Large, medium and small fibers with lengths of >500 μm , 400-500 μm , and 150-200 μm , respectively were added to the scaffolds. The investigators hypothesized that the composite mechanical properties would depend on fiber length, which is essential for developing a composite that will ensure sufficient energy transfer occurs from the matrix to the dispersed phase under mechanical loading.⁴⁵ Mechanical analyses of the scaffolds showed that microfiber incorporation and length affected both the dynamic and equilibrium moduli of composites. Composites with fiber lengths of 200 μm appeared to fall below the critical length, and failed to provide adequate stress transfer along the fibers. The critical length in this study was determined to be 500 μm . This length provided sufficient fiber overlap and resulted in increased stiffness. The highest Young's modulus was observed for silk scaffolds reinforced with 500 μm fibers (34 +/- 3.1 kPa). This test group also exhibited the highest dynamic modulus at 1 Hz (357.2 +/- 45.7 kPa).

Given that silk is a naturally occurring biopolymer, it is likely that the critical lengths of fibrin microthreads (also a naturally occurring biopolymer) in a fibrin hydrogel are shorter than the lengths currently used in the scaffolds. In this thesis, the fiber lengths extended through the entire length of the construct (12 mm). However, it is possible that smaller fragments could still function as continuous fibers and provide significant mechanical reinforcement. With smaller segments, it is possible that the compaction throughout the material may be more uniform than what was observed in this work. If the fibrin microthreads were behaving as a barrier in the current format, then shorter, aligned microthreads may be able to overcome that issue.

Aligning shorter fragments of fibrin microthreads will present a challenge. While the work in this thesis, fibers were aligned prior to integration with a hydrogel, one potential solution may be to cast fibers in a hydrogel and align the fibers as the hydrogel is polymerizing. A simple technique for aligning collagen fibrils during hydrogel polymerization requiring no specialized equipment was presented by Guo and Kaufman.⁴⁶ The method involves casting the hydrogel solution with magnetic beads. A magnet is placed adjacent to the polymerizing sample. This work demonstrated that alignment of the collagen fibrils was achieved, and was attributed to the magnetic field and the flow created by the beads. While this work was aligning fibrils of a biopolymer, a similar method may assist with aligning small microfibers in a hydrogel matrix. Furthermore, the method may align the fibrils of fibrin resulting in increased alignment of the composite material.

6.3.3 Incorporation of Vasculature in Composite Patch

Vascularization of tissues is required for oxygen and nutrient diffusion, as well as removal of waste products. Additionally, incorporated endothelial cells provide paracrine signaling, which promotes cardiomyocyte function and viability.⁴⁷ Furthermore, if this cardiac patch were to be used for drug testing, a vasculature would provide a route for delivery of drugs.⁴⁷ The diffusion limit for oxygen is 100 -200 μm .^{23, 29-30} With this thesis work, all samples were maintained *in vitro* with an initial layer thicknesses of $\sim 300 \mu\text{m}$. Upon implantation *in vivo*, the patch will not have media on both sides of the construct but will rather need to rely on transport through a vascular system. Cells incorporated in a cardiac patch will need to be within 100-200 μm of a vasculature. This need is especially strong for cardiac tissue due to the high

metabolic demands of the heart.⁴⁸ When considering the thickness of a laminated patch, this thesis showed that two acellular layers laminated together were ~600 μm thick. Individual 10-thread and 20-thread composite layers compacted to thicknesses of ~200 μm when cultured for 14 days. As was determined in Aim 3, Produce a Biomimetic Patch with Material Properties Comparable to Native Myocardium, in order to achieve a patch with stiffness values in the range of ventricular myocardium, a patch thickness of ~1.5 cm is required. With each layer having a thickness at the upper limit for oxygen diffusion, a patch will require a vascular layer laminated between each composite layer.

Current work in the Pins lab is focused on the development of a fibrin hydrogel vascular network. To generate the vascular layer, channels are formed in a fibrin hydrogel using a sacrificial gelatin mold. In a pilot study, an unaligned 5-thread composite layer was cultured for 14 days with rat neonatal ventricular myocytes incorporated. Following culture, the layer was placed on top of a fibrin-based vascular layer. The only source of fluid was the fluid flowing through the vasculature. A 2 μM calcein AM dye in dPBS solution was flowed through 25 gauge needles at the inlet and outlet of the vascular layer for 75 minutes. Calcein AM is non-fluorescent until converted to a green-fluorescent calcein after hydrolysis by intracellular esterases in live cells. Following the incubation period, the combined composite layer and vascular layer were detached from the pump set-up and placed on a slide to image. Images were acquired at 400X (**Figure 6.1**) on an upright fluorescent microscope.

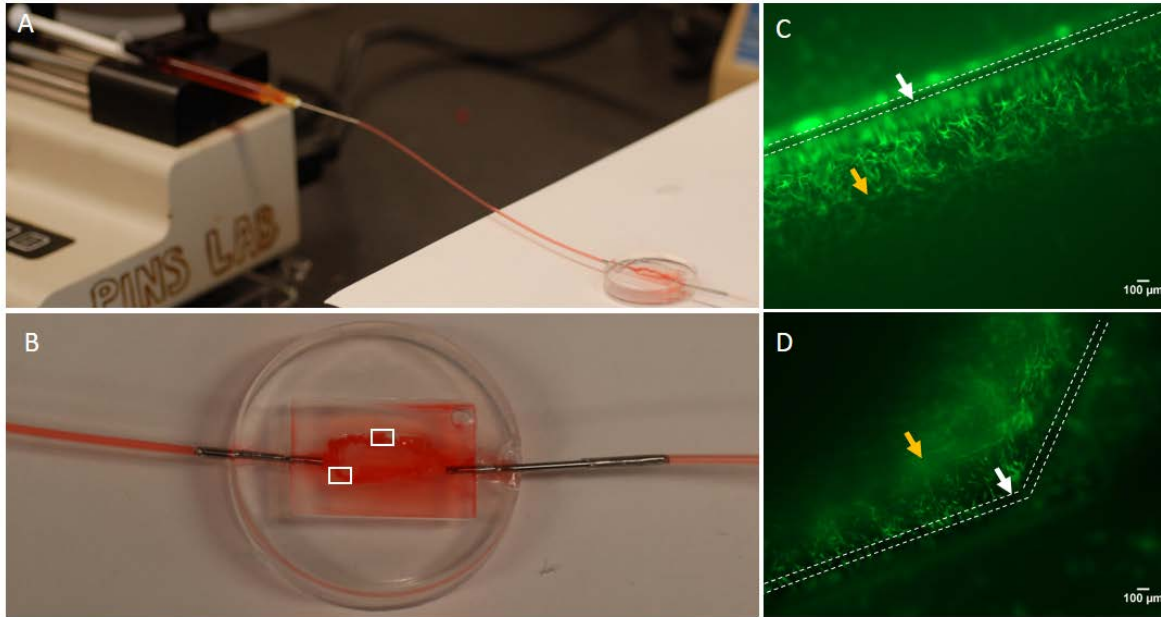


Figure 6.1. Vascular layer fabrication and combination with composite layer. The vascular layer is a fibrin hydrogel with embedded channels and defined inlet and outlet ports. The inlet and outlets can connect to a syringe pump (A), and fluid (in image, water with red food coloring) can be flowed through the construct (B). When a composite layer is placed on top of the vascular layer and calcein AM solution is flowed through, cells near the channels (white arrows, white dotted lines) fluoresce green (C, D). C shows a straight channel and D shows a rounded curve. These areas of interest are boxed in B. Yellow arrows in C and D show fibrin microthreads.

In **Figure 6.1**, cells near the channels of the vascular layer fluoresced green while cells further from the channels did not fluoresce. These images demonstrate that diffusion of fluid from the vasculature to the composite layer is possible. Additionally, it is visible how it is critical that the vascular layer be designed to have channels with spacing that ensures diffusion of nutrients uniformly across adjacent composite layers. Work on the vascular layer continues for establishing diffusion distances, optimizing the channel spacing, endothelializing the vascular channels and ultimately, lamination with a composite patch to maintain cell viability throughout the construct.

6.3.4 Fibrin Composite Layers as a Platform Technology

To promote functional tissue regeneration in a clinical application, an engineered scaffold must recapitulate the structural and mechanical properties of the native tissue. This provides cells with appropriate signaling cues to direct a sustained regenerative environment.⁴⁹ Native tissue constructs are complex; they are comprised of protein-based fibrillar elements arranged into

hierarchically ordered constructs. The structural arrangements are tissue-dependent, and enable the tissue functionality.⁵⁰ Conventional biofabrication strategies for the production of engineered scaffold materials lack the multiscale combination of properties to create tissue constructs comparable to native tissue.

Biopolymer microthreads have been explored for tissue engineering applications ranging from skeletal muscle^{2, 51-52} and cardiac tissue,⁵³⁻⁵⁵ to tendon and ligament.⁵⁶⁻⁵⁹ Microthreads are appealing as a scaffold because they can be engineered to biomimetic, hierarchical structures with tissue-specific morphologies. Additionally, microthreads can provide mechanical and biochemical cues to promote regeneration. Furthermore, through manipulations such as crosslinking, degradation rates and mechanical properties can be finely tuned to mimic material properties of native tissues.⁶⁰ Although these scaffolds are promising, a composite material may be able to better recapitulate the material and biochemical environment enabling greater tissue regeneration.

With the development of the composite material in this thesis work, there is an exciting opportunity to utilize the material as a platform technology. By combining different materials into one, a range of better, or different, properties can be achieved. One potential application may be the incorporation of therapeutic proteins to promote endogenous regeneration of tissues.⁶⁰ With a composite material, there is the opportunity to incorporate proteins in multiple places potentially yielding different release profiles that could ultimately better mimic the various stages of tissue regeneration. Considering most tissues in the body are composites, we hypothesize that the fibrin-based composite material developed will be applicable across a wide variety of engineered tissues.

6.4 FINAL CONCLUSIONS

In this thesis, we developed a composite material for use as cardiac patch. We evaluated how volume fraction manipulation of the fibrin microthreads impacted the modulus of the composite material. An increasing volume fraction correlated with an increasing modulus; the same trend as was predicted using composite theory. With the increasing volume fractions, we evaluated the impact on incorporated cardiomyocyte function. Through high density mapping (HDM) analysis, we found that all composite layers had contractile strains and contractile

frequencies comparable to fibrin hydrogel controls. This demonstrated that the increase in volume fraction of microthreads did not attenuate cell function. Additionally, cells in regions within 100 μm of a fibrin microthread showed increased nuclear alignment. This showed that the fibrin microthreads influenced regional cell orientation.

Without cellular alignment across the entire layer, functional integration with host tissue will not be efficient. We developed a culturing method that capitalized on the tension produced through the composite material by cell-mediated gel compaction. By constraining two ends of the scaffold, we utilized the tension to increase alignment of incorporated cells. Nuclear alignment of constrained samples showed distributions qualitatively similar to human heart tissue and greater than unaligned controls. When evaluating cell function through HDM, composites with improved alignment also had increased contractile strains and contractile areas relative to unaligned composite layers and gelatin-coated coverslip controls.

Contractile wave propagation through the layers was evaluated and showed that aligned regions had anisotropic signal propagation although the speeds shown were still well below those observed in healthy heart tissue. This was likely due to immature gap junction formation. This hypothesis was further supported by the immature connexin 43 expression observed in all composite layers. To improve function, a shift from rat neonatal ventricular myocytes to induced pluripotent stem cell derived cardiomyocytes may be beneficial. Additionally, to improve maturity, mechanical and electrical stimulation mimicking *in vivo* stimulations should be explored.

Finally, we showed that strategic lamination of composite layers could be achieved to produce a patch with material properties comparable to ventricular myocardium. Using a model based on generalized Hooke's law and assuming a plane stress state, we evaluated the impact angular offsets of microthreads from the direction of applied load would have on the material modulus. We found that microthreads need to be in the direction of applied load to ensure material properties comparable to ventricular myocardium. We laminated layers together at a 90° offset using fibrin glue and found that the configuration met all of the required material properties except stiffness. This is likely because the geometry of the patch did not match the geometry of the assumed defect size. In order to match the needed stiffness values, a patch with a thickness of 1.5 cm will be needed. For a cell-populated patch to remain viable with this

thickness, a vasculature system is needed. Future efforts will need to focus on continuing the development of vascular system for the composite cardiac patch.

6.5 REFERENCES

1. Callister, W. D.; Rethwisch, D. G., *Fundamentals of materials science and engineering : an integrated approach*. 4th ed.; Wiley: Hoboken, N.J., 2012; p xxv, 910 p.
2. Grasman, J. M.; Pumphrey, L.; Dunphy, M.; Perez-Rogers, J.; Pins, G. D., Static axial stretching enhances the mechanical properties and cellular responses of fibrin microthreads. *Acta biomaterialia* **2014**, *10* (10), 4367-76.
3. Kochupura, P. V.; Azeloglu, E. U.; Kelly, D. J.; Doronin, S. V.; Badylak, S. F.; Krukenkamp, I. B.; Cohen, I. S.; Gaudette, G. R., Tissue-engineered myocardial patch derived from extracellular matrix provides regional mechanical function. *Circulation* **2005**, *112* (9 Suppl), I144-9.
4. Jacot, J. G.; McCulloch, A. D.; Omens, J. H., Substrate stiffness affects the functional maturation of neonatal rat ventricular myocytes. *Biophysical journal* **2008**, *95* (7), 3479-87.
5. Radisic, M.; Christman, K. L., Materials science and tissue engineering: repairing the heart. *Mayo Clinic proceedings* **2013**, *88* (8), 884-98.
6. Forte, G.; Pagliari, S.; Ebara, M.; Uto, K.; Tam, J. K.; Romanazzo, S.; Escobedo-Lucea, C.; Romano, E.; Di Nardo, P.; Traversa, E.; Aoyagi, T., Substrate stiffness modulates gene expression and phenotype in neonatal cardiomyocytes in vitro. *Tissue engineering. Part A* **2012**, *18* (17-18), 1837-48.
7. Marsano, A.; Maidhof, R.; Wan, L. Q.; Wang, Y.; Gao, J.; Tandon, N.; Vunjak-Novakovic, G., Scaffold stiffness affects the contractile function of three-dimensional engineered cardiac constructs. *Biotechnol Prog* **2010**, *26* (5), 1382-90.
8. Bursac, N.; Loo, Y.; Leong, K.; Tung, L., Novel anisotropic engineered cardiac tissues: studies of electrical propagation. *Biochemical and biophysical research communications* **2007**, *361* (4), 847-53.
9. Bian, W.; Jackman, C. P.; Bursac, N., Controlling the structural and functional anisotropy of engineered cardiac tissues. *Biofabrication* **2014**, *6* (2), 024109.
10. Black, L. D., 3rd; Meyers, J. D.; Weinbaum, J. S.; Shvelidze, Y. A.; Tranquillo, R. T., Cell-induced alignment augments twitch force in fibrin gel-based engineered myocardium via gap junction modification. *Tissue engineering. Part A* **2009**, *15* (10), 3099-108.
11. Chung, C. Y.; Bien, H.; Entcheva, E., The role of cardiac tissue alignment in modulating electrical function. *J Cardiovasc Electrophysiol* **2007**, *18* (12), 1323-9.
12. Pong, T.; Adams, W. J.; Bray, M. A.; Feinberg, A. W.; Sheehy, S. P.; Werdich, A. A.; Parker, K. K., Hierarchical architecture influences calcium dynamics in engineered cardiac muscle. *Exp Biol Med (Maywood)* **2011**, *236* (3), 366-73.
13. Sommer, G.; Schriefl, A. J.; Andra, M.; Sacherer, M.; Viertler, C.; Wolinski, H.; Holzapfel, G. A., Biomechanical properties and microstructure of human ventricular myocardium. *Acta biomaterialia* **2015**, *24*, 172-92.
14. Rudnicki, M. S.; Cirka, H. A.; Aghvami, M.; Sander, E. A.; Wen, Q.; Billiar, K. L., Nonlinear strain stiffening is not sufficient to explain how far cells can feel on fibrous protein gels. *Biophysical journal* **2013**, *105* (1), 11-20.
15. Eschenhagen, T.; Didie, M.; Munzel, F.; Schubert, P.; Schneiderbanger, K.; Zimmermann, W. H., 3D engineered heart tissue for replacement therapy. *Basic research in cardiology* **2002**, *97 Suppl 1*, I146-52.
16. Bian, W.; Liau, B.; Badie, N.; Bursac, N., Mesoscopic hydrogel molding to control the 3D geometry of bioartificial muscle tissues. *Nature protocols* **2009**, *4* (10), 1522-34.
17. Taylor, R. J.; Moody, W. E.; Umar, F.; Edwards, N. C.; Taylor, T. J.; Stegemann, B.; Townend, J. N.; Hor, K. N.; Steeds, R. P.; Mazur, W.; Leyva, F., Myocardial strain measurement with feature-tracking cardiovascular magnetic resonance: normal values. *European heart journal cardiovascular Imaging* **2015**.
18. Kim, D. H.; Lipke, E. A.; Kim, P.; Cheong, R.; Thompson, S.; Delannoy, M.; Suh, K. Y.; Tung, L.; Levchenko, A., Nanoscale cues regulate the structure and function of macroscopic cardiac tissue constructs. *Proceedings of the National Academy of Sciences of the United States of America* **2010**, *107* (2), 565-70.
19. Capulli, A. K.; MacQueen, L. A.; Sheehy, S. P.; Parker, K. K., Fibrous scaffolds for building hearts and heart parts. *Adv Drug Deliv Rev* **2016**, *96*, 83-102.

20. Angst, B. D.; Khan, L. U.; Severs, N. J.; Whitely, K.; Rothery, S.; Thompson, R. P.; Magee, A. I.; Gourdie, R. G., Dissociated spatial patterning of gap junctions and cell adhesion junctions during postnatal differentiation of ventricular myocardium. *Circulation research* **1997**, *80* (1), 88-94.
21. Yang, X.; Pabon, L.; Murry, C. E., Engineering adolescence: maturation of human pluripotent stem cell-derived cardiomyocytes. *Circulation research* **2014**, *114* (3), 511-23.
22. Guyette, J. P.; Charest, J. M.; Mills, R. W.; Jank, B. J.; Moser, P. T.; Gilpin, S. E.; Gershlak, J. R.; Okamoto, T.; Gonzalez, G.; Milan, D. J.; Gaudette, G. R.; Ott, H. C., Bioengineering Human Myocardium on Native Extracellular Matrix. *Circulation research* **2016**, *118* (1), 56-72.
23. Vunjak-Novakovic, G.; Tandon, N.; Godier, A.; Maidhof, R.; Marsano, A.; Martens, T. P.; Radisic, M., Challenges in cardiac tissue engineering. *Tissue engineering. Part B, Reviews* **2010**, *16* (2), 169-87.
24. Sommer, G.; Haspinger, D. C.; Andra, M.; Sacherer, M.; Viertler, C.; Regitnig, P.; Holzapfel, G. A., Quantification of Shear Deformations and Corresponding Stresses in the Biaxially Tested Human Myocardium. *Annals of biomedical engineering* **2015**.
25. Grossman, W.; Jones, D.; McLaurin, L. P., Wall stress and patterns of hypertrophy in the human left ventricle. *The Journal of clinical investigation* **1975**, *56* (1), 56-64.
26. Moore, C. C.; Lugo-Olivieri, C. H.; McVeigh, E. R.; Zerhouni, E. A., Three-dimensional systolic strain patterns in the normal human left ventricle: characterization with tagged MR imaging. *Radiology* **2000**, *214* (2), 453-66.
27. Clark, N. R.; Reichek, N.; Bergey, P.; Hoffman, E. A.; Brownson, D.; Palmon, L.; Axel, L., Circumferential myocardial shortening in the normal human left ventricle. Assessment by magnetic resonance imaging using spatial modulation of magnetization. *Circulation* **1991**, *84* (1), 67-74.
28. Yeh, H. L.; Yeh, H. Y., A dimensionless analysis of young's modulus and stress distribution for orthotropic materials. *Journal of Aeronautics and Aerospace Engineering* **2014**, *3* (1).
29. Carmeliet, P.; Jain, R. K., Angiogenesis in cancer and other diseases. *Nature* **2000**, *407* (6801), 249-57.
30. Novosel, E. C.; Kleinhans, C.; Kluger, P. J., Vascularization is the key challenge in tissue engineering. *Adv Drug Deliv Rev* **2011**, *63* (4-5), 300-11.
31. Herper, M., The Truly Staggering Cost of Inventing New Drugs. *Forbes, Pharma & Healthcare* **2012**, 38.
32. Lavery, H.; Benson, C.; Cartwright, E.; Cross, M.; Garland, C.; Hammond, T.; Holloway, C.; McMahon, N.; Milligan, J.; Park, B.; Pirmohamed, M.; Pollard, C.; Radford, J.; Roome, N.; Sager, P.; Singh, S.; Suter, T.; Suter, W.; Trafford, A.; Volders, P.; Wallis, R.; Weaver, R.; York, M.; Valentin, J., How can we improve our understanding of cardiovascular safety liabilities to develop safer medicines? *Br J Pharmacol* **2011**, *163* (4), 675-93.
33. Connolly, R.; Kanellias, M.; Stratica, H., *Design of a Universal Microscope Incubator for Drug Screening of 3D Models of Engineered Myocardium*. Worcester Polytechnic Institute: Worcester, MA, 2017.
34. Chen, A.; Lee, E.; Tu, R.; Santiago, K.; Grosberg, A.; Fowlkes, C.; Khine, M., Integrated platform for functional monitoring of biomimetic heart sheets derived from human pluripotent stem cells. *Biomaterials* **2014**, *35* (2), 675-83.
35. Smith, A. S.; Macadangang, J.; Leung, W.; Laflamme, M. A.; Kim, D. H., Human iPSC-derived cardiomyocytes and tissue engineering strategies for disease modeling and drug screening. *Biotechnology advances* **2017**, *35* (1), 77-94.
36. Takahashi, K.; Yamanaka, S., Induction of pluripotent stem cells from mouse embryonic and adult fibroblast cultures by defined factors. *Cell* **2006**, *126* (4), 663-76.
37. Chin, M. H.; Mason, M. J.; Xie, W.; Volinia, S.; Singer, M.; Peterson, C.; Ambartsumyan, G.; Aimiwu, O.; Richter, L.; Zhang, J.; Khvorostov, I.; Ott, V.; Grunstein, M.; Lavon, N.; Benvenisty, N.; Croce, C. M.; Clark, A. T.; Baxter, T.; Pyle, A. D.; Teitell, M. A.; Pelegri, M.; Plath, K.; Lowry, W. E., Induced pluripotent stem cells and embryonic stem cells are distinguished by gene expression signatures. *Cell stem cell* **2009**, *5* (1), 111-23.
38. Wilson, K. D.; Venkatasubrahmanyam, S.; Jia, F.; Sun, N.; Butte, A. J.; Wu, J. C., MicroRNA profiling of human-induced pluripotent stem cells. *Stem cells and development* **2009**, *18* (5), 749-58.
39. Mauritz, C.; Martens, A.; Rojas, S. V.; Schnick, T.; Rathert, C.; Schecker, N.; Menke, S.; Glage, S.; Zweigerdt, R.; Haverich, A.; Martin, U.; Kutschka, I., Induced pluripotent stem cell (iPSC)-derived Flk-1 progenitor cells engraft, differentiate, and improve heart function in a mouse model of acute myocardial infarction. *European heart journal* **2011**, *32* (21), 2634-41.

40. Ebert, A. D.; Yu, J.; Rose, F. F., Jr.; Mattis, V. B.; Lorson, C. L.; Thomson, J. A.; Svendsen, C. N., Induced pluripotent stem cells from a spinal muscular atrophy patient. *Nature* **2009**, *457* (7227), 277-80.
41. Dimos, J. T.; Rodolfa, K. T.; Niakan, K. K.; Weisenthal, L. M.; Mitsumoto, H.; Chung, W.; Croft, G. F.; Saphier, G.; Leibel, R.; Goland, R.; Wichterle, H.; Henderson, C. E.; Eggan, K., Induced pluripotent stem cells generated from patients with ALS can be differentiated into motor neurons. *Science* **2008**, *321* (5893), 1218-21.
42. Park, I. H.; Arora, N.; Huo, H.; Maherali, N.; Ahfeldt, T.; Shimamura, A.; Lensch, M. W.; Cowan, C.; Hochedlinger, K.; Daley, G. Q., Disease-specific induced pluripotent stem cells. *Cell* **2008**, *134* (5), 877-86.
43. Yodmuang, S.; McNamara, S. L.; Nover, A. B.; Mandal, B. B.; Aganwal, M.; Kelly, T. A. N.; Chao, P. H. G.; Hung, C.; Kaplan, D. L.; Vunjak-Novakovic, G., Silk microfiber-reinforced silk hydrogel composites for functional cartilage tissue repair. *Acta biomaterialia* **2015**, *11*, 27-36.
44. Chao, P. H.; Yodmuang, S.; Wang, X.; Sun, L.; Kaplan, D. L.; Vunjak-Novakovic, G., Silk hydrogel for cartilage tissue engineering. *Journal of biomedical materials research. Part B, Applied biomaterials* **2010**, *95* (1), 84-90.
45. Lee, S. M., *Handbook of composite reinforcements*. VCH: New York, 1993; p xiv, 715 p.
46. Guo, C.; Kaufman, L. J., Flow and magnetic field induced collagen alignment. *Biomaterials* **2007**, *28* (6), 1105-14.
47. Ogle, B. M.; Bursac, N.; Domian, I.; Huang, N. F.; Menasche, P.; Murry, C. E.; Pruitt, B.; Radisic, M.; Wu, J. C.; Wu, S. M.; Zhang, J.; Zimmermann, W. H.; Vunjak-Novakovic, G., Distilling complexity to advance cardiac tissue engineering. *Science translational medicine* **2016**, *8* (342), 342ps13.
48. Post, M. J.; Rahimi, N.; Caolo, V., Update on vascularization in tissue engineering. *Regen Med* **2013**, *8* (6), 759-70.
49. Cutiongco, M. F.; Tan, M. H.; Ng, M. Y.; Le Visage, C.; Yim, E. K., Composite pullulan-dextran polysaccharide scaffold with interfacial polyelectrolyte complexation fibers: a platform with enhanced cell interaction and spatial distribution. *Acta biomaterialia* **2014**, *10* (10), 4410-8.
50. Atala, A.; Kasper, F. K.; Mikos, A. G., Engineering complex tissues. *Science translational medicine* **2012**, *4* (160), 160rv12.
51. Grasman, J. M.; Do, D. M.; Page, R. L.; Pins, G. D., Rapid release of growth factors regenerates force output in volumetric muscle loss injuries. *Biomaterials* **2015**, *72*, 49-60.
52. Grasman, J. M.; Zayas, M. J.; Page, R. L.; Pins, G. D., Biomimetic scaffolds for regeneration of volumetric muscle loss in skeletal muscle injuries. *Acta biomaterialia* **2015**, *25*, 2-15.
53. Tao, Z. W.; Favreau, J. T.; Guyette, J. P.; Hansen, K. J.; Lessard, J.; Burford, E.; Pins, G. D.; Gaudette, G. R., Delivering stem cells to the healthy heart on biological sutures: effects on regional mechanical function. *Journal of tissue engineering and regenerative medicine* **2014**.
54. Guyette, J. P.; Fakharzadeh, M.; Burford, E. J.; Tao, Z. W.; Pins, G. D.; Rolle, M. W.; Gaudette, G. R., A novel suture-based method for efficient transplantation of stem cells. *Journal of biomedical materials research. Part A* **2013**, *101* (3), 809-18.
55. Proulx, M. K.; Carey, S. P.; Ditroia, L. M.; Jones, C. M.; Fakharzadeh, M.; Guyette, J. P.; Clement, A. L.; Orr, R. G.; Rolle, M. W.; Pins, G. D.; Gaudette, G. R., Fibrin microthreads support mesenchymal stem cell growth while maintaining differentiation potential. *Journal of biomedical materials research. Part A* **2011**, *96* (2), 301-12.
56. Cornwell, K. G.; Pins, G. D., Discrete crosslinked fibrin microthread scaffolds for tissue regeneration. *Journal of biomedical materials research. Part A* **2007**, *82* (1), 104-12.
57. Horan, R. L.; Collette, A. L.; Lee, C.; Antle, K.; Chen, J. S.; Altman, G. H., Yarn design for functional tissue engineering. *Journal of biomechanics* **2006**, *39* (12), 2232-2240.
58. Gentleman, E.; Lay, A. N.; Dickerson, D. A.; Nauman, E. A.; Livesay, G. A.; Dee, K. C., Mechanical characterization of collagen fibers and scaffolds for tissue engineering. *Biomaterials* **2003**, *24* (21), 3805-3813.
59. Pins, G. D.; Christiansen, D. L.; Patel, R.; Silver, F. H., Self-assembly of collagen fibers. Influence of fibrillar alignment and decorin on mechanical properties. *Biophysical journal* **1997**, *73* (4), 2164-72.
60. O'Brien, M. P.; Carnes, M. E.; Page, R. L.; Gaudette, G. R.; Pins, G. D., Designing Biopolymer Microthreads for Tissue Engineering and Regenerative Medicine. *Curr Stem Cell Rep* **2016**, *2* (2), 147-157.

Appendix 1: Summary of Functional Behavior

Table A.1. Summary table of functional behavior. Values shown are averages +/- standard error.

Group	N	Time Point (days)	Max Contractile Strain (%)	Average Contractile Strain (%)	Frequency (Hz)
GCS	8	7	4.97 +/- 0.51	2.14 +/- 0.12	0.9 +/- 0.2
	7	10	4.17 +/- 0.31	2.08 +/- 0.06	1.2 +/- 0.2
	4	14	4.21 +/- 0.38	2.12 +/- 0.18	1.4 +/- 0.2
FGC	8	7	7.18 +/- 0.35	3.16 +/- 0.16* (p=0.023)	2.5 +/- 0.1* (p<0.001)
	7	10	7.19 +/- 0.78* (p=0.010)	3.15 +/- 0.31* (p=0.023)	1.6 +/- 0.1 [‡] (p<0.001)
	6	14	6.34 +/- 0.67	2.94 +/- 0.27	1.5 +/- 0.3 [‡] (p<0.001)
5tC	9	7	6.32 +/- 0.46	3.29 +/- 0.42* (p=0.006)	2.1 +/- 0.2* (p<0.001)
	10	10	7.77 +/- 0.48* (p<0.001)	3.41 +/- 0.25* (p=0.001)	1.9 +/- 0.1* (p=0.035)
	9	14	5.35 +/- 0.59 [†] (p=0.007)	2.66 +/- 0.20 [†] (p=0.048)	1.9 +/- 0.2
10tC	9	7	6.52 +/- 0.66	3.29 +/- 0.24* (p=0.006)	2.3 +/- 0.1* (p<0.001)
	9	10	7.93 +/- 0.95* (p<0.001)	3.25 +/- 0.18* (p=0.006)	1.7 +/- 0.2 ^g (p=0.006)
	9	14	6.65 +/- 0.63	3.10 +/- 0.18	1.9 +/- 0.2
20tC	8	7	6.08 +/- 0.52	2.97 +/- 0.24	2.2 +/- 0.2* (p<0.001)
	10	10	6.50 +/- 0.62* (p=0.044)	3.33 +/- 0.17* (p=0.002)	1.9 +/- 0.1* (p=0.037)
	9	14	5.81 +/- 0.29	2.91 +/- 0.22	2.0 +/- 0.2

* Denotes significant difference from GCS at respective time point.

[†] Denotes significant difference from 5tC at Day 10

[‡] Denotes significant difference from FGC at day 7.

^g Denotes significant difference from 10tC at day 7.

Appendix 2: Comparison of Media Formulations on 2D and 3D Cultures with Rat Neonatal Ventricular Myocytes

A.2.1 INTRODUCTION

Media components can cause changes in cell behavior. In a study completed by Franke et al, media supplemented with fetal bovine serum (FBS) or horse serum (HS) was used to culture primary equine bronchial fibroblasts. Data from this study demonstrated that media supplemented with FBS promoted enhanced proliferation and had faster doubling times relative to HS.¹ With rat neonatal ventricular myocytes (rNVMs), a similar trend has been reported; horse serum can limit fibroblast proliferation.² This is desirable as fibroblasts can overtake a primary isolation culture,³ hindering contractile function of incorporated myocytes. This is especially problematic in 2D cultures as a 3D environment can help to limit fibroblast proliferation, possibly due to contact inhibition.³

Additionally, chick embryo extract (CEE) is a supplement that has been used in rNVM cultures.⁴ It has been demonstrated that following the development of a contractile rNVM engineered tissue scaffold, when HS and CEE were withdrawn from the media, contractile activity rapidly ceased.⁵ An additional study showed that the force development of cells incorporated in a 3D scaffold was greatly reduced or entirely absent when CEE or HS was not included in the media, respectively.⁶

For Aim 1 of this thesis work, the media formulation had a combination of FBS and HS, and no CEE supplementation. In this study, we were interested in comparing this media formulation to a published media formulation containing CEE and HS.⁷ We compared 2-dimensional (2D) and 3-dimensional (3D) samples seeded with rNVMs and cultured with either media. We evaluated the contractile strains, contractile frequencies, and contractile areas. Additionally, we performed LIVE/DEAD staining to evaluate the relative number and viability of incorporated cells

throughout the culture period. The goal of this study was to determine what media formulation should be used with future experimentation.

A.2.2 MATERIALS and METHODS

For more detailed methods on scaffold preparation, please refer to Chapter 4: Alignment of Cardiomyocytes in a Fibrin Microthread-Based Composite Layer Enhances Contractile Function.

A.2.2.1 Microthread Extrusion

Fibrin microthreads were generated by co-extruding two solutions; a 70 mg/mL solution of fibrinogen (from bovine plasma, Sigma, St. Louis, MO) in HEPES (N-[2-Hydroxyethyl] piperazine-N'-[2-ethanesulfonic acid]) buffered saline (HBS, 20 mM HEPES, 0.9% NaCl; pH 7.4) and a 6 U/mL solution of thrombin isolated from bovine plasma (Sigma) in HBS and CaCl₂ solutions.⁸⁻¹¹ The solutions were extruded through polyethylene tubing (BD, Sparks, MD) and threads were hand-drawn into a 10 mM HEPES buffer bath (pH 7.4) in a Teflon coated pan at a flow rate of 0.225 mL/min. Following a polymerization time of 10-15-minutes, the scaffolds were stretched to ~150% of their original length and hung to dry.¹¹

A.2.2.2 Fibrin Microthread Organization

Dried fibrin microthreads were organized as previously reported,¹² using a purpose-built fibrin microthread spacer. For this work, evaluations were completed utilizing composite layers with 5 fibrin microthreads (5tC) evenly spaced across a 12 mm width. Once organized, threads were secured using medical grade silicone adhesive (Vendor, City, State) to precut vellum frames.

A.2.2.3 Rat Neonatal Ventricular Myocyte (rNVM) Isolation

All work involving animals was submitted to and approved by the Institutional Animal Care and Use Committee at Worcester Polytechnic Institute. rNVMs were isolated following a previously described protocol.¹³ Ventricles of excised hearts of 2 and 3 day old neonatal Sprague Dawley rats (Charles River, Wilmington, MA) were separated from atria, and minced. Serial digestion using type II collagenase (Thermo Fisher Scientific, Waltham, MA) was completed. Cells were pre-plated for 45 minutes, then immediately used for experimentation.⁷

A.2.2.4 Fabrication of Composite Layers

Organized fibrin microthreads on vellum frames were rehydrated in phosphate buffered saline (PBS) for 1 hour, then placed on either polydimethylsiloxane (PDMS) sheets (for unaligned composite layers – UAC) or custom PDMS casting devices (for aligned layers- AC) coated with 1% Pluronic-F127 (Sigma, St. Louis, MO) in DI water. 150 μ L of hydrogel solution consisting of 4×10^6 cells/mL, 4% (v/v) 40 U/mL thrombin, and 28% (v/v) 11 mg/mL fibrinogen was mixed on ice, cast over the vellum frames and spread using a pipette tip to provide an even layer. The paper outlining the media formulation containing CEE and HS also included a methodology for creating aligned fibrin-based hydrogels.⁷ The hydrogel formulation was similar to the hydrogel formulation described here, but included Matrigel. To evaluate if Matrigel in combination with HS and CEE supplemented media provided the best combination for promoting cardiomyocyte contractile function, an additional sample group (UACMAT M2) was included with a hydrogel formulation of 4×10^6 cells/mL, 2% (v/v) 40 U/mL thrombin, 20% (v/v) 11mg/mL fibrinogen, 10% (v/v) Matrigel and 20% (v/v) 2X DMEM. The 2X DMEM solution was made by rehydrating powdered DMEM (Gibco, cat. no. 31600034) with half of the recommended volume of distilled water yielding a DMEM solution that was twice the concentration of regular DMEM. Following a 30-minute incubation time, samples were transferred to wells. UAC layers were free-floating, while aligned samples were transferred to culturing devices and secured to the PDMS posts of the device with silicone o-rings (McMaster-Carr, Princeton, NJ).

A.2.2.5 Seeding of Gelatin-Coated Glass Coverslip Controls (GCS)

Gelatin coated coverslips (GCS) were used to assess 2D cultures. Glass coverslips (VWR) were coated with sterile 0.7% gelatin (Sigma Aldrich) in DI water for 4 hours, then secured to the bottom of wells in a 12 well plate using vacuum grease. 100 μ L of cell suspension (2×10^6 cells/mL) was seeded on each coverslip and incubated at 37°C for 18 hours. Samples were then rinsed and covered with medium for extended culture.

A.2.2.6 Media Preparation and Extended Culture

Two media formulations (M1 and M2) were evaluated for this assessment and are summarized in **Table A.2.1**. For all samples, culture was maintained for 14 days with medium changes every other day.

Table A.2.1. Media formulations evaluated for experiment. Media formulation 1 (M1) is what had been utilized in Aim 1. Media formulation 2 (M2) is based on a published formulation.⁷

<i>Media Component</i>	<i>Media Formulation 1</i>	<i>Media Formulation 2</i>
<i>Iscove's Modified DMEM</i>	~82.5%	----
<i>DMEM +L-glutamine</i>	----	85%
<i>FBS</i>	10%	----
<i>HS</i>	2%	10%
<i>pen strep</i>	1%	1%
<i>Amphotericin B</i>	1%	1%
<i>Aprotinin (5mg/mL)</i>	1%	1%
<i>Chick Embryo Extract</i>	----	2%
<i>Gentamicin</i>	0.5%	----
<i>Glutamax</i>	1%	----
<i>B-mercaptoethanol</i>	0.007%	----
<i>1.2mM CaCl₂ and 0.8 mM MgCl₂ in DiH₂O</i>	1%	----

To thoroughly compare the conditions, the following schema was utilized (**Table A.2.2**):

Table A.2.2. Outline of sample nomenclatures and study design to compare media formulations in 2D and 3D cultures.

	<i>Base Nomenclature</i>	<i>Media 1, Name/ n#</i>	<i>Media 2, Name/ n#</i>
<i>Gelatin-Coated Coverslips (2D)</i>	GCS	GCS M1/ n=3	GCS M2/ n=3
<i>Aligned Composites (3D)</i>	AC	AC M1/ n=3	AC M2/ n=3
<i>Unaligned Composites (3D)</i>	UAC	UAC M1/ n=5*	UAC M2/ n=3
<i>Unaligned Composites +Matrigel (3D)</i>	UACMAT	-----	UACMAT M2/ n=5*

*: Extra samples were prepared for LIVE/DEAD analysis at days 7 and 14.

A.2.2.7 Cardiomyocyte Functional Analysis Through High Density Mapping (HDM)

Spontaneous contractions were recorded at days 7, 10 and 14 for ~1300 frames at 100X magnification and 60 frames per second with a high speed camera (HiSpec 4, Fastec Imaging Corp, San Diego, CA) attached to an inverted microscope (DMIL, Leica Microsystems, Buffalo Grove, IL). There were visible differences regionally for AC samples. Because of this, two regions per sample were recorded per time point: one at a region of larger global movements (as identified by thread movement) and one at a region of low global movements (as identified by little if any thread movement). High density mapping (HDM), was used to evaluate regional mechanical function.¹⁴ Regions of interest (ROI) selected for each sample (size: 1200 x 986 pixels) were divided into 16 x 16 pixel subwindows. An 8 pixel shift and 5 averaging windows were used to track pixel displacements of sequential frames.¹⁵⁻¹⁶ The resulting displacement fields were then used to determine the maximum principal contractile strain, the average principal contractile strain, frequency of contractions and total contractile area.

A.2.2.8 LIVE/DEAD Staining

LIVE/DEAD staining was completed after 7 and 14 days in culture on UAC M1 and UACMAT M2 samples (1/ time point). It is important to note that samples from each group could not be stained due to the limited number of cells (and therefore, limited number of samples) from the isolation. These groups were chosen for staining as there were extra samples in each. Following

the manufacturer’s protocol (Molecular Probes, Waltham, MA), a 2 μ M calcein AM and 4 μ M ethidium homodimer-1 (Ethd-1) solution was prepared in Dulbecco’s phosphate-buffered saline (D-PBS). Samples were rinsed with D-PBS, then incubated with the prepared staining solution for 30-45 minutes at 37°C. Following incubation, samples were imaged at 100X using a fluorescent Zeiss inverted microscope (Zeiss, Thornwood, NY). Because of the difference in cell densities at day 7 and 14, samples could not be imaged at the same exposure times and were adjusted for each sample group (**Figure A.2.1**). Because of this, qualitative comparisons between images were made but were not quantified as different exposure times can change potential outcomes.

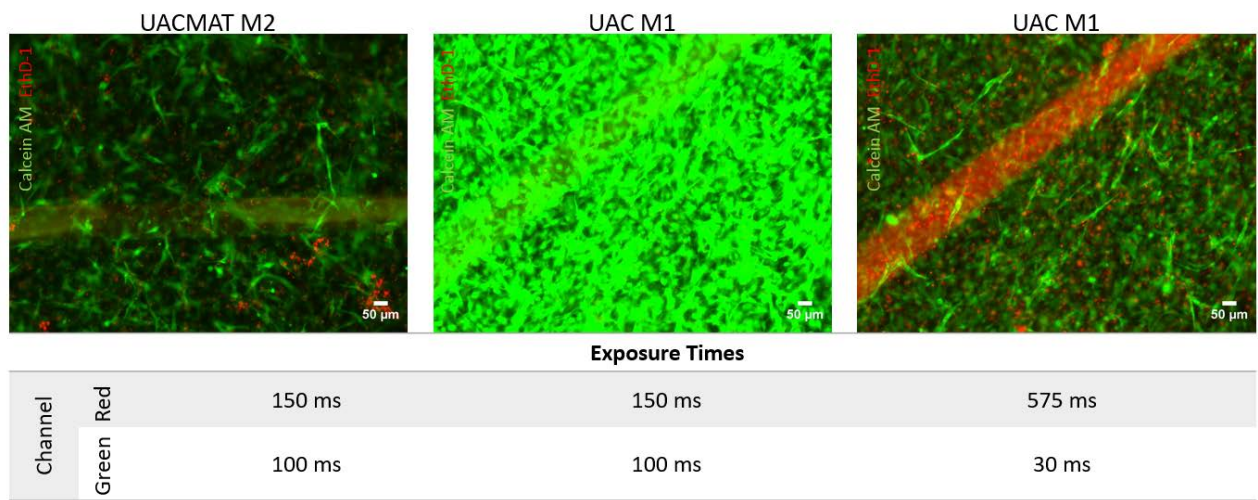


Figure A.2.1. Exposure times for fluorescently labeled samples. When imaging UACMAT M2 and UAC M1 samples, each sample group required different exposure times to clearly visualize the LIVE/DEAD stain. Exposure times shown for the left and right images are the times used for all samples within those groups, respectively. The center sample is an example of why the same exposure times could not be used as the settings for UACMAT M2 resulted in over-exposure of cells in the UAC M1 samples.

A.2.2.9 Statistical Analyses

Statistical analyses were run using SigmaPlot 13 software. For all comparisons, a significance level of $p < 0.05$ was utilized. For contractile strains, areas and frequencies, comparisons were made at each time point using a One-way ANOVA with Holm-Sidak post hoc analysis. For all data presented, data are reported as means \pm standard deviation.

A.2.3 RESULTS

A.2.3.1 M2 Media Promotes Increased Functional Behavior in a 14-Day Culture

There were striking differences in the functional parameters evaluated for samples cultured in M1 relative to M2. When evaluating the maximum contractile strains, samples cultured in M2 had an increasing trend in strains over time (**Figure A.2.2**) while samples cultured in M1 had a decreasing trend in strains over time. At day 10, AC M2 Max samples had significantly higher maximum contractile strains than all other samples cultured in M1 media ($12.6\% \pm 5.2$, $0\% \pm 0$, $2.7\% \pm 0.7$, $3.3\% \pm 0.1\%$, $2.9\% \pm 0.4$ for AC M2 Max, GCS M1, UAC M1, AC M1 Max and AC M1 Min, respectively). By day 14, a similar pattern to day 10 was observed where all samples cultured in M2 media trended higher than all samples cultured in M1 media. Average principal contractile strains followed very similar trends to maximum principal strains. At day 10, both AC M2 Max and AC M2 Min groups were significantly greater than all samples cultured in M1 media ($1.8\% \pm 0.1$, $1.9\% \pm 0.1$, $0\% \pm 0$, $1.1\% \pm 0.1$, $1.2\% \pm 0.1$, $1.1\% \pm 0$ for AC M2 Max, AC M2 Min, GCS M1, UAC M1, AC M1 Max and AC M1 Min, respectively). At day 14, all M2 samples had higher average contractile strain values than all M1 samples.

At day 7, UAC samples cultured in M1 had comparable contractile areas to all M2 samples ($79.0\% \pm 7.6$, $82.4\% \pm 3.5$, $86.1\% \pm 7.3$, 79% , 73% , $79.4\% \pm 11.2$ for UAC M1, GCS M2, UAC M2, AC M2 Max, AC M2 Min and UACMAT M2, respectively). By day 14 of culture, all M2 samples apart from GCS M2 had significantly higher contractile areas than all M1 samples. At this point, measurable contractions were no longer observed for any M1 sample except for UAC M1. While all M1 samples appeared to decrease in strain and area values, the M2 samples appeared to increase in these parameters over the culture period.

There were no significant differences in contractile frequencies among samples that had measurable contractions. When groups began having contractions that we could no longer evaluate using the imaging and HDM parameters outlined in this study, we began seeing significant differences. Again, with the exception of the GCS M2 samples, all samples cultured in M2 had measurable contractions over the 14 day culture period. Only the UAC M1 samples continued to have measurable contractions by day 14 out of all samples cultured in M1 media.

The UACMAT M2 group had a slightly different hydrogel formulation relative to the UAC M2 group. Matrigel was incorporated in the UACMAT M2 samples but not the UAC M2 samples. Both sample groups were cultured in M2 media. At no time point for any functional parameter did these two groups have significant differences.

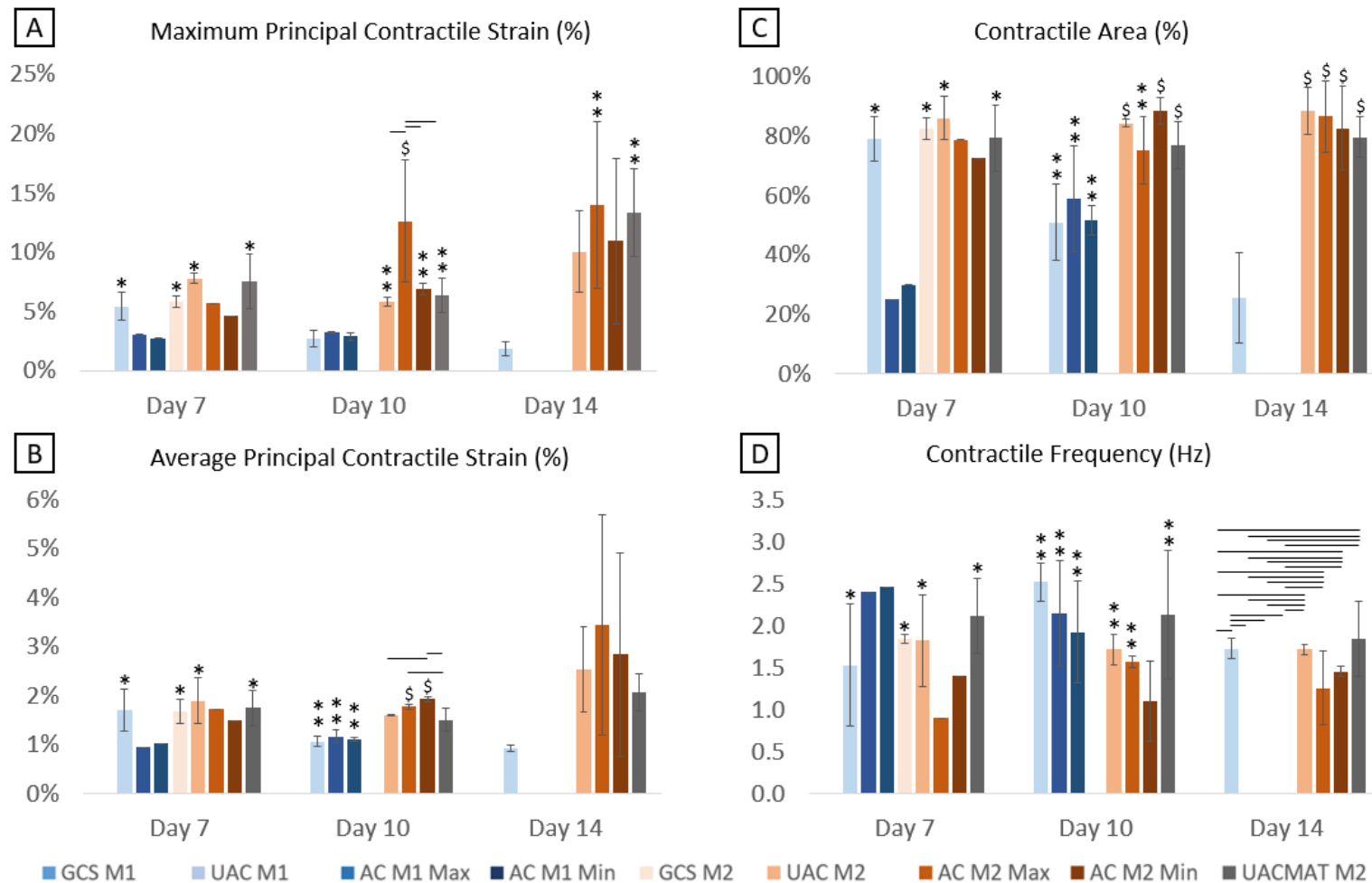


Figure A.2.2. Summary of functional data for 2D and 3D samples in M1 and M2 cultures. M1 samples showed decreasing patterns for functional parameters over a 14 day culture (blue bars) while samples cultured in M2 media (Orange and gray bars) had increasing trends in functional parameters. All significant differences were determined through a One-Way ANOVA with holm-sidak post hoc analysis, $p < 0.05$. All data are shown as averages \pm standard deviations. *: Significant difference from GCS M1. **: Significant difference from GCS M1 and GCS M2. \$: Significant difference from all M1 samples. Bar: Significant difference between two groups.

A.2.3.2 M1 Media May Promote Proliferation of Fibroblasts

Qualitative comparisons were made for LIVE/DEAD staining of UACMAT M2 and UAC M1 samples. The comparisons demonstrated that although samples were initially seeded with the same number of cells, there was evidence of an increased number of cells in the UAC M1 samples at days 7 and 14 (**Figure A.2.3**). At both time points, the UACMAT M2 samples have less green (Calcein-AM positive) and less red (Ethd-1 positive) stained cells, suggesting there are less cells in those constructs at both time points. In the images, there appear to be at least two cell types; an elongated cell and a smaller, more compact cell. The smaller, more compact cells appear to increase in number for both sample groups from day 7 to day 14 and are potentially fibroblasts. Taken together, the observations listed here suggest that the M2 formulation may limit fibroblast proliferation relative to M1 medium.

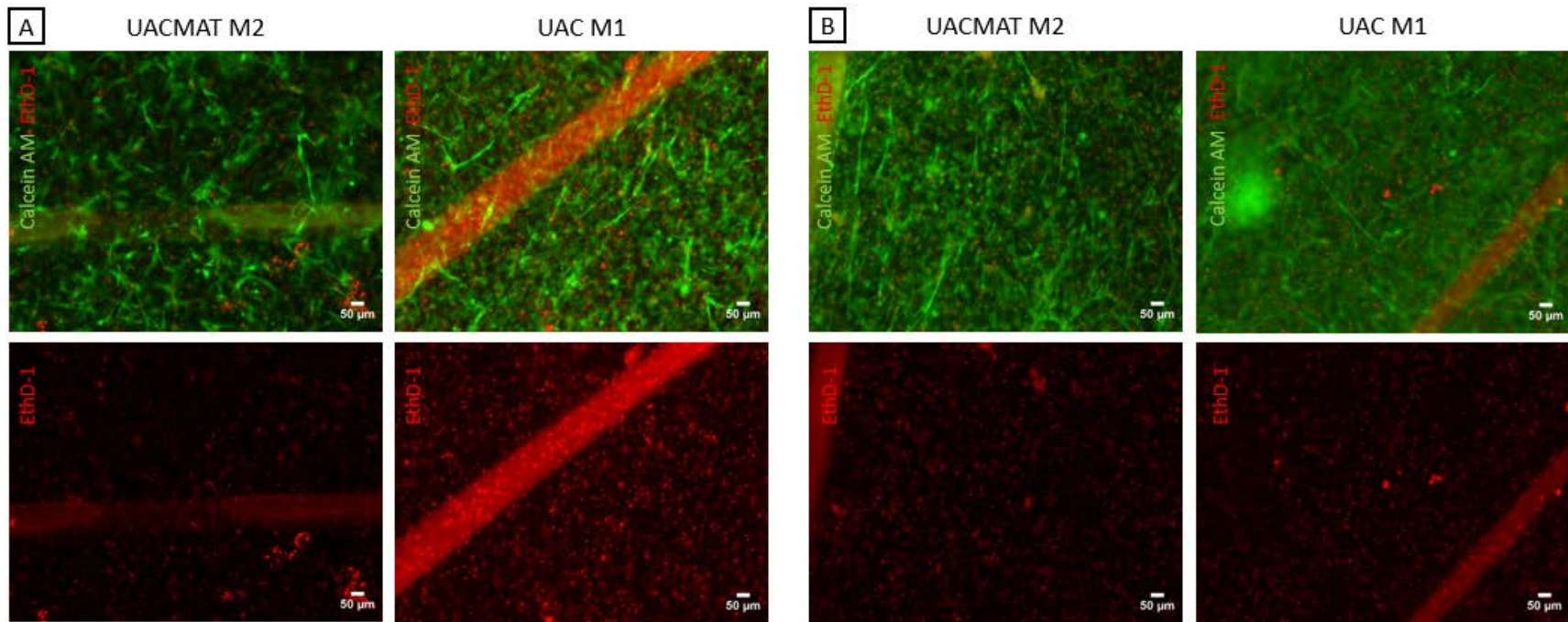


Figure A.2.3 LIVE/DEAD staining of composite samples. Samples cultured in M1 and M2 were compared using LIVE/DEAD staining. The green channel shows live cells (calcein -AM positive) while the red channel shows dead cells (Ethd-1 positive). In the UACMAT M2 samples, less cells appear to be present (larger black spaces visible) at day 7 (A) and day 14 (B), even though samples were seeded with the same number of cells. Direct quantitative comparisons were not made as exposure times had to be adjusted on a group basis to ensure clear visibility of the stains.

A.2.4 DISCUSSION

The cellular composition of tissue engineered cardiac scaffolds is heavily influential on the resultant functional behavior. While cardiomyocytes are functional cells that generate contractile force and propagate an electrical signal, other cells play critical roles. Fibroblasts, stromal and endothelial cells influence matrix deposition, paracrine signaling and vascularization.¹⁷ While action potential speeds increase with an increasing purity of cardiomyocytes, contractile forces have been reported to be optimized with cardiomyocytes comprising 60-80% of the total cell population.¹⁸ While it is generally agreed that non-myocytes like fibroblasts are beneficial to cardiomyocyte maturation and function, when present in too great amounts function can be compromised.¹⁷ Therefore, it is critical that the media utilized not promote fibroblast proliferation as this cell type can overtake cardiomyocytes in culture. This study demonstrated that CEE and HS had large impacts on the resultant cell function. It is likely that this was due to limited fibroblast proliferation. This hypothesis is further supported by the LIVE/DEAD staining showing a potentially increasing cell population over time for samples not cultured with CEE or 10% HS. As such, subsequent work for this thesis utilized M2 media formulation for all cell culture.

UACMAT M2 and UAC M2 samples enabled comparison of hydrogel formulations that contained or did not contain Matrigel, respectively. In this study, these sample groups never significantly differed from one another for any functional evaluations at any time point. As such, Matrigel addition does not appear to impact resulting cell function. The lack of increase in cell function with Matrigel was justification for excluding Matrigel from all hydrogel formulations in subsequent thesis work.

A.2.4.1 Study Limitations

The goal of this study was to evaluate the impact of two media formulations on rat neonatal ventricular myocytes cultured in 2D and 3D formats. More specifically, the goal of this work was to determine which media formulation should be utilized for work following Aim 1 of this thesis. The comparisons of interest required 9 sample groups with the study design described. A limiting factor influencing the study design was the number of cells obtained from the cell isolation. A more thorough study would separate the media components of interest (CEE and HS) to determine how each impacted the resulting function of incorporated cells, as well as the combination of supplements. Additionally, another limitation of this study was that the base media components

were slightly different between the two formulations. A more robust study would remove those variables to ensure all impacts to function were caused by the CEE or HS supplements. The data presented does show clear differences in cell function, but does not fully elucidate the causality of those changes. For our goal, this study was sufficient for determining which media promoted greater cell function, and which media was used for subsequent work of this thesis.

Because of the limited number of cells and therefore samples, LIVE/DEAD staining could not be completed for all sample groups, and was not completed at all time points. Only UAC M1 and UACMAT M2 groups were compared. The UACMAT M2 group not only was cultured in M2 media, but also had Matrigel incorporated in the hydrogel formulation. The qualitative differences observed therefore, are only suggestive but not indicative of how the media formulations impact the incorporated cells. With more resources available, it would have been preferable to evaluate UAC M2 samples that did not include Matrigel. This would have more clearly shown the differences resulting from the media formulations. Matrigel addition did not impact cell function relative to UAC M2 samples. As such, it is possible that the Matrigel addition did not change the phenotype of incorporated cells or proliferation rates. This is speculative, and would need to be confirmed.

We had no measurable contractions for GCS M1 samples throughout the culture period which seems contradictory to the results of Aim 1 where GCS samples in the same media had measurable contractions at all time points. The reason for this difference is the change in recording and HDM analysis parameters. Because of the high function observed with samples cultured in M2, the HDM parameters used in Aim 1 were not sufficient for evaluating cell function. In Aim 1, we recorded samples at a magnification of 400X. With global movements occurring in M2 samples, quantitative evaluations became difficult at this magnification. For this assessment, a magnification of 100X enabled quantification of all 3D samples regardless of global movements. While contractions were likely occurring for GCS M1 samples, they were not above the noise threshold when imaged at 100X. In all subsequent thesis work, recordings were taken at 100X.

We only had measurable contractions at D7 for GCS M2 samples. We did however, have measurable contractions at all time points for these same samples in subsequent work summarized in Aim 2. In this particular study, we had limited number of samples and the data pulled for the

GCS M2 samples was unfortunately very noisy. While contractions were observed, we had difficulty quantifying the functional behavior.

A.2.5 CONCLUSIONS

In this work, we demonstrated that samples cultured in M2 media formulation had increased cell function relative to samples cultured in M1. As fibroblast proliferation has been shown to hinder cardiomyocyte function, a possible explanation is that the 10% HS and CEE supplements in M2 helped limit proliferation relative to M1. This hypothesis is further supported with the LIVE/DEAD data obtained where samples cultured in M1 appeared to have more cells present within the constructs than samples cultured in M2 at days 7 and 14. Further, when comparing samples cultured in M2 media that did or did not contain Matrigel, no significant difference in function was observed at any time point for any functional parameter. Following this study, we chose to continue all subsequent work for this thesis with M2 media and to not include Matrigel in the hydrogel formulation used with our composite layers.

A.2.6 ACKNOWLEDGEMENTS

This work was funded by NIH R01-HL115282 (G.R.G.), NSF IGERT DGE 1144804, and NIH 1R15HL137145-01.

A.2.7 REFERENCES

1. Franke, J.; Abs, V.; Zizzadoro, C.; Abraham, G., Comparative study of the effects of fetal bovine serum versus horse serum on growth and differentiation of primary equine bronchial fibroblasts. *BMC Vet Res* **2014**, *10*, 119.
2. Wendel, J. S.; Ye, L.; Zhang, P.; Tranquillo, R. T.; Zhang, J. J., Functional consequences of a tissue-engineered myocardial patch for cardiac repair in a rat infarct model. *Tissue engineering. Part A* **2014**, *20* (7-8), 1325-35.
3. Radisic, M.; Christman, K. L., Materials science and tissue engineering: repairing the heart. *Mayo Clinic proceedings* **2013**, *88* (8), 884-98.
4. Naito, H.; Melnychenko, I.; Didie, M.; Schneiderbanger, K.; Schubert, P.; Rosenkranz, S.; Eschenhagen, T.; Zimmermann, W. H., Optimizing engineered heart tissue for therapeutic applications as surrogate heart muscle. *Circulation* **2006**, *114* (1 Suppl), I72-8.
5. Eschenhagen, T.; Didie, M.; Munzel, F.; Schubert, P.; Schneiderbanger, K.; Zimmermann, W. H., 3D engineered heart tissue for replacement therapy. *Basic research in cardiology* **2002**, *97* Suppl 1, I146-52.
6. Zimmermann, W. H.; Melnychenko, I.; Eschenhagen, T., Engineered heart tissue for regeneration of diseased hearts. *Biomaterials* **2004**, *25* (9), 1639-47.
7. Bian, W.; Liao, B.; Badie, N.; Bursac, N., Mesoscopic hydrogel molding to control the 3D geometry of bioartificial muscle tissues. *Nature protocols* **2009**, *4* (10), 1522-34.

8. Cornwell, K. G.; Pins, G. D., Discrete crosslinked fibrin microthread scaffolds for tissue regeneration. *Journal of biomedical materials research. Part A* **2007**, 82 (1), 104-12.
9. Grasman, J. M.; O'Brien, M. P.; Ackerman, K.; Gagnon, K. A.; Wong, G. M.; Pins, G. D., The Effect of Sterilization Methods on the Structural and Chemical Properties of Fibrin Microthread Scaffolds. *Macromolecular bioscience* **2016**, 16 (6), 836-46.
10. Grasman, J. M.; Page, R. L.; Dominko, T.; Pins, G. D., Crosslinking strategies facilitate tunable structural properties of fibrin microthreads. *Acta biomaterialia* **2012**, 8 (11), 4020-30.
11. Grasman, J. M.; Pumphrey, L. M.; Dunphy, M.; Perez-Rogers, J.; Pins, G. D., Static axial stretching enhances the mechanical properties and cellular responses of fibrin microthreads. *Acta biomaterialia* **2014**, 10 (10), 4367-76.
12. Chrobak, M. O.; Hansen, K. J.; Gershlak, J. R.; Vratanos, M.; Kanellias, M.; Gaudette, G. R.; Pins, G. D., Design of a fibrin microthread-based composite layer for use in a cardiac patch. *ACS Biomaterials Science & Engineering* **2016**.
13. Morgan, K. Y.; Black, L. D., 3rd, Mimicking isovolumic contraction with combined electromechanical stimulation improves the development of engineered cardiac constructs. *Tissue engineering. Part A* **2014**, 20 (11-12), 1654-67.
14. Hansen, K. J.; Favreau, J. T.; Gershlak, J. R.; Laflamme, M. A.; Albrecht, D. R.; Gaudette, G. R., Optical Method to Quantify Mechanical Contraction and Calcium Transients of Human Pluripotent Stem Cell-Derived Cardiomyocytes. *Tissue engineering. Part C, Methods* **2017**.
15. Kelly, D. J.; Rosen, A. B.; Schuldt, A. J.; Kochupura, P. V.; Doronin, S. V.; Potapova, I. A.; Azeloglu, E. U.; Badylak, S. F.; Brink, P. R.; Cohen, I. S.; Gaudette, G. R., Increased myocyte content and mechanical function within a tissue-engineered myocardial patch following implantation. *Tissue engineering. Part A* **2009**, 15 (8), 2189-201.
16. Tao, Z. W.; Favreau, J. T.; Guyette, J. P.; Hansen, K. J.; Lessard, J.; Burford, E.; Pins, G. D.; Gaudette, G. R., Delivering stem cells to the healthy heart on biological sutures: effects on regional mechanical function. *Journal of tissue engineering and regenerative medicine* **2014**.
17. Ogle, B. M.; Bursac, N.; Domian, I.; Huang, N. F.; Menasche, P.; Murry, C. E.; Pruitt, B.; Radisic, M.; Wu, J. C.; Wu, S. M.; Zhang, J.; Zimmermann, W. H.; Vunjak-Novakovic, G., Distilling complexity to advance cardiac tissue engineering. *Science translational medicine* **2016**, 8 (342), 342ps13.
18. Zhang, D.; Shadrin, I. Y.; Lam, J.; Xian, H. Q.; Snodgrass, H. R.; Bursac, N., Tissue-engineered cardiac patch for advanced functional maturation of human ESC-derived cardiomyocytes. *Biomaterials* **2013**, 34 (23), 5813-20.